Bioengineering Functional Human Jejunal Grafts for Intestinal Failure

Laween Meran

BMedSci BMBS MRCP

Thesis submitted to University College London for the Degree of Doctor of Philosophy

UCL Great Ormond Street Institute of Child Health

and

The Francis Crick Institute

2020

Declaration

I, Laween Meran, confirm that the work presented in the thesis is my own. Where information has been derived from other sources, I confirm that this has been indicated in the thesis.

Signed:

Date:

PhD Publications

Meran L., Massie I., Campinoti S., … De Coppi, P & Li, V.S.W. (2020) Engineering transplantable jejunal mucosal grafts using patient-derived organoids from children with intestinal failure. Nature Medicine. 2020;10.1038/s41591-020-1024-z.

Giobbe, G., Crowley, C., Luni, C., Campinoti, S., Khedr, M., Kretzschmar, Kai., De Santis, M., Zambaiti, E., Michielin, F., **Meran, L**., Hu, Q., …De Coppi, P. (2019). Extracellular matrix hydrogel derived from decellularized tissues enables endodermal organoid culture. Nature Communications. 10, 5658 (2019) doi:10.1038/s41467-019-13605-4.

Schwerd, T., Bryant, R. V., Pandey, S., Capitani, M., **Meran, L**., Cazier, J. B., … Uhlig, H. H. (2018). NOX1 loss-of-function genetic variants in patients with inflammatory bowel disease. Mucosal Immunology, 11(2), 562–574. doi:10.1038/mi.2017.74

Lee S.E., Massie I., **Meran L** & Li V.S.W. Advances in Stem Cells and their Niches. Volume 2, (2018), Pages 99-140. Chapter Four - Extracellular matrix remodelling in intestinal homeostasis and disease

Meran, L.*, Baulies, A.*, & Li, V.S.W (2017). Intestinal stem cell niche: the extracellular matrix and cellular components. Stem Cells International, 2017, 7970385. doi:10.1155/2017/7970385

* co-authorship

PhD Prizes

Jeremy Powell-Tuck First Prize Winner for Best Abstract, June 2015

Awarded by the British Association of Parenteral and Enteral Nutrition Society

Best Oral Communication, Digestive Diseases Federation 2015

Awarded by the British Society of Gastroenterology

Best Poster Prize Award, July 2015

Awarded at the 6th NIHR Infrastructure Doctoral Research Training Camp

'Research Images as Art' Runner Up Prize, January 2021

Awarded by University College London

Abstract

Intestinal failure (IF), following extensive anatomical or functional loss of small intestine, has debilitating long-term effects on infants born with this condition. Priority of care is to increase the child's length of functional intestine, jejunum in particular, to improve nutritional independence. Children with irreversible IF suffering complications of parenteral nutrition may be referred for intestinal transplantation. However, mortality rates are as high as 60% at 5 years. The aim of my project was to develop an innovative treatment strategy to rebuild the patients' own jejunum for autologous transplantation. Here I report the reconstruction of transplantable intestinal mucosal grafts using primary human materials. Human jejunal intestinal organoids derived from paediatric patients with IF can be cultured and expanded efficiently *in vitro* with region-specific markers preserved. Decellularised human intestinal matrix with intact ultrastructure is used as biological scaffold. I show that the biochemical composition of decellularised human small intestine and colon matrix are virtually analogous, suggesting that they both can be used as scaffolds for jejunal graft reconstruction. Functional jejunal grafts with digestive enzyme-producing enterocytes can be efficiently engineered by repopulating human intestinal scaffolds with human jejunal organoids and fibroblasts *in vitro*, which can further survive and mature after *in vivo* transplantation. These primary human material based jejunal grafts provide proof-of-concept data for autologous transplantation of tissue engineered intestine in patients with IF.

To

Leylan and Dastan

You bring out the best in me

“See with your mind, hear with your heart”

Impact Statement

The small intestine is the primary site of digestion in the human body and can grow to approximately 6 metres in length. Intestinal failure occurs when disease or injury to the small intestine prevents adequate absorption of food and drink, leading to malnutrition and dehydration. A common cause of irreversible intestinal failure is short bowel syndrome, where large sections of the small intestine have been surgically removed. These patients are supported by providing essential nutrients directly into their veins. In severe cases they may be referred for intestinal transplantation, however donor organs are in shortage and survival rates are very low even after transplantation. This PhD project seeks to develop human intestinal tissue engineering techniques, to rebuild human small intestine for children with intestinal failure requiring transplantation. The research aim is to make a personalised graft using the patient's own intestinal cells wherever possible.

Here I present my work in successfully engineering functional patient-specific jejunal grafts using autologous cells sources. This has resulted in significant impact on both clinical and the research fields. Clinically, the banking patient organoids at the point of intestinal resection in at risk cases, such as neonates with necrotising enterocolitis, may become the norm in the future. This work also introduces the new research concept of 'recycling' human colonic tissue to grow small intestinal grafts. The new protocols I developed of jejunal graft engineering maintained in dynamic flow bioreactors could also have a strong impact in drug screening and drug discovery fields. In addition, the physiologically relevant human intestinal grafts provide platforms for human disease modelling, as an alternative to using animals in research. Most importantly, the publication of my data represents a significant translational step forwards, pushing organoid technologies and regenerative medicine further towards clinical application. Finally, the research impact of this work was maximised by disseminating our data widely through press releases, such that its publication generated an 'Alimetric score' of 947 within a week, as over a hundred global news outlets reported on this work.

Acknowledgements

I am grateful to UCL, the Crick and Great Ormond Street NIHR Biomedical Research Centre for funding my clinical research training fellowship. I thank my incredibly kind and inspiring supervisors, Dr Vivian Li and Prof Paolo De Coppi, for providing excellent supervision and allowing me the freedom to explore this project's translational potential fully. It has been a steep learning curve but one that will guide my work ethos forever. I am also greatly appreciative of the academic guidance of Simon Eaton and Paola Bonfanti. UCL's Academic Careers Office team, in particular Colby Benari and Geraint Rees, have been invaluable for their support on my return from maternity leaves - thank you! I am also grateful for the unique mentorship of Professor Chris Hawkey, who gave so much of his time to me, very early on in my training.

For project specific work, I would like to highlight the unique kindness and expertise of Anne Weston and Riana Gaifulina. I also thank Alan Ling and his mechanical engineering workshop at the Crick, for their patience with my various evolving sketches of bioreactor components that were crucial to these studies. I am grateful for the support of the Science and Technology Platforms at the Francis Crick Institute, in particular Chizzy Oguejiofor and Nick Baidoo in Experimental Histopathology, and Peter Faull in the Mass Spectrometry laboratories. I am thankful to all members of Paolo's lab at ICH and Vivian's lab at the Crick, past and present, for all the fun and banter.

Most of all I would like to thank my mother and father for their spiritual, practical and intellectual encouragement. Without the love and support of my parents, my husband, 'ate' Gerly, my siblings and true friends (near and far), I would not have been able to embark upon this PhD work whilst also becoming a new mother. My daughter Leylan and son Dastan, born in the second and final year of my PhD respectively, made this period of study a far more colourful (…and sleepless) one!

Contents

Table of Figures

Abbreviations

ALPI - Alkaline phosphatase
AB-PAS - Alcian blue and periodic acid Schiff
BMP - Bone morphogenic protein
CBC - Crypt base columnar
CHGA - Chromogranin A
COX 2 - Cyclooxygenase-2
ECM - Extracellular matrix
EGF - Epidermal growth factor
EN - Enteral nutrition
ESC - Embryonic stem cell
FEnS - Fetal enterospheres
FN - Fibronectin
GAG - Glycosaminoglycans
GI - Gastrointestinal
GFP - Green fluorescence protein
HA - Hyaluronan
hiPSC - Human induced pluripotent stem cells
HSPG - Heparan sulphate proteoglycan
HUVEC - Human umbilical vein endothelial cell
IF - Intestinal failure
ISC - Intestinal stem cell
LCT - Lactase
LRP6 - Low density lipoprotein receptor-related protein 6
LGR5 - Leucine Rich Repeat Containing G Protein-Coupled Receptor 5
MLC - Myosin light chain
MMP - Matrix Metalloproteinase
MUC2 - Mucin 2
OLFM4 - Olfactomedin 4
PDOs - Patient derived organoids
PN - Parenteral nutrition
RGD - Arginylglycylaspartic (domain)
SBS - Short bowel syndrome
SI - Small intestine
SIS - Small intestine submucosa
SOX 9 - SRY-box 9
SBS-IF - chronic intestinal failure due to short bowel syndrome
TAZ - Transcriptional coactivator with PDZ-binding motif
TESI - Tissue Engineered Small Intestine
TIMP - Tissue inhibitors of metalloproteinases
TLR4 - Toll like receptor 4
UEA1 - Ulex Europaeus Lectin 1 antibody
Wnt - Wingless-related integration
YAP - Yes association protein

1. Introduction

1.1 The Healthy Gastrointestinal Tract

A competent Gastrointestinal (GI) tract is essential for human health. This remarkable organ represents the largest mucosal surface area of the human body, estimated to be 200m^2, serving its chief role in nutrient digestion and absorption[1]. In addition, its functional importance as an immunologic organ is well established as the gut is richly populated with immune cells and lymphoid tissue[2]. As the primary interface of interaction between host and environment, the tract is densely populated with a microbial community that metabolises indigestible carbohydrates and produces essential vitamins[3]. Whilst modulating mucosal immunity, the small intestine (SI) must also mount protective responses against invading pathogenic microorganisms in order to maintain intestinal homeostasis[3,4]. Meanwhile, the colon acts as the main reservoir of the microbial flora, the maintenance of which is essential for health and dysregulation has been implicated in multiple digestive disorders[5,6], as well as more widespread pathological processes from neurological disorders to chronic systemic inflammatory conditions[7-9].

Anatomically, the intestinal component of the GI tract consists of the SI (duodenum, jejunum, ileum) and large intestine (colon and rectum). Nutrient absorption primarily occurs in the SI, whereas water resorption occurs in the colon. The intestinal epithelium is constantly renewing and is organised along a crypt-villus axis. The villi, present in SI only, are covered in a range of differentiated cells that project into the lumen so that as food passes by, nutrient breakdown and absorption is maximised. Intestinal crypts are formed by invaginations of the epithelium from the mucosa into the deeper mesenchyme. Six major differentiated cell types of the intestinal epithelium perform the functions of the intestine: [1] absorptive enterocytes[10,11]; [2] mucus secreting goblet cells[12]; [3] hormone secreting enteroendocrine cells[13]; [4] antimicrobial secreting Paneth cells[14,15]; [5] taste-chemosensory tuft cells[16] and [6] immunosurveillance microfold “M” cells[17]. Renewal of the epithelium is driven by

dedicated adult intestinal stem cells (ISCs) which are restricted to the base of the crypt compartment, called crypt base columnar (CBC) cells. Leucine rich repeat containing G protein-coupled Receptor 5 (*LGR5*), expressed exclusively in CBC cells, is a stem cell marker of the intestine[18]. The ISCs divide and give rise to daughter cells entering the transit-amplifying (TA) zone which then proliferate and migrate upwards towards the crypt-villus junction. Here, they terminally differentiate before reaching the villus tip and are shed into the lumen, with the exception of Paneth cells that will migrate downwards back to the stem cell zone[18-20]. Paneth cells are situated adjacent to the ISCs, acting as a major source of secreted growth factors such as Wnt, EGF and Notch ligands, crucial for stem cells survival[19,21]. The whole ISC proliferation to differentiation journey from the base of the crypt to the villus tip lasts approximately 3-5 days in mice[20].

The multifaceted functional dimensions of the GI tract make it one of the most fascinating organs of the human body to study, with wide reaching implications on human health. The functional differences between the SI and colon are reflected in differences in mucosal micro-architecture and epithelial cell composition. Most obviously, the colonic epithelium lacks villi structure but retains crypt compartments, where the ISCs reside. However, subtle differences in epithelial cell properties also exist. For example, Goblet cells secreting MUC2 mucin glycoproteins are more abundant in the colon than the small intestine. The secreted antimicrobial glycocalyx mucous layer not only forms a barrier against bacteria, but also serves to protect the epithelium from the physical and mechanical stress during peristalsis[12]. The mucous layer sits directly above the epithelium acting to concentrate Paneth cell secreted antimicrobial peptides close to the epithelial cells, thereby producing an antibacterial gradient from the cells towards the lumen. Interestingly, the properties of the mucus barrier system differ between colon and SI[22]. In the colon, a double layered mucous barrier, formed of an inner adherent layer and an outer more porous layer exists. Whilst in the SI, it is a single non-adherent mucous layer with higher porosity, allowing microbes to penetrate the mucus relatively more easily[22].

Paneth and goblet cells are derived from a common secretory progenitor, and as such continue to share similar characteristics[23]. Antibacterial peptides secreted from crypt Paneth cells are crucial for maintaining stem cell homeostasis and modulating the microbiome[15,21]. However, Paneth cells are only present in the SI. In the colon, cells termed "Paneth-like" exist, which are in fact a subset of colonic goblet cells that are distinctly cKit+ (a receptor tyrosine kinase)[24]. These Paneth-like cells are predominantly situated in the proximal colon or at sites of inflammation[21]. These cells mimic Paneth cells as they are interdigitated with $Lgr5^+$ stem cells in the colon crypts. They are regulated by Notch signalling and function similarly to Paneth cells in the SI to support $Lgr5^+$ stem cells. Since much fewer "Paneth-like" cells exist in the colon resulting in relatively less antimicrobial defence, this might explain the greater need for a more robust double-layered mucus barrier present in the colon but not the SI.

Given these functional differences, both SI and colon are required for optimal health. However, whilst many patients are able to maintain a good life following a colectomy[25], resections of the small bowel leading to intestinal failure are much more disruptive and life-threatening to patients, children in particular[26], discussed further below.

1.2 Intestinal Failure - the clinical problem

Intestinal failure (IF) is defined as a reduction of functional gut mass below the minimal amount necessary for digestion and absorption required to satisfy nutrient and fluid requirements for maintenance in adults, or growth in children[27]. Short bowel syndrome (SBS) describes a malabsorptive state that often follows massive resection of the SI, and is the most common cause of chronic irreversible IF (SBS-IF)[28].

Patients with IF comprise a heterogeneous group due to the multiple underlying causes and differences in residual bowel structure and function. In the paediatric population, the causes of IF can broadly be separated into three main pathogenesis groups: (i) anatomical loss due to SBS which may be secondary to intestinal resections due to necrotising enterocolitis, Crohn's disease or congenital malformations such as intestinal atresia and gastroschisis; (ii) dysmotility due to neuromuscular

intestinal diseases such as Hirschsprung's disease or chronic intestinal pseudo-obstruction (CIPO); (iii) congenital epithelial defects of the intestine such as microvillus inclusion disease and tufting enteropathy[29]. In the adult population, the causes of IF include extensive bowel resections following vascular insults to the intestine, such as in mesenteric ischaemia, thrombosis or trauma. Severe Crohn's disease, leading to multiple resections is also a common cause for SBS-IF, as in the paediatric population. Radiation enteritis causing epithelial inflammation and scarring leading to IF is more commonly seen in adult patients with malignancy[30].

The role of artificial nutrition in the care of patients with IF has been evolving for over 50 years. Following significant intestinal resection, the early postoperative phase is frequently characterized by administration of parenteral nutrition (PN) with the aim to transition gradually to enteral nutrition (EN), followed by the subsequent reintroduction of oral nutrition. EN is generally favoured over PN as clear physiological advantages have been documented in both animal studies and human clinical trial data when comparing subjects receiving EN versus PN. For example, mucosal hypoplasia is observed in the SI of fasted rats receiving parenteral nutrition[31]. This implies that food passing through the gut has an important role in preserving normal physiology, mucosal immune function and systemic inflammation[32-35].

The progression from PN to EN may be hindered by bacterial overgrowth, persistent micronutrient deficiency and metabolic complications such as electrolyte imbalances and acute kidney injury. In general, the majority of patients with less than 100cm of small bowel will become dependent on PN[36]. Underlying intestinal conditions such as Crohn's disease, radiation enteritis or pseudo-obstruction increase the risk of a patient being persistently dependent on PN. IF patients that become dependent on PN may suffer numerous complications including bacterial overgrowth, line sepsis, central venous access thrombosis or PN-related liver disease[37,38]. Ultimately, patients with irreversible IF suffering complications of PN may be referred for small bowel transplantation. However due to shortage of suitable organs many patients die on the transplant wait list. Among children who received a

transplant, mortality at 5 years is as high as 60 % due to sepsis, graft failure and complications of long-term immunosuppression[39].

At a population level, accurate international data on the epidemiology of IF in children is difficult to attain owing to the condition's rarity and the complex heterogeneous cohort of patient backgrounds associated with the condition[40]. The 'Paediatric IF Consortium', consisting of 14 sites across the United States of America and Canada, report SBS to be the leading cause of IF in children, as well as being the underlying cause in almost half of all patients requiring home PN[40-42]. The incidence of IF in infancy was reported to be 24.5 cases per 100,000 live births, based on a single-centre study in Toronto in 2004[43]. Data gathered from across 33 hospitals in the UK indicate a fourfold increase in the number of children on long-term home PN between the years 1993 to 2012, with a regional point prevalence varying from 1.76 to 41.4 patients per million[44]. More recently, in 2014 the Committee for Orphan Medicinal Products (COMP) estimated that SBS affects less than 1 in 10,000 people in the European Union (equivalent to approximately 51,000 people), therefore qualifying SBS as a rare disease as defined by the European Medicines Agency (EMA). Given the growing numbers of children on home PN, the limited success of current treatment strategies and high morbidity and mortality associated with IF, there is an urgent unmet clinical need for research into novel treatments for these patients.

1.3 Intestinal adaptation and regeneration

Intestinal adaptation and regeneration are two distinct but crucially important events that take place in response to loss of or damage to the small intestine. Adaptation occurs following massive resection of the intestine, whereby the organ exhibits a morphological compensatory change in order to expand the absorptive surface area per unit length of the intestine. The main features of intestinal adaptation include an increase in the crypt depth and elongation of villus height as well as enhanced rates of epithelial proliferation and apoptosis[45-47]. This is accompanied by changes in intestinal blood flow and intestinal motility, that all together increase the absorptive capacity of the remaining intestine[48]. Additionally, in mouse models of SBS, where 50% of the proximal small intestine has been

resected, ileal enterocytes were able to reprogram their regional identity towards a more proximal enterocyte identity[49]. This indicates another feature of intestinal adaptation, maximising carbohydrate, protein and lipid digestion and micronutrient absorption which occurs mostly in the duodenum and jejunum[50].

The glucagon-like peptides (GLP-1 and GLP-2) are synthesised and released from enteroendocrine cells in the small and large intestine, in response to nutrient ingestion. GLP-1 regulates blood glucose by stimulating insulin secretion from pancreatic islet beta cells[51]. In addition, GLP-1 action results in the inhibition of gastric emptying and acid secretion, reduction of food ingestion and secretion of glucagon[51]. Meanwhile, GLP-2 is recognised as a potent epithelial trophic hormone, promoting nutrient absorption by stimulating crypt cell proliferation and inhibiting enterocyte apoptosis[52]. GLP-2 also reduces epithelial permeability and intestinal motility. The actions of GLP-2 are mediated by a distinct receptor, thought to be expressed on a subset of enteroendocrine cells in the epithelium[53], and on enteric nervous cells[54,55] with downstream actions mediated via subepithelial fibroblasts[56]. Thus, GLP-2 functions as a key regulator of mucosal integrity, permeability and nutrient absorption. Both GLP-1 and GLP-2 are rapidly inactivated by the exopeptidase enzyme, dipeptidyl peptidase IV (DPP-IV), resulting in a half-life of several minutes *in vivo*[57,58]. The process of natural intestinal adaptation having a clinically significant effect on a patient with IF (i.e. the patient becoming independent of EN or PN), is slow and can take up to 2 years. However, this process can be accelerated pharmacologically by the drug Teduglutide (Brand names Gattex or Revestive®), licenced for clinical use in PN-dependent SBS-IF patients. Teduglutide is an analog of glucagon-like-peptide-2 (GLP-2) and differs from GLP-2 by one amino acid substitution. This substitution confers a much longer half-life than endogenous GLP-2, as it is more resistant to proteolysis from dipeptidyl peptidase-4 (DPP-4)[59]. In patients with IF, Teduglutide treatment increases villus height and crypt depth of the intestinal mucosa[60], offering some hope for improvement in their nutritional state.

On the other hand, intestinal regeneration describes the ability of the organ to renew itself in order to maintain function. The regenerative capacity of the gut is characterised by the relatively short half-life of intestinal epithelial cells. Hence the intestinal mucosa has one of the fastest self-renewal rates of all mammalian tissues. Under normal homeostasis conditions, this rapid turnover is driven by dedicated, mitotically active $Lgr5^+$ CBCs (Figure 1.1). However, upon exposure to luminal pathogens or chemical insults that cause damage to the crypts and the CBC cells, the regenerative capacity is partially preserved[61]. This indicates that there are "back-up" mechanisms of injury-induced regeneration in place. These include (i) the presence of quiescent '+4' cells; (ii) distinct populations of reserve stem cells; and (iii) cellular plasticity - whereby differentiated cells undergo "dedifferentiation" regaining their previous ISC phenotype in order to replenish the ISC pool and repair the epithelial damage quickly[62,63]. Intestinal cells demonstrating plasticity in order to contribute to the regenerative process have been observed in +4/5 position progenitor cells (expressing a range of various markers that include $Tert^+$, $Prox1^+$, $Bmi1^+$, $NeuroD1^+$, $Atoh1^+$, $Hopx^+$, $Krt19^+$, Dll^+)[64-71]; +6 position $Alpi^+$ enterocytes[72]; +4 position enteroendocrine cells[69,73]; +3 position secretory precursors $Lgr5^+$ label retaining cells[74]; and fully differentiated Paneth cells[75-77]. Most recently in 2019, a "revival stem cell" (revSC) that is able to revive the homeostatic stem cell compartment and regenerate the intestinal epithelium was described.[71] RevSCs are marked by high clusterin expression at the +4 position and are able to give rise to all major cell types of the intestine including $Lgr5^+$ CBCs, after irradiation damage or dextran sodium sulphate induced damage to the mouse intestine.[71] Overall, these studies suggest that cellular plasticity may be a feature in distinct cell populations, in response to critical damage to intestinal crypts.

1.4 Intestinal stem cells and their niche

The fast turnover rate of intestinal epithelium is supported by the ISCs located at the intestinal crypt. The intestinal crypt is enriched by a multitude of growth factors originating intrinsically from the crypt base cells and extrinsically from the extracellular matrix surrounding the crypts (Figure 1.1).

Alongside the regulatory signalling cascades governing ISC fate, the ECM also provides important stromal cell factors and biomechanical factors that are important in maintaining the ISC niche. The proteins of the intestinal crypt basement membrane are of mixed origin, being produced by cells of the epithelial compartment as well as the stromal compartment. The basement membrane consists of two layers: (i) the basal lamina positioned directly beneath epithelial cells and (ii) the underlying reticular sheet of matrix that anchors the epithelium to the lamina propria[78]. The basement membrane is therefore hypothesised to be a key site for epithelial-mesenchymal cross-talk. Under homeostatic conditions, the ECM enables regulated bi-directional interaction despite the physical separation between stromal cells and intestinal epithelial cells. In this section the cellular and structural components of the ISC niche are discussed.

1.4.1 Signalling pathways regulating intestinal stem cells

A carefully orchestrated regulatory network exists to maintain a fine balance between ISC maintenance, proliferation and differentiation, thus protecting the niche when it is confronted with environmental fluctuations (such as toxins or infections) that could potentially lead to intestinal injury and disease.

The highly conserved Wnt signalling pathway is of fundamental importance in the maintenance and proliferation of ISCs[79,80]. Wnt ligands are secreted by Paneth cells (Wnt 3, 6 and 9b) and pericryptal stromal cells (Wnts 2b, 4, 5a and 5b)[81,82]. Stromal cells also secrete the potent Wnt agonist R-spondin[82]. Likewise, Notch signalling is also essential for ISC maintenance whereby inhibition of the pathway results in dampened stem cell proliferation[83,84]. Paneth cells express membrane bound Notch ligands (Delta-like 1 and 4) that, when presented to notch receptors of neighbouring ISCs, activate the notch signalling pathway leading to crypt proliferation and epithelial regeneration[85]. Subsequently, inactivation of Notch signalling drives the differentiation of progenitor cells towards the secretory lineage[86,87]. Conversely, Bone Morphogenetic Protein (BMP) signalling restricts ISC expansion and promotes differentiation[88]. Higher BMP ligands are expressed in the villus compartment whilst BMP

antagonists (Noggin, Gremlins 1 and 2) are secreted by pericryptal stromal cells, thereby generating a BMP-low environment in the intestinal crypts[89]. The Hippo pathway also has a central role in determining cell-fate and GI tissue homeostasis, in particular controlling organ size by regulating ISC proliferation, differentiation and apoptosis[90-92]. Here, the transcriptional co-activators YAP and TAZ transduce ECM mechanical-cytoskeletal cues, leading to changes in cell shape, proliferation and differentiation, with significant crosstalk between Hippo and Wnt signalling pathways. Finally, Hedgehog signalling has a key role in stem cell homeostasis and tissue regeneration and maintenance of the crypt-villus axis[93]. Inhibition of Hedgehog signalling blocks villus formation whilst boosting ISC proliferation through enhancing Wnt/β-catenin activity[94].

An understanding of the cross-talk between all these signalling pathways is essential in order to accurately recreate the natural ISC niche *in vitro* on scaffolds for the purpose of intestinal tissue engineering.

1.4.2 Stromal - epithelial interactions

Paneth cells, as discussed above, provide essential niche signals to their neighbouring stem cells[95]. Alongside Paneth cells, crosstalk between the epithelium and the subepithelial stromal cells are also of critical influence on intestinal function and regeneration in the ISC niche. The mesenchymal compartment of the intestinal lamina propria contains multiple stromal cell populations with distinct phenotypes and function. The cell populations able to secrete ECM proteins, growth factors and ligands essential in the ISC niche include fibroblasts, myofibroblasts, mesenchymal stromal cells, endothelial cells, pericytes, neural cells and smooth muscle cells[96,97].

The predominant cells of the intestinal stroma are fibroblasts, of which there is significant phenotypic heterogeneity. Fibroblasts drive tissue repair processes such as wound healing, but are also implicated in carcinogenesis. Intestinal subepithelial myofibroblasts (ISEMFs), a member of the fibroblast family, are located in pericryptal regions and throughout the lamina propria. Of all the stromal cells present in the ECM, ISEMFs have received the most academic attention for their importance in the ISC niche,

given their ability to secrete Wnt ligands and BMP antagonists[81,89,97,98]. TGFβ is thought to be a key inducer of myofibroblast differentiation, which exhibit qualities of smooth muscle cells as they are able to exert a contractile force[98]. Upon normal wound healing, ECM remodelling is mediated by an inflammatory trigger of matrix catabolism by matrix metalloprotease enzymes (MMPs) secreted by ISEMFs[98]. Once the healing process resolves, ISEMFs undergo apoptosis, mediated in part by IL-1β[98]. Meanwhile, excessive ECM deposition is associated with a pathological persistence of activated ISEMFs, such as in inflammatory bowel diseases (IBD)[99,100].

Multipotent mesenchymal stromal cells (MSCs) are non-haematopoietic progenitor cells that were originally isolated from bone marrow but have been found to reside in all post-natal organs and tissues[101,102]. They have functional roles in immunomodulation and regeneration[102-104], however their specific function in the gut has not been extensively explored. In mouse models of radiation injury, the systemic administration of MSCs was shown to improve intestinal epithelial repair[105-107]. Indeed, several clinical trials are underway to investigate the therapeutic utility of MSCs in several diseases, including IBD, with contradictory long term results[108-112]. It will be crucial to understand the exact role of MSCs in the maintenance of the ISC niche *in vivo*, in order to improve their clinical applications for intestinal diseases.

Smooth muscle cells, present in close association with ISEMFs, form a thin layer of muscle (muscularis mucosa) to separate the lamina propria from the submucosa. The smooth muscle cells contract and relax to keep the muscularis mucosal layer under constant agitation[97]. This function serves to expel potentially toxic luminal contents out of the crypts and away from the ISC niche. Similar to ISEMFs, smooth muscle cells also secrete BMP antagonists to repress the differentiative BMP signal and maintain the Wnt activity in the crypt base[89].

Endothelial cells present in the lamina propria are important in maintaining epithelial homeostasis. Previously published mouse model studies showed that radiation-induced injury triggered rapid endothelial apoptosis prior to epithelial death *in vivo* [113]. Importantly, loss of epithelial stem cells did

not occur when endothelial apoptosis was blocked by administration of a basic fibroblast growth factor (bFGF) treatment or by genetic deletion of the acid sphingomyelinase (*ASMase*) - a gene that is required for radiation-induced endothelial apoptosis. Endothelial cells are also implicated in the induction of intra-mucosal immune responses[114,115]. However, their full role in homeostasis of the ISC niche remains to be discovered.

Pericytes are peri-endothelial myofibroblast-like contractile cells wrapping around the capillaries, which regulate angiogenesis and capillary wall permeability via paracrine signalling[116]. However, the identity of the pericytes remains controversial, specifically regarding their ontogeny and progeny. Distinction between populations of pericytes and myofibroblasts is challenging since they express similar molecular markers[117]. Subsets of pericytes have been reported to be multipotent progenitors that may participate in tissue regeneration[118]. The comprehensive role of pericytes in the ISC niche remains unclear. It is thought that pericytes may function similarly as ISEMFs based on their close developmental origin and identity[116,117].

Neural cells are also present in the ISC niche and important for intestinal epithelial growth. The enteric nervous system consists of a large number of neurons and enteric glia cells (EGCs) that are interconnected to form the two ganglionated plexuses – the myenteric and the submucosal plexuses. EGCs are located both within the ganglia and in the extraganglionic regions, such as the lamina propria with close proximity to the intestinal crypts[119,120]. Bjerknes and colleagues showed that enteric neurons participate in the feedback loop that regulates epithelial growth and repair by expressing the glucagon-like peptide 2 (GLP-2) receptor[121]. In addition to their neuroprotective function, these mucosal EGCs are thought to play crucial roles in maintaining the intestinal epithelial barrier. Recent data show that EGCs homeostasis postnatally is dependent on functional host-microbe interactions, indicating their role in regulating immune responses in the gut[122]. The EGCs also exert protective functions on the intestine by secreting factors such as epidermal growth factor (EGF) and TGFβ isoforms following inflammation or injury[123,124].

Finally, it is important to acknowledge the lamina propria is also rich in immune cells such as dendritic cells, macrophages and T-regulatory cells[2,125]. A full discussion of the intestine's mucosal immune system is not within the remit of this thesis, but has been reviewed extensively in the literature[125,126]. Most recently, an important study used single-cell RNA sequencing to identify MHC class II machinery enrichment in two subsets of $Lgr5^+$ ISCs, followed by functional studies co-culturing intestinal organoids with $CD4^+$ T helper cells[127]. It was demonstrated that pro-inflammatory signals (IFNγ, IL-17a IL-13) promote intestinal epithelial cell differentiation whilst regulatory signals (IL-10) promoted ISC self-renewal. Furthermore, both in T cell depleted mice and in an MHCII knock out mouse model, the pool of ISCs expands. This indicates the important role of the Th1/2/17 immune axis in the ISC niche.

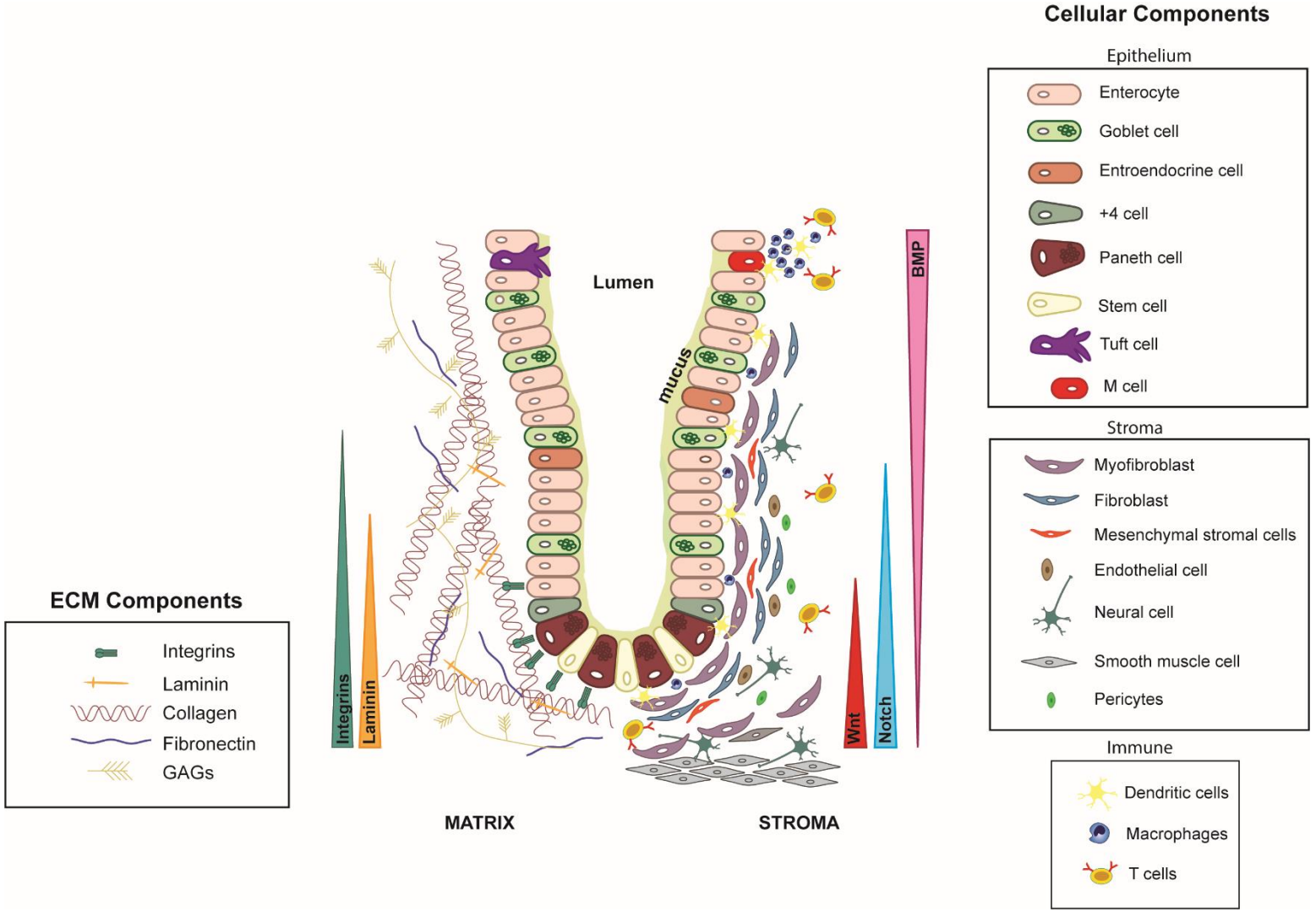

Figure 1.1 - The extracellular matrix and cellular components of the intestinal stem cell niche: The crypt surrounding microenvironment is made up of both physical/structural and cellular niche to regulate ISC homeostasis. The physical niche includes collagen fibres, integrins, fibronectin filaments, laminins, and glycosaminoglycan, which form a highly structured network named as the extracellular matrix (ECM). The cellular niche includes pericryptal myofibroblasts, fibroblasts, mesenchymal stromal cells, endothelial cells, pericytes, neural cells, smooth muscle cells and immune cells. The ECM and cellular niche interact and communicate with each other via different signalling pathways to maintain homeostasis of the intestinal epithelium, which includes: enterocytes, goblet cells, enteroendocrine cells, Paneth cells, tuft cells, M cells and intestinal stem cells.

1.4.3 The extracellular matrix of the intestinal stem cell niche

In addition to the cellular residents of the intestine's ECM, the biomechanical parameters of the ECM are also important influences on the ISC niche (Figure 1.1). Several structural proteins make up the ECM, including fibronectins, laminins, collagens, glycosaminoglycans (e.g. heparan sulphate proteoglycans - also known as percalan) and integrins are reported to be enriched at the intestinal crypt base, suggesting their potential role in ISC regulation[78,128-138]. All these components influence intestinal epithelial proliferation and differentiation during migration from crypts to villus tips, healing following mucosal insult and injury, inflammatory bowel disease, and malignant transformation.

Laminin is a major glycoprotein constituent of the intestinal crypt basement membrane (together with fibronectin, type IV collagen and heparan sulphate proteoglycan) and is recognised to be particularly important in the establishment of epithelial cell polarity[132,139]. Laminin subtypes are key for the constitution of SI and colon basement membranes. Laminin α1 and α2 were shown to be enriched at the crypt regions, while laminin α5 was expressed strongly at the villus basement membrane[139-141]. Laminin α5 is believed to play a crucial role in establishing the mucosal pattern of the SI by maintaining the villus architecture[140,142]. The recent study on the designer matrices for intestinal organoid culture has further demonstrated that laminin-111 ($\alpha_1\beta_1\gamma_1$) is important to enhance ISC survival and proliferation[143].

Fibronectin (FN) is a versatile high molecular weight adhesive glycoprotein found in a wide range of tissues and plays important roles in cell adhesion, migration, growth, and differentiation. In the intestinal ECM, it is secreted by myofibroblasts as well as being expressed by epithelial cells, and is located predominantly in the basement membrane, but also throughout the lamina propria[131,136,144]. Changes in the deposition pattern of FN correlates with several intestinal disease states. For example, an upregulation of fibronectin throughout epithelial cells is seen in conditions associated with intestinal fibrosis such as IBD[129]. Strain forces exerted in the ECM *in vitro* have been shown to induce FN mediated epithelial cell migration by activating the extracellular signal-regulated kinase (ERK) and

myosin light chain (MLC) signalling pathways, indicating the importance of FN in wound closure and epithelial migration[145]. Furthermore, FN is postulated to be an activator of the nuclear factor-κB signalling pathway in the context of intestinal inflammation[129]. FN is likely to have multifunctional roles since it contains binding sites for other ECM proteins such as collagens and glycosaminoglycans, as well as RGD binding sites for cell surface receptors of the integrin superfamily[129].

The integrin superfamily is a group of structurally and functionally related heterodimeric receptors, consisting of α and β subunits that link the ECM with the intracellular cytoskeleton as part of the RGD-adhesion system, and are particularly relevant in discussion of the ISC niche[128,146]. Drosophila studies demonstrated integrin signalling to be obligatory for the maintenance and proliferation of ISCs, reputedly anchoring them in the crypts during the physical compression and stretching forces associated with peristaltic muscle contraction as food is propelled across the length of the gut[147]. In the same study, several integrin subunits and signalling components were found to be expressed at high levels in ISCs but low levels in differentiated cells of the Drosophila midgut[147]. β1 integrins are essential in regulating the proliferation of ISCs of a genetic mouse model, by mediating Hedgehog signalling[148]. In human tissue, many biological effects of fibronectin are mediated through the transmembrane α1β5 integrin receptor. In addition, integrin α8β1 is thought to be a crucial mediator of intestinal crypt cell-matrix interaction, through the focal adhesion kinase (FAK) signalling pathway pathway[149-151]. Human intestinal epithelial cells have also been shown to be regulated by Integrin-linked kinase (ILK) through a fibronectin dependent mechanism[152]. Overall, these studies provide evidence of an essential role for integrins in promoting ISC homeostasis and potentially intestinal tumorigenesis when integrin mediated mechanisms are disturbed.

Collagen is the most abundant structural ECM protein in the human body. The collagen superfamily contains at least 19 different subtypes, with types I, III, IV and VIII being secreted by fibroblasts being uniformly distributed in the health intestinal ECM[135,153,154]. However, increasing evidence points to type VI collagen (which interacts closely with type IV collagen of the basement membrane) as a chief

regulator of the mechanical microenvironment of the intestinal crypt cells, via fibronectin and RGD-dependent crypt cell interactions[128,133]. Indeed, intestinal crypt epithelial cells have been demonstrated to secrete type VI collagen into the basal lamina of the intestinal basement membrane[133]. Increases in ECM collagen deposition leads to increased tissue stiffness which alters integrin focal adhesions, growth factor receptor signalling and acto-myosin and cytoskeletal dependent cell contractility[155]. However, in a dysregulated environment, as is seen in IBD, histological findings of excessive collagen cross-linking is found, associated with intestinal fibrosis and stricturing disease[156,157].

Glycosaminoglycans (GAGs) are present abundantly in the ECM and provide lubrication and structural integrity to cells owing to their high viscosity and low compressibility. These properties enable them to form a passageway between cells, facilitating cell migration[158,159]. GAGs can operate as organisers of collagen fibre deposition, stimulating angiogenesis and inhibiting coagulation[160]. The specific GAGs of physiological interest in the intestine are heparan sulphate proteoglycan (HSPG), hyaluronic acid, heparin, and chondroitin sulphate.

One of the most intensely studied GAGs in the intestine is HSPG, which are present in the ECM as linear polysaccharides of repeating disaccharide units of glucuronic acid and N-acetyl glucosamine, able to bind to Wnt, Hedgehog, TGF-β, and FGF in Drosophila and Xenopus studies[134,161-163]. Intestine-specific HSPG is found on the basolateral surface of intestinal epithelial cells. Their role in the ISC niche has been implicated to be through their ability to modulate the Wnt/β-catenin signalling pathway during regeneration of small intestinal crypts[134,164]. This study demonstrated that γ-radiation induced intestinal epithelial injury in mice deficient in intestine specific-HSPG led to a loss of Wnt target gene expression and reduced nuclear staining of β-catenin. This coupled with a reduced phosphorylation of low-density lipoprotein receptor-related protein-6 (LRP6) by stimulation with Wnt3a in the epithelial cells of HSPG-deficient mice, strongly proposes that HSPG present on the cell surface enhances binding of Wnt ligands to intestinal cells, thereby promoting intestinal regeneration[134].

In the healthy gut, another GAG named hyaluronic acid (HA) exists abundantly throughout the matrix as a chemically simple, high molecular weight, non-branching polymer of repeating units of N-acetyl-glucosamine. However, in disease processes such as in excessive inflammation, these polymers are cleaved to fragments of lower molecular weight that take on signalling roles[165,166]. Though the mechanisms for HA degradation are incompletely understood, it has been recently demonstrated that fibroblasts in the guts of active Crohn's disease secrete the protein KIAA1199, which leads to excessive degradation of HA and the generation of pro-inflammatory HA fragments. HA binds to CD44, which is expressed on the plasma membrane of many cell types, and also binds to the Toll-like receptors TLR2 and TLR4, which are widely distributed in the gastrointestinal tract and are important in mediating the host response to both commensal and pathogenic bacteria[166,167]. Indeed, it has been shown that HA injected intraperitoneally to mouse models of radiation enteritis demonstrated a TLR4 and COX-2 mediated increase in intestinal crypt survival[167,168].

Application of knowledge on the intestinal ECM was demonstrated by Gjorevski *et al.* when they devised a modular synthetic hydrogel to study the effect of various ECM parameters on ISC behaviour *in vitro*[143]. They showed that enrichment of hydrogels individually with ECM components including FN, laminin-111, collagen IV and HSPG enhanced ISC survival, when compared with inert matrix gels providing physical support alone. The combination of Laminin-111 together with FN's RGD (Arg-Gly-Asp) peptide in mechanically dynamic gels that demonstrated the greatest influence on intestinal organoid culture efficiencies in a dose dependent fashion[143]. Central to the study of biomechanics of the ECM is the Hippo signalling pathway, which incorporates mechanosensing and interacts with most of the major signalling pathways including Notch and Wnt. Cells interact with physical stimuli via cell adhesion molecules at their periphery, which allow the cytoskeleton to connect with the adjacent ECM structures. This enables microenvironmental forces to be sensed and translated into intracellular messages, in a process termed mechanotransduction[169]. ECM signals act on the two transcriptional co-activators YAP (yes-associated protein) and TAZ (transcriptional co-activator with PDZ-binding motif). Indeed, YAP displays nuclear translocation and activation in

response to mechanical tension, hence is important in cellular mechanosensing and mechanotransduction[170,171]. Gjorevski *et al.* demonstrated that ISCs embedded in hydrogel-based matrices of low stiffness correlated with poor proliferation and cytoplasmic localisation of YAP. Whereas increasing stiffness leads to the nuclear translocation and activation of YAP. Initial higher matrix stiffness enhanced YAP activation and ISC expansion, while the formation of organoids was vitally dependent on a dynamic softening profile of the matrix[143].

In vivo ECM morphology, and therefore its mechanical properties, is under constant dynamic remodelling, whereby components are deposited, degraded or modified by cues conveyed to the matrix by cells. The process of intestinal ECM remodelling is strongly associated with angiogenesis, cell migration and differentiation, deposition and destruction via the matrix metalloproteinases (MMPs) family[172]. MMPs comprise a large family of at least 25 zinc-dependent endopeptidases capable of degrading all components of the ECM. They are classified according to substrate specificity, and are themselves inhibited by tissue inhibitors of metalloproteinases (TIMPs). The role of MMPs in maintaining homeostasis of the ISC niche was confirmed through *in vitro* studies showing that intestinal organoids cultured in RGD based hydrogels that are susceptible to rapid degradation by MMPs, promoted a pro-inflammatory phenotype in the organoids[143]. These findings provide direct evidence that the physical properties of the ECM influence ISCs regulation.

1.5 Intestinal tissue engineering

Tissue engineering is an interdisciplinary field that comprises the combination of biomaterials to form scaffolds and stem cells for cellular regeneration, in order to create a construct to replace lost human tissues. Previous studies have reported pre-clinical developments of tissue engineering in many soft tissue organs including oesophagus, skeletal muscle, liver and lung reconstruction[173-179]. Whilst engineering of simpler tissues such as skin and cornea are well established in clinical practice[180,181], examples of successful clinical applications of more complex organs have only been demonstrated in a few clinical case reports of trachea and bladder reconstruction[182,183]. Intestinal

tissue engineering, through combination of biomaterials and patient-derived cells, offers a novel treatment approach for IF patients[184]. This approach could render immunosuppression needless, thereby circumventing complications of graft-host rejection and malignancy[39]. To date there have been no clinical studies of bioengineered SI grafts in humans. Furthermore, tissue engineering strategies are adaptable to enable personalised grafts whereby length, diameter and composition may be modified based on the individual patient's underlying disease aetiology. For example, in SBS inadequate enteral absorption follows massive full thickness anatomical resection of the small intestine[38,43]. The most predominant pathologies resulting in SBS include necrotizing enterocolitis (NEC), intestinal atresia, gastroschisis, malrotation with volvulus and Crohn's disease[37]. Hence in these circumstances, constructing a full thickness intestinal wall graft (including mucosa, submucosa and muscularis layers) in neonatal dimensions is essential. In purely neuromuscular intestinal diseases, such as extensive Hirschsprung's disease or chronic intestinal pseudo-obstruction (CIPO), patients have a healthy intestinal epithelium but dysfunctional neuromuscular wall. Hence constructing a neuromuscular graft capable of peristalsis is paramount. Finally, in congenital epithelial defects such as in Microvillus Inclusion Disease or Intestinal Epithelial Dysplasia, the patient retains good neuromuscular function. Hence reconstruction of a purely mucosal graft would be of utmost significance in these patient groups.

Overall, tissue-engineered grafts are most suited to patients who have lost nutritional autonomy following an acute insult to the gut, as is the case in congenital malformations or necrotising enterocolitis. In these situations, the graft is unlikely to be vulnerable to ongoing disease processes. In contrast, chronic relapsing and remitting conditions such as Crohn's disease will render the tissue-engineered graft susceptible to systemic inflammatory responses and end organ damage. In these clinical cases, optimisation of medical therapies prior to surgery will be crucial for the success of transplanted gut (whether cadaveric or tissue engineered). Similarly, in conditions such as Hirschsprung's disease or congenital epithelial defects, *ex-vivo* correction of the cellular and genetic defects prior to recellularisation will be an essential step to longevity of the engineered intestinal graft.

In all cases, in order to maintain long-term viability after transplantation the engineered grafts require a vascular network to facilitate graft survival. Inducing neo-angiogenesis is also a key priority for intestinal tissue engineering. Similarly, the lymphatic system of the intestine must not be overlooked during tissue engineering studies. Intestinal lymphatics are essential for dietary lipid and fat-soluble vitamin absorption, as well as transporting antigens and antigen presenting cells[185]. Lymphatic vasculature is a one-way drainage system for interstitial fluid and immune cells. Fluid drains in to blind ending permeable lymphatic capillaries to form "lymph". Lymph is then transported to lymph nodes by collecting vessels, before re-entering the blood circulation via the thoracic duct[185]. Indeed, loss or damage to the intestinal lymphatics results in severe gut inflammation, sepsis and death in mouse studies using diphtheria toxin administered selectively to ablate intestinal lymphatics[186].

Finally, since this thesis focuses on infants and children with IF, it is important to consider the need for a tissue-engineered construct to grow in dimension at an appropriate rate for the child's age and size. Previous studies of transplanted tissue-engineered constructs in children offer some insight into this question. The 4-year follow up study of one child who successfully received a tissue-engineered trachea at the age of 10 as a treatment of last resort, reported that engineered tracheal graft was vulnerable to malacia and stenosis[187,188]. This observation may be related to the growth dynamics and properties of cartilaginous tissue. Interestingly, long-term follow up publications on patients receiving engineered smooth muscle bladder constructs have not reported similar findings[189,190]. In long-term follow up canine studies of bladder augmentation with porcine SI matrix scaffolds indicated that the grafts can be remodelled and replaced by host tissue[191]. More longitudinal studies tracking the growth of the matrix as well as cells on engineered graft will be an essential step prior to adopting tissue-engineered therapies in situations other than ' the last resort'.There have been important pre-clinical studies on tissue engineering of the intestine[192-198]. The ongoing debate regarding the best source of cells and scaffolds for intestinal tissue engineering is discussed further below.

1.5.1 Sources of intestinal cells

There are several sources of intestinal epithelial cells for *ex-vivo* expansion and transplantation purposes (Figure 1.2). These include human adult somatic intestinal stem cells (hISCs); human induced pluripotent stem cells (hiPSCs); human embryonic stem cells (hESCs) and human fetal enterospheres (FEnS). This body of work focuses on the use of adult somatic hISCs for tissue engineering and transplantation purposes. All these cellular sources are discussed in this section.

Previous attempts to establish the *in vitro* expansion of ISCs were extremely difficult without inducing genetic transformations. In 1992, Evans *et al.*, first demonstrated primary adult intestinal crypt cultures that consisted of both epithelial and mesenchymal cells on collagen-type 1 coated plates[199]. However, only short-term cultures lasting up to two weeks was possible using this method[199-201]. In 2007, Barker *et al*., made the landmark discovery that ISCs were marked by the Wnt target gene *Lgr5* in CBC cells of both the SI and colon[18]. The increasing knowledge of the dynamics of ISC biology paved the way for the establishment of novel organoid "mini-gut" culture systems, first established by Sato *et al*., in 2009[202]. The study showed that a single Lgr5-expressing ISC was able to grow three-dimensionally into crypt-villus budding structures in a Matrigel-based culture, and in the absence of a mesenchymal niche. This has proven to be another key milestone in the field of ISC biology, with significant research applications[203,204]. Prior to this publication it was not possible to reliably culture ISCs that retained multipotency of all differentiated intestinal cell types in the lab. One month after the Sato *et al.* publication, another group led by Calvin Kuo in Stanford published an alternative collagen matrix-based air-liquid interface culture system, which also enabled long-term *in vitro* intestinal epithelial cultures. A key advantage of this method is preservation of epithelial-mesenchymal interactions the immune microenvironment. Once established, these organoids could be maintained for at least 1 year exhibiting proliferation and multi-lineage intestinal epithelial differentiation. However, this method has only been demonstrated to work for embryonic or neonatal murine cultures and the organoids cannot be expanded by passaging. Therefore Sato *et al. methods*

for both mouse and human intestinal organoid cultures have been more widely adopted in the field, since this method demonstrates unconstrained capacity for expansion with karyotype stability[202,205].

There have since been several intestinal organoid transplantation studies demonstrating regenerative medical applications of the 'mini-gut' organoids. For example, mouse intestinal organoids were injected into the colon lumen where they demonstrated a capacity for mucosal healing and regeneration, by integrating into the damaged mucosa of the mouse colon[204]. Particularly noteworthy, is the ability of the engrafted SI organoids to maintain their original tissue identity to form villi when transplanted ectopically in the mouse colon[206]. However, this finding was not replicated when GFP labelled murine fetal enterospheres (derived from the proximal fetal intestine) were implanted in a colonic injury model. These fetal-derived cells in this model engrafted at sites of denuded colon epithelium and expressed the marker carbonic anhydrase, specific to colon[207]. This introduced new debate as to whether the regional and functional identities of the ISCs are determined by extracellular signals or the intrinsic cellular programme of the transplanted organoids were more important in determining the final functional identity of the cells. More recently, human colon organoids have been xenotransplanted orthotopically, using a Lgr5-CreER knockin to enable genetic lineage tracing[208]. Here, they demonstrated that the human colon cells maintained multipotency and self-renewal, with a slower cycling status than the mouse colonic epithelium.

HiPSCs are another attractive source for cell therapy. They are generated by forced expression of OCT3/4, SOX2, KLF4 and c-MYC in differentiated adult cells such as fibroblasts[209]. Once in their pluripotent state, they have been used to generate intestinal epithelium of all lineages *in vitro*[210,211]. These cells were ectopically transplanted under the kidney capsule of NSG NOD SCID mice, in the absence of a scaffold, where crypt-villus structures formed[211]. Although not clinically relevant for human transplantation at these small scales without scaffolds, this *in vivo* model using human pluripotent stem cells (either embryonic or induced) has proven to be an important system for modelling intestinal diseases. When combined with human vagal neural crest cells (NCCs) that were

differentiated into neurons and glial cells, and implanted in the kidney capsule of mice for 6-10 weeks, a functional enteric nervous system developed. This was further used to investigate the cell and molecular basis for Hirschsprung's disease[212].

However, translation of this technology as cellular therapy in human clinical trials faces major hurdles. For example, viral vectors are commonly used for efficient reprogramming[213]. Furthermore, transplantation of hiPSCs poses a risk of teratoma formation *in vivo*[214]. In contrast, since adult somatic hISCs are multipotent and fate restricted, their potential to induce teratoma formation is abolished. Additional concerns have also been raised over genetic mutations and chromosomal aberrations evolving during the reprogramming process, which may lead to malignancy[215-218]. On the other hand, a key advantage of hiPSCs is the ability to non-invasively obtain donor cells from autologous sources, which is particularly important for IF patients who have very little or no small intestine left *in situ*. Recently, a pre-clinical study on intestinal reconstruction using hiPSCs on rat scaffolds was reported[193] (discussed in further detail in section 1.5.2). hiPSCs are currently in clinical trials for adult diseases such as age-related macular degeneration[219], Parkinson's disease[220] and severe heart failure[221]. However, for conditions of infancy and childhood, substantial concerns persist over the use of hiPSCs and hESCs not only due to the risk of teratoma formation, but also because of chromosomal aberrations during the reprogramming process which increase the risk of malignancy. In addition, it is accepted that iPSCs retain a degree of epigenetic memory of their original tissue, which may have influence on the behaviour of cells *in vivo*[222]. Finally, hiPSCs have been shown to be immunogenic in mice[223]. This may mean that their uses in regenerative medicine may be limited as patients receiving such transplants will require immunosuppression.

Embryonic stem cells (ESCs) are derived from totipotent cells of the blastocyst stage of the early mammalian embryo (i.e. less than 8 weeks after fertilisation) and are capable of unlimited, undifferentiated proliferation *in vitro*[224]. Mouse ESCs have been induced to differentiate into functional intestinal tissue[225,226]. Using similar protocols, human ES cell lines (commercially available)

have also been used to form intestinal tissue when engrafted in the kidney capsule of NSG mice. After 6 weeks in vivo, the cellular grafts contained most of the intestinal epithelial, mesenchymal and smooth muscle cell types found in the developing gut[211]. Interestingly, when seeded into synthetic scaffolds (discussed further in section 1.5.2), smooth muscle cells were not present implying some loss of pluripotency in these conditions[227]. Since the derivation of ESCs from human embryos is associated with significant ethical obstacles, this is likely to hinder their widespread use in translational clinical research.

Somewhat related is the development of protocols to generate human FEnS[207], derived from immature gut epithelium of first-trimester human fetuses (i.e. after 8 weeks from fertilisation) following elective abortions. However, the functional characterisation of human FEnS and fetal organoids *in vitro* remains relatively limited. Most of the data in this paper focuses on mouse FEnS, where Fordham *et al.* show that they are refractory to differentiation *in vitro* but demonstrate some potential for differentiation in a mouse model of colonic injury. Whilst mouse FEnS have been passaged for up to 180 days showing a normal karyotype[207] and can be passaged for up to 2 years, human FEnS have thus far been reported to be maintained for over 2 months. In addition, it is still unclear whether fetal cells transplanted for regenerative medicine purposes will display immune privilege, echoing the maternal acceptance of the fetus during pregnancy. There is some evidence that allogeneic transplantation of fetal cells may evoke an immune response in the recipient, as demonstrated in some *in vitro* studies with human fetal retinal cells[228]. This may represent challenges regarding their use in clinical translation.

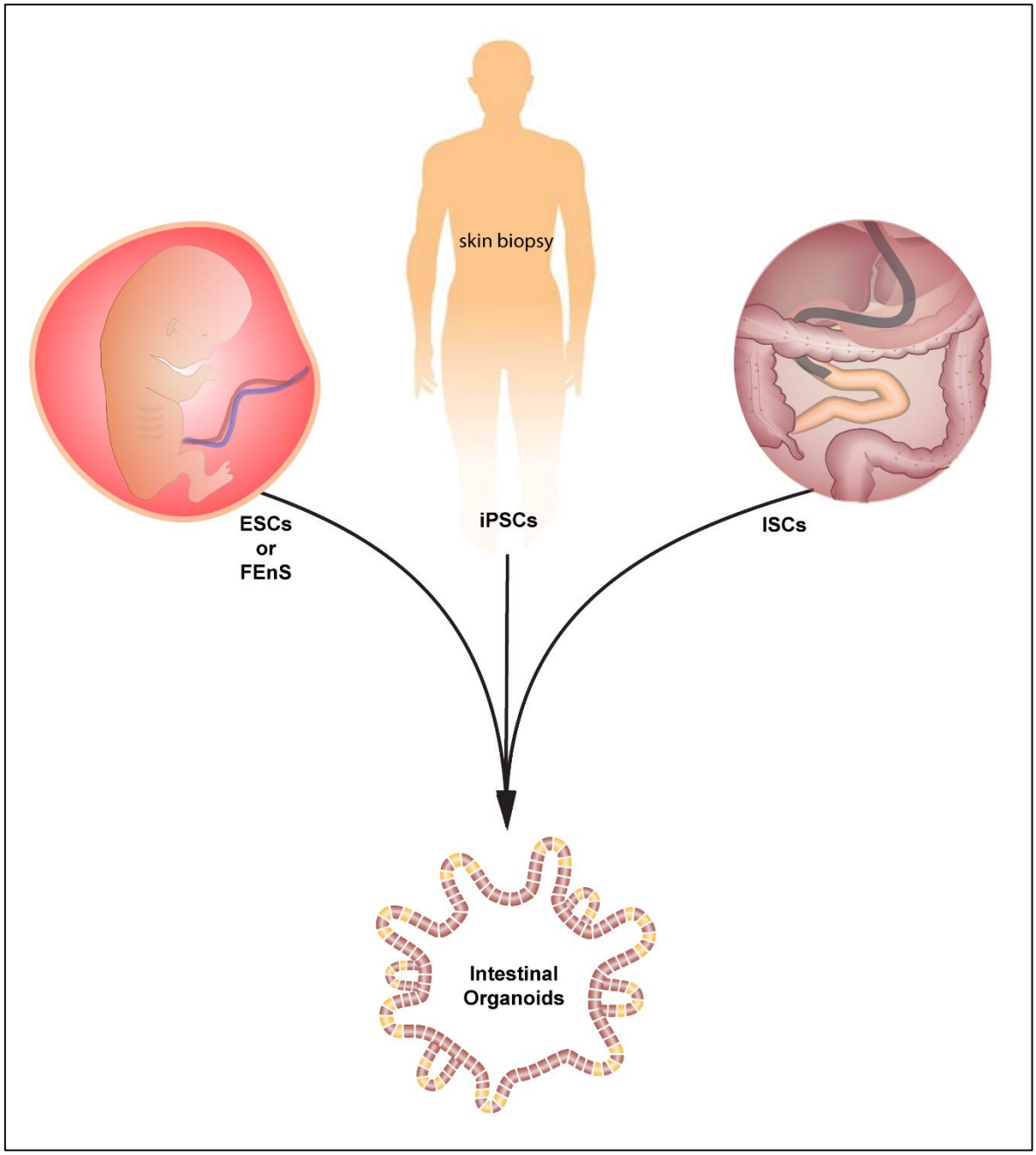

Figure 1.2 - Sources of human intestinal stem cells for tissue engineering: Schematic diagram summarising that intestinal organoids have been generated from (i) Embryonic Stem Cells (ESCs) or Fetal Enterospheres (FEnS); (ii) induced pluripotent stem cells derived from skin fibroblasts and (iii) adult somatic intestinal stem cells (ISCs).

1.5.2 Sources of intestinal scaffolds

Scaffolds are essential for tissue engineering as they act as a physical platform and support network, guiding three dimensional cell growth (Figure 1.3)[229]. Scaffolds should ideally mimic the natural ECM that exists *in vivo* as closely as possible. Biodegradability of the scaffold is also an important consideration, since this is important to limit ongoing foreign body reactions and inflammation. In the context of the intestine, retaining the characteristic crypt-villus axis is of utmost importance. Biomaterials used to generate scaffolds may be either synthetic or biological or a combination of the two. Furthermore, scaffold composition and design significantly impact cell behavior and identity[173,176,196-198,227,229-231].

The choice of scaffold source depends on the desired mechanostructural properties required for the engineered organ, as well as cellular behaviour on the scaffold. Synthetic scaffolds are generally derived from biodegradable polymers and are moulded into the desired organ shape, or designed using 3D printers. The great advantage of synthetic scaffolds is the potential to develop an "off the shelf" product that is widely available and can be manufactured in large scale production lines. However, these polymers do not retain any of the natural nanotopography of the native intestine, nor any bioactivity. In contrast, biological scaffolds are those that are derived directly from the ECM of native organ through a process of decellularization, which describes the process whereby an organ is perfused with various chemical or biological solutions in order to remove all cellular and immunogenic material[232]. Professor Badylak's research group have led extensive preclinical studies in the use of several biological scaffolds, including porcine small intestine submucosa (SIS), for use in a wide range of tissue environments such as oesophageal, skeletal muscle, tendon, vascular, abdominal wall and bladder repair[229,233-236]. Notably, the bioactivity of important growth factors is retained in studies of porcine SIS scaffolds, including transforming growth factor-β (TGF- β), basic fibroblast growth factor (b-FGF), and vascular endothelial growth factor (VEGF) following decellularization[237-239]. Therefore, an understanding of the mechanisms by which biological scaffolds promote site appropriate tissue

reconstruction, as well as their remodelling *in vivo* are instrumental to anticipating the host response and the long-term graft survival post-transplantation. Retaining bioactivity of the ECM is important after decellularization since excessive processing can reduce the amount of ECM molecules present. Badylak's group also showed that the use of ionic detergents can reduce the amount of glycosaminoglycans present[240]. It is therefore important to achieve the fine balance between complete decellularization and over-processing or using excessively harsh biochemical solutions that may also damage the microarchitecture and remove important organic signals of biological scaffolds. In addition, several clinical studies have demonstrated the use of porcine SIS in promoting wound healing and restoration of a wide range of tissue function, from chronic skin wounds such as burns to chest wall reconstruction[241-244]. As such, porcine SIS is commercially available and approved by the Food and Drug Administration for a variety of clinical applications. However, porcine SIS is not currently routinely used for intestinal reconstruction. There is growing evidence for the use of SIS in SI tissue repair in rat, rabbit and canine models[245-248]. In canine models, SIS grafts measuring approximately 7cm by 3cm in dimension were shown to encourage tissue repair in a model of partial small bowel wall resection[244]. Encouragingly, this study demonstrated *in vivo* remodelling of the SIS to include histologically discreet villi on the mucosa as well as submucosa, smooth muscle and serosal layers by 6 months. Similar results were also seen in the rat models when 2cm-length tubular rat-SIS grafts were implanted[245,247]. Meanwhile, porcine-SIS tubular grafts, 3cm in length, assessed in rat models were reported to enable rapid regeneration of mucosa and well as smooth muscle layers of the gut[248]. However, full characterisation data of the neo-intestinal morphology was limited and it is unclear whether the central portion of the tubular graft was fully recellularised. All together, these studies indicate the intestinal matrix to be rich in biological characteristics, favourable for cell growth and regeneration *in vivo* and support the use of human biological intestinal decellularized scaffolds for intestinal tissue engineering in this thesis.

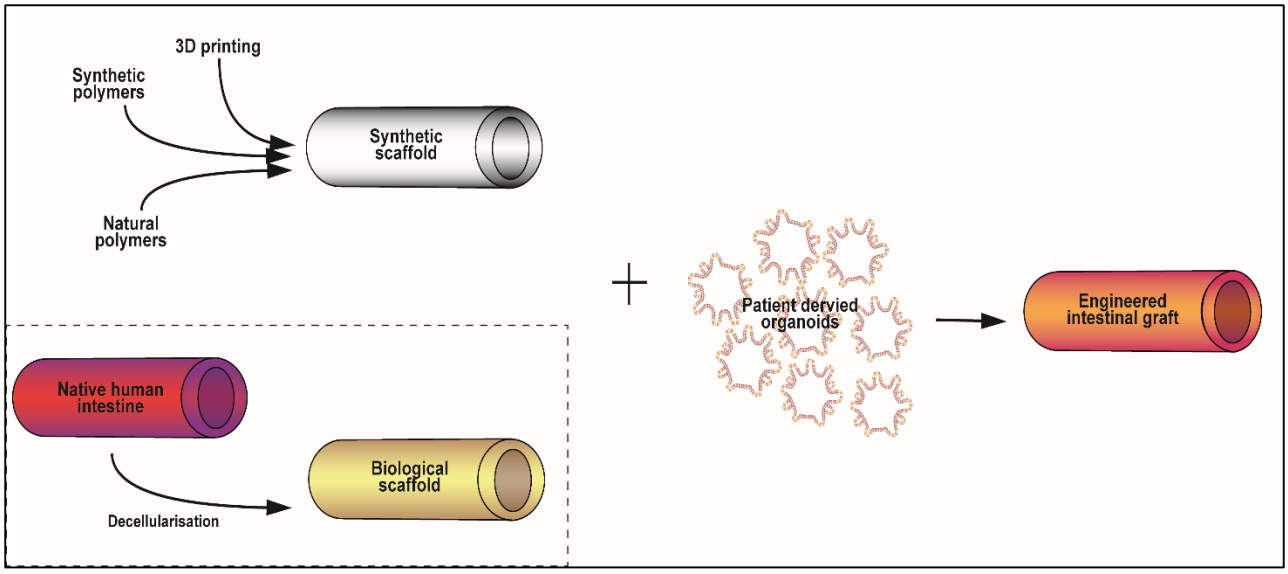

Figure 1.3 - Sources of intestinal scaffolds for tissue engineering: Schematic diagram summarising that engineered grafts for intestinal tissue engineering have been derived from either synthetic sources or biological sources via decellularisation and combined with patient derived organoids.

1.5.3 Recent advances in intestinal tissue engineering

To date, intestinal biological scaffolds have been derived from native rat[193,230], pig[193,227] and human intestines[227,249,250]. Despite this, published studies on engineering transplantable human intestinal grafts using biological scaffolds are surprisingly limited.

The most sophisticated and pertinent of these studies is from 2017 by Kitano *et al.*, where they described the seeding of hiPSC-derived intestinal organoids onto rat decellularised scaffolds with intact vasculature[193]. Characterisation of a polarised columnar epithelium *in vitro* showed differentiation to enterocytes, enteroendocrine cells, stromal cells and proliferative cells. However, goblet and Paneth cell differentiation *in vitro* and crypt-villus morphology was missing. In parallel, the rat scaffold vascular tree was re-endothelialised by infusing human umbilical vein endothelial cells (HUVECs). The functional capacity of the regenerated intestinal constructs to absorb basic nutrients (glucose and medium-chain fatty acids) from the lumen was demonstrated *in vitro*. The engineered grafts were then transplanted heterotopically in the cervical region of immunodeficient rats, whereby the superior mesenteric artery and vein of each graft was anastomosed to the right carotid artery and

right internal jugular vein respectively. The epithelial morphology following 4 weeks of *in vivo* transplantation showed presence of all differentiated cells (Paneth cells, goblet cells, enteroendocrine cells and enterocytes), indicating more optimal conditions for maturation of the grafts *in vivo*. Functional tests were repeated after 2 weeks *in vivo*, and showed glucose and fatty acid absorption. Positron emission tomography and computer tomography (PET-CT) was further used to trace the incorporation of glucose analog 18F-fluorodeoxyglucose delivered into the lumen of the graft, which showed prominent accumulation in the brain of the rats.

Another important study in 2016 utilised biological intestinal scaffolds to model colorectal cancer. Chen *et al.,* described the engineering of an organotypic *ex vivo* colon cancer model using a biological human colon scaffold that was recellularised with primary human colon organoids and colon myofibroblasts derived from healthy individuals[250]. Commercially acquired microvascular endothelial cells were also used to re-populate the scaffolds. However, the co-culture of human colon organoid and myofibroblast cells were immortalised with human telomerase reverse transcriptase (hTERT) to prevent premature senescence and ensure their long-term growth potential. This may have artificially conferred an advantage to repopulating the scaffolds, a method which would not be translatable for clinical transplantation studies. Overall, their *ex vivo* system captures the pathological progression from APC-mutant neoplasia to a submucosal invasive tumour. Their data also included characterisation of the engineered colon epithelium with good crypt structure and demonstrated $Lgr5^{+}$ proliferating cells at the base of crypts, alongside differentiated goblet cells and enteroendocrine cells higher up. However, absorptive enterocyte differentiation was not demonstrated in this paper and scaffold integrity could have been compromised since their seeding methods involved detachment of the mucosa from the submucosa. Details on the methods of culture were somewhat limited but implied that the engineered grafts were less than 1cm in size and were maintained in static conditions for up to 7 weeks in mutagenesis experiments. Though not directly related to tissue engineering for transplantation purposes, this study highlighted human biological intestinal scaffolds to be superb physiological platforms for cellular regeneration.

The use of synthetic scaffolds for intestinal tissue engineering has also been demonstrated in several notable studies[227,251-254]. The scaffolds were derived from polyglycolic/poly L lactic acid (PGA/PLLA) polymers that were moulded into a tubular shape[251]. Initial studies with these scaffolds used rat intestinal cells called "organoid units" are multicellular units derived from neonatal rat intestine containing a mesenchymal core surrounded by a polarised intestinal epithelium[201]. These units contain mucosa, submucosa and muscle layers of the intestine (first described by Evans et al in 1992)[199]. The intestinal cultures were seeded onto synthetic scaffolds to form "Tissue Engineered Small Intestine" (TESI) constructs. There was no *in vitro* culture period as the TESI was immediately transplanted into rat models of SBS. Results showed that rats receiving TESI had reduced mortality compared to controls[254]. In subsequent studies, the same technique was used to construct and test TESI *in vivo*, in a Yorkshire swine model[255]. Here, the seeded scaffolds were implanted by wrapping the scaffolds into the omentum or mesentery. Seven weeks later, the animals were sacrificed and the TESI constructs were harvested for analysis. The results demonstrated that all constructs retained engineered portions of intestine with crypt-villus axis preservation and stromal cell presence. Proliferation, as indicated by PCNA, was constrained to the crypt compartments. In addition, goblet and enteroendocrine cells were identified as well as the ganglion cells in Auerbach's and Meissner's plexi. However, there was no preservation of the intestinal smooth muscle layers, which was present in the original neonatal rat "organoid units". Human TESI was also produced using similar protocols[192,256]. Although there are physiological advantages of TESI that consists of all layers of the intestine, this methodology proved to be unfeasible for clinical translation as large lengths of donor intestinal tissue is required to generate relatively low numbers of "organoid units" for scaffold seedings, since the maintenance of these cultures were limited to 2 weeks (as discussed earlier).

Subsequent studies in 2015 using these synthetic scaffolds moved away from seeding multicellular "organoid units" and replaced them with hESC-derived intestinal organoids, the main advantage being their pluripotency and unlimited expansion potential[227]. In these studies, embryonic derived intestinal organoids were seeded on both the PGA/PLLA synthetic scaffolds and porcine derived native

decellularised matrices. The grafts were cultured *in vitro* for 2 weeks, before being implanted subcutaneously into the omentum or under the kidney capsule. Interestingly, only synthetic scaffolds retained engineered intestinal epithelium with good epithelial morphology and presence of differentiated cells after 13 weeks *in vivo*. Vimentin positive stromal cells were also identified. However, despite the pluripotent origin of the embryonic derived organoids, no enteric nervous system (ENS) or smooth muscle cells were present in the grafts. In parallel experiments using the same protocols, seedings of hESC-derived intestinal organoids on native porcine produced largely negative results *in vivo*, the reasons for this remains unclear[227]. No functional analyses data was included in this study. Although human intestinal decellularized scaffolds (derived from a cadaveric donor) were presented in supplementary figure 1 of this paper, no data demonstrating the seedings of embryonic derived organoids on that human decellularized intestinal scaffold was presented, suggesting that these experiments were either unfeasible or unsuccessful.

Finally, most recently in 2019, Ladd *et al.* published a study where synthetic scaffolds formed of poly glycerol sebacate (PGS) were fabricated using laser ablation to recreate the nanotopography of the villi but not crypts[257]. Here, either CACO-2 cells or mouse GFP-labelled intestinal organoids (termed "enteroids" in the paper) were used for cell seedings. The results showed poor epithelial cell morphology with no signs of columnar monolayers or polarisation shown. The article focussed on the physical characteristics of the scaffold and biodegradability once implanted in omental pouches of mice. Morphology of the graft epithelium did not improve post-transplantation.

Altogether, these summarised published data indicate the great importance of selecting the appropriate intestinal cell source and scaffold type, which has significant influence on determining the eventual structural and functional identity of engineered intestinal grafts.

1.6 Research Aim, Hypotheses and Objectives

The prevailing research aim of this PhD thesis is to advance the recent developments in the field of intestinal tissue engineering towards clinical translation as much as possible for the target IF patient group. My particular focus is reconstruction of the intestinal mucosa. Specific objectives and associated research hypotheses are:

1. To build a "living biobank" of organoids derived from paediatric patients, specifically seeking endoscopic intestinal biopsies from children with established IF or those who are diagnosed with conditions that increase their risk of developing IF in their future.

- Hypothesis: The regenerative potential of ISCs is preserved in IF patients and can be exploited through organoid culture for expansion *in vitro*.

2. To generate a library of human intestinal scaffolds derived from paediatric patients undergoing intestinal resections, and perform in-depth characterisation of the biological scaffold matrix composition and microarchitecture.

- Hypothesis: Decellularised scaffolds derived from SI and colon are biosimilar in ECM composition

3. To define the conditions required to effectively reconstruct the innermost layer of the intestine - the mucosa - and demonstrate the morphological and functional characteristics of the engineered intestinal constructs.

- Hypothesis: Decellularised SI and colon scaffolds are equally ideal platforms for engineering functional SI mucosal grafts.

4. To test the engineered intestinal mucosal constructs *in vivo*, and generate proof-of-concept data of graft maturation and survival in small animal transplantation models.

- Hypothesis: The survival and morphology of intestinal grafts is influenced by the *in vivo* transplantation site.

2. Material and Methods

2.1 Ethical Approval

Ethical approval for the use of human intestinal tissue was obtained from the Bloomsbury NRES committee (REC references 04-Q0508-79 and 18/EE/0150). The Committee was constituted in accordance with the Governance Arrangements for Research Ethics Committees and complied fully with the Standard Operating Procedures for Research Ethics Committees in the UK. Informed consent for the collection and use of human tissue was obtained from all patients, parents or legal guardians at Great Ormond Street Hospital, London.

2.2 Human Tissue

Wherever possible, endoscopic intestinal epithelial biopsies for organoids or fibroblast isolations were primarily sought from paediatric patients known to the intestinal failure multidisciplinary team at Great Ormond Street Hospital. For comparative experiments, tissue was also sought from other paediatric cases who, due to complex clinical backgrounds were at risk of developing intestinal failure. The full list of patient materials collected over the course of this thesis is listed in Appendix 1. Intestinal tissue for scaffold fabrication were sought from a broader clinical background of paediatric patients undergoing intestinal resection related procedures also listed in Appendix 1.

2.3 Animals

Immune deficient NOD-SCID IL-2Rγnull (NSG) female mice, aged 9 - 14 weeks old, were used in all experiments (obtained from the Francis Crick Institute Biomedical Research Facility). All mice were housed in the animal facility at the Francis Crick Institute. All experiments were performed with ethical approval under Home Office Project License PPLs 70/8904 and PEF3478B3.

Porcine (Sus scrofa domesticus) SI from the 'Pietrain' breed was used to derive piglet SI scaffolds. Piglets up to 3 kg in weight were euthanized following criteria outlined by the JSR veterinary advisors. Once sacrificed, the animals were transported to the lab via courier and the intestine was harvested immediately on arrival (within 6 hours of euthanasia).

2.4 Patient-Derived Organoid and Fibroblasts and HUVEC Culture

Endoscopic biopsy specimens were cut into finer pieces and washed in cold PBS. For organoid isolations, the tissue fragments were incubated in 2mmol/L EDTA cold chelation buffer, consisting of distilled water with 5.6mmol/L Na2HPO4, 8mmol/L KH2PO4, 96.2mmol/L NaCl, 1.6mmol/L KCl, 43.4 mmol/L sucrose, 54.9 mmol/L D-sorbitol, 0.5mmol/L DL-dithiothreitol) for 30 minutes at 4°C as previously reported[205]. Following this incubation period, crypts were released from the fragments by shaking vigorously. The supernatant was centrifuged at 800RPM for 5 minutes at 4°C, to form a pellet of intestinal crypts, which were washed in Advanced Dulbecco's modified Eagle medium (DMEM) / F12 supplemented with 5% penicillin/streptomycin, 10mmol/L HEPES and 2mM of GlutaMAX. The crypts were then resuspended in Basement Membrane Extract® (BME®) and seeded in a single droplet on pre-heated 48-well plates. The BME® was polymerised for 20 minutes at 37°C, before adding 250µL/well of either human IntestiCult™ Organoid Growth Medium (STEMCELL Technology, #06010) or human organoid basal culture media consisting of conditioned media produced using stably transfected L cells (Wnt 50%; R-spondin 20%; Noggin 10%) and the following growth factors: B27 1X (Invitrogen), Nicotinamide 10mM (Sigma-Aldrich), N-acetyl cysteine 1mM (Sigma-Aldrich), TGF-β type I receptor inhibitor A83-01 500nM (Tocris), P38 inhibitor SB202190 10µM(Sigma-Aldrich), Gastrin I 10nM (Sigma-Aldrich), EGF 50ng/ml (Invitrogen). Rho-kinase inhibitor Y-27632 was added to the culture media for the first week in culture at a concentration of 10µM. The media of each well was changed every 2 days. Organoids were expanded by passaging, as previously described[205]. Briefly, the organoid culture medium was replaced with fresh basal culture medium. Organoids and BME® were mechanically disrupted using a P1000 pipette and transferred into a 15-ml falcon tube, and placed on ice. Further mechanical dissociation was achieved using a fire polished Pasteur pipette. Dissociated organoids were washed with 10 ml of basal culture medium and centrifuged at 800RPM for 5 min at 4°C. To achieve single cell dissociation of organoids, 500µl of TrypLE™ (Gibco) was added to the pellet of organoid, mixed gently with a P1000 pipette and incubated at 37°C for 3 minutes. 10% FBS/ADMEM was then added to the suspension to stop trypsinization, before repeating the centrifugation step at

1000RPM for 5 minutes at 4C. The supernatant was discarded, the pellet resuspended with fresh BME® and organoid culture medium was added. To enhance the expansion rate, organoids were cultured with 3µM CHIR99021 (CHIR) added to the alternate day media changes. The addition of CHIR enabled organoids to be passaged at least once a week, with an expansion ratio of 1:10 wells of a 24-well tissue culture plate. Organoids in differentiation phase were cultured in 10µM DAPT for 48 hours. For the isolation of human intestinal fibroblasts, intestinal fragments left over from the chelation step above were washed in PBS and placed on the bottom of tissue culture dishes with DMEM supplemented with 10% heat inactivated Fetal Bovine Serum (FBS) (Sigma-Aldrich), 5% penicillin/streptomycin and 1x insulin-transferrin-selenium solution (both ThermoFisher). Fibroblasts grew from the fragments within 3-4 days. Cells used for seeding experiments were between passages 3-10. HUVECs were cultured in EGM-2 endothelial medium bullet kit (Lonza, cat.no. CC-3162) and were not used beyond passage 15.

2.5 Real time quantitative Reverse Transcription PCR analyses

RNA was extracted according to the manufacturer's instructions (Qiagen RNAeasy). cDNA was prepared using High-Capacity cDNA Reverse Transcription Kit (Applied Biosystems, #4368813). Quantitative PCR detection was performed using PowerUp™ SYBR® Green Master Mix (Applied Biosystems, A25742). Assays for each sample were run in triplicate and were normalised to the housekeeping gene β-actin. Primer sequences are listed in Appendix 2.

2.6 Western Blotting

BME droplets containing organoids in either basal, expansion (3µM CHIR) or differentiation (10µM DAPT) conditions were disrupted using ice cold Advanced Dulbecco's modified Eagle medium (DMEM) / F12 supplemented with 5% penicillin/streptomycin, 10mmol/L HEPES and 2mM of GlutaMAX, pelleted at 1000RPM for 5 minutes and lysed in ice cold protein lysis buffer (150mmol/L NaCl, 30mmol/L Tris (pH 7.5), 1mmol/L EDTA, 1% Triton X-100, 10% glycerol, 0.1mmol/L phenylmethylslfonyl fluoride, 0.5mmol/L dithiothreitol, protease inhibitor cocktail tablets (EDTA-free) (Roche) and phosphatase inhibitor cocktail tablets (Roche)). Lysates were pelleted for 10 minutes at

13000PRM and supernatants stored at -80ºC until analysis. Protein quantification was by Bradford assay. 40µg protein was loaded onto sodium dodecyl sulfate-polyacrylamide gels (SDS-PAGE) and transferred to membranes, which were blocked using 5% milk in Tris-buffered saline (50mM Tris, 150mmol/L NaCl, pH6) containing 0.1% Tween-20 (TBST) for 1 hour. Primary antibodies (as in Table S5) were added in 3% bovine serum albumin in TBST as follows: lysozyme (1:1000), Sox9 (1:1000), Olfm4 (1:1000), SI (1:200) overnight at 4ºC. Membranes were washed in TBST before appropriate HRP-conjugated secondary antibodies were added at 1:5000 in 5% milk in TBST for 1 hour. Antibody binding was detected using chemiluminescence ECL Prime Western Blotting Substrate (GE Healthcare). Membranes were reprobed with anti-β actin peroxidase antibody (Sigma, A3854, 1:25000) for 10 minutes before ECL development. Band intensity was quantified in ImageJ and normalised to βactin.

2.7 Histology

Samples were fixed in 10% Neutralised Buffered Formalin (Sigma) at room temperature overnight, dehydrated in graded alcohols, paraffin embedded and sectioned at 4µm. Tissue slides were stained according to manufacturers' instructions with Haematoxylin and Eosin (H&E) (Thermo Fisher), Alkaline Phosphatase (Vector Laboratories), Alcian-Blue Periodic Acid Schiff (Sigma). Picrosirius Red (PR), Elastic Van Gieson (EVG) and Alcian Blue (AB) (Thermo Fisher) staining was used to assess retention of collagen, elastin and glycosaminoglycans respectively.

2.8 Immunofluorescence and Immunohistochemistry

For immunofluorescence studies, paraffin embedded slides were rehydrated, permeabilized with 0.3% Triton X100 (Sigma, UK) for 30 minutes at room temperature. Heat mediated antigen retrieval was performed using a sodium citrate buffer (pH6). For whole mount immunostaining of intestinal organoids, cells were fixed with 4% PFA at room temperature for 20 minutes. Primary antibodies were diluted in 1% BSA/PBS/0.01% Triton X-100 and applied overnight at 4°C. Samples were incubated with Alexa Fluor secondary antibodies (Invitrogen) for 45 min at room temperature, washed and mounted with ProLongTM Diamond Antifade Mountant with DAPI (ThermoFisher). EdU staining with the Click-

iT EdU Alexa Fluor 568 Imaging kit (Life Technologies) followed the manufacturer's protocol. DNA was stained with DAPI (Molecular Probes). Images were acquired using a Leica SP5 confocal microscope. For immunohistochemistry, antigen retrieval was performed using a sodium citrate buffer. Slides were permeabilized using a 0.2% Triton X100 (Sigma, UK) for 30 minutes at room temperature, and blocked with 5% bovine serum albumin (BSA) for 30 minutes. Primary antibodies were detected using peroxidase conjugated secondary antibodies using standard protocols as described previously. Image analysis and capture was performed using a Leica stereomicroscope or an inverted Nikon microscope. All antibodies used are listed in Appendix 3. Images were processed using ImageJ and Adobe Photoshop. Quantifications were performed on raw images however for presentational clarity, adjustments of brightness and contrast were applied equally to all panels of a given figure.

2.9 Scaffold Fabrication

The detergent-enzymatic treatment (DET) for decellularization, previously established on rat small bowel[230], was adapted for porcine[258] and human intestine samples. One cycle of DET consisted of the following steps: (i) 24 hours of deionised water at 4°C; (ii) 4 hours of 4% sodium deoxycholate (Sigma) at room temperature; (iii) 1 hour of deionised water at room temperature; (iv) 3 hours of 2000kU DNase-1 (Sigma) in 1M NaCl (for human tissue) or 0.15M NaCl and 10mM CaCl (for piglet tissue) at room temperature. After harvesting piglet small intestine, the mesenteric artery, mesenteric vein and lumen were cannulated using a 29-gauge surgical cannula. The lumen of the intestine and the mesenteric artery were perfused with continuous fluid delivery of DET solutions using a Masterflex L/S variable speed roller pump at 3ml/min, for two cycles. Whole sections of human intestinal tissue collected from surgery were washed in cold PBS containing 5% penicillin/streptomycin to remove luminal contents, before starting decellularization by immersion in DET solutions and gentle agitation on a roller. For human scaffolds, two to three cycles of DET were performed, depending on both age of the patient and weight of the tissue received from the theatre. Specifically, age of patients: <6month: 1-2 cycles; 6 months - 1 year: 2-3 cycles; >1year: 3 cycles; weight of tissue: <3g: 1-2 cycles;

3-20g: 2-3 cycles; >20g: 3 cycles. Gamma irradiation at a dose of 16000Gy for 15 hours was applied to sterilise the scaffolds and then preserved at 4°C, in PBS containing 1% penicillin/streptomycin prior to use in cell culture.

2.10 Mechanical Testing

Age-matched SI or colon scaffolds were cut into transverse strips measuring approximately 10mm wide by 15mm long and blotted dry using tissue. The thickness of each sample was measured using electronic callipers. Tape was added to the ends of each sample before they were loaded into the grips of an Instron Tensile Tester 5565, equipped with a 500N load (Instron, High Wycombe, UK). A pressure of 3 bar was applied by the grips to hold both ends of the scaffold in place. Extension was at 5mm/minute until failure across the middle of the scaffold. Any scaffolds that slipped before failure were excluded from analysis. BlueHill 3 software (Instron) was used to generate stress-strain curves and Young's modulus. Samples were measured in duplicate (with the exception of one colon sample since the dimensions of the tissue obtained was insufficient).

2.11 Electron Microscopy and Micro-CT imaging

For routine SEM imaging, decellularized human scaffold samples were fixed in 2% glutaraldehyde in 0.1 M phosphate buffer and kept at 4°C for 24 hours. Samples were then washed with 0.1 M phosphate buffer and cut into segments of approximately 1 cm in length and cryoprotected in 25% sucrose, 10% glycerol in 0.05 M PBS (pH 7.4) for 2 hours, then fast frozen in nitrogen slush and freeze fractured at -160°C. Samples were then returned to the cryoprotectant solution and allowed to thaw at room temperature. After washing in 0.1 M phosphate buffer (pH 7.4), the material was fixed in 1% OsO_4 in 0.1 M phosphate buffer (pH 7.4). After rinsing with distilled water, specimens were dehydrated in a graded ethanol-water series to 100% ethanol, critical point dried from CO_2 and mounted onto aluminium stubs using sticky carbon tabs. Samples were coated with a thin layer of Au/Pd using an ion beam coater (Gatan UK). Images were recorded using a Jeol 7401 field emission gun scanning electron microscope.

For routine TEM, MicroCT imaging, serial block face SEM imaging and montage SEM imaging, recellularised scaffold grafts were fixed overnight at room temperature in 10% neutralised buffered formalin (Sigma) followed by a second fixation step in 2.5% glutaraldehyde/4% paraformaldehyde in 0.1 M phosphate buffer (pH7.4). The sample was post-fixed in 2% reduced osmium (4% OSO4, 1.5% K3FE(CN)6) for 60 minutes on ice and then washed in ddH_20.

To check the orientation of cells on recellularised scaffolds, the sample was embedded in CYGELTM (BioStatus, Leicestershire, UK) in an Eppendorf tube and a microCT scan was performed at 4kV/3W, with no filter, 1601 projections and a pixel size of 7.3379 µm using an Xradia 510 Versa (Zeiss). The data was automatically reconstructed using Scout-and-ScanTM Control System Reconstructor software (Zeiss) and viewed in TXM3DViewer software (Zeiss). With the presence of cells confirmed, the sample was immersed in ice, the CYGELTM washed off the sample with ddH20 and the sample trimmed to approximately 1 mm^3 blocks. The trimmed blocks were then incubated in 1% aqueous thiocarbohydrazide at room temperature for 20 minutes then washed in ddH_20. The blocks were incubated in 2% aqueous osmium tetroxide for 30 minutes at room temperature and washed in ddH_20. This was followed by a further incubation in 1% aqueous uranyl acetate at 4°C overnight. The blocks were washed in ddH_20 and then incubated in Walton's lead aspartate for 30 minutes at 60°C before being dehydrated through a graded series of ethanol, infiltrated with Durcupan resin (Sigma-Aldrich) and polymerised for 48 hours at 60°C.

For routine TEM, 70 nm sections were cut on a UC6 ultramicrotome (Leica), picked up on formvar-coated slot grids and imaged in a Tecnai G2 Spirit Biotwin (ThermoFisher) with an Orius CCD camera (Gatan UK). For Serial Block Face SEM, Samples were trimmed to the region of interest, mounted on an aluminium pin (Leica Microsystems) and sputter coated with 2 nm of platinum. See Supplementary Table 6 for serial block face SEM imaging conditions. For SEM montage images, after the orientation of the cells within the block was determined by microCT, 200 nm sections were cut on a Powertome ultramicrotome (RMC) and picked up on ITO-coated coverslips. The coverslips were mounted on SEM

pin stubs (Agar Scientific) using a sticky carbon tab and sputter coated with 0.5 nm platinum. Sections were viewed in a Quanta FEG scanning electron microscope (ThermoFisher) using a backscattered electron (BSE) and large montage images acquired using MAPS 1.1 software (ThermoFisher). See Supplementary Table 7 for SEM montage imaging conditions. The montaged image in figure 5.5 was generated by stitching together individual images using TrakEM2, a plug-in of the FIJI framework[259]. The montaged images in figure 6.5 were generated by stitching together individual images using MAPS 1.1 software (ThermoFisher).

2.12 Raman Spectroscopy

Raman imaging was conducted using a Renishaw RA816 Biological Analyser coupled to a 785 nm laser excitation source that is reshaped using cylindrical lenses to produce a line illumination (Renishaw plc, Wotton-under-edge, UK). A total laser intensity of approximately 158mW was focused onto the sample through a 50×/NA 0.8 objective. A 1500 lines/mm grating was used to disperse the laser light providing a spectral range of 0 to 2100 cm^{-1} in the low wavenumber range. The RA816 series undergoes a fully automated calibration and optimization sequence to ensure optimal performance, including calibration to the 520.5 cm^{-1} silicon peak. Raman imaging was conducted on colonic and small intestine sections previously embedded in paraffin wax and cut at 8 µm. Sections were mounted onto stainless steel slides, deparaffinised in xylene and rehydrated in graded alcohol and distilled water prior to Raman analysis. A total of thirty single point spectra were acquired from each histological region of both the large and small intestine (mucosa, submucosa and muscularis propria) using a 15 seconds integration time. Large Raman maps were acquired using the Renishaw StreamLine™ mode using a 4.4 µm step size and 1.1 seconds integration time per pixel. A total of 8,544 spectra were acquired across the colon map and 22,825 spectra across the small intestine map. Prior to any analysis all spectra were pre-processed to remove all non-chemical effects of the data acquisition process. All spectra were truncated between 400 - 1800 cm^{-1} which encompasses the fingerprint region where the majority of all biological signal lies. Cosmic ray removal was conducted using the width of feature and nearest neighbour methods in Renishaw's WiRE 5 software. Spectra

were then imported into MATLAB R2017a (MathWorks, Natick, MA, USA) where baseline correction to a third order polynomial was conducted using the modified polyfit method37. Spectra were vector normalised and then analysed in both WiRE 5 and MATLAB R2017a.

Point spectra obtained from each distinct histological site in the colon and small intestine (mucosa, submucosa and muscularis propria) before and after decellularization were averaged and plotted on the same axis. The most obvious differences pre- and post-decellularization were highlighted. Principal component analysis (PCA) was then carried out to ascertain whether the biochemical difference between each distinct intestinal layer post-decellularization could be observed. This is an unsupervised multivariate analysis technique that allows an effective reduction in the dimensionality of the spectral dataset and hence facilitates the identification of combinations of highly correlated variables that best describe the variance in the data. Both of these procedures were carried out in MATLAB R2017a. The large high spatial resolution Raman maps were analysed in WiRE 5 (Renishaw plc, Wotton-under-Edge, UK) using unsupervised Multivariate Curve Resolution - Alternating Least Squares (MCR-ALS) approach for initial exploratory analysis to determine the global composition of each specimen. Using the reconstructed component curves, it was possible to identify some of the components abundant within each histological layer. Direct Classical Least Squares Component analysis was then used to acquire component images of a number of known biomolecules using previously acquired reference spectra. This enabled the mapping of the spatial distribution of known biomolecules within the full thickness of the intestinal wall.

2.13 Mass Spectrometry

Four biological replicates of both decellularized colon and SI ECM scaffolds were used for mass spectrometry analysis. Samples were prepared for analysis as previously reported[260]. Briefly, 1mg of lyophilised decellularized tissue was solubilised in 8M urea containing 10mM dithiothreitol. Iodoacetamide was added to a final concentration of 55mM and incubated for 30 minutes at room temperature protected from light. Proteins were treated with PNGaseF (25,000 units/mg) overnight. An initial protein digest using Lys-C (10 µg/mg for 4 hours) was followed up with two successive tryptic

digests (20 µg/mg overnight; 10 µg/mg for 4 hours). All enzyme reactions were performed at 37°C. Four biological replicates each of colon and intestine scaffolds were processed. Peptide material was cleaned up using C18 Sep-Pak columns (Waters 50 mg sorbent, WAT054955). Eluates were dried in a speedvac concentrator. Dried peptides were solubilised in 0.1 % trifluoroacetic acid (TFA) to a concentration of approx. 5 µg/µl, then diluted to 0.25 µg/µl in a glass auto-sampler vial immediately prior to analysis. Each of the eight samples were analysed in technical triplicate (approx. 1 µg per injection) using a ThermoFisher Scientific QExactive mass spectrometer coupled to an UltiMate 3000 HPLC system for on-line liquid chromatographic separation. Each sample was initially loaded onto a C18 trap column (ThermoFisher Scientific Acclaim PepMap 100; 5 mm length, 300 µm inner diameter) then transferred onto a C18 reversed phase column (ThermoFisher Scientific Acclaim PepMap 100; 50 cm length, 75 µm inner diameter). Peptides were eluted at a flow rate of 250nL/min with a stepped gradient of 5-25% buffer B (80% acetonitrile, 0.1% formic acid, 5% DMSO) for 60 minutes followed by 25-40% for 20 minutes. Higher energy Collisional Dissociation (HCD) was used for MS/MS peptide fragmentation. Singly-charged and unknown charge state precursor ions were not analysed. Full MS spectra were acquired in the orbitrap (m/z 300–1800; resolution 70k; AGC target value 1E6) with the MS/MS spectra of the ten most abundant precursors from the preceding MS survey scan then acquired (resolution 17.5k, AGC target value 1E5; normalised collision energy 28 eV; minimum AGC target 1E2). Selected precursors were dynamically-excluded for 15 s.

Raw data files were processed using MaxQuant software (version 1.6.0.13) for protein identification and quantification using intensity based absolute quantification (iBAQ). iBAQ values were calculated for colon and SI by combining technical and biological replicates. A SwissProt Homo sapiens protein database (downloaded July 2017 containing 26,389 reviewed sequences) was searched with a fixed carbamidomethylation of cysteine modification and variable oxidation of methionine and protein acetylation (N-term) modifications. Protein and peptide false discovery rates were set at 1 %. The MaxQuant protein groups output file was imported into Perseus software (version 1.4.0.2) for further statistical analysis and data visualisation. Common contaminant proteins and reverse sequences were

removed. Intensity values were log2 transformed and Gene Ontology cellular compartment (GOCC) descriptions were added by Perseus. Protein detection was called when it was detected in at least 3 out of the 4 biological replicates of either colon or SI scaffolds. This resulted in 377 total proteins detected in these intestinal scaffolds (Appendix 4 and 5).

2.14 Scaffold Seeding Protocol

Sterilised sections of acellular intestinal scaffolds were immobilised in custom made mini platforms and placed at the bottom of 12 well tissue culture plates. When seeding scaffolds were intended for transplantation, human jejunal fibroblasts were trypsinised and resuspended in DMEM before seeding by multiple microinjections via 26g cannulae (Terumo SKU:SR+DU2619PX) into the lateral walls of the scaffolds, at a density of $1x10^6$ cells/cm^2 and cultured in static conditions for 3 days. Human jejunal organoids were trypsinised and seeded onto the mucosal surface of the scaffolds at a density of $1x10^6$ cells/cm^2. The cells were allowed to engraft for a period of 30 minutes at 37°C, before covering the whole scaffold with basal human intestinal organoid culture media. The scaffolds were maintained for another 4 days in static culture conditions, before transferring the scaffolds into perfusion plates (Amsbio #AMS.AVP-KIT-5) and connecting this to a bioreactor circuit. For in vitro functional and histology analyses, graft cultures were maintained for 14 days in dynamic culture conditions, with media circulating at a rate of 3ml/min. For *in vivo* transplantation, dynamic culture times were reduced to 7 days. For vascularisation experiments, HUVECs were injected at a density of $1x10^6$ cells/cm^2 into the lateral walls of the grafts submucosally, 24 hours before transplantation into mice. Piglet scaffold seedings were seeding in a similar manner, without pre-injections of fibroblasts or HUVECs due to the lack of accuracy of injection in the thin scaffold walls.

2.15 Perfusion Bioreactor

The bioreactor circuit consisted of a media reservoir (custom made by Chem Glassware UK Manufacturers Ltd, London) with a 0.22µm air filter, inlet and outlet tubing (Cole Parmer cat.no. 224-2081), a peristaltic pump (Cole Parmer cat.no. 224-1505) and 3-way stopcocks (Becton Dickinson UK Ltd cat.no. 394601) for media sampling at both inlet and outlet points of the circuit.

2.16 Citrulline Quantification Assay

Graft culture supernatants were collected and citrulline levels quantified by spectrophotometry according to methods reported previously[261]. Briefly, 20µl of each test sample was added to 20µl of water and 10µl of working urease solution, then incubated at 37°C for 30 minutes. 150µl of chromogenic reagent was then added to the solution and incubated for a further 60minutes at 100°C to allow colour development. Absorbance was read at 520nm in a 96 well microtitre plate using a Tecan microplate reader (Infinite® M1000 PRO). Concentration was determined by comparison to a citrulline standard curve.

2.17 Disaccharidase Functional Assay

Grafts in dynamic culture were transferred from the bioreactor circuit into 6 well plates. The scaffolds were washed in PBS three times then incubated with a solution of 56mM sucrose in PBS (or PBS alone in control wells) for 60 minutes. Aliquots of the solution were then sampled for glucose detection using the AmplexTM Red glucose/glucose oxidase assay kit (ThermoFisher cat.no. A22189) according to manufacturer's protocol. Briefly, 50µl of the reaction working solution was added to 50µl of the test samples in a 96 well black flat bottom microtitre plate in triplicates, and incubated in the dark for 30 minutes at room temperature. The fluorescence (excitation 535nm, emission 590nm) was measured using a Tecan microplate reader (Infinite® M1000 PRO). Concentration was determined by comparison to a glucose standard curve.

2.18 β-Ala-Lys-AMCA Peptide Uptake Assay

Grafts in culture (or unseeded scaffolds as controls) were transferred from the bioreactor circuit into a 6 well plate and rinsed several times with PBS. They were then incubated with fresh human organoid culture media containing 25µM β-Ala-Lys-AMCA for 2 hours at 37°C. After incubation the media was removed and the graft was rinsed in cold PBS three times. The grafts (or unseeded scaffolds as controls) were fixed in 4% paraformaldehyde for 30 minutes at room temperature. Whole mount immunostaining was performed as described above, with Alexa Fluor 568 phalloidin staining to mark

cellular boundaries. The samples were then imaged using a Leica SP5 inverted confocal microscope. The fluorescence signal of β-Ala-Lys-AMCA was acquired using the UV laser.

2.19 Dipeptidyl peptidase IV assay

Grafts in culture (or unseeded controls) were removed from culture and washed in PBS three times. Gly-Pro p-nitroanilide hydrochloride (Sigma cat.no. G0513) was dissolved in PBS at a concentration of 1.5mM and added to the grafts for 1 hour at 37°C before supernatant was collected. Optical density (415nm) was measured in duplicate and concentration determined by comparison to a 4-nitroaniline (Sigma cat.no. 185310) standard curve.

2.20 FITC-Dextran barrier function assay

Piglet scaffolds were mounted into CellCrowns (Sigma cat.no. Z742381) (instead of onto custom made mini-platforms) before seeding with organoids and culture as described above. Grafts in culture (or unseeded controls) were removed from culture and washed in PBS three times before 100µl of 500µg/ml FITC-Dextran (Sigma cat.no. 46944-100MG-F) in media was added to the apical chamber of the CellCrown. 900µl of media was added to the basal chamber. Samples were incubated for 2 hours at 37°C. Media was then collected from the basal chamber into individual wells of a flat-bottomed, black-walled 96-well plate in duplicate. Presence of FITC-Dextran was determined by measuring fluorescence (excitation 490nm, emission 520nm). Percentage permeability of cellular grafts was calculated by comparison to unseeded scaffolds.

2.21 Lentiviral Preparation and Human Organoid Labelling

The lentiviral vector pHIV-LUC-ZsGreen (Addgene Inc. MA, USA, Plasmid #39196, kind gift from Dr Bryan Welm, Department of Surgery, University of Utah) was used to generate a lentivirus containing both ZsGreen fluorescent protein and firefly luciferase from an EF1-alpha promoter. Human jejunal organoids were labelled by lentiviral transduction as previously reported[262]. Briefly, LUC-ZsGreen lentivirus was produced by co-transfecting 293T cells with the above plasmid along with packaging vectors PAX2 and VSV-G envelope plasmid (kind gifts from Dr Hans Clevers). Transfection was performed according to manufacturer's instructions for 8 hours at 37°C. The medium (Opti-MEM®)

was exchanged for virus collection. After 24 hours, the virus-containing medium was purified by centrifugation at 2500 rpm (4 °C) and filtered through a 0.45µm membrane and ¼ volume of PEG-itTM was added to the filtered supernatant before ultracentrifugation at 2300 x g for 30 mins at 4°C (SW28 rotor, Optima LE80K Ultracentrifuge, Beckham). The viral pellet was resuspended in 1ml of pre-cooled Opti-MEM® (Gibco), aliquoted and stored at −80 °C. Human organoids were dissociated into single cells and cultured in the presence of 250µl 2x organoid culture media and 250µl viral particles and 2.5µl of TransDux^{TM}. Transduction efficacy was determined measured as the proportion of cells expressing the fluorescent protein ZsGreen 72 h after transduction.

2.22 *In Vivo* Transplantation Studies

NSG mice were anaesthetized with a 2-5% isoflorane: oxygen gas mix for induction and maintenance. The dorsum of each animal was shaved and the skin cleansed with 70% ethanol and povidone-iodine solution. For kidney capsule transplantation (n=3), each seeded graft (cultured as 1cm^2 patches) was carefully cut in half and gently folded to maintain the epithelial surface internally, before immediately inserting the graft under the capsule of the kidney. For subcutaneous transplantation (n=12), closed blunt scissors were used to create subcutaneous pockets bilaterally in the dorsum of each mice and one folded graft segment was inserted in each pocket. Subcutaneous Teduglutide or vehicle (PBS) was administered at a dose of 0.2 mg/kg/daily after implantation. The mice were sacrificed at 7 or 14 days for analysis. 2 hours prior to culling, each mouse was administered a dose of EdU (3ul/g of a stock solution of 10mg/ml).

2.23 Bioluminescence Imaging (BLI)

BLI was performed using an IVIS Spectrum in vivo imaging system (PerkinElmer, Waltham, MA, USA) and Living Image 4.3.1 software (PerkinElmer). Mice were injected intraperitoneal with 150 mg/kg D-luciferin (PerkinElmer) twenty minutes prior to imaging. All images were taken at field of view C or D, with automatic exposure time, pixel binning set to 8, f-stop 1 and open emission filter. This generated pseudo-coloured scaled images overlaid on grey scale photographs, providing 2-dimensional

localization of the source of light emission. All images were analysed using Living Image 4.3.1 software (PerkinElmer). Regions of interest (ROI) were drawn manually and the light emission was quantified in photons s−1. ROI shapes were kept constant between images within each experiment.

2.24 Three-Dimension Volume Rendering of Transplantation Data

Serial sections were cut of the paraffin embedded sample. Odd numbered slides were stained with H&E while even numbered slides were kept unstained for further immunostaining analyses. Odd numbered H&E slides were then serially scanned (Olympus VS120 slide scanner) and the region of interest was aligned manually using Amira Software (ThermoFisher). Using the aligned slices, the kidney, scaffold, epithelial ring and lumen were segmented manually and saved as four separate label fields before generating 3D surfaces. A movie was created using Amira Animation Director.

2.25 Quantification of *In Vivo* data - Lumens and Vessels

Odd numbered H&E slides were scanned and images opened in QuPath software (University of Edinburgh)[263]. Each slide was checked for presence of epithelial lumen and blood vessels and this was quantified as a percentage across all sections.

2.26 Statistical Analyses

Statistical analysis was conducted on data from three or more biologically independent experimental or biological replicates wherever possible, as stated in the figure legends. Given the small sample sizes, the Shapiro-Wilk test of normality was performed. This indicated data distribution to be normal for the data presented in figures 3.2; 3.3; 4.5. Data in figures 6.5 and 6.6 did not pass the Shapiro-Wilk test of normality. Results are expressed as the mean ± s.e.m. Statistical significance was analyzed using unpaired Student's t tests (two sided) or Mann Whitney U tests, for comparisons between two different groups. For analysis among more than two groups, statistical significance was analyzed using one-way ANOVA with Dunnett's or Tukey's post hoc multiple-comparisons test. *P < 0.05, **P < 0.01, ***P < 0.001, ****P < 0.0001 were considered significant. All attempts at replication were successful. Statistical analysis was carried out using Prism 8 (GraphPad Software).

3. **Results I** - Expansion of Patient Derived Intestinal Cells

3.1 Introduction

The physiological characteristics of the intestinal epithelium varies greatly along the cephalo-caudal axis of the GI tract[50]. The SI is divided into three parts, based on anatomical, histological and functional specialisations: duodenum, jejunum and ileum. The duodenum receives gastric contents, bile, and digestive enzymes from the pancreas. Here, absorption of iron, calcium, and water-soluble vitamins takes place[50]. The jejunum has the largest surface area of the small intestine whereby the majority of dietary lipids, carbohydrates and proteins are digested and absorbed[50]. The ileum absorbs residual nutrients and mediates transport of bile acids and vitamin B12[50,264]. Therefore, biological geography within the longitudinal axis of the SI is an important factor in determining the functional identity of epithelial cells once transplanted onto scaffolds. A previous study confirmed that intestinal region specific gene expressions are intrinsically programmed and are independent of extracellular and stromal cell signals[265]. This indicates that in order to engineer a mucosal graft with jejunal function, organoids must be derived from biopsies of the jejunum, which is more challenging to access endoscopically and less frequently operated on surgically. Engineering a graft with jejunal function was prioritised in this thesis, as restoration of jejunal function is more likely to be associated with clinical improvements in nutritional autonomy and reducing PN requirements. This is because 90% of nutrient absorption and digestion occurs in the proximal 100-150cm of jejunum[266,267].

Considering the significant ethical and translational hindrances to the use of embryonic and induced pluripotent cells in clinical trials, discussed in the introduction chapter, an early decision was taken to focus on the use of primary ISCs resident in the human gut for this thesis. The main advantage of primary sources of ISCs are their high expandability, lineage restriction and genetic stability, when cultured using organoid methods. Therefore, this source is currently the safest option for use in tissue engineering of the gut. However, one potential disadvantage of the primary human intestinal organoid

technology is that it is a purely epithelial culture system[202]. This means that, unlike iPSC or embryonic derived intestinal cultures, only epithelial cell populations are readily expanded *in vitro* for each patient from endoscopic biopsies. Although the epithelium is the major functional component of the intestinal mucosa, non-epithelial cells such as fibroblasts, neural cells, muscle cells and endothelial cells have important niche roles. Isolating these important non-epithelial cell populations remains an important challenge in the effort to generate autologously sourced engineered grafts.

Finally, intestinal biopsies for the study were specifically sought from children with IF. This task may be complicated by the underlying cause of IF in the patient. For example, it is well recognised that chronic inflammation and tissue damage eventually depletes the regenerative capacity of many tissues[268]. Therefore, isolating and expanding intestinal epithelial stem cells from patients with conditions such as IBD may prove more challenging. In addition, the efficiency of forming primary intestinal organoids from patients with IF, who have limited functional native gut *in situ*, has not been demonstrated to date. Therefore, in order to apply this biotechnology to patients with IF specifically, it is necessary to optimise the organoid culture conditions for this specific patient group. This points the focus towards expanding the intestinal cells from each patient rapidly *in vitro,* whilst preserving multilineage differentiation potential. This objective is guided by a previous study which demonstrated that the use of two small molecules, CHIR99021 and valproic acid, can increase to colony-forming efficiency of intestinal organoids by about 100 fold[269].

3.2 Isolation and expansion of patient derived intestinal organoids from endoscopic biopsies.

To achieve maximal clinical relevance, I initiated a restriction of using a maximum of two endoscopic intestinal epithelial biopsies that were about 2mm in size, from each paediatric patient involved in the study (Fig. 3.1 a). In total, patient derived organoids (PDOs) were established from 12 children who had IF or are at risk of developing IF due to co-morbidities or complex surgical histories (Appendix 1). On average, three to five organoids were established by week four in culture following isolation. This was further expanded to over ten million cells by week eight of culture, passaging at a

ratio of roughly 1:8 to 1:10, depending on the density of organoids per well (Fig. 3.1 a-b). Once established in culture (i.e. after the 4-week point), the expansion efficiency was similar in all three regions (duodenum, jejunum or ileum) of the small intestine (Fig. 3.1 c), and did not vary across different clinical backgrounds. However, I noted that it took more time in culture to establish organoids derived from Crohn's disease materials with (Patients 6 and 7 - appendix 1). However, once the organoids were established, the proliferation and differentiation potential of these organoids were indistinguishable from other PDOs, suggesting that in our culture conditions, the clinical background of these patients did not affect PDO production.

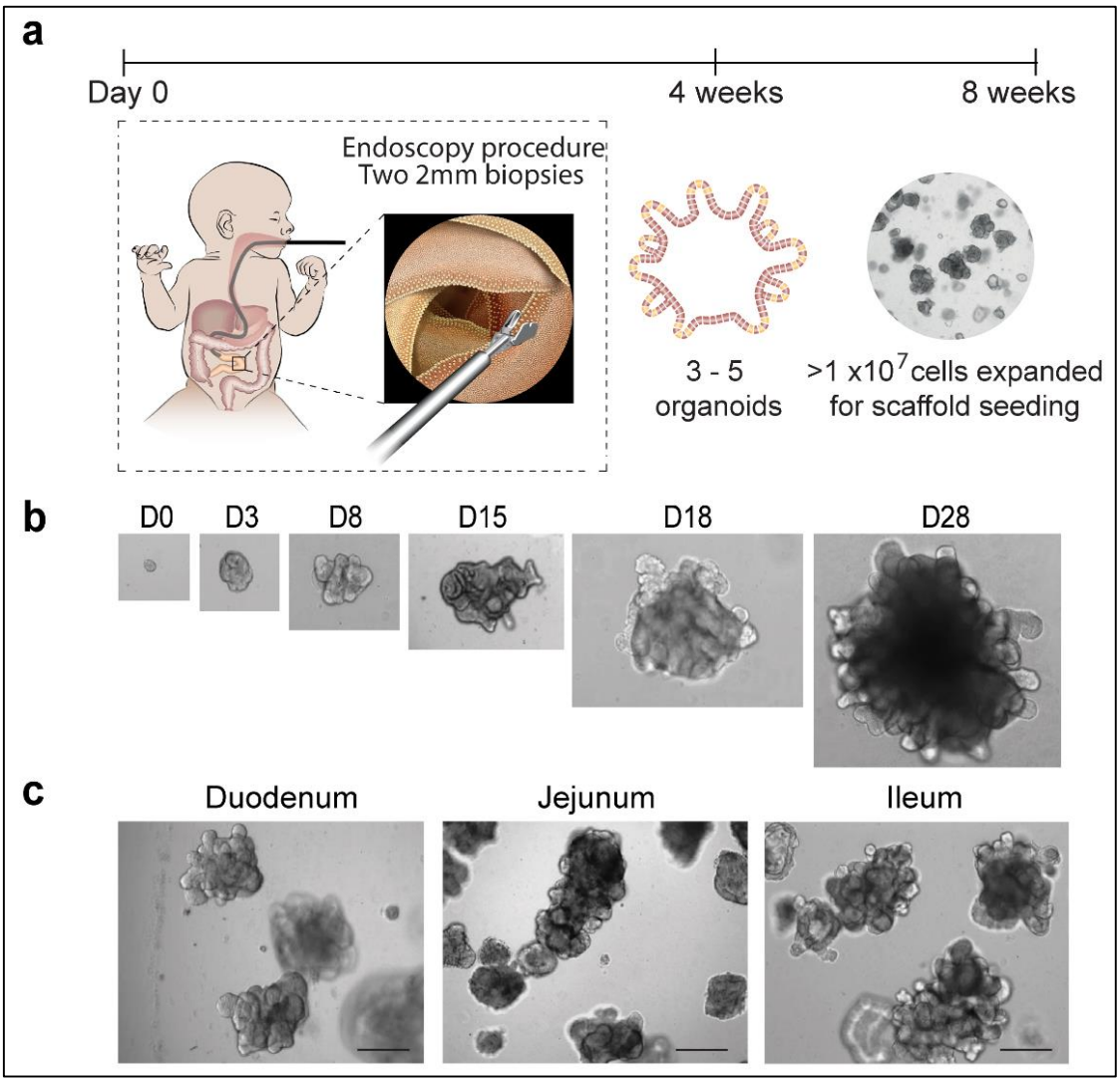

Figure 3.1 - Isolation and expansion of patient derived organoids from endoscopic biopsies: (a) Schematic overview demonstrating the expansion timeline after harvesting intestinal crypts endoscopically from paediatric patients. Each patient biopsy sample yields ~3-5 organoids by week 4

and over 10 million cells by week 8 after successive passaging as indicated by a representative phase contrast image of organoids in culture at week 8. (b) Phase contrast images of human intestinal organoids cultured in BME® [patient 6] established from isolation at the indicated time points. Original magnifications: X20 (days 0); X10 (days 3, 8); X5 (days 15, 18, 28). (c) Representation phase contrast images of first passage expansion cultures of duodenal [patient 9] (left), jejunal [patient 2] (middle) and ileal [patient 3] organoids (right), all cultured in BME®. Scale bars represent 200μm. All images (b, c) are representative of 3 experiments.

3.3 Intestinal cell location specificity is retained following extended passaging *in vitro.*

Among the 12 PDOs established, there were 3 duodenal, 3 jejunal and 6 ileal organoids (Appendix 1). Previously study showed that the SI exhibits regionality in nutrient digestive and absorptive function[265]. Quantitative reverse transcription-PCR (qRT-PCR) confirmed that PDOs generated from epithelial biopsies expressed region-specific functional markers appropriately. Duodenal organoids expressed the apical brush border enzyme cytochrome b reductase 1 (CYBRD1) and the iron transporter solute carrier family 40 member 1 (SLC40A1); jejunal organoids express the brush border digestive enzymes sucrase isomaltase (SI) and lactase (LCT); and ileal organoids expressed the apical bile acid transporter (SLC10A2) and the basolateral organic solute transporter (OSTB) (Fig. 3.2 a). Next, I focussed on the expansion of PDOs derived from the jejunum of 3 patients [patients 2, 7 and 8 - appendix 1], since 90% of digestion and absorption occurs in the proximal 100–150 cm of the jejunum. To reach cell numbers in the order of >10 million cells for each patient, organoids were passaged rapidly in culture. The expression of jejunal specific markers SI and LCT were verified after significant passaging time (P > 25), showing that the intrinsically programmed regional identity of intestinal cells is maintained despite long-term culture in vitro (Fig. 3.2 b).

3.4 Differentiation potential of PDOs following extensive expansion

In order to expand the organoids in the shortest amount of time possible, PDOs were cultured in the previously published human intestinal organoid media[205], with the addition of the GSK3β inhibitor (CHIR99021) to boost Wnt signalling and promote proliferation[269]. qRT-PCR analysis showed that stem cell markers (OLFM4 (olfactomedin 4) and LGR5 (leucine rich repeat-containing G-protein-

coupled receptor 5)) and Paneth cell (LYZ (lysozyme)) genes were significantly upregulated in these conditions (Fig. 3.3 a). This was confirmed at protein level, by expression of EdU (ethynyl-2'-deoxyuridine) and KI67, indicating proliferation, and crypt compartment markers LGR5, SOX9 and LYZ

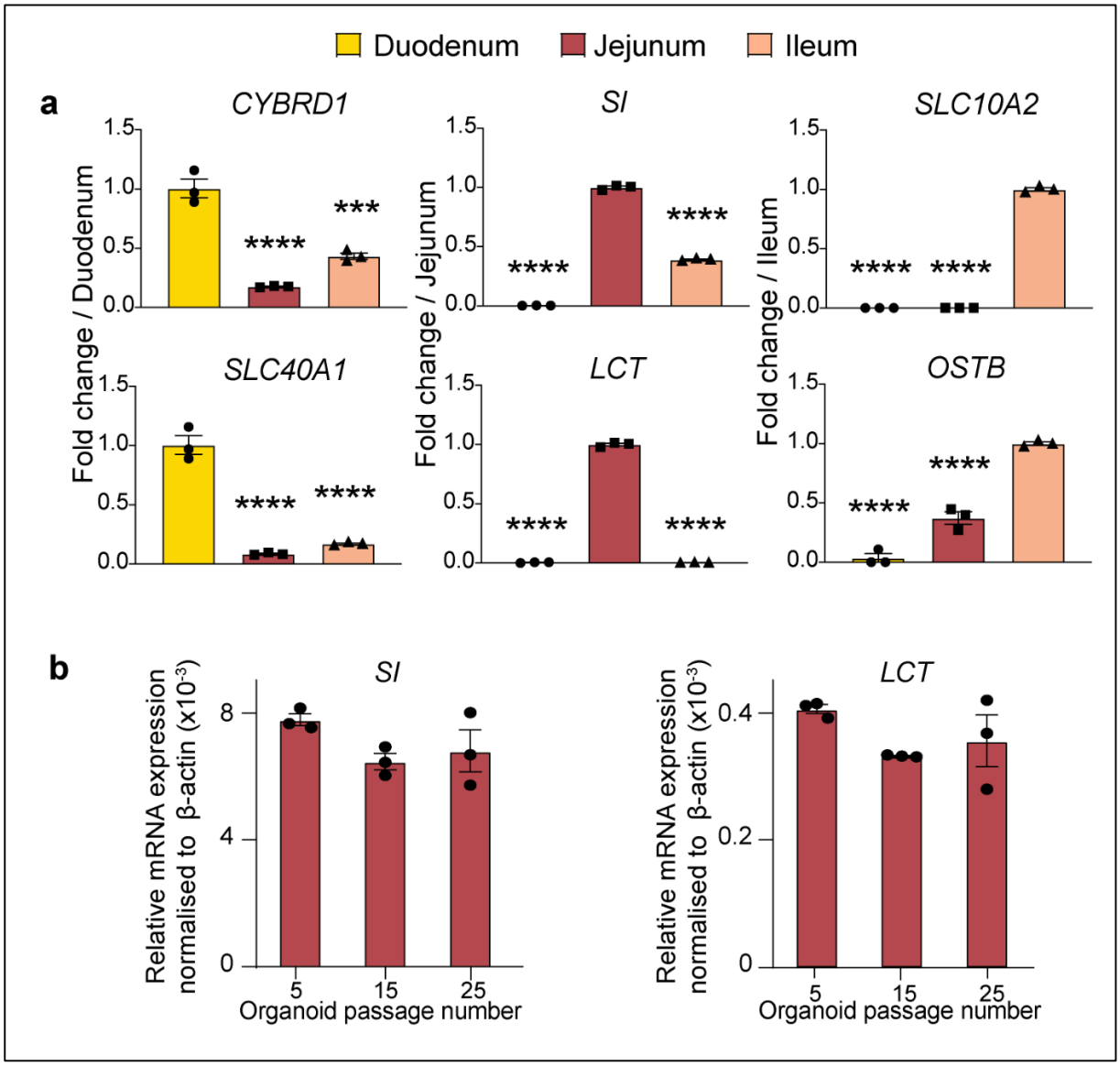

Figure 3.2 - Intestinal region specific characterisation of organoids in culture: (a) Quantitative RT-qPCR analysis of human duodenal [patient 10], jejunal [patient 2] and ileal [patient 14] organoids for functional duodenal markers (CYBRD1; SLC40A1), jejunal markers (SI; LCT) and ileal markers (SLC10A2; OSTB). (b) Quantitative RT-qPCR analysis of human jejunal organoids [patient 2, 7, 8] at passages 5, 15 and 25 for jejunal specific markers SI and LCT. Quantitative data shown in represents mean ± s.e.m. of n = 3 experimental replicates (a) or of n = 3 biologically distinct replicates (b). Differences were analyzed by one-way ANOVA with Dunnett's multiple comparisons test. *p<0.05, **p<0.01, ***p<0.001, ****p<0.0001 were considered significant; n.s., not significant.

Data acquired with Isobel Massie and Nikos Angelis (Crick)

(Fig. 3.3 b, c (upper panel)). Next, the differentiation capacity of these jejunal PDOs were tested after prolonged expansion culture conditions. This was done by the addition of the gamma-secretase inhibitor (DAPT) to inhibit Notch signalling. qRT-PCR analysis showed that differentiation genes (MUC2 (mucin 2), ALPI (alkaline phophatase) and CHGA (chromogranin A)) were upregulated upon DAPT-treatment, alongside a loss of stem and Paneth cell markers (Fig. 3.3 a). This was confirmed at protein level by immunostaining for differentiation markers UEA-1, ALPI and CHGA (Fig. 3.3 c (lower panel)).

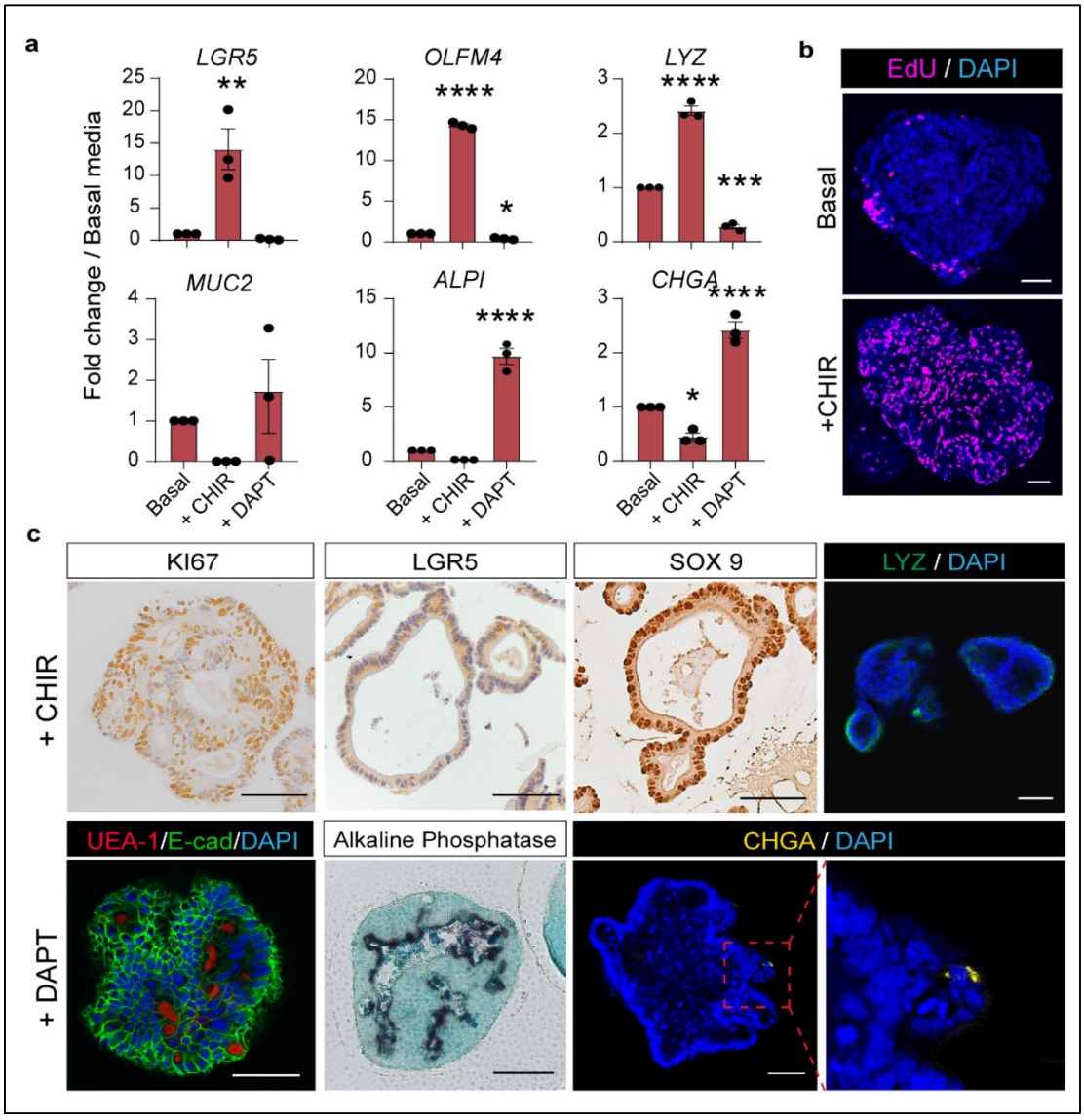

Figure 3.3 - Differentiation potential of patient derived jejunal organoids: (a) Quantitative RT-qPCR analysis of human jejunal organoids [patients 2, 7, 8] cultured in basal media culture conditions as indicated in the method, treated with the GSK3β inhibitor CHIR99021 (CHIR), or the Notch inhibitor DAPT. (b), Representative stainings for EdU and DAPI of human jejunal organoids [patient 2] in basal culture conditions and expansion conditions (+CHIR). Scale bars represent 30µm. (c) Representative immunostaining of human jejunal organoids [patient 2] cultured in expansion conditions (+CHIR) or

differentiation conditions (+DAPT) using the indicated antibodies to mark proliferating cells (Ki67), stem cells (LGR5 and SOX9), Paneth cells (LYZ), goblet cells (UEA-1), epithelial cells (E-cad), enterocytes (alkaline phosphatase) and enteroendocrine cells (CHGA). Scale bars represent 100µm. Images are representative of 2 (b) or 3 (c) experiments. Quantitative data shown in (a) represents mean ± s.e.m. of n = 3 biologically distinct replicates. Differences were analyzed by one-way ANOVA with Tukey's multiple comparisons. *p<0.05, **p<0.01, ***p<0.001, ****p<0.0001 were considered significant; n.s., not significant.

3.5 Isolation and expansion of human intestinal fibroblasts

I further generated primary human intestinal fibroblasts isolated from the same intestinal tissues used to derive organoids or SI scaffolds (Appendix 1). Primary human intestinal fibroblasts could be cultured and expanded for up to 10 passages while retaining strong expression of typical stromal matrix markers fibronectin (F-NEC), vimentin, fibroblast surface protein marker-1 (FSP-1), laminin α5 (LAMA5) and with scattered weaker co-expression of alpha-smooth muscle actin (αSMA) (Fig. 3.4). This indicates a mixed population of intestinal fibroblasts and myofibroblasts, which are both essential stromal niche for the survival and maintenance of human ISCs. These cells were used for seedings of jejunal grafts intended for *in vivo* transplantation experiments, discussed further in chapters 5 and 6.

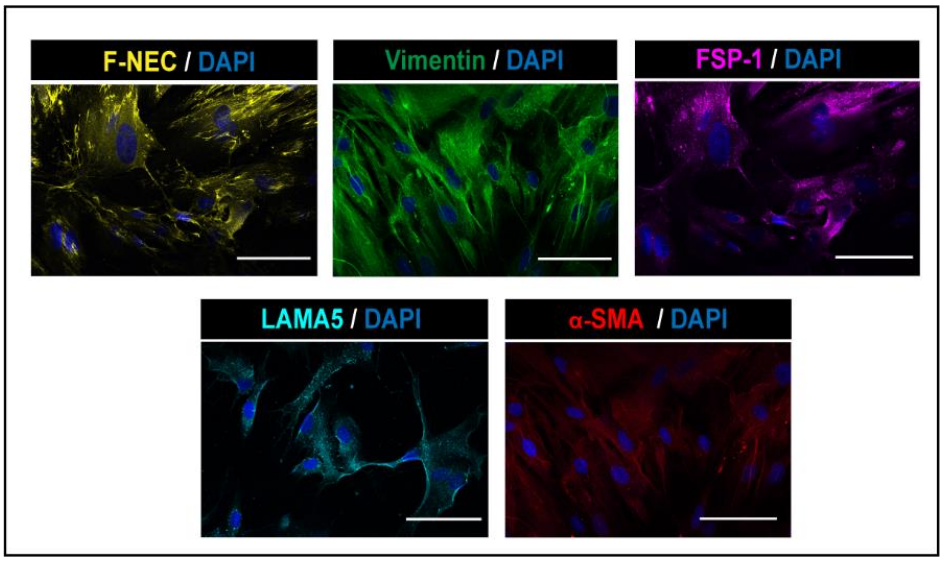

Figure 3.4 - Characterisation of human intestinal fibroblasts: Representative immunofluorescent images of primary human jejunal fibroblasts [patient 2] showing fibronectin (F-NEC, yellow), vimentin (green), fibroblasts surface protein marker-1 (FSP-1, magenta), laminin alpha 5 (LAMA5, cyan) and alpha-smooth muscle actin (α-SMA, red).

3.6 Discussion

All together, these results demonstrate that PDOs can be generated robustly children with IF, from as little as two 2mm sized epithelial biopsies. The organoids multiply rapidly *ex vivo* under expansion media (+CHIR) while maintaining their original intestinal regional identity and differentiation potential upon Notch inhibition (+DAPT). This data is in keeping with results from previously published studies using human and mouse intestinal organoids[265,269]. Using the same tissue samples, human SI fibroblasts could also be isolated and expanded from the IF patient group.

Clinically, the small bowel length in a term neonate measures just above 200cm and there is a correlation between those with ≥10% of their predicted small-bowel length and their ability to wean off parenteral nutrition (PN)[266]. Therefore, in order for these methods of intestinal organoid expansion to be relevant to the most severe patient cases (i.e. a baby who has lost their entire small intestine), the methods described would need to be scaled up to provide enough cells to engineer a 20cm length graft. This current work focuses on engineering $1cm^2$ sized grafts, for which I need $1x10^6$ intestinal epithelial cells. Consequently, in order to scale up to a tubular construct, since [Area = $2\pi rl$], assuming a neonatal small intestine luminal radius (r) of 1cm and length (l) of 20cm, the area to be repopulated is approximately $125cm^2$. Since $1x10^6$ cells are required to repopulate $1cm^2$ of scaffold, the number of cells required to repopulate a 20cm tubular neonatal scaffold will be 125 million.

Using methods outlined here, the conditions for robust epithelial cell expansion has been optimised whereby 10 million cells can be obtained by 8 weeks. Once the organoids are established at this point, they can quadruple every 7-9 days under expansion condition. Based on these parameters, I estimate that it would require around 10 weeks in total from a starting material of 2 endoscopic epithelial biopsies to achieve 125 million cells for reconstruction of a 20cm jejunal graft. Increasing the volume of starting biopsy material may further shorten the time required to expand enough number of cells for scaffold seeding. I therefore n conclude this timescale to be achievable when extrapolating to hypothetical clinical scenarios.

4. **Results II** - Fabrication and characterisation of decellularised human intestinal scaffolds

4.1 Introduction

The ECM acts as a support network and serves as functional scaffolding to cells, as well as providing key biological signals for cell proliferation and differentiation. Resident cells of the matrix secrete the structural and organ specific functional molecules that impact epithelial cell behaviour[143,238,258,270,271]. For these unique advantages, an early decision was taken to focus exclusively on using biological ECM human intestinal scaffolds generated by decellularisation methods in this thesis. From here on, the term "scaffold" refers to decellularized human or piglet ECM intestinal materials.

Previous work from the De Coppi lab at UCL described decellularization protocols to generate rodent or piglet small intestinal (SI) ECM scaffolds[230,258], named the "Detergent-Enzymatic Treatment" (DET). DET involves 3 steps: Firstly, the tissue is washed in deionised water, which results in cell lysis by osmotic shock. Next, the tissue is washed in a detergent solution of 4% sodium deoxycholate, to solubilise cell and nucleic membranes. In the final step, the tissue is washed in 2000kU DNase-I to catalyse the hydrolysis of deoxyribonucleotide chains. Other groups have also generated decellularised porcine and human intestinal matrices using different decellularisation protocols[193,227,249]. Results of cell seeding on decellularised scaffolds can be highly dependent on the method of decellularization. For example, a recent study fabricated human SI ECM decellularized scaffolds but did not include any characterisation data of the decellularized scaffolds in the publication. Furthermore, the human decellularized scaffolds were not used to demonstrate successful seedings or transplantation with these scaffolds[227]. Indeed, in the same study suboptimal results were achieved when seeding intestinal cells onto piglet ECM decellularized scaffolds over PGA/PLLA synthetic scaffolds for transplantation studies. This may indicate to problems with the decellularization technique, or possible residual detergents on the scaffolds post-decellularization.

Hence, decellularization of tissue is a precise skill that must ensure reproducibility of the scaffold product in order to generate the desired tissue engineered results.

In this chapter, I apply the DET protocol to optimise the decellularization of both human SI and colonic scaffolds acquired from paediatric patients undergoing intestinal resection surgeries (listed in Appendix 1). I proceed to fully characterise the structural and biophysical features of the scaffolds, using electron microscopy, Raman spectroscopy and mass spectrometry. Whilst electron microscopy is a standard tool used to assess scaffold microarchitecture in this field of study, Raman spectroscopy and mass spectrometry are less widely employed to characterise decellularized scaffold composition. Raman spectroscopy is a vibrational light scattering technique that provides a biochemical fingerprint of tissue composition. It is a valuable tool that enables the extraction of a wealth of quantitative biomolecular information regarding the specific biochemical conformation of proteins, carbohydrates, lipids and nucleic acids with submicrometer spatial resolution[272]. Combining Raman spectroscopy with mass spectrometry, provides valuable insight into the spatial distribution and global composition of decellularized scaffolds generated for tissue engineering.

4.2 Scaffold decellularisation and microarchitecture preservation

To increase the translational impact of this research, I fabricated decellularized scaffolds from native SI and colon tissue that was collected from paediatric patients undergoing intestinal resection (Appendix 1). Due to the nature of the surgeries, excess tissues is often collected without intact mesentery, thus cannot be decellularized via perfusion. Instead, I optimised the decellularisation of the native intestinal tissues using the DET protocol previously published[230]. The main adjustment of protocols was in performing the decellularization through a series of immersion and agitation in the 3 main steps, rather than by perfusion. The number of cycles required to achieve decellularization whilst maintaining crypt-villus architecture ranged from one to three cycles, depending on the age of the patient and the weight of tissue acquired. By age of patient: < 6 months required 1-2 cycles; 6 months to 1 year required 2-3 cycles; > 1 year required 3 cycles. By weight of tissue: < 3g required 1-2 cycles;

3-20g required 2-3 cycles; >20g required 3 cycles. Judgement on the number of cycles required was based on histological analysis by H&E and DAPI staining of the scaffold, rather than DNA quantification.

I first show that applying the DET protocol in this way resulted in full removal of cellular and nuclear material as revealed histologically by H&E and DAPI staining in the decellularized scaffolds (Fig 4.1a-b top and lower panel). Furthermore, the intestinal crypt-villus axes were well preserved (Fig. 4.1a-b middle panel). Immunofluorescent staining confirmed the presence of the key ECM protein collagen in both SI and colonic decellularized scaffolds (Fig. 4.1a-b lower panel). The ultrastructure of the ECM scaffolds was examined using scanning electron microscopy (SEM), showing remarkable preservation of the microarchitecture of mucosa, submucosa and muscularis layers. Importantly, intact crypt-villus axis of the SI scaffold and crypts of the colonic scaffold in the mucosal layer was clearly identified after decellularization (Fig. 4.1c), which offer ideal natural nanotopography for intestinal graft construction. Several patients were undergoing intestinal resections for IBD (Crohn's disease) strictures. When scaffolds were generated from these samples and examined with SEM, significant distortion was seen in all 3 layers of the intestine, for both SI and colon samples (Fig 4.2). Therefore, these decellularized scaffolds were excluded from further studies in tissue engineering grafts.

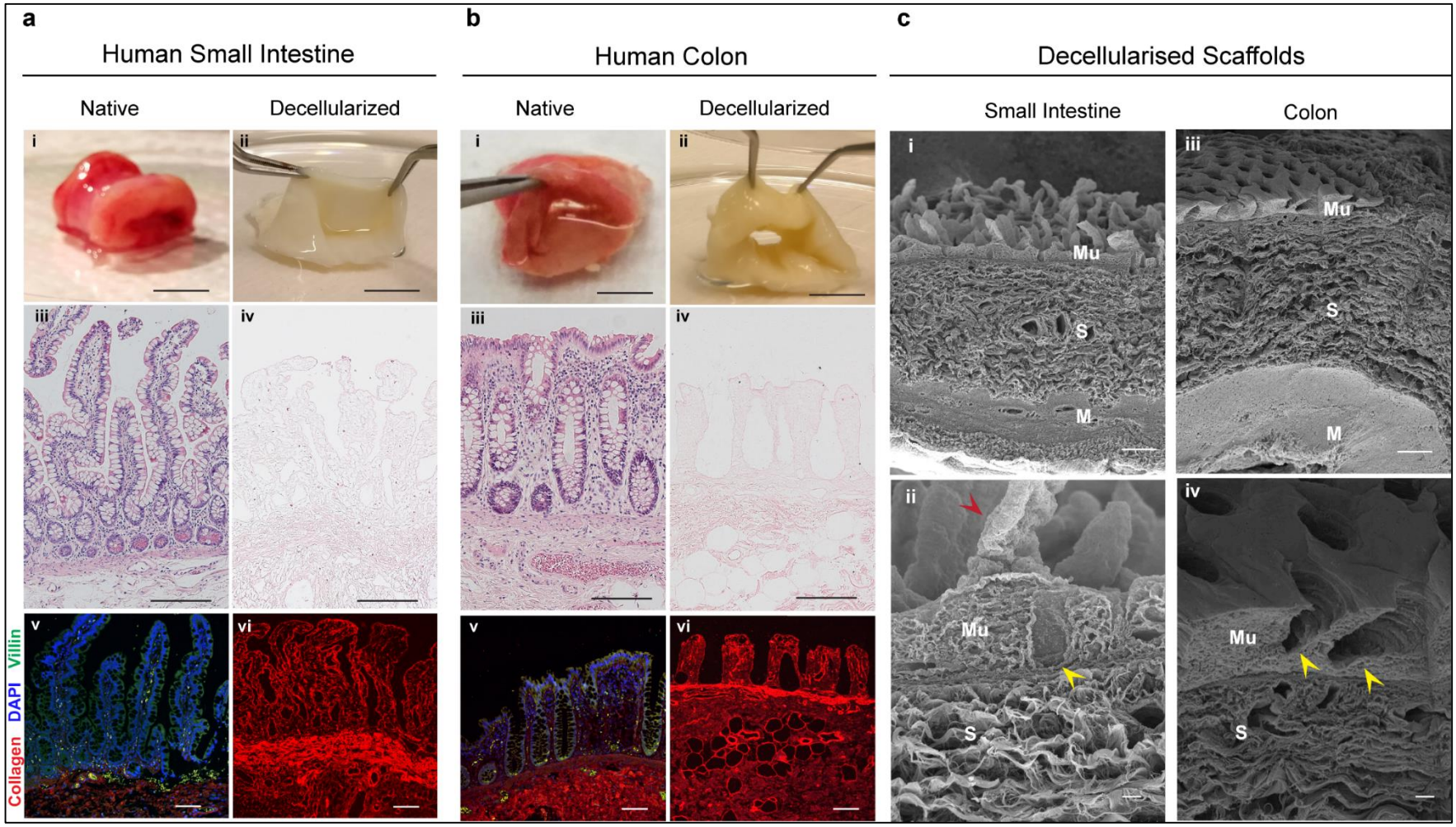

Figure 4.1 - Fabrication of human decellularised intestinal scaffolds: (a, b) Representative images of SI [patient 1] (**a**) and colon [patient 18] (**b**) samples before (native) and after decellularization. Top, macroscopic images; middle, H&E histological images; bottom, immunofluorescent staining using the indicated antibodies. Scale bars: top, 1cm; middle, 200µm; bottom, 100µm. (c) Representative scanning electron micrographs of decellularized SI [patient 1] and colon [patient 18] scaffolds highlighting the microarchitecture of the mucosa (Mu) submucosa (S) and muscularis (M). Yellow arrowheads indicate intestinal crypts. The red arrow head indicates villi structure present on the SI scaffold. Scale bars: top, 100µm; bottom, 10µm.

Electron microscopy data acquired with Elizabeth Hirst (NIMR)

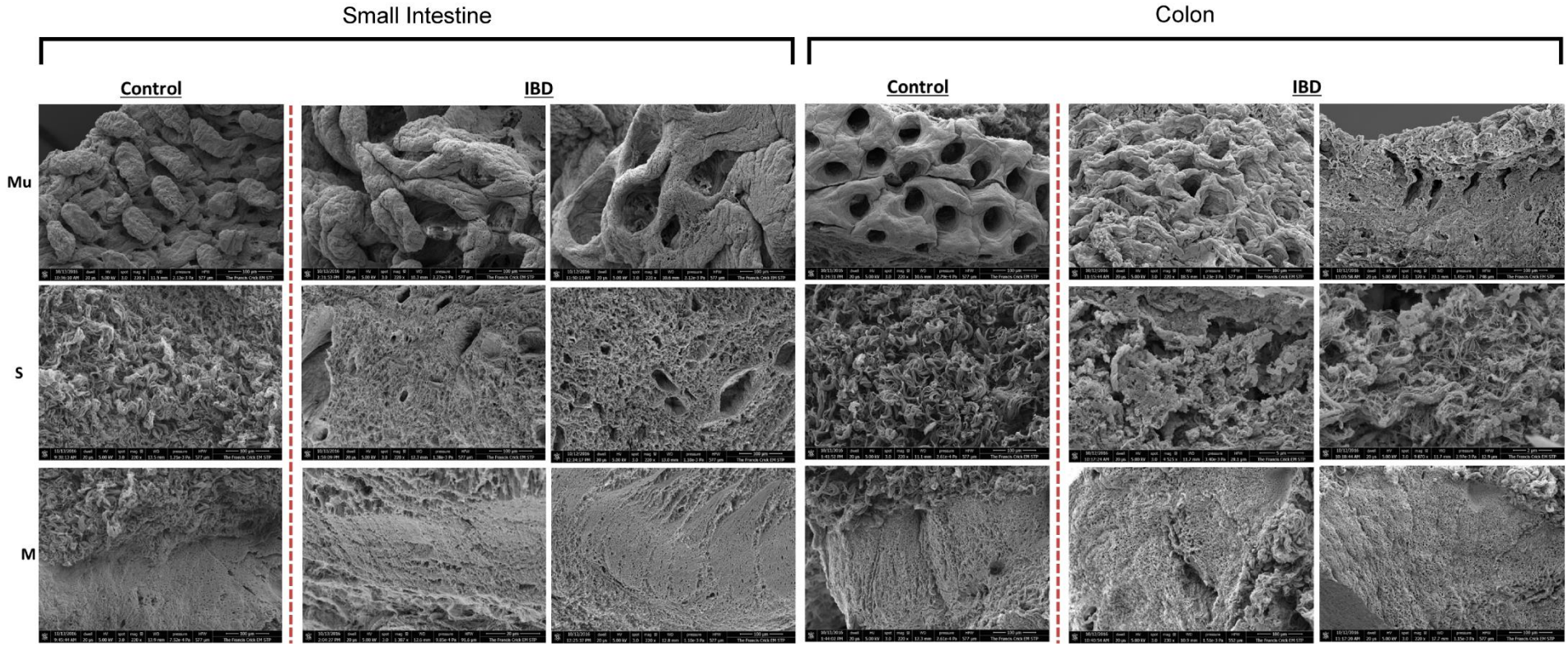

Figure 4.2 – Microarchitectural intestinal ECM changes in Inflammatory bowel disease (IBD): Scanning electron micrographs showing a comparison of healthy (Control – patients 1 and 18) versus diseased scaffolds (IBD – patients 29 and 30) derived from the small intestinal and colon. Mucosa (Mu) shown in the top row. Submucosa (S) shown in the middle row. Muscularis (M) shown in the bottom row. Scale bars 100 micron (top and middle rows) and 30 microns (bottom row).

Electron microscopy data acquired with Julia König (Crick)

To conserve the use of human decellularized scaffolds, piglet decellularized SI scaffolds were used in optimisation experiments of seedings. These scaffolds were provided by kind collaboration from members of Prof De Coppi's lab at UCL (characterisation data shown in Appendix 4). Importantly, the decellularized tissue did not differ substantially from the native porcine intestine in ECM structure. The major difference when compared to the paediatric human intestinal decellularized scaffolds, was in scaffold wall thickness.

4.3 Raman spectral analyses

In order to establish the effect of DET processing on the biomolecular profile of human SI and colon scaffolds, I used Raman microspectroscopy to compare the average spectra of the distinct microstructural layers of native intestinal tissue and their corresponding decellularized scaffolds.

In native SI and colon tissue, regions with dense cellular populations such as the mucosa exhibit distinct peaks at 726 cm^{-1} and 780 cm^{-1}, which are characteristic of ring breathing modes of nucleotides contained within DNA (Fig. 4.3a). This is indicative of the high density of cell populations in this region. These nucleic acid signals however were not captured from the muscle cells within the muscularis propria. This likely reflects the sparse distribution of nuclei in stretched out muscle cells, compared to the tightly packed columnar cells and their nuclei of the mucosa.

The characteristic lipid peaks at 1078cm^{-1} and 1303cm^{-1}, indicative of the ν(C-C) skeletal of acyl backbone of lipids and methylene bending mode, was also noted to be more intense in both native mucosa and muscle spectra, which could be associated with the lipid-rich cellular membranes of these two cell-enriched layers. This feature is also characteristic of regions containing dense cell populations as it is absent from the submucosa known to be predominantly composed of connective tissue, where cells are more sparsely distributed. The native SI is noted to have weaker lipid signals than observed in the native colon. These combined spectral features disappear from the decellularized tissue supporting the conclusion that DET processing successfully removes all cellular material without having a significant impact on the remaining spectral profile of the intestinal ECM.

One of the most notable spectral features in the decellularized tissue of both SI and colon decellularized scaffolds were peaks at 570 cm^{-1} and 1418 cm^{-1}, these peaks were also more obvious in the submucosa of native SI and colon, known to be primarily composed of connective tissue. The spectral peak at 570 cm^{-1} has previously been attributed to CO_2 rocking and the S-S bridge of cysteine, proline and tryptophan, and is therefore likely to be characteristic of the ECM[273]. The prominence of the 1418 cm^{-1} peak, attributed to CH_2 bending mode of proteins and lipids, within the submucosa is indicative of its dominance in the structural matrix. The enrichment of these two peaks in the decellularized scaffolds highlights the unique properties of the structural ECM scaffolds that lack a dense cell population.

Interestingly, minimal difference in peak intensity of the spectra profile was observed between native and decellularized scaffolds in the submucosal region that contains the least cellular density, suggesting that the main difference between the native and decellularized tissues is likely due to be the removal of the cellular mass rather than the DET process itself. Furthermore, the overall spectra profiles between SI and colonic decellularized scaffolds were highly analogous, suggesting that the biochemical composition is largely conserved between SI and colonic decellularized scaffolds.

Next, spectral data of SI and colon decellularized scaffolds with similar profiles were grouped to enable a visualisation of their spatial localisation with heatmaps (Fig. 4.3b). In particular, it is noted that collagen was mainly localised to the submucosal layer, while phenylalanine - indicating most proteinaceous regions - was most abundant in the muscularis propria. Meanwhile GAGs, indicated by glucosamines spectra, were highly enriched in the mucosal layer. Consistent to the spectra profiling, the ECM component distributions were also highly similar between SI and colonic decellularized scaffolds. The results highlight the distinct biomolecular compositions for each histological layer of the scaffolds after decellularization processing, which offer essential structural and biochemical cues for cellular reconstitution.

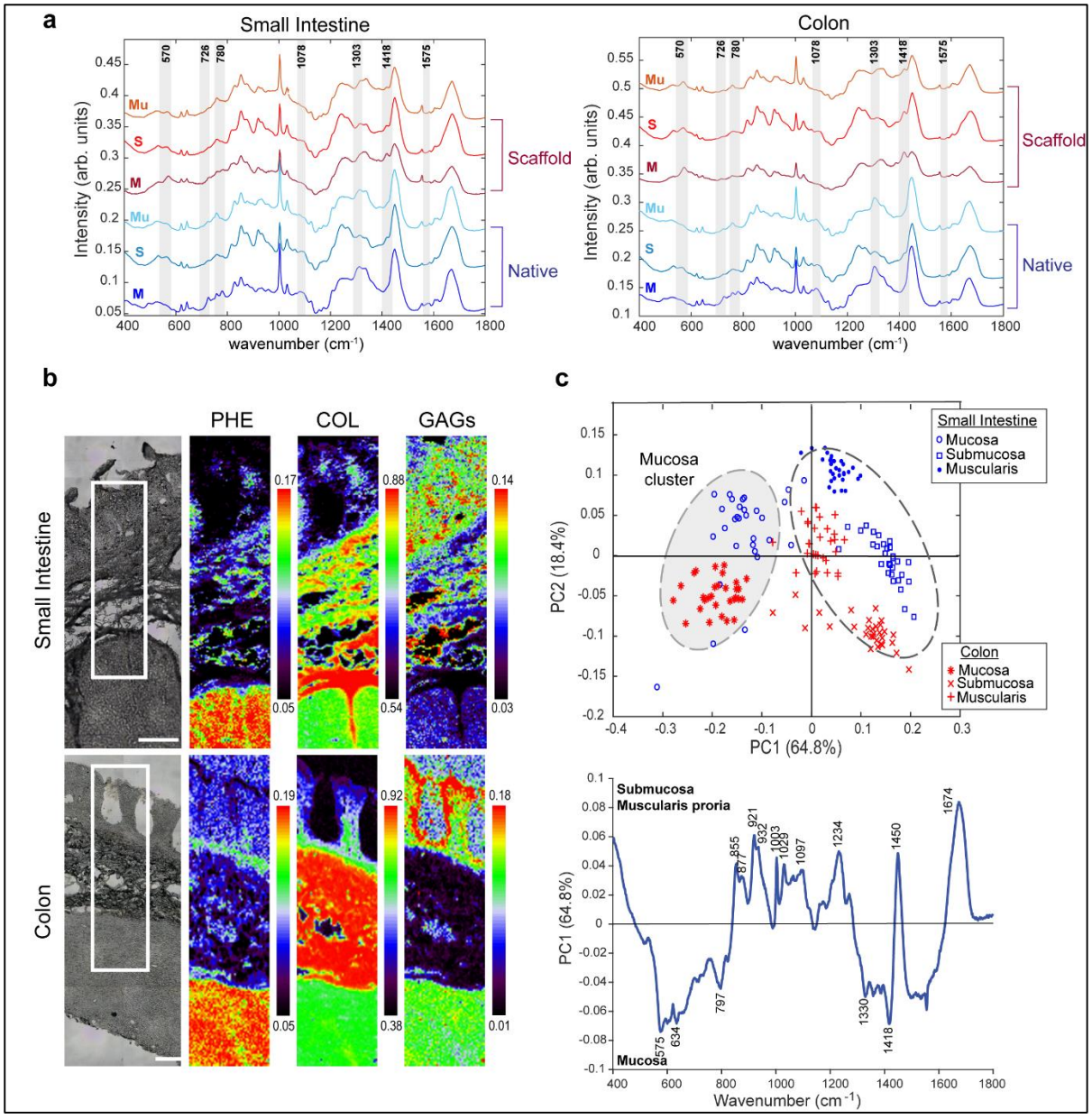

Figure 4.3 - Compositional analyses of the ECM of intestinal scaffolds: (a) Raman spectral analysis of comparable histological regions (mucosa (Mu), submucosa (S) and muscularis (M)) of the native tissue (blue lines) and decellularized scaffolds (red lines) of SI [patient 1] (left) and colon [patient 18] (right) samples. Peaks at 726 and 780 cm^{-1} were assigned to ring breathing vibrations of nucleic acids whilst peaks at 1078 and 1303 cm^{-1} were assigned to δ(CH2) and ν(C-C)/ν(C-O) modes of lipids. (b) False coloured heat maps representing direct classical least squares component analysis of Raman maps using previously acquired reference spectra of purified biomolecules. Distinct spatial distribution of Phenylalanine (PHE), Collagen (COL) and Glycosaminoglycans (GAGs) in SI [patient 1] and colon [patient 18] scaffolds is shown. Scale bars represent 50µm. Images representative of 2 experiments. (c) Top - Score plot from principal component analysis differentiates the distinct Raman biochemical spectral profiles of each distinct histological layer of the SI [patient 1] (blue) and colon [patient 18] scaffolds (red). Bottom - PC1 loading plot associated with the PC1 vs PC2 scores plot.

Raman spectroscopy data acquired with Riana Gaifulina, (UCL)

Principal component analysis of the spectra profiles readily segregated the spectra into distinct clusters based on their layer identities (Fig. 4.3c). The intensity of the corresponding peaks found within the loadings plot indicate their influence on the separation in the scores plotted along the associated axis. Remarkably, the mucosal spectra of both SI and colonic decellularized scaffold was tightly clustered together, which was distinct from the submucosal and muscularis spectra which are positively characterised (Fig. 4.3c). The data suggest that the biochemical composition of the mucosal layer from both SI and colon decellularized scaffolds are more similar to each other than their corresponding deeper histological layers.

4.4 Proteomic profiling

To further characterise the biomolecular profiles, mass spectrometry was used to generate a global proteomic profile of the decellularized SI and colonic ECM scaffolds (n=4 each). This revealed a total of 377 proteins detected in the decellularized scaffolds, among which 126 were ECM proteins (Appendices 5 and 6). Strikingly, majority of the proteins were detected in both SI and colonic scaffolds, while only 11/377 total proteins and 2/126 ECM proteins were detectable in either SI or colonic scaffolds (Fig. 4.4a). These included 17 collagen subtypes and 5 Laminin subtypes (Fig 4.4 and Appendix 5). Only 11 of 377 total proteins were detected in either SI or colon scaffolds (Appendix 6). Among the 2 ECM proteins, Defensin-5A (DEFA5) was detectable only in SI scaffold while Thrombospondin-4 (THBS4) was detectably only in colonic scaffolds. Immunohistochemical staining confirmed the restricted expression of DEFA5 in native SI but not native colon tissue, which is in keeping with this protein being known to be secreted by SI-specific Paneth cells (Fig 4.4b). THBS4, on the other hand, was found to be expressed in both native SI and native colon tissue (Fig. 4.4c), suggesting that the difference noted in mass spectrometry might be due to the detection limit in the SI ECM decellularized scaffolds rather than actual expression difference.

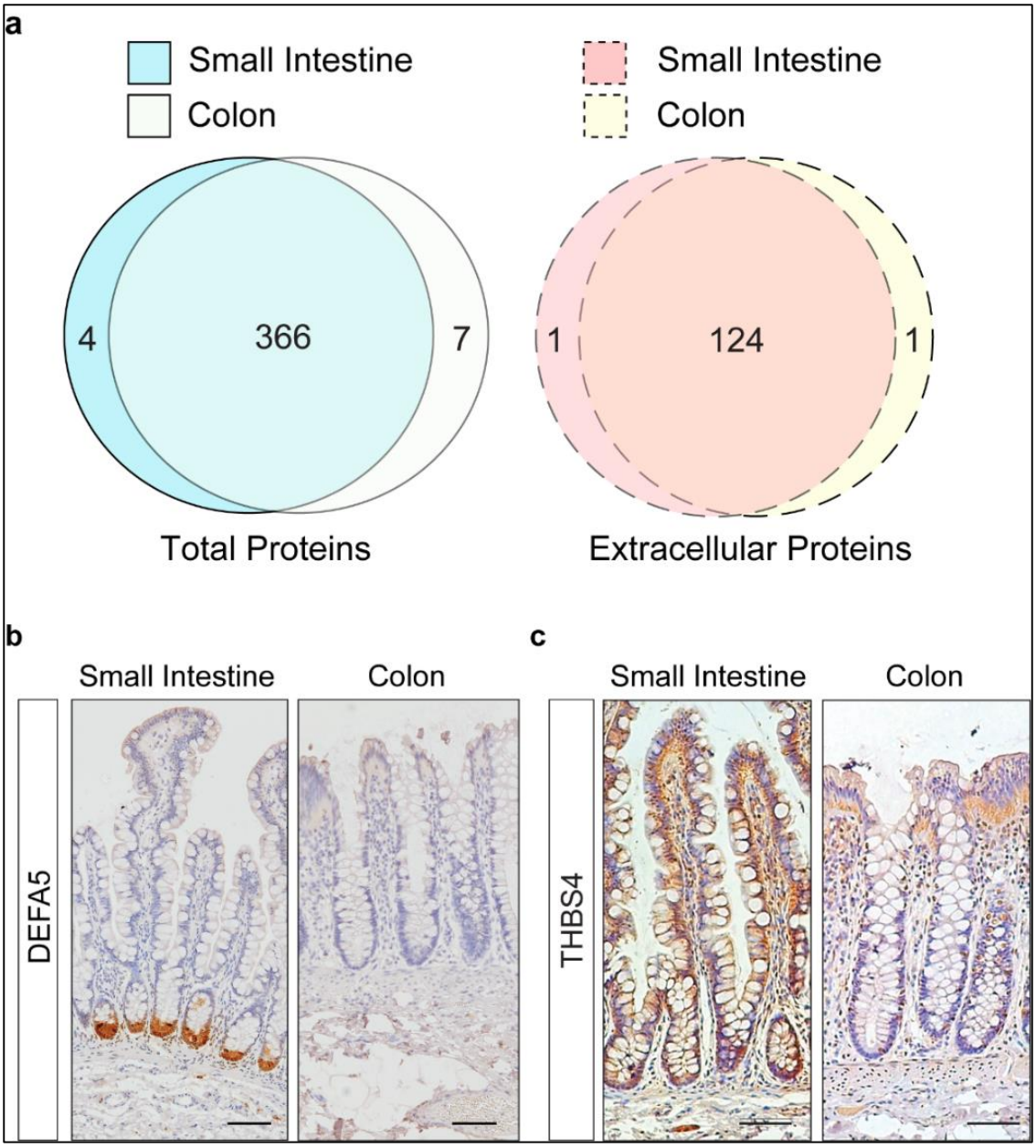

Figure 4.4 - Proteomic profiles of SI and colon scaffolds: (a) Venn diagrams showing total and extracellular proteins detected in the SI [patients 4, 11, 12, 13] and colon [patients 2, 15, 16, 17] scaffolds by mass spectrometry. Proteomics data represents samples from 4 biologically independent patient samples in each group. (b, c) Representative immunohistochemical staining of the native paediatric SI [patient 1] and colon [patient 18] tissue using the indicated antibodies, n = 2 biologically distinct patient tissue samples. Scale bars represent 100µm.

Proteomic data acquired with Peter Faull, (Crick)

Altogether, comprehensive analysis of the proteomic profiles of the decellularized intestinal scaffolds demonstrate the vastly similar biochemical composition between human SI and colonic matrix, implying that both can potentially be used for jejunal graft reconstruction.

4.5 Mechanical testing

Finally, the mechanical properties of human SI and colon scaffolds were assessed, given the importance of this characteristic in future clinical translation studies, when surgically anastomosing grafts to the native intestine. When tensile stress and strain across the transverse axis of age-matched scaffolds (n=3) was quantified, no significant differences in Young's modulus was found (Fig 4.5a-b). However, SI scaffolds tended to have higher break points on the stress-strain curves (Fig. 4.5a).

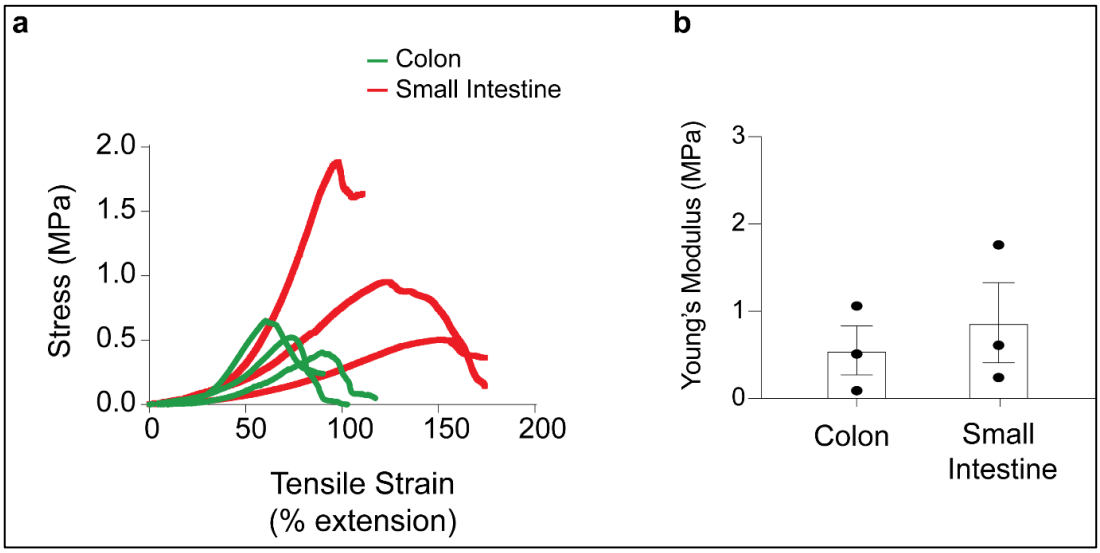

Figure 4.5 – Mechanical properties of human SI and colon scaffolds: (a) Stress-strain curves of human colon [patients 19, 20, 21] and small intestine [patients 21, 23, 24] scaffolds. (b) Corresponding calculated Young's modulus of the same scaffolds in (a). Data represent mean ± s.e.m. of n=3 biologically distinct patient samples. No significant differences identified between human SI and colon samples; unpaired t test, p = 0.5871. This experiment was performed once.

Data acquired with Lucinda Tullie and Isobel Massie (Crick)

4.6 Discussion

Developing and standardising methods to assess each scaffold produced by decellularization is an essential step when setting up a quality assurance process and ensuring reproducibility, prior to scaling up and using these biomaterials in future human clinical trials. In this chapter, I used several modalities to characterise the biophysical characteristics of the intestinal scaffolds derived from human tissue: Histological analyses, SEM, Raman spectroscopy, mass spectrometry and tensile testing. To conserve the numbers of human scaffolds available for seeding experiments, homogenising scaffolds in order to quantify DNA before and after decellularization was not performed in these experiments. There is no international consensus on the definition of decellularization, and the FDA does not currently establish tissue decellularization standards. In future experiments with human intestinal decellularized scaffolds, the additional confirmation of a reduction in scaffold DNA to less than 50ng per mg of dry weight, or a reduction of DNA fragments to less than 200 base pairs will be important to meet the 3-point criteria for defining decellularized tissue, set by prominent previous publications[274,275].

SEM is the gold standard method for assessing the nanotopography and architecture of biomaterials. It was important to assess whether the crypt villus architecture was maintained, since it is known that physical stimuli and topography significantly impact stem cell behaviour[276,277]. Although decellularisation via perfusion of the vasculature of the organ is best practice[278], I show that the DET protocol can be applied to segments of intestinal tissue without intact vasculature and good microarchitectural results. The advantage this represents is that it doesn't limit the sole use of human intestinal tissue resected with an intact vascular supply, thereby increasing the opportunity for perioperative tissue that may be accessed for decellularisation. Since fibrosis and scarring of the matrix can impact cell behaviour through cellular mechanosensing, tissue from children undergoing surgical resections for fibrotic IBD were found to have distorted matrix architecture after decellularization, and were therefore excluded from this study.

Conventionally, the techniques used to characterise the composition of collagen and GAGs in scaffolds often include biochemical assays and histological tissue staining[179]. However, biochemical assays only yield the bulk concentration of matrix constituents in the tissue, whilst histological staining provides a limited qualitative representation of spatial distribution. I therefore used Raman spectroscopy to study the human SI and colon scaffolds, comparing them to their native counterparts as well as to each other. The key advantage is that it is a non-invasive, label-free technique that provides both quantification and localisation of biomolecular constituents within tissue. To my knowledge, Raman spectroscopy has not been used in the assessment of intestinal decellularized scaffolds before. The data show that aside from delineating features specific to the loss of cells, the spectral profiles between the native and decellularized samples are largely conserved. When comparing SI and colon scaffolds against each other, I observed that the spectral profiles and distribution of ECM components on Raman heat-maps are highly analogous. Indeed, the biochemical composition of the mucosal layer of both scaffold types are more similar to each other than their corresponding deeper histological layers (submucosa and muscularis). This indicates that both may be equally as effective as each other, when used as a platform for jejunal graft engineering. Hence both scaffold types are used in subsequent seeding experiments, explained further in chapter 5. Overall, this data supports the use of Raman Spectroscopy in tissue engineering, in analysing scaffolds and constructs.

Mass spectrometry was used to confirm the Raman spectral findings, and also to map the global proteomic profile of the scaffolds. This challenging task required several months of optimisation, since the ECM is primarily formed of fibrillary components such as collagen and elastin that are resistant to solubilisation. Mass spectrometry pipelines require proteins to be solubilised and digested into peptides. Therefore, comprehensive and accurate scaffold proteome analyses is dependent on reproducibly generating peptides from the entirety of proteins present in the scaffolds. Initial experiments failed to provide a representative global proteomic profile of the scaffolds as solubilisation of the scaffolds was visibly incomplete using standard sample preparation protocols[279]. I therefore adopted a method whereby the scaffolds were snap frozen and grinded into a power with

a pestle and mortar in a bath of liquid nitrogen first, prior to lyophilisation. Samples were then denatured, reduced and alkylated, deglycosylated and digested by proteases LysC and trypsin, based on the methods described in a previous publication[260]. This reproducible method provided interesting insights into the ECM signature, or "matrisome", of the SI and colon showing that there is significant overlap between them. Attempts at gaining a more quantitative approach, for example to assess the relative amounts of specific proteins between SI and colon scaffold samples were unsuccessful due to the small sample sizes (4 biological replicates only) and concern about variation between experimental replicates. Nevertheless, the mass spectrometry data acquired provides important qualitative insights into the similarities between SI and colon scaffolds, which is a new contribution to the research field but has a lot of scope for further development. For example, one previous study used filter associated sample preparation (FASP) on decellularized rat livers and human lungs to identify remnant cellular immunogenic proteins that may result in tissue rejection upon transplantation[275,280,281].

Next, the mechanical properties of both SI and colon decellularized scaffolds were tested. This was important on two levels. Firstly, on a practical level this information is relevant to the surgical integrity of these biomaterials when anastomosed to the native intestine in future translational studies. The desired mechanical properties of surgical grafts depend on the site of organ transplantation, and must take into consideration factors such as permeability, porosity, pore size, elasticity and biodegradability[282-284]. When considering the intestine, scaffolds that are prone to disintegration would be poor candidates for intestinal transplantation, due to the risk of deformation, enteric wound dehiscence and anastomotic leaks leading to intra-abdominal sepsis. Secondly, I was particularly interested to know if scaffolds derived from colonic tissue, that propel more solid material through the lumen, had significantly different properties to scaffolds derived from SI tissue, that propel more liquid material. In our work, only tensile testing was employed, whereby deformation of the intestinal scaffolds was measured with gradual increases in the force applied to the samples. Although this is quite a basic mechanical testing method, the data did not demonstrate any significant differences between the two decellularized scaffold types, however SI scaffolds tended to have higher break

points. This may be due to the presence of villi in SI scaffolds resulting in higher tenacity, which may be a surgical advantage *in vivo* but would require further testing in orthotopic transplantation models. Unfortunately, the mechanical data set presented in this thesis lacks comparison to native gut, as fresh tissue it was not accessible at the time of mechanical testing experiments. However, our findings may be considered alongside data previously published on tensile testing in native human SI and colon, where maximal tensile stress values were reported to be 0.5MPa and 0.9MPa respectively[285]. When progressing to orthotopic transplantation models, it will be important to test mechanical properties in both axial and transverse directions. End-to-end anastomoses of the graft to native tissue may be further assessed by suture testing in future work.

5. Results III - *In vitro* intestinal graft engineering

5.1 Introduction

The major burden of nutritional digestion and absorption is taken on by the proximal 100-150cm of jejunum. Hence, the focus of this chapter was to engineering intestinal mucosal grafts with jejunal specific function. In this way, even modest increases in jejunal surface area could restore nutritional autonomy in a child. Since data from the previous chapter indicates SI and colon scaffolds to be unanimous in biophysical features, both are used in this chapter for jejunal organoid seedings. This raises the important research question: What are the contributing roles of the origin of ISCs versus origin of the decellularised matrices, in determining the eventual functional identity of the final engineering graft?

In addition, several studies have previously reported techniques to develop physiological *in vitro* intestinal models, useful for drug discovery and disease modelling. Porous silk protein scaffolds were used in combination with commercially available human colon cancer cell lines (CACO-2 and HT-29-MTX) and myofibroblasts (H-InMyoFibs)[197]. In this *ex vivo* static culture system, the epithelial layer retained a functional double mucus barrier and modelling interactions with the intestinal pathogenic bacterium *Yersinia pseudotuberculosis* was demonstrated. However, the main limitation to this system was that function of the model decreased over time in culture. A second *in vitro* modelling approach, developed by Professor Allbritton's research group, uses human SI or colon organoids for seeding onto rat tail collagen based hydrogels[286-289]. This creates a 2D monolayer of epithelial cells that is expandable by mechanical and chemical breakage of the 2D layer and re-seeding onto new collagen hydrogels. The 2D layers are converted into 3D models by using PDMS stamps to recapitulate the crypt-villus axes on a transwell set-up. Using biochemical gradients across the epithelial layer, they show to proliferation is restricted to the crypt compartments whilst differentiation is present outside of the crypt regions. A third example is from a study in 2016, where human intestinal organoids were expanded and seeded as single cells on to biological scaffolds derived from porcine SIS scaffold[195].

Cultures were maintained in Transwell-like settings. After 7 days the presence of differentiated cells (goblet and enteroendocrine) were identified on the scaffold. Furthermore, dynamic culture conditions using a perfusion bioreactor had beneficial effects on epithelial morphology[195]. Whilst all these studies are not directly translational for clinical transplantation purposes, the methods described provide important insights into the optimal *in vitro* conditions to achieve barrier function and differentiation on engineered jejunal grafts prior to transplantation.

5.2 Static culture conditions

To assess conditions required for cell engraftment, PDOs were expanded and trypsinised for seeding onto human colon scaffolds at a density of $1x10^6$ cells/cm^2 of scaffold, where the scaffold was fully submerged in organoid culture media (Fig 5.1). A lower seeding density resulted in patchy cell engraftment with significant areas of the scaffolds left blank. Similarly, a higher seeding density also resulted in patchy cell engraftment with significant blank areas of the scaffold. Excessive cell debris and cell death was also noted in the scaffold culture supernatant. This is likely due to increased cellular demands on a fixed volume of media covering the tissue culture well, where the scaffolds are maintained.

At a density of $1x10^6$ cells/cm^2, intestinal epithelial cells were noted to have good epithelial coverage of the scaffold (Fig. 5.1a), including the crypt compartments (Fig 5.1b) after 10 days in culture. This indicated conditions were adequate for cellular engraftment. However, the morphology of the epithelial layer was suboptimal. Although a brush border was noted at higher magnification (Fig 5.1b), cells were largely vacuolised and unpolarised. This led me to explore a period of dynamic culture in the subsequent experiments to improve epithelial morphology.

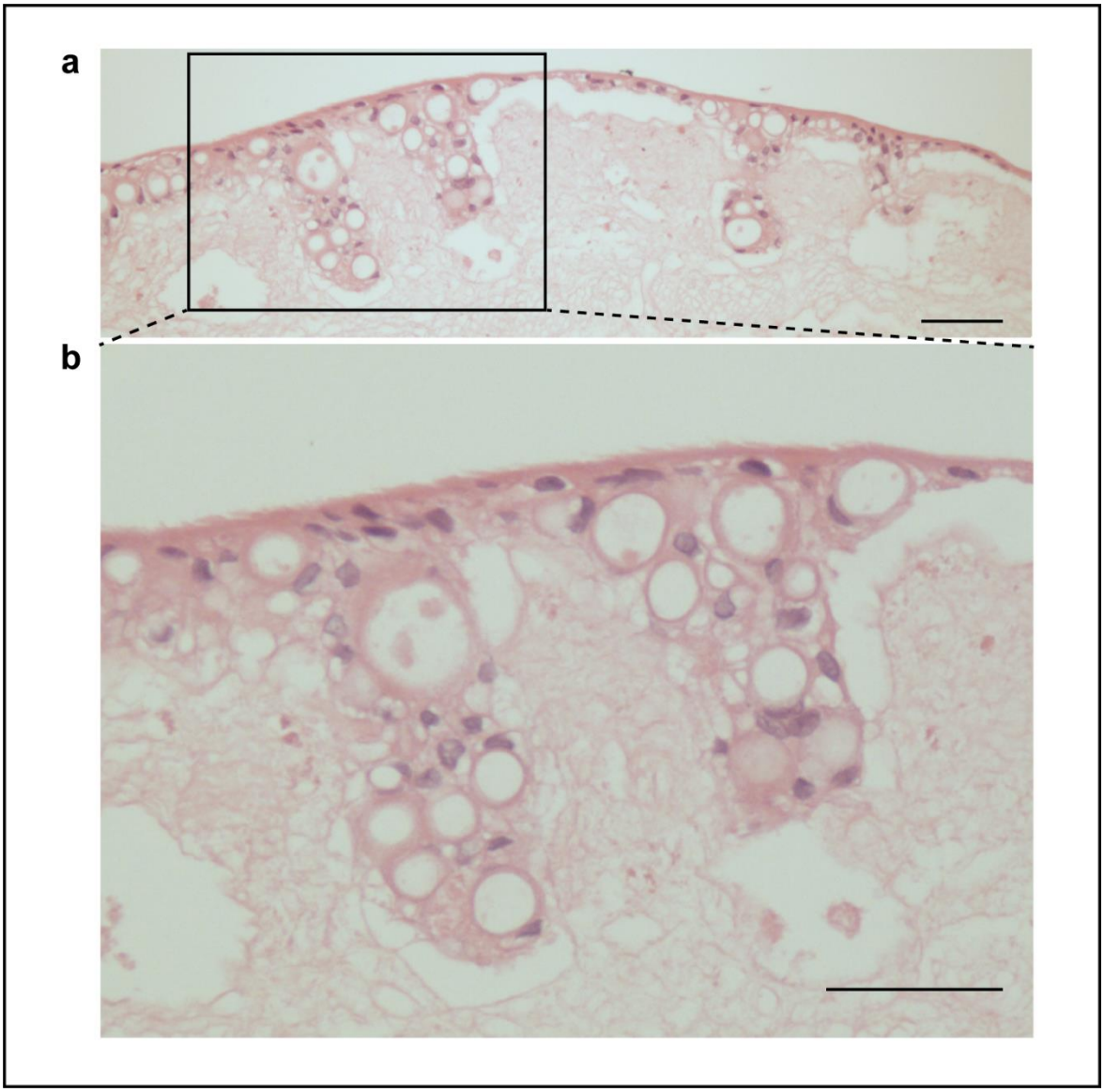

Figure 5.1 - Morphology of the intestinal epithelial layer in submerged static culture conditions: (a) Representative H&E staining of human duodenal graft after 10 days in static culture on human colon scaffolds. (b) High magnification of vacuolised and unpolarised cells covering the crypt compartments. All organoids in this figure originate from patient 10. Scaffolds originate from patient 18. Scale bars represent 50 microns.

5.3 Bioreactor design and dynamic culture conditions

To establish dynamic conditions, primary human jejunal organoids were seeded onto the luminal surface of scaffolds which were individually mounted on a customised scaffold holder (Fig 5.2a-b). The mounted grafts were submerged in media and maintained under static conditions for 4 days, after which, they were transferred to dynamic culture conditions using a perfusion bioreactor (Fig. 5.2a-c). The grafts remained submerged and were maintained under dynamic conditions for at least 14 days before performing histological analyses.

For initial optimisations, human jejunal organoids were seeded on piglet SI scaffolds in order to conserve more limited human intestinal scaffolds. Micro-CT imaging was performed on the seeded scaffolds as the first step of analyses. This enabled a quick assessment of the volume and distribution of epithelial cells on the scaffold. I show that surface area coverage by cells on the scaffolds remained high after introducing a dynamic culture period (Fig 5.3).

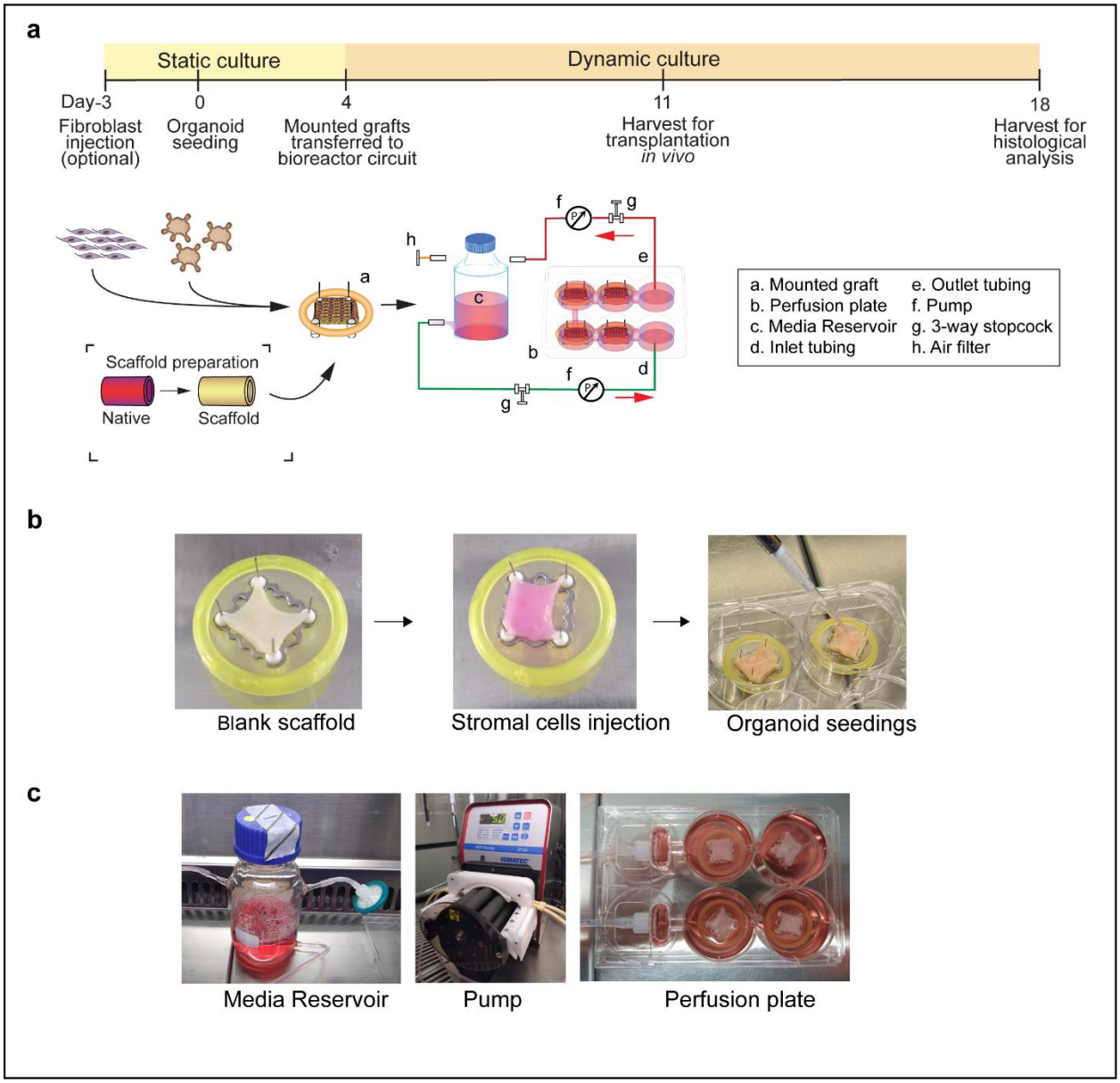

Figure 5.2 - Bioreactor set-up for *in vitro* submerged graft culture: (a) Schematic outline of the scaffold seeding strategies using a bioreactor circuit. The timeline shows seeding of each cellular component onto the scaffolds and the time periods in static and dynamic cultures (top). The bioreactor circuit design and all individual components are indicated (bottom). (b) Representative images showing a blank scaffold (left), after stromal cell injection (middle) and during organoid cell seeding (right). (c) Photographs showing the media reservoir (left), the peristaltic pump (middle) and the perfusion plate (right) holding 4 individually mounted grafts.

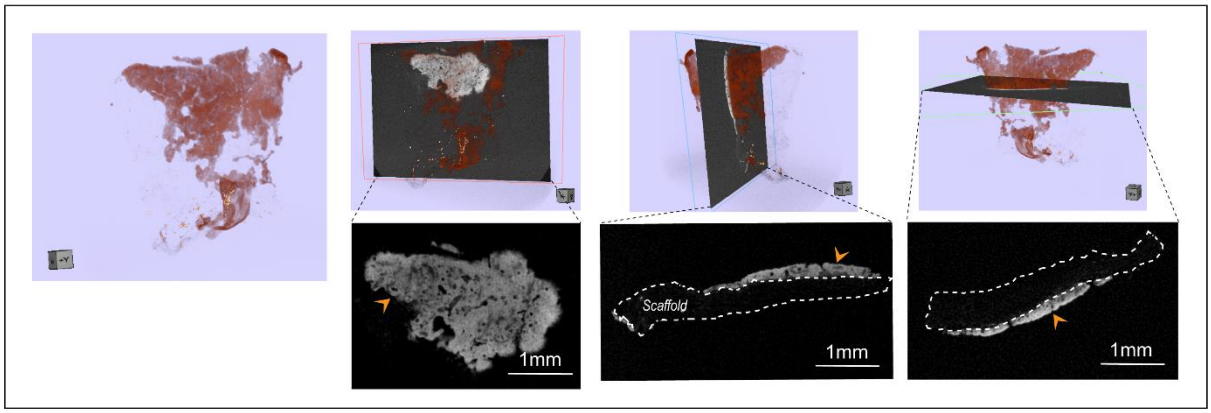

Figure 5.3 - MicroCT imaging of jejunal grafts formed on piglet SI scaffolds: a, 3D volume rendering of micro CT virtual slices showing jejunal epithelial layer (bright white and indicated by orange arrowheads) on a piglet scaffold (outlined by dashed white line) at different angles. Scale bars indicate 1mm.

MicroCT data acquired with Anne Weston (Crick)

After a period of static culture followed by dynamic culture, histological analyses of the jejunal grafts using piglet SI scaffolds showed an improved morphology, expected of the intestinal epithelium. An organised monolayer of columnar cells extending to cover the crypt compartments was noted (Fig 5.4 a-b). However, variability in morphology was noted as regions of collagen-positive new matrix deposition were detected, with structures resembling new villi (Fig 5.4 b-c). This variability may be due to the impact of an uneven flow of media across the scaffolds, using the perfusion plate system.

In addition, all intestinal cell types were readily detected in the graft, including lysozyme-positive Paneth cells, AB-PAS-positive goblet cells and alkaline phosphatase-positive enterocytes (Fig. 5.4 d-f). Proliferation marker Ki67 was also identified in the graft (Fig 5.4g). Importantly, the jejunal-specific enzyme, sucrase isomaltase, was also widely detected on the brush boarder of the epithelial cells (Fig 5.4h). This indicates that jejunal region-specific identity was preserved in the engineered grafts using piglet SI scaffolds.

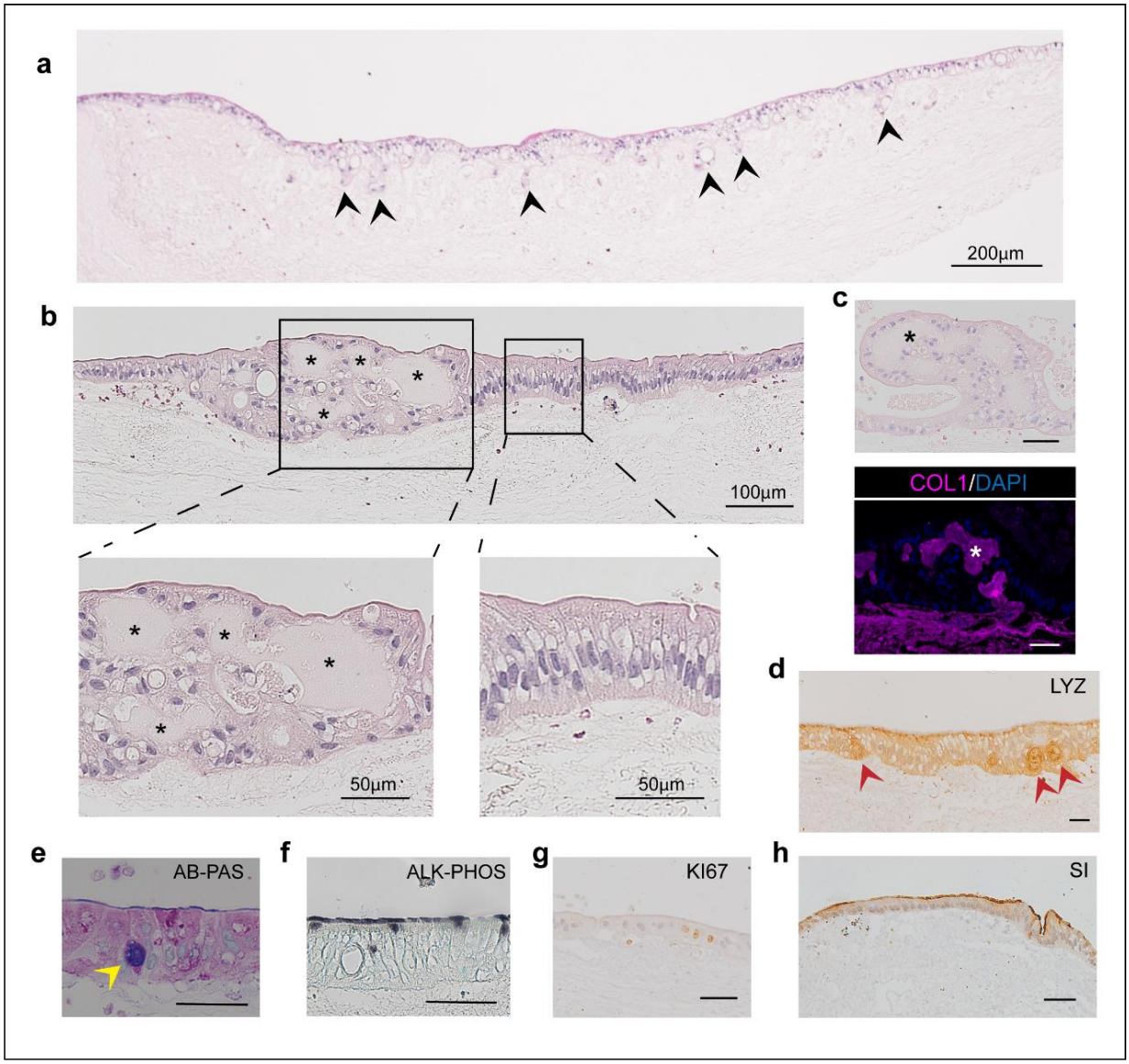

Figure 5.4 - Characterisation of engineered jejunal grafts cultured *in vitro* using piglet SI scaffolds: (a) Representative H&E staining of a jejunal graft showing epithelial lining with invaginated crypts (black arrowheads). (b) H&E staining of a jejunal graft showing regions of columnar epithelial monolayers (bottom right) as well as regions of new matrix deposition (black asterisks, top and bottom left). (c) New matrix deposition indicated by black asterisk in H&E image (top) stains positive for collagen-1 (magenta, white asterisk, bottom). (d-h) Representative immunohistochemistry images of engineered jejunal grafts using the indicated antibodies. Paneth-like cells are indicated with red arrowheads in (d) and goblet-like cells are indicated with yellow arrowheads in (e). Enterocytes are indicated by brush border staining with alkaline phosphatase (ALK-PHOS) (f) and sucrase isomaltase (SI) (h). Proliferating nuclei are indicated by Ki67 staining (g). All scale bars represent 50µm unless specified otherwise. Images are representative of 3 independently cultured grafts. All organoids in this figure originate from patient 2.

Next, I examined engineered graft epithelial morphology when seeding human jejunal organoids onto either human SI or human colonic scaffolds.

Similar to piglet scaffold data, histological analyses revealed a continuous monolayer of columnar epithelial cells distributed evenly along the decellularized human SI scaffold surfaces (Fig. 5.5a). Immunostaining confirmed that proliferation (as indicated by PCNA) and differentiation (ALPI to mark enterocytes and AB-PAS to mark goblet cells) potential was maintained in the reconstructed grafts. These findings were also observed when jejunal graft reconstruction was performed using identical methods onto human colon scaffolds, where proliferation and differentiation were all detected (Fig. 5.5b). Interestingly, immunofluorescent staining of collagen showed new matrix deposition in multiple regions underneath the epithelial cells, suggesting ECM remodelling mediated by epithelial cells on both scaffold types (Fig. 5.5 a-b immunofluorescent images). This pattern of matrix deposition was also seen in earlier optimisation experiments with piglet SI scaffolds (Fig 5.4c). This is indicative of active ECM remodelling driven by the intestinal epithelial cells on all scaffolds types. The expression of tight junctions (as marked by ZO1) and polarity (indicated by Na+/K+/ATPase) was assessed in these areas of matrix remodelling, on sections of the graft where new matrix deposition was identified(Fig. 5.5c). This indicates abnormal polarity of cells involved in matrix deposition.

Electron microscopy analysis further demonstrated the presence of microvilli (brush boarder of enterocytes); basement membrane (as indicated by basal lamina and reticular lamina features between the scaffold and the epithelial cells); goblet cell mucous vesicles and Paneth cell secretory vesicles (Fig. 5.5d-e). The presence of both basement membrane microstructure, composed of basal lamina and reticular lamina, as well as tight junction markers is encouraging, as both are essential components for epithelial barrier function of the intestine.

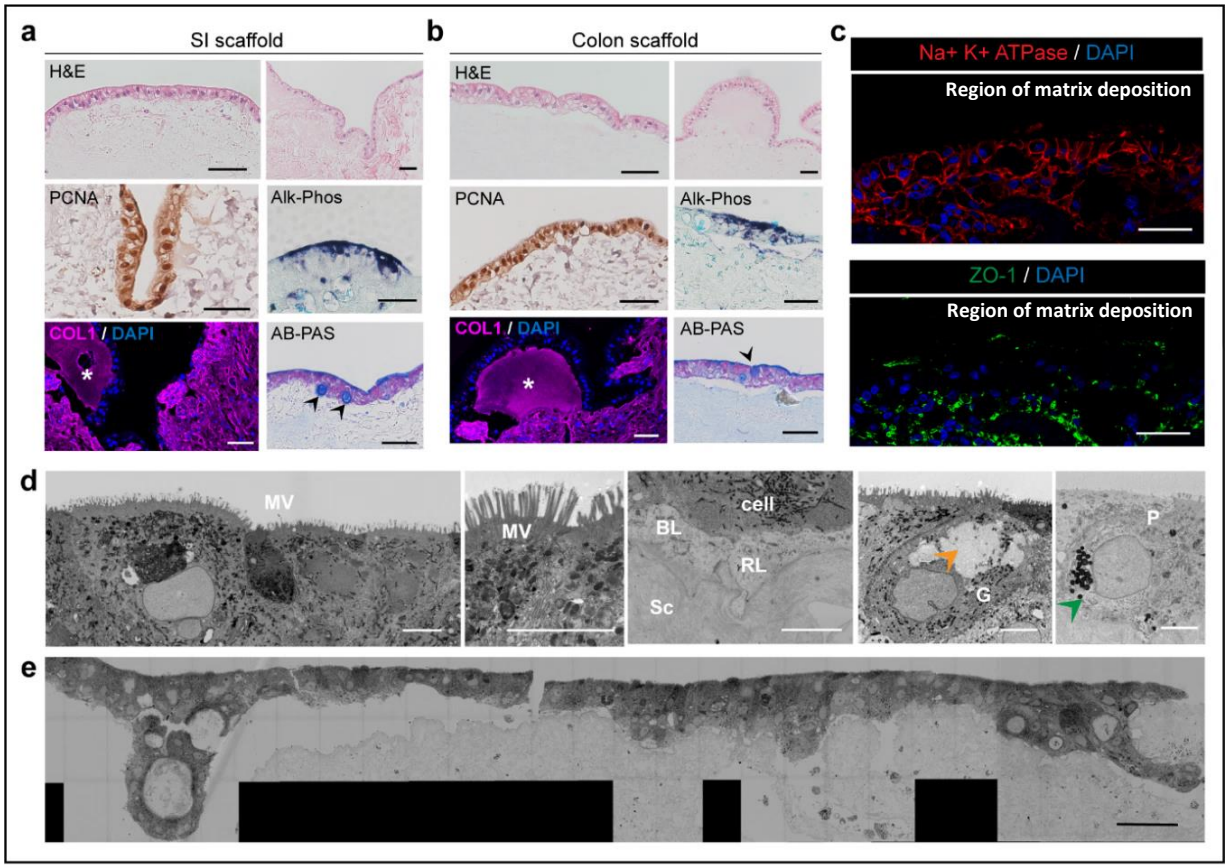

Figure 5.5 - Characterisation of engineered jejunal grafts cultured *in vitro* using human scaffolds. (a-b) Representative histological and immunostaining images of jejunal grafts reconstructed using human SI scaffolds [patient 13] (a) or human colon scaffolds [patient 16] (b) at day 18. New matrix deposition is shown by newly synthesized collagen (white asterisks). Black arrowheads indicate AB-PAS-positive goblet cells. Scale bars represent 50µm. (c) Representative immunofluorescent images of a jejunal graft seeded on human SI scaffolds, in a region of new matrix deposition, [patient 5] using the indicated antibodies. Scale bars represent 50µm. (d) Representative electron micrographs of a jejunal construct [SI scaffold - patient 5] showing microvilli (MV) (left and second from the left); basement membrane with basal lamina (BL) and reticular lamina (RL) at the scaffold (Sc) border (middle); Goblet cell (G) with mucous vesicles indicated by the orange arrow head (second from the right) and Paneth cell (P) with secretory vesicles indicated by the green arrow head (right). Scale bars represent 5µm. (e) Electron micrograph showing a monolayer of epithelial cells on a graft [SI scaffold – patient 5]. Scale bar represents 50µm. All organoids in this figure originate from patient 2. Images are representative of at least 3 independent graft cultures.

Electron microscopy data acquired with Anne Weston (Crick)

5.4 Functional analysis

Next, the absorptive and digestive function of the bioengineered grafts at various time points of *in vitro* culture was examined (Fig. 5.6a). First, the absorptive capacity of the reconstructed jejunal grafts was tested at day 18 of culture by incubating the grafts with fluorescently labelled peptide β-Ala-Lys-AMCA. Immunofluorescent staining confirmed the presence of β-AMCA peptides incorporated within the boundaries of intestinal epithelial cells on the grafts (Fig. 5.6b). This indicates that the engineered graft possesses peptide absorptive function and the presence of active peptide transporters on the graft epithelium.

Digestive capacity was assessed by demonstrating the function of the jejunal enterocyte brush border enzyme, sucrase isomaltase. Here, the jejunal constructs were challenged with sucrose and measuring the subsequent glucose (one of the metabolic products) production at various time point of culture. This method tests the disaccharidase activity, since sucrase isomaltase hydrolyses sucrose into two glucose molecules. Remarkably, glucose production was detected as early as day 4 culture in all three scaffold types, indicating that the enzyme sucrase isomaltase is functional throughout the *in vivo* culture timeline (Fig. 5.6c).

Plasma citrulline levels positively correlate to enterocyte mass and absorptive function, and are used as a clinical biomarker of intestinal failure[290]. Therefore, graft culture supernatants were sampled to quantify the citrulline concentration as a surrogate biomarker of enterocyte mass on the scaffolds. This was done at days 0, 11 and 25 of the culture. The data shows an increase in citrulline levels from day 0 to day 25 in the jejunal grafts regenerated from all three scaffold types. This further indicates the formation of healthy functional enterocytes in all constructs (Fig. 5.6d).

Digestive capacity was also detected by assessing the activity of the enzyme dipeptidyl peptidase IV. This was achieved by incubating the grafts with the compound Gly-Pro p-nitroanilide hydrochloride to and measuring the release of nitroaniline (Fig. 5.6e). This indicates cleavage activity of dipeptidyl peptidase IV on the engineered grafts.

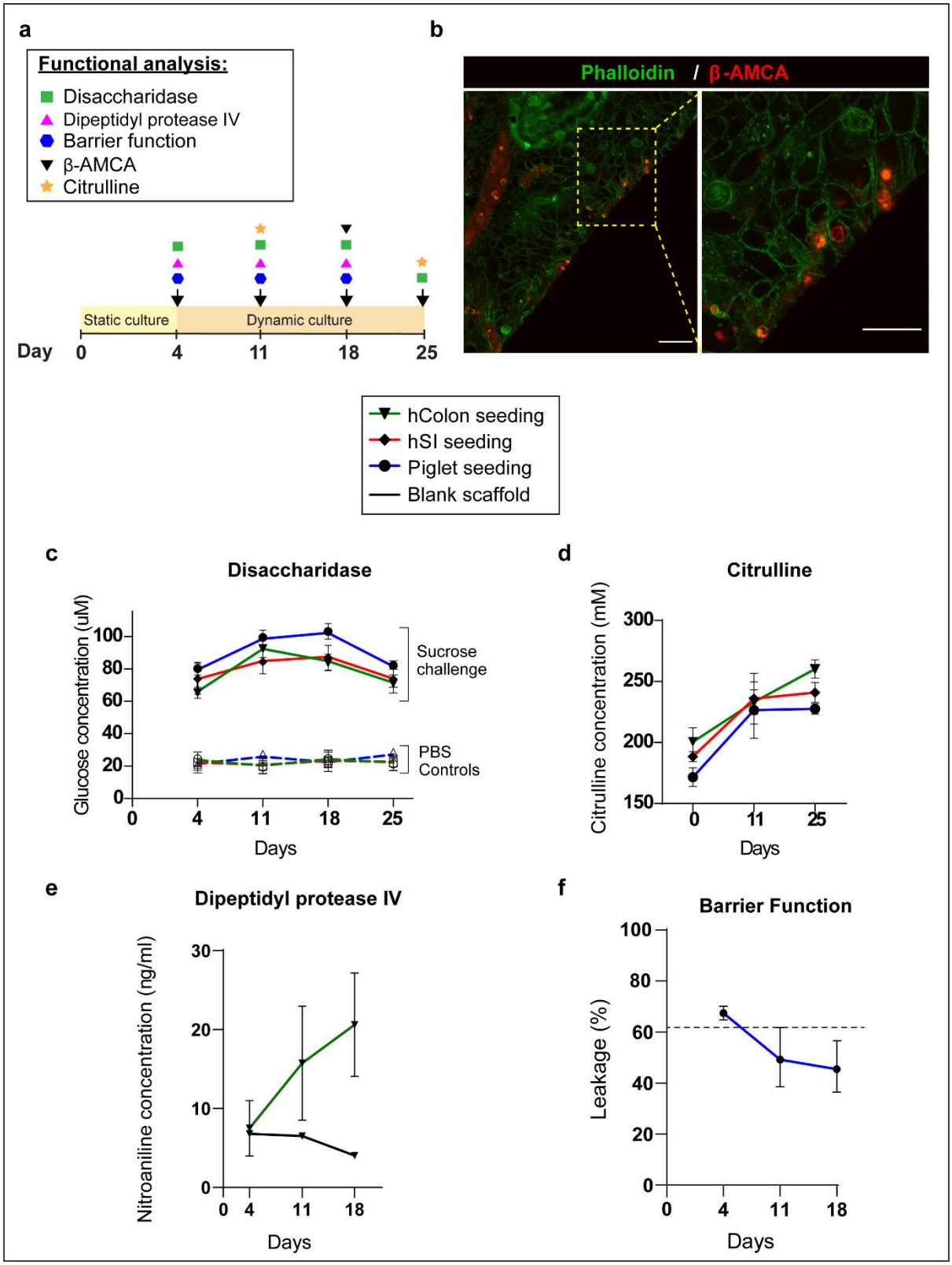

Figure 5.6 - Functional assessment constructed jejunal grafts *in vitro*: (a) Timeline indicating the experimental sampling (marked by each coloured symbol) of jejunal grafts for functional analyses. (b) Immunofluorescent staining showing uptake of β-AMCA peptide (red) on a jejunal graft (piglet SI scaffold). Phalloidin staining (green) indicates epithelial cell boundaries. Scale bars, 30µm. Images representative of two experiments. (c-f) Functional analysis using jejunal grafts seeded on human colon scaffolds (green lines), human SI scaffolds (red lines), piglet scaffold (blue lines) or unseeded

blank scaffolds (black lines). (c) Disaccharidase enzyme activity, showing sucrose (solid lines) or PBS control (dashed lines). (d) Graft supernatant citrulline concentration over time. (e) Nitroaniline concentration from jejunal grafts over time. (f) Barrier function as indicated by percentage leakage on jejunal grafts over time. Blank scaffolds show an average of 61% baseline leakage (dashed line). All organoids used in this figure originated from patient 2. Data represent the mean ± s.e.m. of three independently cultured jejunal grafts.

Data acquired with Isobel Massie (Crick) and Simon Eaton (UCL)

Finally, barrier function was assessed by measuring the percentage leak of FITC-labelled dextran through jejunal grafts constructed with piglet SI scaffolds, which is more permeable than human scaffolds. This was expressed as a measurement from the 'luminal side' to the 'serosal side'. Blank piglet SI scaffolds showed an average baseline leakage of 61% (as indicated by the dashed line) and this was reduced to 45% by day 18 of graft culture (Fig. 5.6 f).

In summary, the results from functional analyses indicate that the engineered jejunal grafts regenerated using either SI or colon decellularized scaffolds, exhibit some aspects of physiological jejunal function, namely (i) peptide absorption, (ii) peptide digestion, (iii) sucrose digestion and (iv) partial improvement in barrier formation over time.

5.5 Discussion

In this chapter, the culture conditions required for epithelial regeneration on decellularized scaffolds were investigated. It is widely accepted that two-dimensional *in vitro* static culture conditions differ significantly from true *in vivo* conditions. Even three-dimensional organoid cultures that are perceived as more biomimetic are still maintained in static conditions, depriving the cells of mechanical stimulation such as shear tress, stretching, compression, contraction and the resulting variability of matrix stiffness. Therefore, the organoid culture system does not adequately recapitulate mechanically induced cell signalling responses which represents an important limitation.

When culturing jejunal grafts in submerged static culture conditions, I found that cells lacked polarity and organisation expected of the intestinal epithelial monolayer. In addition, cells appeared

vacuolised which histopathologically is often associated with cell death. Indeed, longer periods of culture in static conditions were more difficult to maintain and resulted in highly variable results in epithelial survival and morphology. Experimental attempts at creating an air-liquid interface culture using the human scaffolds were largely unsuccessful. This may be attributed to the significant thickness of the human scaffolds, and the relative impermeable properties of it. Air-liquid interface culture set ups require cells to take up nutrients from the media compartment via their basolateral membrane. The thickness of the human scaffolds represented a barrier to this process, resulting in poor cell survival. Alternative approaches to achieving good air-liquid cultures would be to reduce the thickness of the intestinal scaffold by dissecting away the muscle layer and using only the mucosa/submucosal layers of the scaffolds. However, this resulted in damage to the mucosal layer and overall was not in keeping with the prevailing research aim of the thesis, which was to translate the use human biomaterials into clinical practice for intestinal tissue engineering. The translational strategy taken from the outset of the project was to adjust my experimental protocols to suit the human biomaterial properties (rather than converse of altering human biomaterial properties to suit the experimental aims). Therefore, I moved on to exploring dynamic culture conditions to improve morphology of the intestinal epithelial cells on the human decellularised intestinal scaffolds. In progressing to dynamic culture conditions, a simple bioreactor circuit consisting of a peristaltic pump and perfusion culture plates produced much improved results in epithelial cell survival and morphology on all scaffold types. Here, some physiological conditions of the native intestine such as shear stress and turbulent fluid pressures, experienced during intestinal peristalsis, are partially recreated.

Interestingly, the data suggest that epithelial cells were remodelling the scaffold matrix as indicated by the deposition of new hyaline matrix on the surface of the scaffolds. This data supports findings already published in the field by Kitano *et. al*.,, who also show evidence of collagen IV deposition by the transplanted epithelial cells was also included in supplementary data[193]. Although definite crypt villus axis was present on the human scaffolds, a clear organisation of cells along the crypt villus axis

was not seen in either this study or that of Kitano and colleagues (i.e. proliferative stem cells at the base of the crypts and differentiated cells at the villi). Compartmentalisation of proliferative and differentiated cells was achieved in earlier publications on transwell set ups where the crypt villus contour had been created using molds[286,289]. In this study, the new matrix deposition may be indicative of early matrix remodelling towards new crypt-villus axis formation that might have been limited by suboptimal dynamic culture conditions. Future experiments allowing longer culture periods would be useful to study the impact of matrix remodelling on compartmentalisation of stem and differentiated cell popuations.

The majority of differentiated intestinal cell types were detected on the engineered grafts, including Paneth cells, goblet cells and enterocytes. Jejunal specific sucrase isomaltase expression was also widely detected on the brush border, signifying maintenance of region-specific identity of the engineered grafts. It is important to note that expression of chromogranin A was not detectable, indicating a lack of terminally differentiated enteroendocrine cells. In some of the human scaffold seedings, lysozyme expression was not detectable, however in-depth electron microscopy analysis did confirm the presence of cells containing multiple secretory vesicles were also identified, which may represent early immature Paneth cells. These findings are comparable to previous studies using hiPSC derived intestinal organoids on rat decellularized scaffolds, which also did not find the full complement of differentiated intestinal cell subtypes of native gut[193]. Specifically, fully differentiated goblet and Paneth cells were not found *in vitro*. However, after transplantation goblet and Paneth cells were abundantly present, suggesting further maturation *in vivo*[193]. To achieve a more global profile of cellular and matrix composition of the graft, future experiments could also employ methodologies such as flow cytometry, RNA extraction for single cell RNA sequencing, imaging mass spectrometry, and other spatial resolution approaches such as MERFISH and imaging CyTOF.

A particular advantage of our bioreactor culture and seeding methods is that we optimise our protocols to the shortest *in vitro* culture times possible (i.e. 14 days) whilst methods described in

previously published studies require longer *in vitro* culture times (28 days)[193]. Shorter culture period (both in the patients' cell expansion phase as well as the bioreactor culture phase) is likely to be advantageous for future clinical translation, particularly when constructing a patient-specific graft for children with intestinal failure.

Most importantly, I show that engineered grafts possessed jejunal specific functions such as nutrient digestion and absorption, regardless of the origin of the scaffolds. Several publications reporting on tissue engineered intestine do not include studies of functional assays of digestion, absorption or barrier integrity at all[194,227,251,253,254]. Whilst one more recent publication the transfer of glucose and medium chain fatty acids from the lumen of the construct to the scaffold vasculature[193]. The concern with their experimental set up is that it does not demonstrate digestive capacity alongside absorptive capacity. This chapter of my thesis contributes new *in vitro* functional assays to the research field, by demonstrating the activity of digestive disaccharidase and peptidase enzymes alongside absorption of peptides into the jejunal grafts. In addition to this, I show that the measurement of citrulline levels in the jejunal graft culture supernatants is a novel application of a non-destructive biomarker method for tracking enterocyte growth on scaffolds. This has important implications in future upscaling of the jejunal graft engineering process. Finally, although evidence of barrier structure was seen on immunostaining and electron microscopy, the FITC-dextran assay performed produced more variable data. This is likely due to micro-tears in the thinner piglet scaffold wall after decellularisation. The functional assay was not performed on the human scaffolds since they are significantly thicker in dimension, and highly impermeable to the FITC-dextran compound. Overall, since the expression of brush border enzymes (sucrase isomaltase and alkaline phosphatase) were detected on engineered grafts that were formed using all scaffold types, I conclude that either SI or colon ECM scaffolds were suitable to proceed with *in vivo* transplantation studies.

6. Results IV - *In vivo* graft transplantation models

6.1 Introduction

Due to the limitations of *in vitro* culture conditions, discussed in chapter 5, the engineered jejunal grafts were tested *in vivo*, to assess the potential for graft survival and further epithelial maturation. Animal transplantation experiments are an essential step when testing the safety and efficacy of tissue engineered organs. There are two types of organ transplantation models: orthotopic (in the correct anatomical position) or heterotopic (in an abnormal position).

Older studies of tissue engineered intestine using synthetic scaffolds were tested orthotopically in rat models of SBS, reported improved survival rates of rats receiving the graft compared to controls[254]. These experiments used full thickness cellular sources, contain mucosa, submucosa and muscle layers of the intestine (first described by Evans et al in 1992)[199]. More recent studies have utilised heterotopic models, whereby the vascularised engineered graft (using rat scaffolds) was anastomosed to the carotid arteries and jugular veins of immunodeficient rats[193]. The grafts constructed over the course of this thesis were purely mucosal and did not have intact vasculature, therefore orthotopic transplantation models were not possible. The options for heterotopic transplantation with these engineered grafts include omental wrapping, insertion under the kidney capsule or subcutaneous transplantation[291,292]. Here, I adopted two approaches to assess the engineered grafts: the kidney capsule model and the subcutaneous model, since these were less invasive and better tolerated by the NSG mice in my experience.

6.2 Kidney capsule transplantation

Jejunal grafts were engineered for all in vivo transplantation experiments as previously described in the previous chapter, using the experimental timeline illustrated in figure 5.2a. In the kidney capsule model, grafts engineered using human scaffolds were more difficult to insert under the tight capsule, due to dimensional limitations. Therefore the jejunal grafts formed using piglet scaffolds were

exclusively transplanted in this model. To recap, no fibroblasts were injected into the piglet scaffolds. Organoids were seeded on day 0 and maintained in static culture conditions for 4 days, before converting the culture to the dynamic system for a further 7 days. At Day 11 on the *in vitro* timeline, grafts were implanted into the animals. Graft epithelial morphology at the point of implantation was equivalent to the data presented in figure 5.4 (i.e. including the presence of differentiated cells). After 7 days *in vivo*, the kidneys were harvested and macroscopic evidence of neovascularisation was noted on the graft (Fig 6.1a).

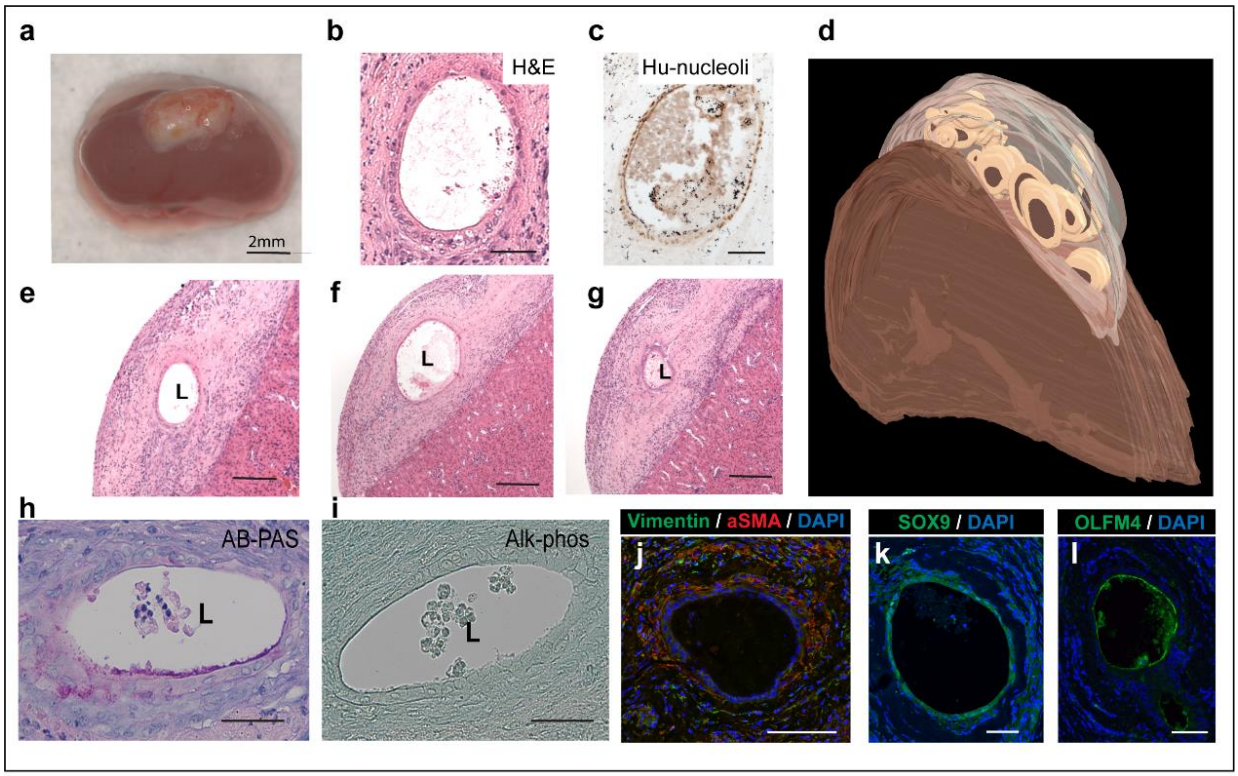

Figure 6.1 - *In vivo* kidney capsule transplantation and characterisation of jejunal grafts: (a) Macroscopic image of the kidney collected after implantation of a jejunal graft in the kidney capsule. (b-c) Histology of a transplanted jejunal graft as analyzed by H&E and human nucleoli staining. (d) 3D volume-rendered model of the jejunal graft structure after transplantation under the kidney capsule. (e-g) Serial H&E staining of a jejunal graft 1 week after transplantation in vivo under the kidney capsule. L indicates graft lumen. (h-i) Histological staining to show the epithelial ring of jejunal grafts are negative for goblet cell (Alcian Blue - Periodic Acid Schiff, AB-PAS) and enterocyte marker (Alkaline Phosphatase, Alk-phos). (j-l) Representative immunofluorescence images of transplanted jejunal grafts obtained using antibodies to the indicated markers.

Surgery performed by Paola Bonftanti (Crick)

Serial histological sectioning along the length of the scaffold demonstrated the presence of continuous rings of intestinal epithelium that were positive for human nucleoli staining (Fig. 6.1b-c, e-g). 3D volume reconstruction of the serial histological section data revealed segments of continuous tubular structures maintained throughout the graft, indicating formation of intestinal lumens (Fig. 6.1d). Unexpectedly, immunostaining of AB-PAS and ALPI was largely negative in the graft, suggesting a lack of goblet cell and enterocyte differentiation in the engineered graft after engraftment under the kidney capsule (Fig. 6.1h-i). No evidence of intestinal cell differentiation was ever seen in any of the experimental replicates grafts that were harvested from the kidney capsule transplantation experiments. However, a large population of cells co-expressing vimentin and αSMA was noted in the stroma surrounding the epithelial rings, indicating that there is a strong infiltration of host myofibroblasts from the kidney into the scaffold (Fig. 6.1j). Immunofluorescent staining confirmed the epithelial cells forming lumen were composed of undifferentiated intestinal cells that demonstrated high expression of stem cell markers OLFM4 and SOX9 (Fig. 6.1k-l).

6.3 Subcutaneous transplantation

In order to enable live *in vivo* tracking of cellular growth on the scaffolds, jejunal PDOs were labelled with a GFP-luciferase reporter prior to seeding on scaffolds (Fig. 6.2a). The GFP reporter in the plasmid construct enabled monitoring of epithelial growth on scaffolds whilst in the *in vitro* culture period (Fig 6.2b). Meanwhile, the luciferase reporter in the plasmid construct enabled the live tracking of cellular growth after transplantation *in vivo* with live bioluminescence imaging (Fig 6.2c).

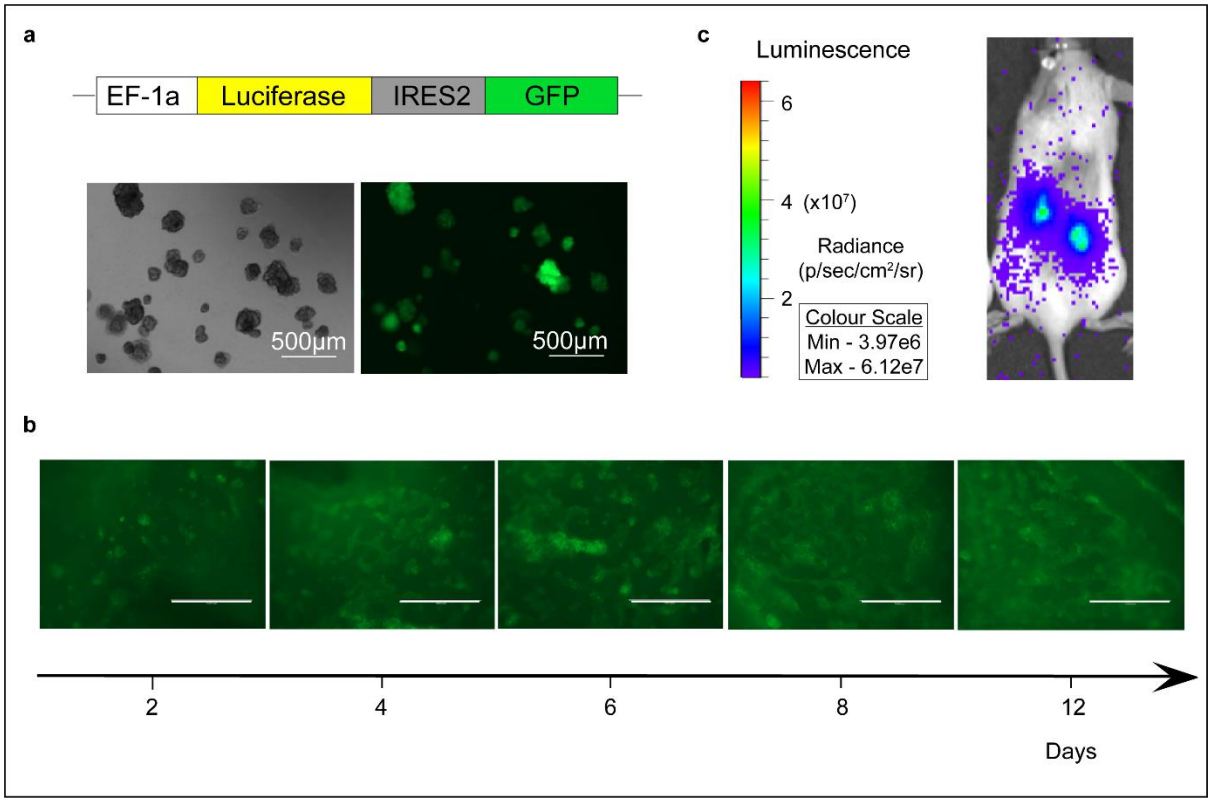

Figure 6.2 - Live tracking of intestinal epithelial cell growth *in vitro* and *in vivo*: (a) Schematic representation of the luciferase-GFP reporter plasmid (top) used to label jejunal organoids (bottom). (b) Live imaging of piglet grafts in culture from days 2 to 12 prior to transplantation. Scale bars represent 1000µm. (c) Left, luminescence scale bar showing bioluminescence signal intensity; Right, representative image of live bioluminescence imaging in the subcutaneous transplantation model.

These engineered grafts were then transplanted in subcutaneous pockets of NSG mice, an approach that allows engraftment of larger dimension constructs. Initial experiments were performed using jejunal grafts formed on piglet scaffolds to allow direct comparison of data with the kidney capsule model. Similar to kidney capsule model, lumens of human nucleoli-positive intestinal epithelial cells were readily detected as early as 7 days after implantation (Fig. 6.3a). However, in contrast to the kidney capsule data, ALPI^{+} enterocytes and AB-PAS^{+} goblet cells were detected in the grafts (Fig. 6.3b-c). It is also important to note that there were significantly less stromal cells surrounding the epithelial rings of the grafts analysed, when compared to grafts in the kidney capsule transplantation.

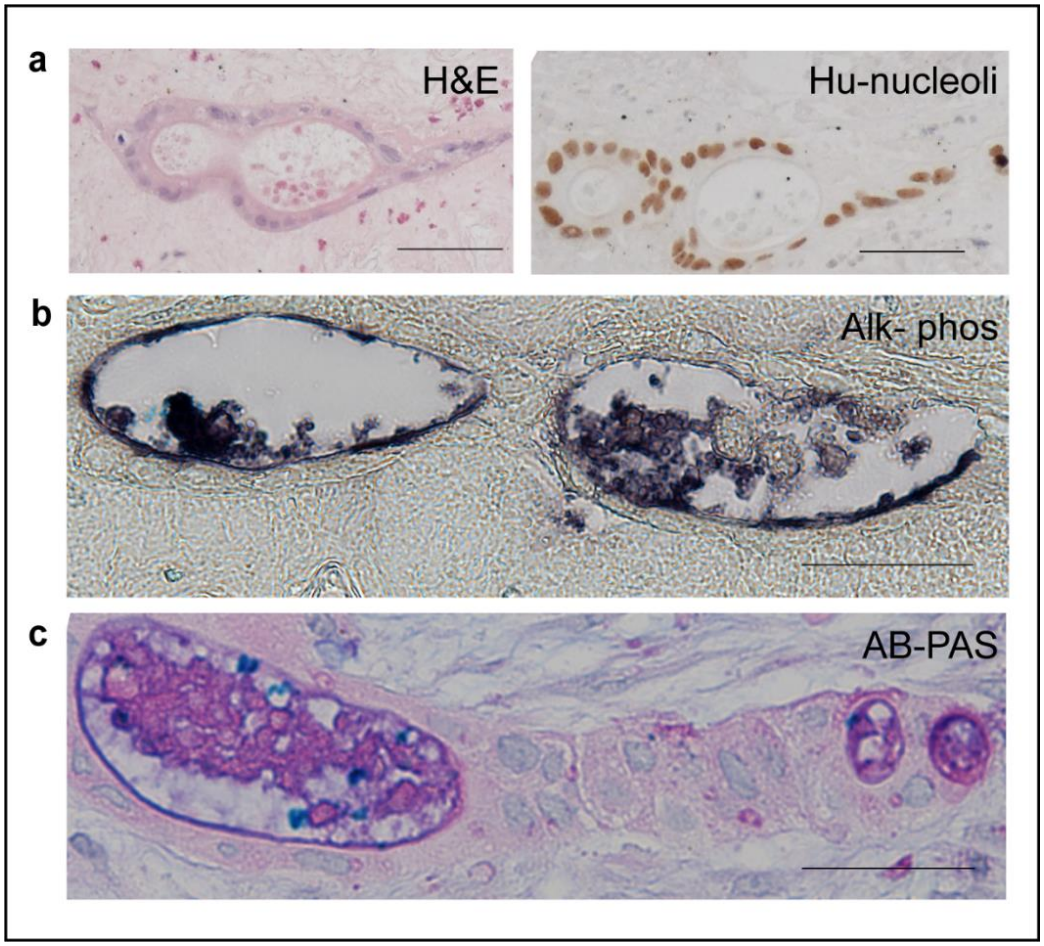

Figure 6.3 - *In vivo* subcutaneous transplantation of jejunal grafts formed using piglet scaffolds: (a) Left, representative image of haematoxylin and eosin staining of the jejunal graft epithelium. Right, representative image of human nucleoli immunostaining marking the jejunal graft epithelium. (b-c) Histological staining with alkaline phophatase (Alk-phos) marking the enterocyte brush border, and alcian blue - periodic acid schiff (AB-PAS) marking goblet cells.

Next, experiments progressed towards transplantation of larger dimensions of jejunal grafts formed on human SI or colon scaffolds. However initial histological analyses yielded largely poor results, with no intestinal epithelial rings seen on serial sectioning of the grafts and minimal stromal cell infiltration from the host.

In order to enhance the survival of transplanted jejunal grafts forming using human scaffolds in this model, the role of Teduglutide was investigated for tissue engineering applications. Teduglutide is a clinically licenced drug used in patients with intestinal failure to promote intestinal adaptation by increasing villus height and crypt depth[59,60]. The receptor (GLP2R) of Teduglutide was fuond to be expressed in both human jejunal fibroblasts and in human jejunal organoids (Fig. 6.4a). Therefore, primary human jejunal fibroblasts (characterisation data shown in section 3.3) were expanded and

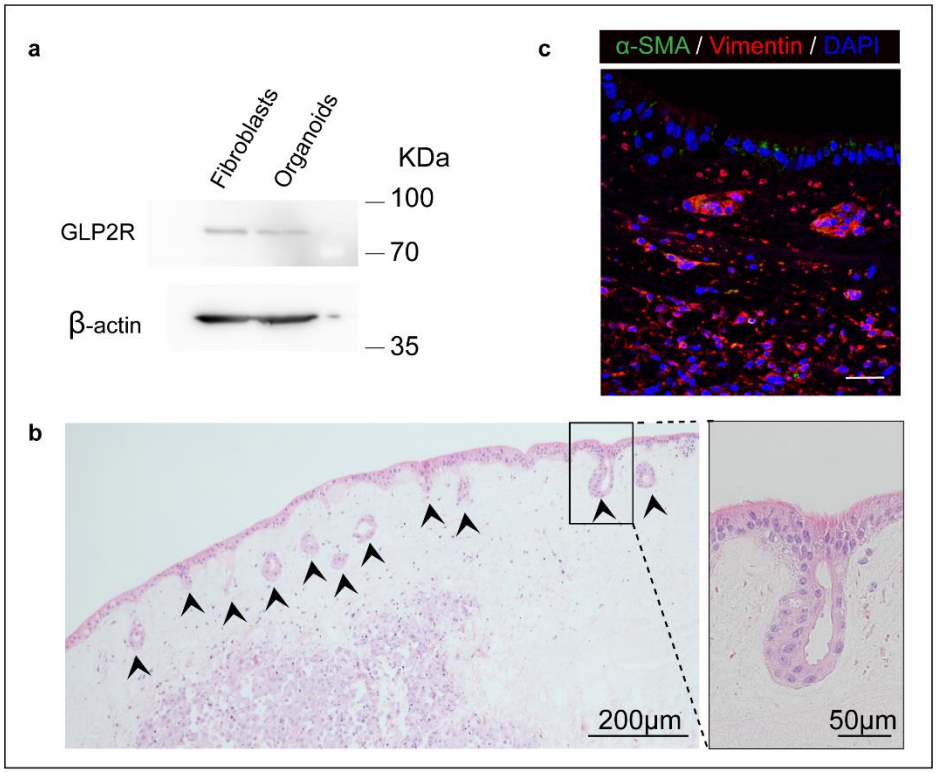

Figure 6.4 - Co-culture of jejunal stromal and epithelial cells on human scaffolds: (a) Western blot analysis confirming the expression of the GLP2R in human jejunal fibroblasts and jejunal organoids [both from patient 2] when co-cultured in vitro. (b) Representative H&E staining of a jejunal graft collected at day 11, showing a monolayer of epithelial cells with invaginating crypt compartments marked by black arrowheads (colon scaffold, patient 2). Left, overview; right, close-up view. (c) Representative immunofluorescent staining of an engineered graft [patient 7 fibroblasts; patient 2 colon scaffold] using the indicated antibodies.

injected into human SI and colon scaffolds intended for *in vivo* subcutaneous transplantation. In these experiments, fibroblasts were first injected into the scaffolds at the mucosal-submucosal boundary, and maintained in static culture for 3 days to recreate the native microenvironment prior organoids seeding (Fig. 5.2a-b). Histological analysis of these grafts showed full coverage by columnar epithelial cells on the scaffold surface with visible crypt units (Fig. 6.4b). Co-staining of the grafts indicated abundant fibroblasts that were predominantly vimentin^{+} and αSMA^{-}, located subepithelially before transplantation (Fig. 6.4c).

Co-cultured grafts were transplanted subcutaneously into NSG mice which were administered either a daily subcutaneous dose of teduglutide (0.2 mg/kg) or vehicle (PBS) after transplantation. Two weeks after transplantation, serial sectioning showed intestinal lumens populated with epithelial cells in 10.4% ± 0.7% of sections for all grafts receiving teduglutide, in comparison to only 0.28% ± 0.6% of sections for all grafts in the control group (P = 0.0271; Fig. 6.5a). Grafts were significantly thicker than earlier analysed piglet scaffolds, where the three histological layers (mucosa, submucosa and muscularis) of the graft were clearly preserved after transplantation (Fig. 6.5b). A distinctive monolayer of human intestinal epithelial cells was formed on the mucosal luminal surface of the implanted grafts. Proliferating cells (indicated by PCNA and EdU staining) were detected in both epithelial and pericryptal stromal cells of the scaffold (Fig. 6.5c). Electron microscopy analysis identified mucous granules within the graft epithelial cells, suggesting the presence of early goblet cell differentiation (Fig. 6.5d). Immunofluorescent staining for pancytokeratin and e-cadherin confirmed the epithelial identity of the epithelial monolayer (Fig. 6.5 e-f). Expression of stromal marker vimentin further confirmed the survival of human intestinal fibroblasts in the injected grafts after transplantation (Fig. 6.5e). Importantly, the jejunal-specific brush border enzyme sucrase isomaltase was broadly expressed in majority of the jejunal graft (Fig. 6.5f), indicating that human ECM scaffold supports and maintains intestinal epithelial cell differentiation towards enterocyte lineage *in vivo*. Similar to piglet scaffold data, co-cultured jejunal grafts formed using human scaffolds were also able to form luminal structures after transplantation (Fig 6.6a) with histological evidence of vascularisation within the graft (Fig. 6.6b).

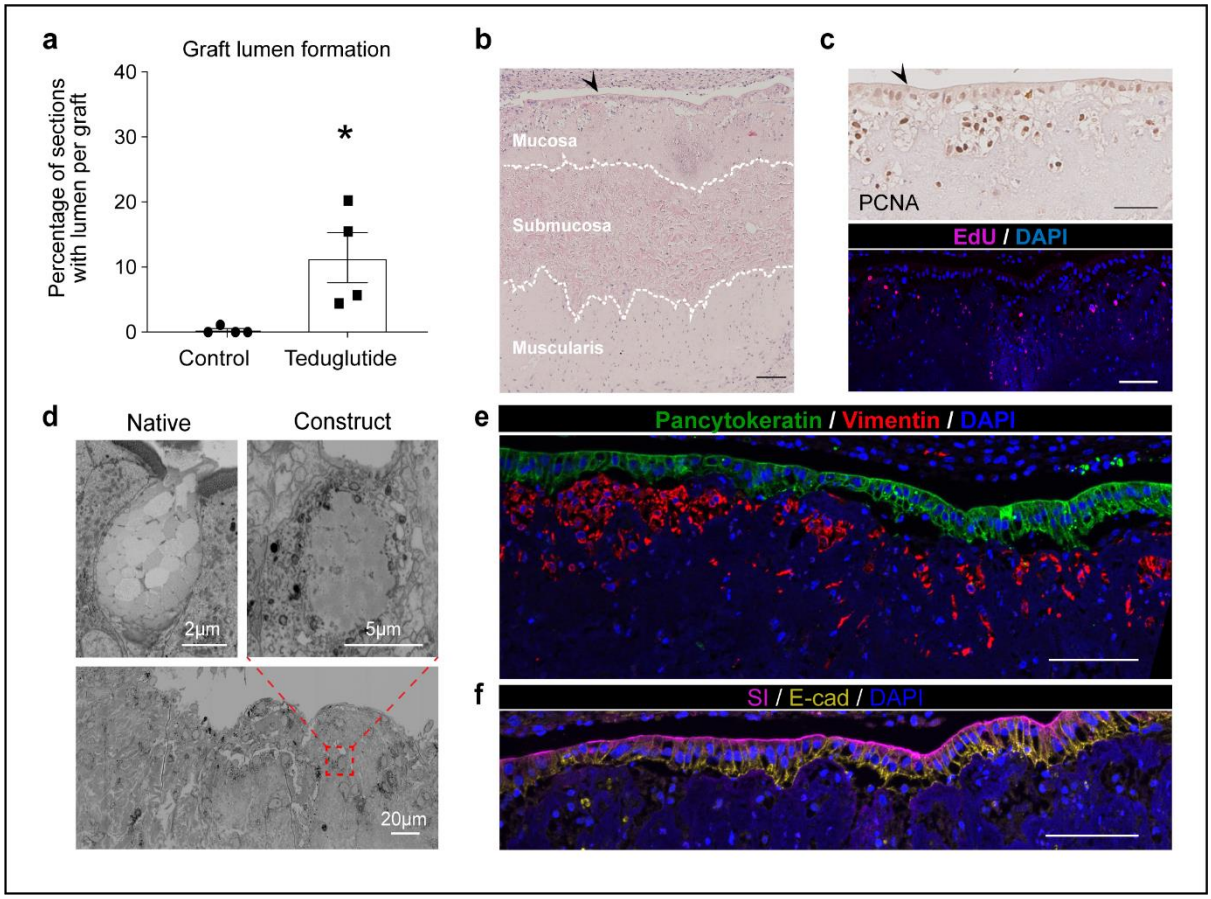

Figure 6.5 - Teduglutide treatment enhances *in vivo* survival of engineered human jejunal grafts: (a) Quantification of the formation of lumens within jejunal grafts following subcutaneous implantation in teduglutide-treated versus control mice. Data represent mean ± s.e.m. for n = 4 independently transplanted jejunal grafts after 2 weeks *in vivo*. Mann Whitney U Test, *P = 0.0286. (b) Representative histology of graft indicating the mucosa, submucosa and muscularis structure. Arrowhead indicates polarized columnar jejunal cells. (c) Immunostaining analyses of cell proliferation as indicated by PCNA (top) and EdU (bottom). Arrowhead indicates the jejunal epithelium. (d) Electron microscopy analysis identifying mucous granules of goblet cells in the native intestine (top left) and a jejunal construct (bottom and top right). (e-f) Representative immunostaining of a jejunal graft using antibodies to epithelial markers (pancytokeratin and e-cadherin), stromal marker (vimentin) and jejunal brush border enzyme (sucrase isomaltase). Grafts in (a) were formed using human colon scaffolds from patient 2. Grafts in (b-f) were formed using human SI scaffolds from patient 1. All organoids and fibroblasts used in this figure originated from patient 2. Scale bars represent 50µm unless specified.

Surgery performed by Paola Bonftanti and Sara Camponiti (Crick)

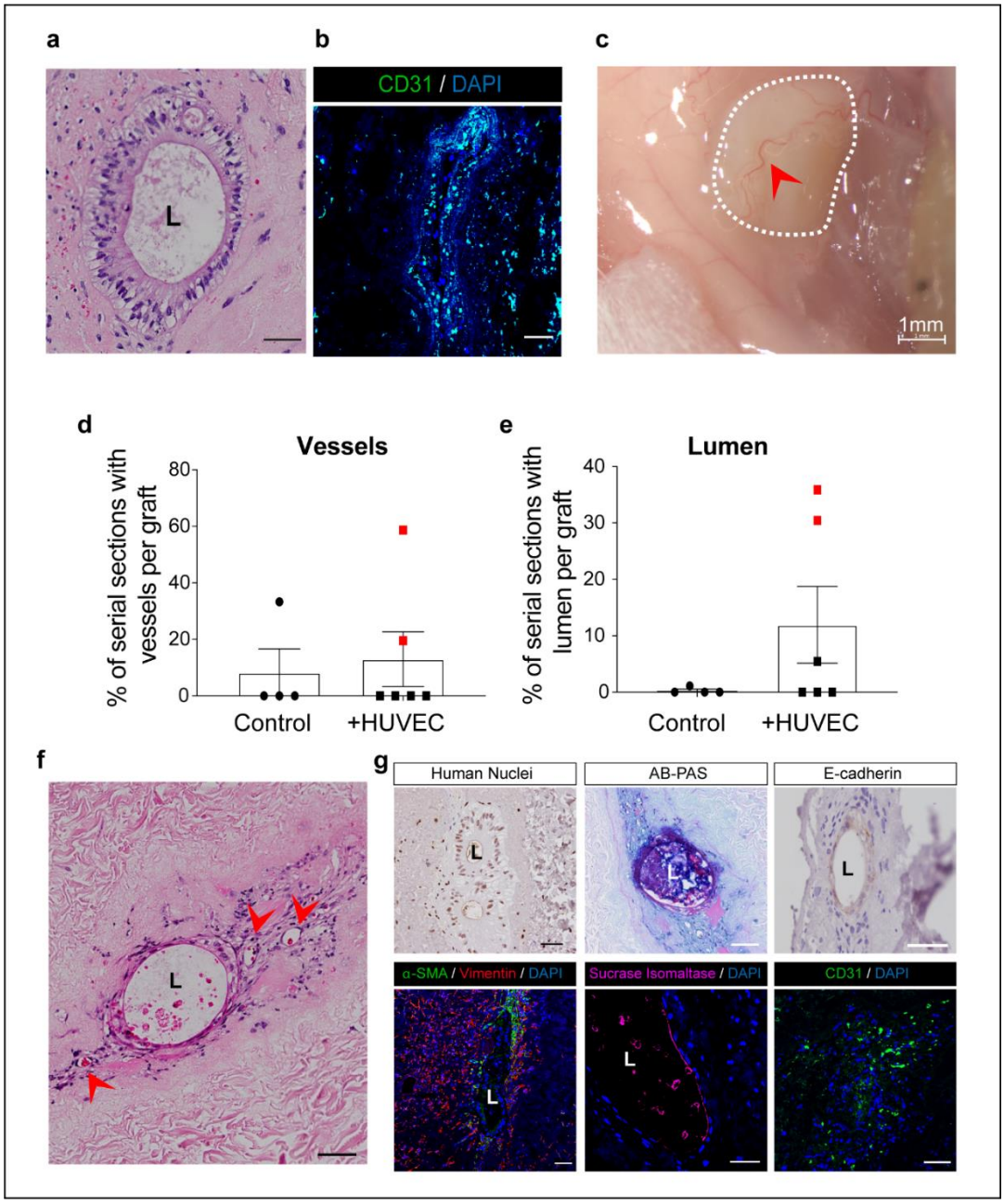

Figure 6.6 - Engineered jejunal graft vascularisation after *in vivo* subcutaneous transplantation (a) H&E staining of luminal ring (L) of intestinal epithelium present on grafts harvested following 2 weeks of subcutaneous transplantation from teduglutide treated mice. (b) Immunostaining of CD31 (green) in the same graft. (c) Macroscopically visible neovascularization (red arrowhead) on a transplanted graft (white outline) formed of human SI scaffold [patient 24]. (d) Quantification of jejunal graft vessel and lumen formation (e) per grafts injected with HUVECs or control (fibroblasts alone). N=6 grafts, [SI scaffold - patient 1 & 24; colon scaffold - patient 2]. Grafts containing vessels are indicated by red points. Data represent mean ± s.e.m. Mann Whitney U test: vessels, p=0.8333; lumen, p=0.2857. (f) Representative image indicating the proximity of blood vessels (red arrowheads) to the epithelial lumen (L) grafts injected with HUVECs. (g) Representative histology of grafts injected with HUVECs, using the indicated antibodies/stainings. L indicates lumen. Intestinal epithelial cells. All scale bars represent 50µm unless specified otherwise.

Data acquired with help from Isobel Massie and Lucinda Tullie (Crick)

Finally, the effect of increased vascularization of the grafts was investigated by introducing an additional injection of human umbilical vein endothelial cells (HUVECs) into human scaffolds 1 day before subcutaneous transplantation. On harvesting grafts from the mice at 2 weeks post transplantation, macroscopically visible vessels were present (Fig. 6.6c). From the six grafts injected with HUVECs, two contained vessels microscopically, and these same two scaffolds had visible lumens on 33% of the serial sections (Fig. 6.6 d-e). Conversely, in the remaining four scaffolds without vessels, lumens were detected in only 1.4 ± 3% of the serial sections (Fig. 6.6 d-e). Blood vessels were often observed in close proximity to the lumens (Fig. 6.6f), suggesting that improved vascularization enhances epithelial cell survival. Histological analysis confirmed the presence of goblet cells and sucrase isomaltase^{+} enterocytes in epithelial lumens surrounded by a mixed population of vimentin^{+} or SMA^{+} fibroblasts (Fig 6.6g). CD31^{+} staining indicates the presence of endothelial cells within the graft (Fig. 6.6g).

6.4 Discussion

In this chapter, two models of *in vivo* models of ectopic transplantation were used to test the potential for survival of the engineered jejunal grafts: [1] under the kidney capsule and [2] in subcutaneous pockets. In contrast, other research groups have commonly adopted ectopic models of omental wrapping transplantation, to test their tissue engineered constructs[251,293]. More recently, in 2017 researchers used a cervical heterotopic transplantation rat model to assess both function and morphology of hiPSC organoid derived grafts formed on rat decellularised SI scaffolds[193]. This particular model has the advantage of being able to connect the vascular supply of the constructs to the carotid artery and jugular vein, whilst standard ectopic transplantation models (omentum, kidney capsule and subcutaneous) do not directly connect to the host vascular system. This heterotopic transplantation approach enables more sophisticated methods of *in vivo* functional testing of the graft by systemic venous sampling and positron emission tomography scanning to confirm uptake of labelled glucose and fatty acids[193].

Neither of the two chosen transplantation models in my studies were completely however both offered distinct *in vivo* microenvironments with regards to stromal cell infiltration, vascularisation and impact on epithelial cell identity. Therefore, both models represented opportunities to learn more about the potential behaviour of the jejunal grafts *in vivo*, informing future studies. Significant differences were noted in epithelial morphology and identity on harvesting and analysing grafts after transplantation. In the kidney capsule transplantation model, the intestinal epithelium of grafts remained in a predominantly undifferentiated state. This may be due to high levels of host myofibroblast infiltration into the graft, that recapitulates the stem cell niche of the intestinal crypt compartment. In contrast, lower levels of stromal cell infiltration seen in the subcutaneous transplantation model seemed to promote more differentiation of the graft epithelium. Although the subcutaneous transplantation models allow more space for larger dimension grafts that are formed using human SI or colon scaffolds, co-culture of fibroblasts with epithelial cells, and the use of teduglutide, were required in order to enhance graft epithelial survival and maturation *in vivo*. This may be due to the increased thickness of these jejunal grafts impeding the infiltration of host endothelial or stromal cells required for epithelial survival. Using an amended *in vitro* culture timeline, jejunal epithelial and stromal cell populations were successfully co-cultured within the scaffolds prior to transplantation. Reduced angiogenesis within tissue-engineered grafts can limit the survival of cells on the graft. HUVECs were therefore injected carefully into seeded grafts one day prior to transplantation to study the impact of this on vessel formation within the human scaffolds, and also lumen formation in grafts. Overall, jejunal specific identity of the grafts was maintained in engineered patient-derived grafts after transplantation *in vivo*.

The most ideal *in vivo* transplantation model would be one where the grafts can be transplanted orthotopically in continuum with native small intestine, however this surgical technique is complex and was beyond the scope of this thesis. These orthotopic experiments have been performed in published studies from 2004, in rats following massive small bowel resection when assessing TESI constructs (discussed earlier in section 1.5.3), with excellent results[254]. The greatest advantage of

orthotopic transplantation models is exposure of the tissue engineered grafts to the native microenvironment and signalling pathways of the gut.

Attempts to increase the length of jejunal graft survival *in vivo* past the 2-week time point using HUVECs were not successful as few luminal rings were seen when grafts were harvested at later time points. This is a particular disadvantage of transplanting large grafts in ectopic sites in small animal studies. Kitano *et al*., demonstrated an elegant solution to the problem of vascularisation *in vivo*, by using HUVECs to revascularise intestinal grafts *in vitro*, prior to seeding hiPSC derived epithelial cells *in vitro* (in a 4-week long bioreactor seeding protocol). When transplanted heterotopically grafts survived for up to 4 weeks. In future studies, replacing HUVECs with primary patient-derived endothelial cells are immensely important for improving the translational value of these experiments for patients in the clinic.

7. Conclusions and Future Perspectives

In this progressive work of engineering transplantable human jejunal mucosal grafts, I sought to derive cells autologously from children with IF, or predisposing conditions, in order to repopulate human decellularised scaffolds. I establish clinically relevant protocols for timely intestinal graft reconstruction using patient-derived materials of post-natal adult somatic intestinal stem cells and human biological intestinal decellularized scaffolds. In doing so, the data presented in this thesis demonstrates the feasibility and proximity of translating this approach in clinical practice in the future, and encourages further studies into bringing tissue engineering technologies using patients' cells and patients' biological scaffolds for children with IF.

Firstly, autologous primary somatic ISCs were derived from relatively small pieces of endoscopically acquired tissue, showing the applicability of this method for children with minimal lengths of residual functional SI *in situ*. The organoids can be efficiently expanded *in vitro* without losing their intrinsic location specific functional identity and differentiation potential. This data would also support proposals to introduce the practice of isolating and banking of intestinal epithelial organoids and stromal cells as a new clinical standard at the point of intestinal resections for at risk children, for example in cases of necrotising enterocolitis in the neonatal period. This would give such a child the prospect of a patient-customised graft being constructed should the clinical need arise in the future.

Other recent studies that opted to use iPSC derived intestinal organoids to reseed rat decellularized scaffolds for tissue engineering, showed excellent *in vitro* and *in vivo* morphology of the engineered epithelial layer together with endothelialisation of the rat scaffolds[193]. Whilst iPSC-sourced intestinal cells have the advantage of being applied to children who have lost their entire small intestine (although rare clinically), autologous sources of primary somatic stem cells remain preferable to induced pluripotent or embryonic stem sources for therapeutic use in children, due to their safety

profile. Importantly, the PDOs and fibroblasts collected in the biobank survived well after repeated freeze-thawing cycles throughout this project.

This data also confirms that under expansion conditions ISCs do not lose their location specific functional identity and differentiation capacity, following significant expansion culture periods *in vitro*. The significance of fibroblasts in the reconstruction of the ISC niche is also demonstrated *in vitro* and *in vivo*, providing support to the epithelial layer of the graft. The organoid characterisation data presented in this thesis on location specification of intestinal organoids expanded from the duodenum, jejunum and ileum confirms the results of previously published studies[265]. This raises an important question on the applicability of this tissue engineering strategy on children who have lost their entire jejunum. Since the data demonstrates that organoids derived from the duodenum have relatively lower expression brush border digestive enzymes sucrase isomaltase, this suggests that in order the form a jejunal graft for a patient, they must have at least a few centimetres of jejunum left *in situ*. This is an important limitation of this data. It is currently unknown whether it is possible to manipulate ISCs-derived from the duodenum or ileum *in vitro*, in order to promote the expression of jejunal specific enterocytes. This would be a significant advantage for patients who have lost their entire jejunum.

Biological scaffolds, derived from human decellularized SI and colon, were used in this study that focussed on engineering transplantable grafts with jejunal-specific nutritional function. This represents a particular novelty of this study, as no other publications have investigated the use of human intestinal decellularized scaffolds for transplantation purposes. One publication extensively investigated the use of human colon decellularized scaffolds for modelling colon cancer, leading to the identification of 38 candidate invasion-driver genes[250]. Another brief publication reported the use human SI decellularized scaffolds with intestinal myofibroblasts, for modelling intestinal fibrosis *in vitro*[249]. Other studies that are focussed on transplantation purposes, rather than *in vitro* modelling purposes, use synthetic scaffold sources or animal biological scaffold sources[193,254,255].

An important limitation to the source of human tissue used in these studies, is not having been able to decellularize the tissue through perfusion of the vascular tree supplying the intestinal explants. However, SEM was used to demonstrate perfect suitability of DET decellularization by gentle immersion and agitation for maintaining the ultrastructure features of human intestinal tissues. This enabled the fabrication of immunologically tolerogenic scaffolds for regenerating the human intestine[230]. The ability of decellularised scaffolds to retain their biological and structural features after cryopreservation has previously been demonstrated, enhancing the potential of these scaffolds to become "off-shelf" clinical products[179].

Previous studies have illustrated the preservation of biological ECM molecules in rodent scaffolds using mainly histological and immunohistochemical evaluations[230]. While these approaches are useful in assessing the spatial distribution of major ECM components, they remain mostly qualitative in their nature. Biochemical quantification of collagens and glycosaminoglycans (GAGs) extracted from digested scaffold material is limited to providing bulk information only. Here, I adopted a three-pronged approach to improving the depth of understanding of the biological properties retained in human derived intestinal scaffolds - namely electron microscopy, Raman spectroscopy and mass spectrometry. Raman spectroscopy is a vibrational laser scattering technique that provides a biochemical fingerprint of tissue composition. It is a valuable tool that provides data on the biochemical conformation of proteins, carbohydrates, lipids and nucleic acids with submicrometer spatial resolution[272]. Raman spectroscopy was employed to provide comparative insights into the complexities of the native human intestinal tissue and their resultant decellularised scaffold biomaterials. The results illustrated the overall conservation of biomolecular cues between the histological layers of the native and scaffold mucosa, submucosa and muscularis histological layers. I then applied Raman imaging approach to compare the spectral signatures arising from the human small intestine and colon scaffolds. Quite remarkably, the data illustrated there to be significant spectral commonality specific to the mucosal layers of both SI and colon scaffolds. Mass spectrometry

comparing the small intestine and colon scaffolds supported the Raman spectroscopy data, confirming overall conservation in the global and matrix protein profiles of the two scaffold products.

The scaffold characterisation data presented here provided an in-depth insight into the biochemical features of the human decellularized intestinal scaffolds, which had not been investigated in previous publications using human SI and colon scaffolds for *in vitro* cancer or fibrosis modelling studies[249,250]. This non-biased approach to exploring the scaffolds' biological characteristics led to the concept of investigating the potential of "recycling" colon scaffolds, utilising them to reconstruct functional SI grafts, by allowing the jejunal derived organoids to drive remodelling of the acellular colon matrix. Undeniably, with good patient education, empowerment resources and appropriate stoma nurse support, patients can lead a relatively good quality of life following significant resection of the colon. This is in stark contrast to the detrimental quality of life significant resections of SI bring, due to the malnutrition and recurrent hospitalisations that ensue.

Hence, I sought to collect both human SI and colon scaffolds for the purpose of *in vitro* seedings with human jejunal organoids. In practice, I found that I was able to retrieve more paediatric colon surgical samples than SI, since resections of colon in children are a more commonly planned occurrence than those of the SI. The concept of recycling colonic biomaterial could be applied in clinical practice to derive a bank of allogeneic donor scaffolds, as an alternative source to cadaveric tissue for the derivation of decellularised scaffolds. As yet, unaddressed research questions remain such as: to what extent is disease held in the structural matrix versus the cellular matrix? Therefore, further studies using Raman spectroscopy, electron microscopy, mass spectrometry, as well as other modalities such as imaging mass spectroscopy, RNA-sequencing and spatial transcriptomics on the recellularised scaffolds, would be useful to characterise the scaffolds of intestinal tissue derived from resections due to dysmotility for example.

Moving forwards, I demonstrate that human jejunal organoids are able to engraft, polarise, proliferate and differentiate to express jejunal specific brush border enzymes, on both SI and colon scaffolds.

Despite preservation of the crypt-villus axis on the human decellularised scaffolds, after re-seeding experiments, compartmentalisation of proliferative cells within the crypt domains or differentiated cells within the villus domains, was not seen, as previously published *in-vitro* modelling studies (also discussed in the introduction chapter)[250,286,289]. The epithelial morphology data presented here is most comparable to previous studies that seeded iPSC-derived intestinal organoids onto rat decellularized intestinal scaffolds, where new matrix deposition was noted to be driven by seeded epithelial cells[193].

Intestinal stromal cells (fibroblasts and myofibroblasts) are important sustainers controlling the assembly and turnover of the structural ECM, secreting fibronectins, laminins, collagens, proteolytic enzymes and inhibitors[96]. They also provide growth factors and ligands essential for the intestinal stem cell niche[96]. Intestinal derived fibroblasts were therefore seeded into both human SI and colon scaffolds to aid the survival of the epithelial graft. These findings support the innovative concept of using colon scaffolds for SI graft reconstruction. There are strong clinical implications of this data for two main reasons. Firstly, colon derived from cadaveric donors or resected in children affected by conditions such as Hirschsprung's disease could be decellularized, stored, and donated for therapy. Secondly, in conditions such as midgut volvulus, in which typically the large bowel is preserved, there is the potential to convert the IF patient's own colon to SI by replacing the mucosal layer with jejunal organoids as an alternative treatment solution.

The engineered jejunal grafts proved to be structurally and functionally competent platforms encouraging cell engraftment and vascularisation when transplanted *in vivo*. However, the physiological behaviour of the intestinal grafts differed depending on the site of implantation. In the kidney capsule transplantation model, I observed a greater amount of host myofibroblast (vimentin$^+$, αSMA$^+$) infiltration into the scaffold surrounding the rings of human intestinal epithelium. This mimics the crypt environment of the ISC niche and resulted in less differentiated epithelial cells. Instead, the cells remained highly expressive of stem cell markers OLF4, SOX9. In contrast, I found less infiltration of host myofibroblasts in the subcutaneous transplantation model. The *in vitro* seedings of stromal

cells was an essential step prior to epithelial cell seeding, to allow me to assess the survival of the graft in this model. Teduglutide (a clinically approved drug for use in human trials of IF, and licenced in the EU) was also administered to the NSG mice. I found this approach aided the survival of the ectopically implanted intestinal grafts, where less host infiltration of the scaffolds occurs, however more studies investigating the use of the drug during recellularisation steps are important. Overall this indicates the dual importance of a robust pre-implantation scaffold seeding protocol and appropriate host cell infiltration, in the survival of engineered intestinal grafts *in vivo*.

In conclusion, the novelty of this work stands in the efforts made to isolate, expand and study jejunal intestinal stem cells and intestinal stromal cells specifically from children with intestinal failure, and use these cells to repopulate human derived intestinal scaffolds and form functional and transplantable mucosal grafts. Although this approach was novel in the research field and important for clinical applicability to the IF patient-population in need, it is important to remember that the causes of IF are heterogeneous. Indeed, sourcing patient ISCs from children with IBD or other conditions that retain epithelial mutations may influence the long-term success of the graft, unless underlying disease pathogenic processes are addressed prior to recellularisation and transplantation. More experiments addressing this specific translational need are required, whereby cells from IBD patients are specifically sought and their long-term cell and matrix phenotype of the engineered grafts are studied *in vivo*. Original approaches were adopted to analyse the human scaffold products and new rationales for utilising colon scaffolds for jejunal reconstruction are proposed from this work, thereby addressing the problem of native organ donation. The relatively simple methods employed here can easily be scaled up for pre-clinical testing in larger animal models of orthotopic transplantation. A purely mucosal engineered graft will have a particular clinical impact on paediatric patients with primarily epithelial defects. However, this work also represents an important advance towards a staged layer approach to future full tubular jejunal intestinal reconstruction. Unlike previous publications that focused on iPSCs, synthetic scaffolds or rodent ECM matrix[192-196,294], the use of primary human materials (both cells and decellularized ECM matrix) in this study is a highly relevant

step towards translation. Additionally, the experiments with teduglutide indicate novel tissue engineering applications, promoting the survival of grafts *in vivo*. Whilst this study represents an important conceptual advance towards full thickness intestinal wall construction, significant challenges persist specifically the efficient co-ordinated expansion of human enteric nerves and smooth muscle cells essential for driving peristalsis of the gut. Critical future steps are to focus on capturing data on the global cellular and ECM profile of the engineered graft at both *in vitro* and *in vivo* transplantation stages. This may be achieved by combining single-cell transcriptomics with spatial transcriptomics to map the distribution of cells and compare this to native intestinal tissue. Furthermore, neuromuscular wall regeneration and vascularisation of grafts are vital future experimental steps, while scaling up to *in vivo* pre-clinical testing in orthotopic transplantation models.

Overall, this work represents the first stepwise scalable approach towards using patient cells and biomaterials, for ultimately reconstructing a full thickness intestinal graft for children with irreversible intestinal failure.

8. References

1. Gebbers, J.O. & Laissue, J.A. Immunologic structures and functions of the gut. *Schweizer Archiv fur Tierheilkunde* **131**, 221-238 (1989).
2. Maloy, K.J. & Powrie, F. Intestinal homeostasis and its breakdown in inflammatory bowel disease. *Nature* **474**, 298-306 (2011).
3. Browne, H.P., Neville, B.A., Forster, S.C. & Lawley, T.D. Transmission of the gut microbiota: spreading of health. *Nature Reviews Microbiology* **15**, 531-543 (2017).
4. Sekirov, I., Russell, S.L., Antunes, L.C. & Finlay, B.B. Gut microbiota in health and disease. *Physiological reviews* **90**, 859-904 (2010).
5. Moran, B.J. & Jackson, A.A. Function of the human colon. *The British journal of surgery* **79**, 1132-1137 (1992).
6. Schirmer, M., Garner, A., Vlamakis, H. & Xavier, R.J. Microbial genes and pathways in inflammatory bowel disease. *Nature Reviews Microbiology* **17**, 497-511 (2019).
7. Lloyd-Price, J*., et al.* Multi-omics of the gut microbial ecosystem in inflammatory bowel diseases. *Nature* **569**, 655-662 (2019).
8. Cryan, J.F., O'Riordan, K.J., Sandhu, K., Peterson, V. & Dinan, T.G. The gut microbiome in neurological disorders. *The Lancet. Neurology* **19**, 179-194 (2020).
9. Durack, J. & Lynch, S.V. The gut microbiome: Relationships with disease and opportunities for therapy. *The Journal of experimental medicine* **216**, 20-40 (2019).
10. Moor, A.E*., et al.* Spatial Reconstruction of Single Enterocytes Uncovers Broad Zonation along the Intestinal Villus Axis. *Cell* **175**, 1156-1167.e1115 (2018).
11. Dickson, I. Enterocyte zonation along the intestinal villus reveals a division of labour. *Nature Reviews Gastroenterology & Hepatology* **15**, 717-717 (2018).
12. Birchenough, G.M.H., Johansson, M.E., Gustafsson, J.K., Bergström, J.H. & Hansson, G.C. New developments in goblet cell mucus secretion and function. *Mucosal Immunology* **8**, 712-719 (2015).
13. Gehart, H*., et al.* Identification of Enteroendocrine Regulators by Real-Time Single-Cell Differentiation Mapping. *Cell* **176**, 1158-1173.e1116 (2019).
14. Clevers, H.C. & Bevins, C.L. Paneth Cells: Maestros of the Small Intestinal Crypts. **75**, 289-311 (2013).
15. Bevins, C.L. & Salzman, N.H. Paneth cells, antimicrobial peptides and maintenance of intestinal homeostasis. *Nature reviews. Microbiology* **9**, 356-368 (2011).
16. Schneider, C., O'Leary, C.E. & Locksley, R.M. Regulation of immune responses by tuft cells. *Nature reviews. Immunology* **19**, 584-593 (2019).
17. Mabbott, N.A., Donaldson, D.S., Ohno, H., Williams, I.R. & Mahajan, A. Microfold (M) cells: important immunosurveillance posts in the intestinal epithelium. *Mucosal Immunology* **6**, 666-677 (2013).
18. Barker, N*., et al.* Identification of stem cells in small intestine and colon by marker gene Lgr5. *Nature* **449**, 1003-1007 (2007).
19. Sato, T*., et al.* Paneth cells constitute the niche for Lgr5 stem cells in intestinal crypts. *Nature* **469**, 415-418 (2011).
20. Gehart, H. & Clevers, H. Tales from the crypt: new insights into intestinal stem cells. *Nature reviews. Gastroenterology & hepatology* **16**, 19-34 (2019).
21. Lueschow, S.R. & McElroy, S.J. The Paneth Cell: The Curator and Defender of the Immature Small Intestine. **11**(2020).
22. Ermund, A., Schütte, A., Johansson, M.E., Gustafsson, J.K. & Hansson, G.C. Studies of mucus in mouse stomach, small intestine, and colon. I. Gastrointestinal mucus layers have different properties depending on location as well as over the Peyer's patches. *American journal of physiology. Gastrointestinal and liver physiology* **305**, G341-347 (2013).

23. Heuberger, J.*, et al.* Shp2/MAPK signaling controls goblet/paneth cell fate decisions in the intestine. *Proceedings of the National Academy of Sciences of the United States of America* **111**, 3472-3477 (2014).
24. Rothenberg, M.E.*, et al.* Identification of a cKit(+) colonic crypt base secretory cell that supports Lgr5(+) stem cells in mice. *Gastroenterology* **142**, 1195-1205.e1196 (2012).
25. Walsh, R.M., Aranha, G.V. & Freeark, R.J. Mortality and quality of life after total abdominal colectomy. *Archives of surgery (Chicago, Ill. : 1960)* **125**, 1564-1566 (1990).
26. Lauro, A. & Lacaille, F. Short bowel syndrome in children and adults: from rehabilitation to transplantation. *Expert review of gastroenterology & hepatology* **13**, 55-70 (2019).
27. O'Keefe, S.J.*, et al.* Short bowel syndrome and intestinal failure: consensus definitions and overview. *Clin Gastroenterol Hepatol* **4**, 6-10 (2006).
28. Booth, C.C. The metabolic effects of intestinal resection in man. *Postgrad Med J* **37**, 725-739 (1961).
29. Goulet, O. & Ruemmele, F. Causes and management of intestinal failure in children. *Gastroenterology* **130**, S16-28 (2006).
30. Kalaiselvan, R.*, et al.* Radiation enteritis leading to intestinal failure: 1994 patient-years of experience in a national referral centre. *European Journal of Clinical Nutrition* **68**, 166-170 (2014).
31. Ghatei, M.A.*, et al.* Proglucagon-derived peptides in intestinal epithelial proliferation: glucagon-like peptide-2 is a major mediator of intestinal epithelial proliferation in rats. *Digestive diseases and sciences* **46**, 1255-1263 (2001).
32. Kudsk, K.A., Li, J. & Renegar, K.B. Loss of upper respiratory tract immunity with parenteral feeding. *Annals of surgery* **223**, 629-635; discussion 635-628 (1996).
33. Lewis, S.J., Egger, M., Sylvester, P.A. & Thomas, S. Early enteral feeding versus "nil by mouth" after gastrointestinal surgery: systematic review and meta-analysis of controlled trials. *BMJ (Clinical research ed.)* **323**, 773-776 (2001).
34. Omata, J.*, et al.* Enteral nutrition rapidly reverses total parenteral nutrition-induced impairment of hepatic immunity in a murine model. *Clinical nutrition (Edinburgh, Scotland)* **28**, 668-673 (2009).
35. Saito, H.*, et al.* The effect of route of nutrient administration on the nutritional state, catabolic hormone secretion, and gut mucosal integrity after burn injury. *JPEN. Journal of parenteral and enteral nutrition* **11**, 1-7 (1987).
36. Messing, B.*, et al.* Long-term survival and parenteral nutrition dependence in adult patients with the short bowel syndrome. *Gastroenterology* **117**, 1043-1050 (1999).
37. Cole, C.R., Hansen, N.I., Higgins, R.D., Ziegler, T.R. & Stoll, B.J. Very low birth weight preterm infants with surgical short bowel syndrome: incidence, morbidity and mortality, and growth outcomes at 18 to 22 months. *Pediatrics* **122**, e573-582 (2008).
38. Vanderhoof, J.A. & Langnas, A.N. Short-bowel syndrome in children and adults. *Gastroenterology* **113**, 1767-1778 (1997).
39. Martinez Rivera, A. & Wales, P.W. Intestinal transplantation in children: current status. *Pediatr Surg Int* **32**, 529-540 (2016).
40. Duggan, C.P. & Jaksic, T. Pediatric Intestinal Failure. *The New England journal of medicine* **377**, 666-675 (2017).
41. Guarino, A. & De Marco, G. Natural history of intestinal failure, investigated through a national network-based approach. *Journal of pediatric gastroenterology and nutrition* **37**, 136-141 (2003).
42. Squires, R.H.*, et al.* Natural history of pediatric intestinal failure: initial report from the Pediatric Intestinal Failure Consortium. *The Journal of pediatrics* **161**, 723-728.e722 (2012).
43. Wales, P.W.*, et al.* Neonatal short bowel syndrome: population-based estimates of incidence and mortality rates. *J Pediatr Surg* **39**, 690-695 (2004).

44. Beath, S.V., Gowen, H. & Puntis, J.W. Trends in paediatric home parenteral nutrition and implications for service development. *Clinical nutrition (Edinburgh, Scotland)* **30**, 499-502 (2011).
45. Sacks, A.I., Warwick, G.J. & Barnard, J.A. Early proliferative events following intestinal resection in the rat. *Journal of pediatric gastroenterology and nutrition* **21**, 158-164 (1995).
46. Doldi, S.B. Intestinal adaptation following jejuno-ileal bypass. *Clinical nutrition (Edinburgh, Scotland)* **10**, 138-145 (1991).
47. McDuffie, L.A*., et al.* Intestinal adaptation after small bowel resection in human infants. *J Pediatr Surg* **46**, 1045-1051 (2011).
48. Tappenden, K.A. Intestinal adaptation following resection. *JPEN. Journal of parenteral and enteral nutrition* **38**, 23s-31s (2014).
49. Seiler, K.M*., et al.* Single-Cell Analysis Reveals Regional Reprogramming During Adaptation to Massive Small Bowel Resection in Mice. *Cellular and molecular gastroenterology and hepatology* **8**, 407-426 (2019).
50. Kiela, P.R. & Ghishan, F.K. Physiology of Intestinal Absorption and Secretion. *Best practice & research. Clinical gastroenterology* **30**, 145-159 (2016).
51. Müller, T.D*., et al.* Glucagon-like peptide 1 (GLP-1). *Molecular metabolism* **30**, 72-130 (2019).
52. Drucker, D.J., Erlich, P., Asa, S.L. & Brubaker, P.L. Induction of intestinal epithelial proliferation by glucagon-like peptide 2. *Proceedings of the National Academy of Sciences of the United States of America* **93**, 7911-7916 (1996).
53. Yusta, B*., et al.* Enteroendocrine localization of GLP-2 receptor expression in humans and rodents. *Gastroenterology* **119**, 744-755 (2000).
54. Guan, X*., et al.* GLP-2 receptor localizes to enteric neurons and endocrine cells expressing vasoactive peptides and mediates increased blood flow. *Gastroenterology* **130**, 150-164 (2006).
55. Pedersen, J*., et al.* The glucagon-like peptide 2 receptor is expressed in enteric neurons and not in the epithelium of the intestine. *Peptides* **67**, 20-28 (2015).
56. de Heuvel, E., Wallace, L., Sharkey, K.A. & Sigalet, D.L. Glucagon-like peptide 2 induces vasoactive intestinal polypeptide expression in enteric neurons via phophatidylinositol 3-kinase-γ signaling. *American journal of physiology. Endocrinology and metabolism* **303**, E994-1005 (2012).
57. Deacon, C.F*., et al.* Both subcutaneously and intravenously administered glucagon-like peptide I are rapidly degraded from the NH2-terminus in type II diabetic patients and in healthy subjects. *Diabetes* **44**, 1126-1131 (1995).
58. Hartmann, B*., et al.* In vivo and in vitro degradation of glucagon-like peptide-2 in humans. *The Journal of clinical endocrinology and metabolism* **85**, 2884-2888 (2000).
59. Kim, E.S. & Keam, S.J. Teduglutide: A Review in Short Bowel Syndrome. *Drugs* **77**, 345-352 (2017).
60. Jeppesen, P.B., Gabe, S.M., Seidner, D.L., Lee, H.M. & Olivier, C. Factors Associated With Response to Teduglutide in Patients With Short-Bowel Syndrome and Intestinal Failure. *Gastroenterology* **154**, 874-885 (2018).
61. Metcalfe, C., Kljavin, N.M., Ybarra, R. & de Sauvage, F.J. Lgr5+ stem cells are indispensable for radiation-induced intestinal regeneration. *Cell stem cell* **14**, 149-159 (2014).
62. de Sousa, E.M.F. & de Sauvage, F.J. Cellular Plasticity in Intestinal Homeostasis and Disease. *Cell stem cell* **24**, 54-64 (2019).
63. Baulies, A., Angelis, N. & Li, V.S.W. Hallmarks of intestinal stem cells. *Development (Cambridge, England)* **147**(2020).
64. Montgomery, R.K*., et al.* Mouse telomerase reverse transcriptase (mTert) expression marks slowly cycling intestinal stem cells. *Proceedings of the National Academy of Sciences of the United States of America* **108**, 179-184 (2011).

65. Tian, H.*, et al.* A reserve stem cell population in small intestine renders Lgr5-positive cells dispensable. *Nature* **478**, 255-259 (2011).
66. Takeda, N.*, et al.* Interconversion between intestinal stem cell populations in distinct niches. *Science (New York, N.Y.)* **334**, 1420-1424 (2011).
67. van Es, J.H.*, et al.* Dll1+ secretory progenitor cells revert to stem cells upon crypt damage. *Nature Cell Biology* **14**, 1099-1104 (2012).
68. Asfaha, S.*, et al.* Krt19(+)/Lgr5(-) Cells Are Radioresistant Cancer-Initiating Stem Cells in the Colon and Intestine. *Cell stem cell* **16**, 627-638 (2015).
69. Yan, K.S.*, et al.* Intestinal Enteroendocrine Lineage Cells Possess Homeostatic and Injury-Inducible Stem Cell Activity. *Cell stem cell* **21**, 78-90.e76 (2017).
70. Castillo-Azofeifa, D.*, et al.* Atoh1(+) secretory progenitors possess renewal capacity independent of Lgr5(+) cells during colonic regeneration. *The EMBO journal* **38**(2019).
71. Ayyaz, A.*, et al.* Single-cell transcriptomes of the regenerating intestine reveal a revival stem cell. *Nature* **569**, 121-125 (2019).
72. Tetteh, P.W.*, et al.* Replacement of Lost Lgr5-Positive Stem Cells through Plasticity of Their Enterocyte-Lineage Daughters. *Cell stem cell* **18**, 203-213 (2016).
73. Sei, Y.*, et al.* Mature enteroendocrine cells contribute to basal and pathological stem cell dynamics in the small intestine. *American journal of physiology. Gastrointestinal and liver physiology* **315**, G495-g510 (2018).
74. Buczacki, S.J.*, et al.* Intestinal label-retaining cells are secretory precursors expressing Lgr5. *Nature* **495**, 65-69 (2013).
75. Yu, S.*, et al.* Paneth Cell Multipotency Induced by Notch Activation following Injury. *Cell stem cell* **23**, 46-59.e45 (2018).
76. Jones, J.C.*, et al.* Cellular Plasticity of Defa4(Cre)-Expressing Paneth Cells in Response to Notch Activation and Intestinal Injury. *Cellular and molecular gastroenterology and hepatology* **7**, 533-554 (2019).
77. Schmitt, M.*, et al.* Paneth Cells Respond to Inflammation and Contribute to Tissue Regeneration by Acquiring Stem-like Features through SCF/c-Kit Signaling. *Cell reports* **24**, 2312-2328.e2317 (2018).
78. Laurie, G.W., Leblond, C.P. & Martin, G.R. Localization of type IV collagen, laminin, heparan sulfate proteoglycan, and fibronectin to the basal lamina of basement membranes. *The Journal of cell biology* **95**, 340-344 (1982).
79. Farin, H.F.*, et al.* Visualization of a short-range Wnt gradient in the intestinal stem-cell niche. *Nature* **530**, 340-343 (2016).
80. Clevers, H. & Nusse, R. Wnt/β-catenin signaling and disease. *Cell* **149**, 1192-1205 (2012).
81. Gregorieff, A.*, et al.* Expression pattern of Wnt signaling components in the adult intestine. *Gastroenterology* **129**, 626-638 (2005).
82. Kabiri, Z.*, et al.* Stroma provides an intestinal stem cell niche in the absence of epithelial Wnts. *Development (Cambridge, England)* **141**, 2206-2215 (2014).
83. VanDussen, K.L.*, et al.* Notch signaling modulates proliferation and differentiation of intestinal crypt base columnar stem cells. *Development (Cambridge, England)* **139**, 488-497 (2012).
84. Demitrack, E.S. & Samuelson, L.C. Notch regulation of gastrointestinal stem cells. *The Journal of physiology* **594**, 4791-4803 (2016).
85. Stamataki, D.*, et al.* Delta1 expression, cell cycle exit, and commitment to a specific secretory fate coincide within a few hours in the mouse intestinal stem cell system. *PloS one* **6**, e24484 (2011).
86. Sancho, R., Cremona, C.A. & Behrens, A. Stem cell and progenitor fate in the mammalian intestine: Notch and lateral inhibition in homeostasis and disease. *EMBO reports* **16**, 571-581 (2015).

87. Philpott, A. & Winton, D.J. Lineage selection and plasticity in the intestinal crypt. *Current opinion in cell biology* **31**, 39-45 (2014).
88. He, X.C.*, et al.* BMP signaling inhibits intestinal stem cell self-renewal through suppression of Wnt-beta-catenin signaling. *Nature genetics* **36**, 1117-1121 (2004).
89. Kosinski, C.*, et al.* Gene expression patterns of human colon tops and basal crypts and BMP antagonists as intestinal stem cell niche factors. *Proceedings of the National Academy of Sciences of the United States of America* **104**, 15418-15423 (2007).
90. Cai, J.*, et al.* The Hippo signaling pathway restricts the oncogenic potential of an intestinal regeneration program. *Genes & development* **24**, 2383-2388 (2010).
91. Barry, E.R.*, et al.* Restriction of intestinal stem cell expansion and the regenerative response by YAP. *Nature* **493**, 106-110 (2013).
92. Beumer, J. & Clevers, H. Regulation and plasticity of intestinal stem cells during homeostasis and regeneration. *Development (Cambridge, England)* **143**, 3639-3649 (2016).
93. van den Brink, G.R. Hedgehog signaling in development and homeostasis of the gastrointestinal tract. *Physiological reviews* **87**, 1343-1375 (2007).
94. Madison, B.B.*, et al.* Epithelial hedgehog signals pattern the intestinal crypt-villus axis. *Development (Cambridge, England)* **132**, 279-289 (2005).
95. Sato, T.*, et al.* Paneth cells constitute the niche for Lgr5 stem cells in intestinal crypts. *Nature* **469**, 415-418 (2011).
96. Meran, L., Baulies, A. & Li, V.S.W. Intestinal Stem Cell Niche: The Extracellular Matrix and Cellular Components. *Stem cells international* **2017**, 7970385 (2017).
97. Powell, D.W., Pinchuk, I.V., Saada, J.I., Chen, X. & Mifflin, R.C. Mesenchymal cells of the intestinal lamina propria. *Annual review of physiology* **73**, 213-237 (2011).
98. Powell, D.W.*, et al.* Myofibroblasts. II. Intestinal subepithelial myofibroblasts. *The American journal of physiology* **277**, C183-201 (1999).
99. Francoeur, C.*, et al.* Degeneration of the pericryptal myofibroblast sheath by proinflammatory cytokines in inflammatory bowel diseases. *Gastroenterology* **136**, 268-277.e263 (2009).
100. McKaig, B.C., McWilliams, D., Watson, S.A. & Mahida, Y.R. Expression and regulation of tissue inhibitor of metalloproteinase-1 and matrix metalloproteinases by intestinal myofibroblasts in inflammatory bowel disease. *The American journal of pathology* **162**, 1355-1360 (2003).
101. da Silva Meirelles, L., Chagastelles, P.C. & Nardi, N.B. Mesenchymal stem cells reside in virtually all post-natal organs and tissues. *Journal of cell science* **119**, 2204-2213 (2006).
102. Uccelli, A., Moretta, L. & Pistoia, V. Mesenchymal stem cells in health and disease. *Nature Reviews Immunology* **8**, 726-736 (2008).
103. Le Blanc, K. & Mougiakakos, D. Multipotent mesenchymal stromal cells and the innate immune system. *Nature Reviews Immunology* **12**, 383-396 (2012).
104. Murphy, M.B., Moncivais, K. & Caplan, A.I. Mesenchymal stem cells: environmentally responsive therapeutics for regenerative medicine. *Experimental & molecular medicine* **45**, e54 (2013).
105. Sémont, A.*, et al.* Mesenchymal stem cell therapy stimulates endogenous host progenitor cells to improve colonic epithelial regeneration. *PloS one* **8**, e70170 (2013).
106. Saha, S.*, et al.* Bone marrow stromal cell transplantation mitigates radiation-induced gastrointestinal syndrome in mice. *PloS one* **6**, e24072 (2011).
107. Chen, H.*, et al.* Pre-activation of mesenchymal stem cells with TNF-α, IL-1β and nitric oxide enhances its paracrine effects on radiation-induced intestinal injury. *Scientific reports* **5**, 8718 (2015).
108. Gong, W.*, et al.* Banking human umbilical cord-derived mesenchymal stromal cells for clinical use. *Cell transplantation* **21**, 207-216 (2012).

109. Dhere, T.*, et al.* The safety of autologous and metabolically fit bone marrow mesenchymal stromal cells in medically refractory Crohn's disease - a phase 1 trial with three doses. *Alimentary pharmacology & therapeutics* **44**, 471-481 (2016).
110. Duijvestein, M.*, et al.* Autologous bone marrow-derived mesenchymal stromal cell treatment for refractory luminal Crohn's disease: results of a phase I study. *Gut* **59**, 1662-1669 (2010).
111. Forbes, G.M.*, et al.* A phase 2 study of allogeneic mesenchymal stromal cells for luminal Crohn's disease refractory to biologic therapy. *Clin Gastroenterol Hepatol* **12**, 64-71 (2014).
112. Liang, J.*, et al.* Allogeneic mesenchymal stem cell transplantation in seven patients with refractory inflammatory bowel disease. *Gut* **61**, 468-469 (2012).
113. Paris, F.*, et al.* Endothelial apoptosis as the primary lesion initiating intestinal radiation damage in mice. *Science* **293**, 293-297 (2001).
114. Owens, B.M. & Simmons, A. Intestinal stromal cells in mucosal immunity and homeostasis. *Mucosal immunology* **6**, 224-234 (2013).
115. Matsumoto, T.*, et al.* Possible role of vascular endothelial cells in immune responses in colonic mucosa examined immunocytochemically in subjects with and without ulcerative colitis. *Clinical and experimental immunology* **78**, 424-430 (1989).
116. Armulik, A., Genove, G. & Betsholtz, C. Pericytes: developmental, physiological, and pathological perspectives, problems, and promises. *Developmental cell* **21**, 193-215 (2011).
117. Mifflin, R.C., Pinchuk, I.V., Saada, J.I. & Powell, D.W. Intestinal myofibroblasts: targets for stem cell therapy. *Am J Physiol Gastrointest Liver Physiol* **300**, G684-696 (2011).
118. Birbrair, A.*, et al.* Pericytes at the intersection between tissue regeneration and pathology. *Clinical science (London, England : 1979)* **128**, 81-93 (2015).
119. Yu, Y.B. & Li, Y.Q. Enteric glial cells and their role in the intestinal epithelial barrier. *World journal of gastroenterology* **20**, 11273-11280 (2014).
120. Furness, J.B. The enteric nervous system and neurogastroenterology. *Nature reviews. Gastroenterology & hepatology* **9**, 286-294 (2012).
121. Bjerknes, M. & Cheng, H. Modulation of specific intestinal epithelial progenitors by enteric neurons. *Proc. Natl. Acad. Sci. U. S. A.* **98**, 12497-12502 (2001).
122. Kabouridis, P.S.*, et al.* Microbiota controls the homeostasis of glial cells in the gut lamina propria. *Neuron* **85**, 289-295 (2015).
123. Neunlist, M.*, et al.* Enteric glia inhibit intestinal epithelial cell proliferation partly through a TGF-beta1-dependent pathway. *Am J Physiol Gastrointest Liver Physiol* **292**, G231-241 (2007).
124. Van Landeghem, L.*, et al.* Enteric glia promote intestinal mucosal healing via activation of focal adhesion kinase and release of proEGF. *Am J Physiol Gastrointest Liver Physiol* **300**, G976-987 (2011).
125. Coombes, J.L. & Powrie, F. Dendritic cells in intestinal immune regulation. *Nature Reviews Immunology* **8**, 435-446 (2008).
126. Whibley, N., Tucci, A. & Powrie, F. Regulatory T cell adaptation in the intestine and skin. *Nature immunology* **20**, 386-396 (2019).
127. Biton, M.*, et al.* T Helper Cell Cytokines Modulate Intestinal Stem Cell Renewal and Differentiation. *Cell* **175**, 1307-1320.e1322 (2018).
128. Benoit, Y.D., Groulx, J.F., Gagne, D. & Beaulieu, J.F. RGD-Dependent Epithelial Cell-Matrix Interactions in the Human Intestinal Crypt. *Journal of signal transduction* **2012**, 248759 (2012).
129. Kolachala, V.L.*, et al.* Epithelial-derived fibronectin expression, signaling, and function in intestinal inflammation. *The Journal of biological chemistry* **282**, 32965-32973 (2007).
130. Simo, P.*, et al.* Changes in the expression of laminin during intestinal development. *Development (Cambridge, England)* **112**, 477-487 (1991).

131. Simon-Assmann, P., Kedinger, M. & Haffen, K. Immunocytochemical localization of extracellular-matrix proteins in relation to rat intestinal morphogenesis. *Differentiation; research in biological diversity* **32**, 59-66 (1986).
132. Simon-Assmann, P.*, et al.* Differential expression of laminin isoforms and alpha 6-beta 4 integrin subunits in the developing human and mouse intestine. *Developmental dynamics : an official publication of the American Association of Anatomists* **201**, 71-85 (1994).
133. Groulx, J.F.*, et al.* Collagen VI is a basement membrane component that regulates epithelial cell-fibronectin interactions. *Matrix biology : journal of the International Society for Matrix Biology* **30**, 195-206 (2011).
134. Yamamoto, S.*, et al.* Heparan sulfate on intestinal epithelial cells plays a critical role in intestinal crypt homeostasis via Wnt/beta-catenin signaling. *American journal of physiology. Gastrointestinal and liver physiology* **305**, G241-249 (2013).
135. Simon-Assmann, P., Kedinger, M., De Arcangelis, A., Rousseau, V. & Simo, P. Extracellular matrix components in intestinal development. *Experientia* **51**, 883-900 (1995).
136. Quaroni, A., Isselbacher, K.J. & Ruoslahti, E. Fibronectin synthesis by epithelial crypt cells of rat small intestine. *Proc. Natl. Acad. Sci. U. S. A.* **75**, 5548-5552 (1978).
137. Teller, I.C.*, et al.* Laminins in the developing and adult human small intestine: relation with the functional absorptive unit. *Developmental dynamics : an official publication of the American Association of Anatomists* **236**, 1980-1990 (2007).
138. Beaulieu, J.F. Differential expression of the VLA family of integrins along the crypt-villus axis in the human small intestine. *Journal of cell science* **102 (Pt 3)**, 427-436 (1992).
139. Teller, I.C. & Beaulieu, J.F. Interactions between laminin and epithelial cells in intestinal health and disease. *Expert reviews in molecular medicine* **3**, 1-18 (2001).
140. Mahoney, Z.X., Stappenbeck, T.S. & Miner, J.H. Laminin alpha 5 influences the architecture of the mouse small intestine mucosa. *Journal of cell science* **121**, 2493-2502 (2008).
141. Simon-Assmann, P., Spenle, C., Lefebvre, O. & Kedinger, M. The role of the basement membrane as a modulator of intestinal epithelial-mesenchymal interactions. *Progress in molecular biology and translational science* **96**, 175-206 (2010).
142. Kedinger, M., Lefebvre, O., Duluc, I., Freund, J.N. & Simon-Assmann, P. Cellular and molecular partners involved in gut morphogenesis and differentiation. *Philos. Trans. R. Soc. Lond. B Biol. Sci.* **353**, 847-856 (1998).
143. Gjorevski, N.*, et al.* Designer matrices for intestinal stem cell and organoid culture. *Nature* **539**, 560-564 (2016).
144. Beaulieu, J.F., Vachon, P.H. & Chartrand, S. Immunolocalization of extracellular matrix components during organogenesis in the human small intestine. *Anatomy and embryology* **183**, 363-369 (1991).
145. Zhang, J., Owen, C.R., Sanders, M.A., Turner, J.R. & Basson, M.D. The motogenic effects of cyclic mechanical strain on intestinal epithelial monolayer wound closure are matrix dependent. *Gastroenterology* **131**, 1179-1189 (2006).
146. Barczyk, M., Carracedo, S. & Gullberg, D. Integrins. *Cell and tissue research* **339**, 269-280 (2010).
147. Lin, G.*, et al.* Integrin signaling is required for maintenance and proliferation of intestinal stem cells in Drosophila. *Developmental biology* **377**, 177-187 (2013).
148. Jones, R.G.*, et al.* Conditional deletion of beta1 integrins in the intestinal epithelium causes a loss of Hedgehog expression, intestinal hyperplasia, and early postnatal lethality. *The Journal of cell biology* **175**, 505-514 (2006).
149. Benoit, Y.D.*, et al.* Integrin alpha8beta1 regulates adhesion, migration and proliferation of human intestinal crypt cells via a predominant RhoA/ROCK-dependent mechanism. *Biology of the cell* **101**, 695-708 (2009).

150. Benoit, Y.D.*, et al.* Integrin alpha8beta1 confers anoikis susceptibility to human intestinal epithelial crypt cells. *Biochemical and biophysical research communications* **399**, 434-439 (2010).
151. Bouchard, V.*, et al.* B1 integrin/Fak/Src signaling in intestinal epithelial crypt cell survival: integration of complex regulatory mechanisms. *Apoptosis : an international journal on programmed cell death* **13**, 531-542 (2008).
152. Gagne, D.*, et al.* Integrin-linked kinase regulates migration and proliferation of human intestinal cells under a fibronectin-dependent mechanism. *Journal of cellular physiology* **222**, 387-400 (2010).
153. Hilska, M.*, et al.* The distribution of collagen types I, III, and IV in normal and malignant colorectal mucosa. *The European journal of surgery = Acta chirurgica* **164**, 457-464 (1998).
154. Followill, D.S. & Travis, E.L. Differential expression of collagen types I and III in consequential and primary fibrosis in irradiated mouse colon. *Radiation research* **144**, 318-328 (1995).
155. Handorf, A.M., Zhou, Y., Halanski, M.A. & Li, W.J. Tissue Stiffness Dictates Development, Homeostasis, and Disease Progression. *Organogenesis* **11**, 1-15 (2015).
156. Graham, M.F.*, et al.* Collagen content and types in the intestinal strictures of Crohn's disease. *Gastroenterology* **94**, 257-265 (1988).
157. Pucilowska, J.B., Williams, K.L. & Lund, P.K. Fibrogenesis. IV. Fibrosis and inflammatory bowel disease: cellular mediators and animal models. *American journal of physiology. Gastrointestinal and liver physiology* **279**, G653-659 (2000).
158. Murch, S.H.*, et al.* Disruption of sulphated glycosaminoglycans in intestinal inflammation. *Lancet* **341**, 711-714 (1993).
159. Hodde, J.P., Badylak, S.F., Brightman, A.O. & Voytik-Harbin, S.L. Glycosaminoglycan content of small intestinal submucosa: a bioscaffold for tissue replacement. *Tissue engineering* **2**, 209-217 (1996).
160. Bonnans, C., Chou, J. & Werb, Z. Remodelling the extracellular matrix in development and disease. *Nature reviews. Molecular cell biology* **15**, 786-801 (2014).
161. Bornemann, D.J., Duncan, J.E., Staatz, W., Selleck, S. & Warrior, R. Abrogation of heparan sulfate synthesis in Drosophila disrupts the Wingless, Hedgehog and Decapentaplegic signaling pathways. *Development (Cambridge, England)* **131**, 1927-1938 (2004).
162. Fuerer, C., Habib, S.J. & Nusse, R. A study on the interactions between heparan sulfate proteoglycans and Wnt proteins. *Developmental dynamics : an official publication of the American Association of Anatomists* **239**, 184-190 (2010).
163. Ohkawara, B., Yamamoto, T.S., Tada, M. & Ueno, N. Role of glypican 4 in the regulation of convergent extension movements during gastrulation in Xenopus laevis. *Development (Cambridge, England)* **130**, 2129-2138 (2003).
164. Oshiro, M.*, et al.* Immunohistochemical localization of heparan sulfate proteoglycan in human gastrointestinal tract. *Histochemistry and cell biology* **115**, 373-380 (2001).
165. Stern, R., Asari, A.A. & Sugahara, K.N. Hyaluronan fragments: an information-rich system. *European journal of cell biology* **85**, 699-715 (2006).
166. de la Motte, C.A. Hyaluronan in intestinal homeostasis and inflammation: implications for fibrosis. *Am J Physiol Gastrointest Liver Physiol* **301**, G945-949 (2011).
167. Riehl, T.E., Foster, L. & Stenson, W.F. Hyaluronic acid is radioprotective in the intestine through a TLR4 and COX-2-mediated mechanism. *Am J Physiol Gastrointest Liver Physiol* **302**, G309-316 (2012).
168. Sherman, L., Sleeman, J., Herrlich, P. & Ponta, H. Hyaluronate receptors: key players in growth, differentiation, migration and tumor progression. *Current opinion in cell biology* **6**, 726-733 (1994).
169. Orr, A.W., Helmke, B.P., Blackman, B.R. & Schwartz, M.A. Mechanisms of mechanotransduction. *Developmental cell* **10**, 11-20 (2006).

170. Aragona, M.*, et al.* A mechanical checkpoint controls multicellular growth through YAP/TAZ regulation by actin-processing factors. *Cell* **154**, 1047-1059 (2013).
171. Dupont, S.*, et al.* Role of YAP/TAZ in mechanotransduction. *Nature* **474**, 179-183 (2011).
172. Said, A., Raufman, J.-P. & Xie, G. The Role of Matrix Metalloproteinases in Colorectal Cancer. *Cancers* **6**, 366 (2014).
173. Quarta, M.*, et al.* Bioengineered constructs combined with exercise enhance stem cell-mediated treatment of volumetric muscle loss. *Nature communications* **8**, 15613 (2017).
174. Jank, B.J.*, et al.* Engineered composite tissue as a bioartificial limb graft. *Biomaterials* **61**, 246-256 (2015).
175. Mazza, G.*, et al.* Decellularized human liver as a natural 3D-scaffold for liver bioengineering and transplantation. *Scientific reports* **5**, 13079 (2015).
176. Uygun, B.E.*, et al.* Organ reengineering through development of a transplantable recellularized liver graft using decellularized liver matrix. *Nature medicine* **16**, 814-820 (2010).
177. Zhou, H.*, et al.* Bioengineering Human Lung Grafts on Porcine Matrix. *Annals of surgery* **267**, 590-598 (2018).
178. Ott, H.C.*, et al.* Regeneration and orthotopic transplantation of a bioartificial lung. *Nature medicine* **16**, 927-933 (2010).
179. Urbani, L.*, et al.* Multi-stage bioengineering of a layered oesophagus with in vitro expanded muscle and epithelial adult progenitors. *Nature communications* **9**, 4286 (2018).
180. Rama, P.*, et al.* Limbal stem-cell therapy and long-term corneal regeneration. *The New England journal of medicine* **363**, 147-155 (2010).
181. Hirsch, T.*, et al.* Regeneration of the entire human epidermis using transgenic stem cells. *Nature* **551**, 327-332 (2017).
182. Elliott, M.J.*, et al.* Stem-cell-based, tissue engineered tracheal replacement in a child: a 2-year follow-up study. *Lancet (London, England)* **380**, 994-1000 (2012).
183. Atala, A., Bauer, S.B., Soker, S., Yoo, J.J. & Retik, A.B. Tissue-engineered autologous bladders for patients needing cystoplasty. *Lancet (London, England)* **367**, 1241-1246 (2006).
184. Martin, L.Y.*, et al.* Tissue engineering for the treatment of short bowel syndrome in children. *Pediatric research* **83**, 249-257 (2018).
185. Bernier-Latmani, J. & Petrova, T.V. Intestinal lymphatic vasculature: structure, mechanisms and functions. *Nature reviews. Gastroenterology & hepatology* **14**, 510-526 (2017).
186. Jang, J.Y.*, et al.* Conditional ablation of LYVE-1+ cells unveils defensive roles of lymphatic vessels in intestine and lymph nodes. *Blood* **122**, 2151-2161 (2013).
187. Gonfiotti, A.*, et al.* The first tissue-engineered airway transplantation: 5-year follow-up results. *Lancet (London, England)* **383**, 238-244 (2014).
188. Hamilton, N.J.*, et al.* Tissue-Engineered Tracheal Replacement in a Child: A 4-Year Follow-Up Study. *American journal of transplantation : official journal of the American Society of Transplantation and the American Society of Transplant Surgeons* **15**, 2750-2757 (2015).
189. Atala, A. Tissue engineering of human bladder. *British medical bulletin* **97**, 81-104 (2011).
190. Atala, A. Tissue engineering of human bladder. *British medical bulletin* **97**, 81-104 (2011).
191. Kropp, B.P.*, et al.* Regenerative urinary bladder augmentation using small intestinal submucosa: urodynamic and histopathologic assessment in long-term canine bladder augmentations. *The Journal of urology* **155**, 2098-2104 (1996).
192. Grant, C.N.*, et al.* Human and mouse tissue-engineered small intestine both demonstrate digestive and absorptive function. *American journal of physiology. Gastrointestinal and liver physiology* **308**, G664-677 (2015).
193. Kitano, K.*, et al.* Bioengineering of functional human induced pluripotent stem cell-derived intestinal grafts. *Nature communications* **8**, 765 (2017).
194. Ladd, M.R.*, et al.* Development of Intestinal Scaffolds that Mimic Native Mammalian Intestinal Tissue. *Tissue engineering. Part A* (2019).

195. Schweinlin, M.*, et al.* Development of an Advanced Primary Human In Vitro Model of the Small Intestine. *Tissue engineering. Part C, Methods* **22**, 873-883 (2016).
196. Shaffiey, S.A.*, et al.* Intestinal stem cell growth and differentiation on a tubular scaffold with evaluation in small and large animals. *Regenerative medicine* **11**, 45-61 (2016).
197. Chen, Y.*, et al.* Robust bioengineered 3D functional human intestinal epithelium. *Scientific reports* **5**, 13708 (2015).
198. Costello, C.M.*, et al.* Synthetic small intestinal scaffolds for improved studies of intestinal differentiation. *Biotechnology and bioengineering* **111**, 1222-1232 (2014).
199. Evans, G.S., Flint, N., Somers, A.S., Eyden, B. & Potten, C.S. The development of a method for the preparation of rat intestinal epithelial cell primary cultures. *Journal of cell science* **101 (Pt 1)**, 219-231 (1992).
200. Stelzner, M.*, et al.* A nomenclature for intestinal in vitro cultures. *American journal of physiology. Gastrointestinal and liver physiology* **302**, G1359-1363 (2012).
201. Choi, R.S. & Vacanti, J.P. Preliminary studies of tissue-engineered intestine using isolated epithelial organoid units on tubular synthetic biodegradable scaffolds. *Transplantation proceedings* **29**, 848-851 (1997).
202. Sato, T.*, et al.* Single Lgr5 stem cells build crypt-villus structures in vitro without a mesenchymal niche. *Nature* **459**, 262-265 (2009).
203. Sato, T. & Clevers, H. Growing self-organizing mini-guts from a single intestinal stem cell: mechanism and applications. *Science (New York, N.Y.)* **340**, 1190-1194 (2013).
204. Yui, S.*, et al.* Functional engraftment of colon epithelium expanded in vitro from a single adult Lgr5(+) stem cell. *Nature medicine* **18**, 618-623 (2012).
205. Sato, T.*, et al.* Long-term expansion of epithelial organoids from human colon, adenoma, adenocarcinoma, and Barrett's epithelium. *Gastroenterology* **141**, 1762-1772 (2011).
206. Fukuda, M.*, et al.* Small intestinal stem cell identity is maintained with functional Paneth cells in heterotopically grafted epithelium onto the colon. *Genes & development* **28**, 1752-1757 (2014).
207. Fordham, R.P.*, et al.* Transplantation of expanded fetal intestinal progenitors contributes to colon regeneration after injury. *Cell stem cell* **13**, 734-744 (2013).
208. Sugimoto, S.*, et al.* Reconstruction of the Human Colon Epithelium In Vivo. *Cell stem cell* **22**, 171-176.e175 (2018).
209. Takahashi, K.*, et al.* Induction of pluripotent stem cells from adult human fibroblasts by defined factors. *Cell* **131**, 861-872 (2007).
210. Spence, J.R.*, et al.* Directed differentiation of human pluripotent stem cells into intestinal tissue in vitro. *Nature* **470**, 105-109 (2011).
211. Watson, C.L.*, et al.* An in vivo model of human small intestine using pluripotent stem cells. *Nature medicine* **20**, 1310-1314 (2014).
212. Workman, M.J.*, et al.* Engineered human pluripotent-stem-cell-derived intestinal tissues with a functional enteric nervous system. *Nature medicine* **23**, 49-59 (2017).
213. O'Doherty, R., Greiser, U. & Wang, W. Nonviral methods for inducing pluripotency to cells. *BioMed research international* **2013**, 705902 (2013).
214. Ben-David, U. & Benvenisty, N. The tumorigenicity of human embryonic and induced pluripotent stem cells. *Nature reviews. Cancer* **11**, 268-277 (2011).
215. Liang, G. & Zhang, Y. Genetic and epigenetic variations in iPSCs: potential causes and implications for application. *Cell stem cell* **13**, 149-159 (2013).
216. Laurent, L.C.*, et al.* Dynamic changes in the copy number of pluripotency and cell proliferation genes in human ESCs and iPSCs during reprogramming and time in culture. *Cell stem cell* **8**, 106-118 (2011).
217. Hussein, S.M.*, et al.* Copy number variation and selection during reprogramming to pluripotency. *Nature* **471**, 58-62 (2011).

218. Gore, A*., et al.* Somatic coding mutations in human induced pluripotent stem cells. *Nature* **471**, 63-67 (2011).
219. Fields, M., Cai, H., Gong, J. & Del Priore, L. Potential of Induced Pluripotent Stem Cells (iPSCs) for Treating Age-Related Macular Degeneration (AMD). *Cells* **5**(2016).
220. Takahashi, J. Preparing for first human trial of induced pluripotent stem cell-derived cells for Parkinson's disease: an interview with Jun Takahashi. *Regenerative medicine* **14**, 93-95 (2019).
221. Cyranoski, D. 'Reprogrammed' stem cells approved to mend human hearts for the first time. *Nature* **557**, 619-620 (2018).
222. Kim, K*., et al.* Epigenetic memory in induced pluripotent stem cells. *Nature* **467**, 285-290 (2010).
223. Zhao, T., Zhang, Z.N., Rong, Z. & Xu, Y. Immunogenicity of induced pluripotent stem cells. *Nature* **474**, 212-215 (2011).
224. Evans, M.J. & Kaufman, M.H. Establishment in culture of pluripotential cells from mouse embryos. *Nature* **292**, 154-156 (1981).
225. Cao, L*., et al.* Intestinal lineage commitment of embryonic stem cells. *Differentiation; research in biological diversity* **81**, 1-10 (2011).
226. Torihashi, S*., et al.* Gut-like structures from mouse embryonic stem cells as an in vitro model for gut organogenesis preserving developmental potential after transplantation. *Stem cells (Dayton, Ohio)* **24**, 2618-2626 (2006).
227. Finkbeiner, S.R*., et al.* Generation of tissue-engineered small intestine using embryonic stem cell-derived human intestinal organoids. *Biology open* **4**, 1462-1472 (2015).
228. Rezai, K.A., Semnani, R.T., Patel, S.C., Ernest, J.T. & van Seventer, G.A. The immunogenic potential of human fetal retinal pigment epithelium and its relation to transplantation. *Investigative ophthalmology & visual science* **38**, 2662-2671 (1997).
229. Hussey, G.S., Cramer, M.C. & Badylak, S.F. Extracellular Matrix Bioscaffolds for Building Gastrointestinal Tissue. *Cellular and molecular gastroenterology and hepatology* **5**, 1-13 (2018).
230. Totonelli, G*., et al.* A rat decellularized small bowel scaffold that preserves villus-crypt architecture for intestinal regeneration. *Biomaterials* **33**, 3401-3410 (2012).
231. Lee, E., Milan, A., Urbani, L., De Coppi, P. & Lowdell, M.W. Decellularized material as scaffolds for tissue engineering studies in long gap esophageal atresia. *Expert opinion on biological therapy* **17**, 573-584 (2017).
232. Crapo, P.M., Gilbert, T.W. & Badylak, S.F. An overview of tissue and whole organ decellularization processes. *Biomaterials* **32**, 3233-3243 (2011).
233. Badylak, S.F., Lantz, G.C., Coffey, A. & Geddes, L.A. Small intestinal submucosa as a large diameter vascular graft in the dog. *The Journal of surgical research* **47**, 74-80 (1989).
234. Clarke, K.M*., et al.* Intestine submucosa and polypropylene mesh for abdominal wall repair in dogs. *The Journal of surgical research* **60**, 107-114 (1996).
235. Lantz, G.C., Badylak, S.F., Coffey, A.C., Geddes, L.A. & Blevins, W.E. Small intestinal submucosa as a small-diameter arterial graft in the dog. *Journal of investigative surgery : the official journal of the Academy of Surgical Research* **3**, 217-227 (1990).
236. Lantz, G.C., Badylak, S.F., Coffey, A.C., Geddes, L.A. & Sandusky, G.E. Small intestinal submucosa as a superior vena cava graft in the dog. *The Journal of surgical research* **53**, 175-181 (1992).
237. McDevitt, C.A., Wildey, G.M. & Cutrone, R.M. Transforming growth factor-beta1 in a sterilized tissue derived from the pig small intestine submucosa. *Journal of biomedical materials research. Part A* **67**, 637-640 (2003).
238. Voytik-Harbin, S.L., Brightman, A.O., Kraine, M.R., Waisner, B. & Badylak, S.F. Identification of extractable growth factors from small intestinal submucosa. *Journal of cellular biochemistry* **67**, 478-491 (1997).

239. Hodde, J.P., Record, R.D., Liang, H.A. & Badylak, S.F. Vascular endothelial growth factor in porcine-derived extracellular matrix. *Endothelium : journal of endothelial cell research* **8**, 11-24 (2001).
240. White, L.J.*, et al.* The impact of detergents on the tissue decellularization process: A ToF-SIMS study. *Acta biomaterialia* **50**, 207-219 (2017).
241. Hodde, J.P. & Allam, R. Small Intestinal Submucosa Wound Matrix for Chronic Wound Healing. *Wounds : a compendium of clinical research and practice* **19**, 157-162 (2007).
242. Demling, R., Niezgoda, J., Haraway, G. & Mostow, E. Small Intestinal Submucosa Wound Matrix and Full-thickness Venous Ulcers: Preliminary Results. *Wounds : a compendium of clinical research and practice* **16**(2004).
243. Murphy, F. & Corbally, M.T. The novel use of small intestinal submucosal matrix for chest wall reconstruction following Ewing's tumour resection. *Pediatr Surg Int* **23**, 353-356 (2007).
244. Chen, M.K. & Badylak, S.F. Small bowel tissue engineering using small intestinal submucosa as a scaffold. *The Journal of surgical research* **99**, 352-358 (2001).
245. Wang, Z.Q.*, et al.* Morphologic evaluation of regenerated small bowel by small intestinal submucosa. *J Pediatr Surg* **40**, 1898-1902 (2005).
246. Demirbilek, S., Kanmaz, T., Özardalı, İ., Edalı, M.N. & Yücesan, S. Using porcine small intestinal submucosa in intestinal regeneration. *Pediatric Surgery International* **19**, 588-592 (2003).
247. Wang, Z.Q., Watanabe, Y. & Toki, A. Experimental assessment of small intestinal submucosa as a small bowel graft in a rat model. *J Pediatr Surg* **38**, 1596-1601 (2003).
248. Ansaloni, L.*, et al.* Experimental evaluation of Surgisis as scaffold for neointestine regeneration in a rat model. *Transplantation proceedings* **38**, 1844-1848 (2006).
249. Giuffrida, P.*, et al.* Decellularized Human Gut as a Natural 3D Platform for Research in Intestinal Fibrosis. *Inflammatory bowel diseases* **25**, 1740-1750 (2019).
250. Chen, H.J.*, et al.* A recellularized human colon model identifies cancer driver genes. *Nature biotechnology* **34**, 845-851 (2016).
251. Sala, F.G.*, et al.* A multicellular approach forms a significant amount of tissue-engineered small intestine in the mouse. *Tissue engineering. Part A* **17**, 1841-1850 (2011).
252. Schlieve, C.R.*, et al.* Neural Crest Cell Implantation Restores Enteric Nervous System Function and Alters the Gastrointestinal Transcriptome in Human Tissue-Engineered Small Intestine. *Stem cell reports* **9**, 883-896 (2017).
253. Hou, X.*, et al.* Short-term and long-term human or mouse organoid units generate tissue-engineered small intestine without added signalling molecules. *Experimental physiology* **103**, 1633-1644 (2018).
254. Grikscheit, T.C.*, et al.* Tissue-engineered small intestine improves recovery after massive small bowel resection. *Annals of surgery* **240**, 748-754 (2004).
255. Sala, F.G., Kunisaki, S.M., Ochoa, E.R., Vacanti, J. & Grikscheit, T.C. Tissue-engineered small intestine and stomach form from autologous tissue in a preclinical large animal model. *The Journal of surgical research* **156**, 205-212 (2009).
256. Levin, D.E.*, et al.* Human tissue-engineered small intestine forms from postnatal progenitor cells. *J Pediatr Surg* **48**, 129-137 (2013).
257. Ladd, M.R.*, et al.* Development of Intestinal Scaffolds that Mimic Native Mammalian Intestinal Tissue. *Tissue engineering. Part A* **25**, 1225-1241 (2019).
258. Giobbe, G.G.*, et al.* Extracellular matrix hydrogel derived from decellularized tissues enables endodermal organoid culture. *Nature communications* **10**, 5658 (2019).
259. Cardona, A.*, et al.* TrakEM2 software for neural circuit reconstruction. *PloS one* **7**, e38011 (2012).
260. Naba, A.*, et al.* The matrisome: in silico definition and in vivo characterization by proteomics of normal and tumor extracellular matrices. *Molecular & cellular proteomics : MCP* **11**, M111.014647 (2012).

261. Boyde, T.R. & Rahmatullah, M. Optimization of conditions for the colorimetric determination of citrulline, using diacetyl monoxime. *Analytical biochemistry* **107**, 424-431 (1980).
262. Maru, Y., Orihashi, K. & Hippo, Y. Lentivirus-Based Stable Gene Delivery into Intestinal Organoids. *Methods in molecular biology (Clifton, N.J.)* **1422**, 13-21 (2016).
263. Bankhead, P.*, et al.* QuPath: Open source software for digital pathology image analysis. *Scientific reports* **7**, 16878 (2017).
264. Thomson, A.B.*, et al.* Small bowel review: Normal physiology, part 1. *Digestive diseases and sciences* **48**, 1546-1564 (2003).
265. Middendorp, S.*, et al.* Adult stem cells in the small intestine are intrinsically programmed with their location-specific function. *Stem cells (Dayton, Ohio)* **32**, 1083-1091 (2014).
266. Spencer, A.U.*, et al.* Pediatric short bowel syndrome: redefining predictors of success. *Annals of surgery* **242**, 403-409; discussion 409-412 (2005).
267. Borgstrom, B., Dahlqvist, A., Lundh, G. & Sjovall, J. Studies of intestinal digestion and absorption in the human. *The Journal of clinical investigation* **36**, 1521-1536 (1957).
268. Wynn, T.A. Common and unique mechanisms regulate fibrosis in various fibroproliferative diseases. *The Journal of clinical investigation* **117**, 524-529 (2007).
269. Yin, X.*, et al.* Niche-independent high-purity cultures of Lgr5+ intestinal stem cells and their progeny. *Nature methods* **11**, 106-112 (2014).
270. Ferreira, S.A.*, et al.* Bi-directional cell-pericellular matrix interactions direct stem cell fate. *Nature communications* **9**, 4049 (2018).
271. Blache, U., Stevens, M.M. & Gentleman, E. Harnessing the secreted extracellular matrix to engineer tissues. *Nature Biomedical Engineering* **4**, 357-363 (2020).
272. Kallepitis, C.*, et al.* Quantitative volumetric Raman imaging of three dimensional cell cultures. *Nature communications* **8**, 14843 (2017).
273. Movasaghi, Z., Rehman, S. & Rehman, I.U. Raman Spectroscopy of Biological Tissues. *Applied Spectroscopy Reviews* **42**, 493-541 (2007).
274. Gilbert, T.W., Freund, J.M. & Badylak, S.F. Quantification of DNA in biologic scaffold materials. *The Journal of surgical research* **152**, 135-139 (2009).
275. Badylak, S.F. & Gilbert, T.W. Immune response to biologic scaffold materials. *Seminars in immunology* **20**, 109-116 (2008).
276. Chen, W., Shao, Y., Li, X., Zhao, G. & Fu, J. Nanotopographical Surfaces for Stem Cell Fate Control: Engineering Mechanobiology from the Bottom. *Nano today* **9**, 759-784 (2014).
277. Dalby, M.J., Gadegaard, N. & Oreffo, R.O.C. Harnessing nanotopography and integrin–matrix interactions to influence stem cell fate. *Nature Materials* **13**, 558-569 (2014).
278. Guyette, J.P.*, et al.* Perfusion decellularization of whole organs. *Nature Protocols* **9**, 1451-1468 (2014).
279. Wiśniewski, J.R., Zougman, A., Nagaraj, N. & Mann, M. Universal sample preparation method for proteome analysis. *Nature methods* **6**, 359-362 (2009).
280. Li, Q.*, et al.* Proteomic analysis of naturally-sourced biological scaffolds. *Biomaterials* **75**, 37-46 (2016).
281. Gilbert, T.W., Sellaro, T.L. & Badylak, S.F. Decellularization of tissues and organs. *Biomaterials* **27**, 3675-3683 (2006).
282. Hollister, S.J. Porous scaffold design for tissue engineering. *Nature Materials* **4**, 518-524 (2005).
283. Akhtar, R., Sherratt, M.J., Cruickshank, J.K. & Derby, B. Characterizing the elastic properties of tissues. *Materials today (Kidlington, England)* **14**, 96-105 (2011).
284. Hendow, E.K.*, et al.* Biomaterials for hollow organ tissue engineering. *Fibrogenesis & Tissue Repair* **9**, 3 (2016).
285. Egorov, V.I., Schastlivtsev, I.V., Prut, E.V., Baranov, A.O. & Turusov, R.A. Mechanical properties of the human gastrointestinal tract. *Journal of biomechanics* **35**, 1417-1425 (2002).

286. Wang, Y.*, et al.* Formation of Human Colonic Crypt Array by Application of Chemical Gradients Across a Shaped Epithelial Monolayer. *Cellular and molecular gastroenterology and hepatology* **5**, 113-130 (2018).
287. Wang, Y.*, et al.* Self-renewing Monolayer of Primary Colonic or Rectal Epithelial Cells. *Cellular and molecular gastroenterology and hepatology* **4**, 165-182.e167 (2017).
288. Ahmad, A.A.*, et al.* Optimization of 3-D organotypic primary colonic cultures for organ-on-chip applications. *Journal of biological engineering* **8**, 9 (2014).
289. Wang, Y.*, et al.* A microengineered collagen scaffold for generating a polarized crypt-villus architecture of human small intestinal epithelium. *Biomaterials* **128**, 44-55 (2017).
290. Fragkos, K.C. & Forbes, A. Citrulline as a marker of intestinal function and absorption in clinical settings: A systematic review and meta-analysis. *United European gastroenterology journal* **6**, 181-191 (2018).
291. Singh, A.*, et al.* Evaluation of transplantation sites for human intestinal organoids. *PloS one* **15**, e0237885 (2020).
292. Rennert, R.C., Sorkin, M., Garg, R.K., Januszyk, M. & Gurtner, G.C. Cellular Response to a Novel Fetal Acellular Collagen Matrix: Implications for Tissue Regeneration. *International Journal of Biomaterials* **2013**, 527957 (2013).
293. Zakhem, E., Tamburrini, R., Orlando, G., Koch, K.L. & Bitar, K.N. Transplantation of a Human Tissue-Engineered Bowel in an Athymic Rat Model. *Tissue engineering. Part C, Methods* **23**, 652-660 (2017).
294. Choi, R.S.*, et al.* Studies of brush border enzymes, basement membrane components, and electrophysiology of tissue-engineered neointestine. *J Pediatr Surg* **33**, 991-996; discussion 996-997 (1998).

Appendix 1 - Patients Demographics Table

Symbols key:
+: established
^ not used in study
n/a: not attempted

ID	Age	Sex	Clinical background	Site of biopsy	Organoids	Scaffolds	Fibroblasts	RNA
1	1	M	Intestinal pseudo-obstruction and dysmotility; **Intestinal failure** on parenteral nutrition	Ileum	+^	+	n/a	n/a
2	8	F	Rett syndrome; Intestinal dysmotility; **Intestinal failure**	Jejunum	+	+	+	n/a
				Colon	n/a	+	n/a	n/a
3	10	F	Severe neuropathic dysmotility; **Intestinal failure** on parenteral nutrition	Ileum	+	+^	n/a	n/a
4	8	M	Intestinal dysmotility; ileostomy; stoma prolapse with necrosis; **Intestinal failure** on parenteral nutrition	Ileum	+^	+	+^	n/a
5	4	F	Intestinal dysmotility; Ileostomy; **Intestinal failure** on parenteral nutrition	Ileum	n/a	+	n/a	n/a
6	15	M	**Crohn's disease**; Orofacial granulomatosis	Duodenum	+	n/a	n/a	n/a
7	15	M	**Crohn's disease**	Jejunum	+	n/a	+	n/a
8	4	F	PEXB11B deficiency; Gastro-oesophageal reflux disease	Jejunum	+	n/a	n/a	n/a
9	11	M	Eosinophilic GI disease, Colitis	Duodenum	+	n/a	n/a	n/a
10	7	M	Hemiplegic cerebral palsy	Duodenum	+	n/a	n/a	n/a
11	1	M	Hypoganglionic bowel dysmotility, mucous fistula	Ileum	n/a	+^	+	n/a
12	1	M	Hirschsprung's disease, enterocolitis	Ileum	n/a	+	+^	n/a
13	10	F	Chronic intestinal pseudo-obstruction, dysfunctioning PEG-J, gastric and oesophageal dilatation, gastrostomy with GJ extension	Ileum	n/a	+	+^	n/a

14	2	F	Autosomal dominant mutation in MNX1 gene, Curriano syndrome, Ano-rectal malformation, perineal fistula, closure of ileostomy	Ileum	+	+^	+^	n/a
15	13	F	Young-simpson syndrome; Gastro-oesophageal reflux; severe constipation	Colon	n/a	+	n/a	n/a
16	8 months	M	**Necrotising enterocolitis** at birth; Left hemicolectomy and end transverse colostomy; Sigmoid colon perforation; Pulmonary stenosis	Colon	n/a	+	n/a	n/a
17	8 months	M	Hirschsprung's disease	Colon	n/a	+	+^	n/a
18	10	F	Colonic neuropathy and intestinal dysmotility	Colon	n/a	+	n/a	n/a
19	5 months	M	Hirschsprung's disease	Colon	n/a	+	n/a	n/a
20	4 months	M	Hirschsprung's disease	Colon	n/a	+	n/a	n/a
21	1	F	**Necrotising enterocolitis**, **Intestinal failure** on parenteral nutrition	Ileum	n/a	+	n/a	+
				Colon	n/a	+	n/a	n/a
22	1	F	Duodenal web	jejunum	n/a	n/a	+^	+
23	6 months	M	Duplication cyst	ileum	+^	+	+	n/a
24	1	M	Neurodevelopmental delay, abdominal distension and stoma formation	ileum	+^	+	unsuccessful - contamination	n/a
25	12	F	Dysmotile colon with diversion colitis, ileostomy	Ileum	n/a	+^	n/a	+
				Colon	n/a	+^	n/a	n/a
26	10	M	SCID, previous bone marrow transplant, constipation and failure to thrive	Duodenum	n/a	n/a	n/a	+
27	5	M	Investigation of rapid transit diarrhoea. Endoscopy and histology normal.	Duodenum	n/a	n/a	n/a	+
				Jejunum	n/a	n/a	n/a	+
				Ileum	n/a	n/a	n/a	+
28	10	M	Coeliac disease	Duodenum	n/a	n/a	n/a	+
29	12	F	Crohn's disease	ileum	n/a	+	n/a	n/a
30	2	F	Early onset Crohn's disease, unresponsive to maximal medical therapy	colon	n/a	+	n/a	n/a

Appendix 2 - Primer Sequences for qRT-PCR

Primer name	Forward	Reverse
human β-**ACTIN**	TTCTACAATGAGCTGCGTGTG	GGGGTGTTGAAGGTCTCAAA
human **CYBRD1**	GCTATTTGTTACAGCTTCTTTCAGG	CAGGATCTCTCAGGGAAAAAATC
human **SLC40A1**	GATGCTGTGGATCCTTGGCCG	CCACATCCGATCTCCCCAAGTAGA
human **SI**	CATACCATTTGATACACAGGTC	GCAGGGTCCAAGATGATGAC
human **LCT**	TCAGGGCGGAAAACTCTCTGTTGTC	CGACCGTGTCCTGGGCAAGC
human **SLC10A2**	GGCGACATGGACCTGAGCGTCAGC	CGAGAGAAACCAGAGATGTACCTATG
human **OSTB**	GGGGCTAAGGGGTCTAAGG	CAGGGCAAGGATGGAATGA
human **OLFM4**	CTTTCCAAAGTGAGGGAATATGTC	GATGTCAATTCGGACAGTTAGG
human **LGR5**	CAGTGCAGTGTTCACCTTCC	AGTGCCAGAACTGCTATGGT
human **LYZ**	CATTGTTCTGGGGCTTGTCC	TCATTACACCAGTAGCGGCT
human **MUC2**	CAACAACTCCGAAGCTGTG	CAAATGTTTCTCGGTCACC
human **ALPI**	TCATCATGAGGGTGTGGCTT	TGTAGGCTTTGCTGTCCTGA
human **CHGA**	GAAGAAGGCCCCACTGTAGT	AGTGCTCCTGTTCTCCCTTC

Appendix 3 - Antibodies for immunofluorescence, immunohistochemistry and immunoblotting

Antibody	Host	Supplier	Cat. Number	Dilution
Beta-actin	mouse	Sigma Aldrich	A3854	1:25000
CD31	mouse	Abcam	ab9498	1:200
ChgA	goat	Santa Cruz	sc-393941	1:500
Collagen-1 (human)	goat	Abcam	ab34710	1:200
Collagen-1 (porcine)	mouse	Abcam	ab6308	1:50
Collagen-4 (porcine)	rabbit	Novabio	NB120-6586	1:200
Defensin-α5	mouse	Abcam	ab90802	1:50
E-cadherin	rabbit	Cell signalling	#3195	1:400
Fibronectin (human)	rabbit	Abcam	ab23750	1:200
Fibronectin (porcine)	mouse	Santa Cruz	sc-59826	1:50
FSP1	mouse	Abcam	ab11333	1:750
GLP2R	rabbit	Abcam	ab188595	1:500
hNucleoli	mouse	Abcam	ab190710	1:200
KI67	rabbit	Abcam	ab16667	1:250
Laminin-α5 (human)	mouse	Abcam	ab210957	1:200
Laminin (porcine)	rabbit	Abcam	ab11575	1:250
LGR5	rabbit	Miltenyi Biotec	#130-104-945	1:100
Lysozyme	rabbit	Dako	a0099	1:500
NA^+K^+ATPase	rabbit	Abcam	ab198367	1:100
OLFM4	rabbit	Cell signalling	#14369	1:200
PanCytokeratin	rabbit	Invitrogen	18-0059	1:100
PCNA	mouse	Abcam	ab29	1:1000
Phalloidin-568		Life technology	A12379	1:500
αSMA	rabbit	Abcam	ab5694	1:100
SOX9	rabbit	Millipore	AB5535	1:1000
Sucrase Isomaltase	mouse	Santa Cruz	sc-393424	1:100
Thrombospondin 4	mouse	Santa Cruz	sc-28293	1:50
UEA-1 (Rhodamine conjugated)		Vector Laboratories	RL-1062	1:200
villin	mouse	Santa Cruz	sc-58897	1:50
vimentin	mouse	Abcam	ab20346	1:1000
ZO-1	goat	Abcam	ab190085	1:200
Alexa fluor anti-mouse 568	Goat	Invitrogen	A1104	1:1000
Alexa fluor anti-rabbit 488	Goat	Invitrogen	A11008	1:1000
Alexa fluor anti-goat 594	Donkey	Invitrogen	A11058	1:1000
HRP secondary	mouse	GE Healthcare	NXA931V	1:5000
HRP secondary	rabbit		NA934V	1:5000
ABC-HRP secondary (IHC)	mouse	Vector Laboratories	BA-2001	1:1000
ABC-HRP secondary (IHC)	rabbit	Vector Laboratories	BA-1000	1:1000
ABC kit		Vector Laboratories	PK-6100	

Appendix 4 - Piglet SI scaffold fabrication and characterisation

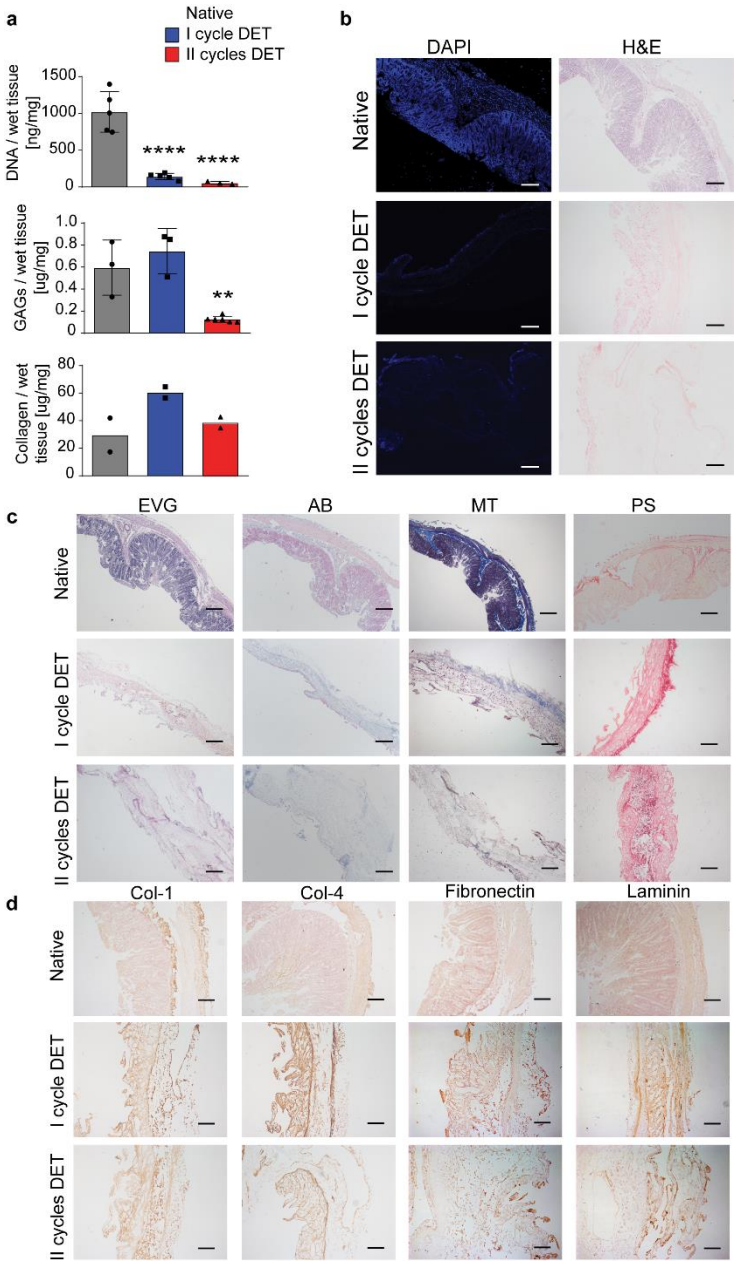

Piglet SI scaffold characterisation: (a) Quantification of DNA, glycosaminoglycans (GAGs) and collagen per milligram of wet tissue in native piglet intestine and following one and two cycles of DET. Data represent mean ± s.e.m of n = 3 biologically distinct piglet intestine samples (DNA and GAG quantification) and of n = 2 biologically distinct samples (collagen quantification). One-way ANOVA with Dunnett's multiple comparisons test. The experiment was performed once. (b) Representative H&E images and DAPI immunostainings of a native piglet intestine and following one and two cycles of DET. Scale bars represent 100µm. (c) Representative histology images of Elastic Van Gieson (EVG) and Alcian blue (AB) stainings confirm preservation of elastin and GAGs respectively following one and two cycles of DET. Masson's trichrome (MT) and Picro-sirius red (PS) histological stainings confirms maintenance of connective tissue and collagens following one and two cycles of DET. Scale bars represent 200µm. (d) Representative immunohistochemical staining for Collagen I (Col-1), Collagen IV (Col-4), Fibronectin, Laminin indicating the preservation of these ECM proteins in a piglet scaffold following two cycles of DET. Scale bars represent 100µm. Images are representative of 3 biological replicates.

This data in its entirety was acquired by Suzanna Eli, Alfonso Tedeschi and Alessandro Pellegata (UCL)

Appendix 5 - Global proteomic profile of human SI and Colon scaffolds

377 total proteins detected in Colon and SI ECM scaffolds using Mass Specreometry

Protein names	Gene names	iBAQ Colon_A	iBAQ Colon_B	iBAQ Colon_C	iBAQ Colon_D	iBAQ SI_A	iBAQ SI_B	iBAQ SI_C	iBAQ SI_D	GOCC name	Score	Q-value	Intensity	Protein IDs	Majority protein IDs	iBAQ Colon_A	iBAQ Colon_B	iBAQ Colon_C	iBAQ Colon_D	iBAQ SI_A	iBAQ SI_B	iBAQ SI_C	iBAQ SI_D	Colon	SI	Colon + SI	Extracellular
Carbamoyl-pho:	**CPS1**	NaN	NaN	NaN	NaN	NaN	14.68677	16.08535	22.25678	cell part;cytoplasmic part;intracellular non-membrane-bounded c	73.658	0	28.55090821	P31327	P31327	0	0	0	0	0	1	1	1	0	3	3	0
HLA class II hist	**HLA-DRB1**	NaN	NaN	NaN	NaN	20.03106	NaN	22.47998	19.05539	cell part;clathrin coated vesicle membrane;clathrin-coated endoc	49.611	0	26.83195239	Q5Y7A7;P0191:	Q5Y7A7;P0191:	0	0	0	0	1	0	1	1	0	3	3	0
Dolichyl-diphos	**DAD1**	NaN	NaN	NaN	NaN	21.36437	NaN	19.72489	22.78654	cell part;cytoplasmic part;endoplasmic reticulum part;integral to	9.2686	0.002	25.68658965	P61803	P61803	0	0	0	0	1	0	1	1	0	3	3	0
Defensin-5;HD5	**DEFA5**	NaN	NaN	NaN	NaN	25.55221	25.4776	29.23911	29.89966	cell part;cytoplasmic membrane-bounded vesicle;cytoplasmic me	23.646	0	33.01100335	Q01523	Q01523	0	0	0	0	1	1	1	1	0	4	4	1
Fatty acid synth	**FASN**	NaN	NaN	11.87071	NaN	14.69632	NaN	17.70698	19.25213	cell part;cytoplasmic membrane-bounded vesicle;cytoplasmic par	31.059	0	26.69418315	P49327	P49327	0	0	1	0	1	0	1	1	1	3	4	0
BTB/POZ domai	**KCTD12;KCTD16**	NaN	NaN	NaN	16.43434	19.07796	NaN	19.16671	19.85784	cell junction;cell part;macromolecular complex;membrane;plasm	15.114	0	24.96322842	Q96CX2;Q68DU	Q96CX2;Q68DU	0	0	0	1	1	0	1	1	1	3	4	0
NADH dehydrog	**NDUFS2**	NaN	NaN	NaN	17.99595	NaN	17.06097	18.41266	20.70117	cell part;cytoplasmic part;intracellular organelle part;intracellular	11.049	0.0021	25.86931313	O75306	O75306	0	0	0	1	0	1	1	1	1	3	4	0
Eukaryotic trans	**EIF3E**	NaN	15.68447	NaN	NaN	16.93779	NaN	15.04631	18.73208	cell part;cytoplasmic part;cytosol;eukaryotic translation initiation	10.713	0.0021	24.11179601	P60228	P60228	0	1	0	0	1	0	1	1	1	3	4	0
Alpha-1-antichy	**SERPINA3**	NaN	NaN	NaN	19.6611	18.43233	NaN	19.17402	19.10562	cell part;extracellular region;intracellular membrane-bounded org	6.5173	0.0032	25.4790184	P01011	P01011	0	0	0	1	1	0	1	1	1	3	4	1
ATP synthase F(	**ATP5F1**	NaN	NaN	17.8396	NaN	19.3992	18.73364	19.32538	21.22376	cell part;cytoplasmic part;intracellular organelle lumen;intracellul	11.54	0	26.09113721	P24539	P24539	0	0	1	0	1	1	1	1	1	4	5	0
Nephronectin	**NPNT**	NaN	NaN	NaN	16.0072	18.46447	14.95882	18.01966	18.76885	cell part;extracellular matrix;extracellular region part;membrane;	7.5993	0.0018	25.33026096	Q6UXI9	Q6UXI9	0	0	0	1	1	1	1	1	1	4	5	1
Phosphoglycera	**PGAM1**	NaN	NaN	21.52712	23.55485	20.27549	NaN	19.45585	24.11688	cell part;cytoplasmic part;cytosol;intracellular membrane-bounde	77.64	0	28.78284913	P18669;P1525!	P18669	0	0	1	1	1	0	1	1	2	3	5	0
Ig alpha-1 chain	**IGHA1**	NaN	NaN	20.58288	22.54934	19.35615	NaN	22.77557	25.17493	extracellular region	62.312	0	29.6713998	P01876	P01876	0	0	1	1	1	0	1	1	2	3	5	1
Myosin-14	**MYH14**	NaN	15.82833	NaN	15.82697	15.483	NaN	16.15117	21.07738	cell part;cytoskeletal part;intracellular organelle part;intracellular	50.661	0	27.90942088	Q7Z406	Q7Z406	0	1	0	1	1	0	1	1	2	3	5	0
Intelectin-1	**ITLN1**	NaN	NaN	19.68017	23.05816	NaN	18.15333	19.80098	24.91552	anchored to membrane;brush border membrane;cell part;cell prc	36.766	0	29.24529058	Q8WWA0	Q8WWA0	0	0	1	1	0	1	1	1	2	3	5	1
Heat shock prot	**HSPB6**	NaN	NaN	22.62687	26.06038	20.17816	NaN	20.36035	21.25667	cell part;cytoplasm;intracellular membrane-bounded organelle;in	29.611	0	29.0875252	O14558	O14558	0	0	1	1	1	0	1	1	2	3	5	0
NADPH--cytoch	**POR**	NaN	NaN	18.73387	16.55346	20.50359	19.14661	NaN	20.93423	cell part;cytoplasmic part;endoplasmic reticulum;endoplasmic ret	26.852	0	27.34350319	P16435	P16435	0	0	1	1	1	1	0	1	2	3	5	0
Complement C4	**C4B;C4A**	NaN	NaN	16.76319	19.14181	17.3699	NaN	19.63394	19.80782	cell part;extracellular region;extracellular region part;extracellula	25.305	0	27.64464572	P0C0L5;P0C0L4	P0C0L5;P0C0L4	0	0	1	1	1	0	1	1	2	3	5	1
T-complex prot	**CCT3**	NaN	NaN	16.83257	20.52076	17.22901	NaN	15.91046	20.31363	cell part;chaperonin-containing T-complex;cytoplasmic part;cytos	24	0	26.53629228	P49368	P49368	0	0	1	1	1	0	1	1	2	3	5	0
Acetyl-CoA acet	**ACAT1**	NaN	18.40557	NaN	21.98468	16.95015	NaN	16.68332	22.30697	cell part;cytoplasmic part;intracellular organelle lumen;intracellul	19.782	0	27.76515445	P24752	P24752	0	1	0	1	1	0	1	1	2	3	5	0
T-complex prot	**CCT8**	NaN	NaN	14.26752	18.91444	16.33293	NaN	16.42017	18.84187	aggresome;cell part;centrosome;cytoplasmic part;cytoskeletal pa	18.779	0	25.34756379	P50990	P50990	0	0	1	1	1	0	1	1	2	3	5	0
Spectrin beta cl	**SPTBN1**	NaN	15.93907	NaN	17.36718	14.49735	NaN	17.59157	18.60957	axolemma;axon part;cell cortex part;cell part;cell projection mem	18.593	0	26.85114702	Q01082	Q01082	0	1	0	1	1	0	1	1	2	3	5	0
NADH-cytochro	**CYB5R3**	NaN	21.94967	NaN	24.17211	20.0696	NaN	17.60052	22.66327	cell part;cytoplasmic part;cytosolic part;endoplasmic reticulum;e	17.928	0	28.68822496	P00387	P00387	0	1	0	1	1	0	1	1	2	3	5	0
Rho GTPase-act	**ARHGAP1**	NaN	15.67964	NaN	20.61207	18.57685	NaN	18.7406	19.52453	cell part;cell projection;cytoplasmic part;cytosol;intracellular mer	14.043	0	26.38172407	Q07960	Q07960	0	1	0	1	1	0	1	1	2	3	5	0
Mitochondrial c	**SLC25A20**	NaN	NaN	19.85387	19.79684	18.92729	NaN	19.24662	22.01257	cell part;cytoplasmic part;integral to membrane;intracellular orga	12.704	0	26.86903067	O43772	O43772	0	0	1	1	1	0	1	1	2	3	5	0
Cullin-associate	**CAND1**	NaN	16.56864	14.77092	NaN	16.92521	NaN	18.48789	19.26986	cell part;cullin-RING ubiquitin ligase complex;cytoplasm;intracellu	12.543	0	26.20696679	Q86VP6	Q86VP6	0	1	1	0	1	0	1	1	2	3	5	0
60S ribosomal p	**RPL18A**	NaN	NaN	19.11954	17.9695	20.21525	NaN	20.58049	21.68239	cell part;cytosolic large ribosomal subunit;intracellular organelle p	11.922	0	25.9041004	Q02543	Q02543	0	0	1	1	1	0	1	1	2	3	5	0
Flotillin-1	**FLOT1**	NaN	16.48032	NaN	18.16649	17.92787	NaN	17.7057	17.95759	caveola;cell part;centriolar satellite;cytoplasmic membrane-boun	10.356	0.002	24.82832479	O75955	O75955	0	1	0	1	1	0	1	1	2	3	5	0
Somatomedin-B	**SBSPON**	17.86949	NaN	NaN	21.72017	18.58167	17.29491	NaN	16.61956	extracellular matrix;extracellular region part;proteinaceous extra	9.2154	0.002	25.75241127	Q8IVN8	Q8IVN8	1	0	0	1	1	1	0	1	2	3	5	1
Translocon-assc	**SSR4**	NaN	18.63895	NaN	20.74065	19.2513	NaN	19.49599	22.00888	cell part;cytoplasmic part;endoplasmic reticulum part;integral to	8.4529	0.0019	25.69200244	P51571	P51571	0	1	0	1	1	0	1	1	2	3	5	0
Ras-related prot	**RAB2A;RAB2B**	18.09032	19.06884	NaN	NaN	18.33534	NaN	19.32635	19.83564	cell part;cytoplasmic membrane-bounded vesicle;cytoplasmic par	7.5531	0.0018	25.1998158	P61019;Q8WUI	P61019;Q8WUI	1	1	0	0	1	0	1	1	2	3	5	0
Immunoglobulir	**IGJ**	21.34164	NaN	18.24665	NaN	NaN	21.11343	21.81902	21.47462	extracellular region	7.11	0.0017	26.4985359	P01591	P01591	1	0	1	0	0	1	1	1	2	3	5	1
Single-stranded	**SSBP1**	NaN	19.73246	NaN	22.26791	NaN	18.27121	20.66926	21.20508	cell part;cytoplasmic part;intracellular non-membrane-bounded c	6.5888	0.0032	26.29932402	Q04837	Q04837	0	1	0	1	0	1	1	1	2	3	5	0
Bifunctional pur	**ATIC**	NaN	16.49251	NaN	19.92764	17.77803	NaN	17.73708	19.90454	cell part;cytoplasmic part;cytosol;intracellular membrane-bounde	6.3035	0.0078	26.50957134	P31939	P31939	0	1	0	1	1	0	1	1	2	3	5	0
Aquaporin-1	**AQP1**	23.84096	22.63014	NaN	NaN	23.92107	22.64273	22.85899	21.58889	apical plasma membrane;basal plasma membrane;brush border r	23.975	0	27.70536714	P29972	P29972	1	1	0	0	1	1	1	1	2	4	6	1
ATP-dependent	**DHX9**	NaN	NaN	15.75937	20.21762	16.82352	17.21987	19.718	20.51258	cell part;centrosome;CRD-mediated mRNA stability complex;cyto	22.443	0	27.82644695	Q08211	Q08211	0	0	1	1	1	1	1	1	2	4	6	0
Heterogeneous	**HNRNPH1;HNRNPF**	NaN	NaN	18.79363	21.06303	21.06842	21.32042	20.86597	22.89441	actin cytoskeleton;catalytic step 2 spliceosome;cell part;cytoplasr	18.205	0	28.20335838	P31943;P52597	P31943;P52597	0	0	1	1	1	1	1	1	2	4	6	0
AP-2 complex su	**AP2A2;AP2A1**	NaN	17.17231	NaN	18.32804	18.95577	17.00383	19.12528	19.5644	AP-2 adaptor complex;apical plasma membrane;AP-type membra	14.62	0	26.84720897	O94973;O9578	O94973;O9578	0	1	0	1	1	1	1	1	2	4	6	0
Hemoglobin sub	**HBD**	20.0308	23.17289	NaN	NaN	20.60666	21.89412	25.29288	24.82449	cell part;cytoplasmic part;cytosolic part;hemoglobin complex;intr	12.408	0	29.83128801	P02042	P02042	1	1	0	0	1	1	1	1	2	4	6	0
LIM and senesc	**LIMS2**	NaN	NaN	17.4492	24.01945	19.00586	18.17431	19.53092	19.16506	adherens junction;anchoring junction;cell junction;cell part;cell-s	11.671	0	28.29338078	Q7Z4I7	Q7Z4I7	0	0	1	1	1	1	1	1	2	4	6	0
Cytochrome c o	**NDUFA4**	NaN	22.4738	21.6894	NaN	23.15879	22.6138	23.62801	24.16576	cell part;cytoplasmic part;intracellular organelle part;intracellular	10.364	0.002	28.34367261	O00483	O00483	0	1	1	0	1	1	1	1	2	4	6	0
Collagen alpha-:	**COL28A1**	NaN	NaN	15.86641	18.94335	18.95319	17.23603	17.94518	17.60711	basement membrane;cell part;collagen;cytoplasmic part;endopla	7.6224	0.0018	26.58505858	Q2UY09	Q2UY09	0	0	1	1	1	1	1	1	2	4	6	1
Unconventional	**MYO5A**	NaN	18.66882	15.68967	NaN	16.06808	15.07944	13.55663	18.77533	actomyosin;cell body;cell part;cell projection;cell projection part;	6.2187	0.0091	26.5791709	Q9Y4I1	Q9Y4I1	0	1	1	0	1	1	1	1	2	4	6	0
Thrombospondi	**THBS4**	NaN	17.40615	16.40085	23.54345	NaN	NaN	NaN	NaN	basement membrane;cell part;cytoplasmic part;extracellular mat	48.69	0	28.89573613	P35443;CON__I	P35443	0	1	1	1	0	0	0	0	3	0	3	1
Sorbin and SH3	**SORBS1**	NaN	15.43195	17.31371	21.94474	NaN	NaN	NaN	NaN	actin cytoskeleton;actin filament bundle;actomyosin;adherens jui	43.274	0	27.92382716	Q9BX66;O9487	Q9BX66	0	1	1	1	0	0	0	0	3	0	3	0
Calcium/calmoc	**CAMK2G;CAMK2A;CAMK2!**	17.06792	NaN	19.02429	22.53251	NaN	NaN	NaN	NaN	axon part;calcium- and calmodulin-dependent protein kinase con	12.43	0	27.32757389	Q13555;Q9UQ!	Q13555;Q9UQ!	1	0	1	1	0	0	0	0	3	0	3	0
Cilia- and flagell	**CFAP46**	16.97668	17.99214	NaN	20.45202	NaN	NaN	NaN	NaN		8.9569	0.0019	27.87554848	Q8IYW2	Q8IYW2	1	1	0	1	0	0	0	0	3	0	3	0
Protein Niban	**FAM129A**	NaN	17.53541	16.94364	20.18628	NaN	NaN	NaN	NaN	cell part;cytoplasm;intracellular membrane-bounded organelle;in	8.3217	0.0019	25.81066165	Q9BZQ8	Q9BZQ8	0	1	1	1	0	0	0	0	3	0	3	0
KN motif and ar	**KANK2**	17.53397	NaN	16.44954	19.9146	NaN	NaN	NaN	NaN	cell part;cytoplasmic part;intracellular membrane-bounded orgar	7.8978	0.0019	25.73308941	Q63ZY3	Q63ZY3	1	0	1	1	0	0	0	0	3	0	3	0
Fructose-bisphc	**ALDOA**	NaN	21.50237	21.0428	23.37332	NaN	NaN	NaN	24.11981	actin cytoskeleton;cell part;contractile fiber part;cytoplasmic mer	138.92	0	29.55217331	P04075	P04075	0	1	1	1	0	0	0	1	3	1	4	1
40S ribosomal p	**RPSA**	NaN	19.50005	16.69656	23.11987	NaN	NaN	NaN	22.90492	90S preribosome;cell part;cytosolic small ribosomal subunit;intra	113.49	0	27.78718459	P08865	P08865	0	1	1	1	0	0	0	1	3	1	4	0
Hydroxymethylg	**HMGCS2**	16.93099	20.49648	NaN	21.06316	NaN	NaN	NaN	25.06714	cell part;cytoplasmic part;cytosol;intracellular membrane-bounde	110.83	0	29.8589021	P54868;Q0158:	P54868	1	1	0	1	0	0	0	1	3	1	4	0
Collagen alpha-:	**COL15A1**	NaN	19.13609	15.3668	21.65517	NaN	NaN	NaN	14.95765	basement membrane;cell part;collagen;collagen type XV;cytoplas	57.027	0	27.37393155	P39059	P39059	0	1	1	1	0	0	0	1	3	1	4	1
Cytochrome c o	**MT-CO2**	NaN	22.53751	18.44225	23.24551	NaN	NaN	NaN	25.40912	cell part;cytoplasmic part;integral to membrane;intracellular orga	37.247	0	28.86100453	P00403	P00403	0	1	1	1	0	0	0	1	3	1	4	0
Integrin alpha-5	**ITGA5**	NaN	18.67366	18.16678	21.76454	NaN	NaN	15.23818	NaN	alphav-beta3 integrin-vitronectin complex;cell part;cell projectior	26.121	0	27.36243923	P08648	P08648	0	1	1	1	0	0	1	0	3	1	4	0
Catechol O-met	**COMT**	NaN	17.367	16.80486	22.26828	NaN	NaN	NaN	21.93423	cell part;cytoplasmic part;cytosol;integral to membrane;intracellu	24.683	0	27.06229356	P21964	P21964	0	1	1	1	0	0	0	1	3	1	4	0
Thioredoxin-dep	**PRDX3**	NaN	19.39058	17.049	20.82889	NaN	NaN	NaN	22.5467	cell part;cytoplasmic part;early endosome;endosome;intracellulai	19.533	0	26.97792866	P30048	P30048	0	1	1	1	0	0	0	1	3	1	4	0
Phosphate carri	**SLC25A3**	NaN	16.63835	18.47718	22.97596	NaN	NaN	NaN	23.13458	cell part;cytoplasmic part;integral to membrane;integral to plasm	16.079	0	28.2654395	Q00325	Q00325	0	1	1	1	0	0	0	1	3	1	4	0
NADH dehydrog	**NDUFV1**	NaN	17.52871	16.00486	18.61709	NaN	NaN	NaN	19.31895	cell part;cytoplasmic part;intracellular organelle part;intracellular	14.485	0	24.84570252	P49821	P49821	0	1	1	1	0	0	0	1	3	1	4	0
PDZ and LIM do	**PDLIM3**	NaN	16.22521	18.96975	22.38853	NaN	NaN	NaN	16.65941	actin cytoskeleton;cell part;contractile fiber part;cytoplasmic part	13.474	0	26.56013805	Q53GG5	Q53GG5	0	1	1	1	0	0	0	1	3	1	4	0
Isocitrate dehyc	**IDH3A**	NaN	17.43184	15.72973	20.13859	NaN	NaN	NaN	20.8949	cell part;cytoplasmic part;intracellular organelle lumen;intracellul	8.5918	0.0019	26.06167575	P50213	P50213	0	1	1	1	0	0	0	1	3	1	4	0
Endothelial prot	**PROCR**	NaN	18.78944	15.34395	19.76888	NaN	NaN	17.31867	NaN	cell part;centrosome;cytoplasmic part;cytoskeletal part;integral t	6.9273	0.0017	23.88716036	Q9UNN8	Q9UNN8	0	1	1	1	0	0	1	0	3	1	4	0
Dynein light cha	**DYNLL2;DYNLL1**	NaN	22.92191	19.94507	23.81646	NaN	NaN	22.47417	NaN	cell part;centrosome;chromosomal part;cytoplasmic dynein comp	6.6798	0.0033	27.13887579	Q96FJ2;P63167	Q96FJ2;P63167	0	1	1	1	0	0	1	0	3	1	4	0
Carbonyl reduct	**CBR1**	NaN	19.71537	19.27814	23.53077	NaN	NaN	21.24377	26.76623	cell part;cytoplasmic part;cytosol;intracellular part	254.98	0	31.04407324	P16152	P16152	0	1	1	1	0	0	1	1	3	2	5	0
Prelamin-A/C;La	**LMNA**	NaN	18.46368	18.05081	24.58394	NaN	NaN	17.77211	22.48709	cell part;cytoplasmic part;cytoskeletal part;cytosol;envelope;inter	129.67	0	30.28383274	P02545;Q0325:	P02545	0	1	1	1	0	0	1	1	3	2	5	0
Trifunctional en	**HADHA**	NaN	15.34002	16.909	21.22134	17.95003	NaN	NaN	22.90991	cell part;cytoplasmic part;fatty acid beta-oxidation multienzyme c	121.73	0	28.71450127	P40939	P40939	0	1	1	1	1	0	0	1	3	2	5	0
Keratin, type I c	**KRT18**	NaN	17.50246	16.13168	20.51297	NaN	NaN	15.65545	25.12904	cell part;centriolar satellite;cytoplasmic part;cytoskeletal part;int	112.59	0	29.89879483	P05783;CON__I	P05783	0	1	1	1	0	0	1	1	3	2	5	0
Alpha-2-macrog	**A2M**	NaN	19.17446	19.84629	21.45739	NaN	NaN	22.54428	22.77545	cell part;cytoplasmic membrane-bounded vesicle lumen;cytoplas	111.67	0	30.24796325	P01023;P20742	P01023	0	1	1	1	0	0	1	1	3	2	5	1
Retinal dehydro	**ALDH1A1**	NaN	21.05245	19.30289	23.41067	NaN	NaN	20.68671	25.21438	cell part;cytoplasmic part;cytosol;intracellular part	85.053	0	30.28713991	P00352	P00352	0	1	1	1	0	0	1	1	3	2	5	0
Ig kappa chain V	**IGKV3D-20**	NaN	19.52744	21.06329	22.71158	NaN	NaN	24.48616	24.54103	cell part;extracellular region;membrane;plasma membrane	66.134	0	28.10464602	P01619;A0A0C4	P01619;A0A0C4	0	1	1	1	0	0	1	1	3	2	5	1
Collagen alpha-:	**COL18A1**	NaN	14.82257	16.55606	20.5792	NaN	NaN	17.31902	18.02025	basement membrane;cell part;collagen;cytoplasmic part;endopla	65.131	0	27.01648323	P39060	P39060	0	1	1	1	0	0	1	1	3	2	5	1
Myosin light pol	**MYL6**	22.22391	23.07287	NaN	27.21891	NaN	NaN	19.95731	24.16216	cell part;contractile fiber part;cytoplasmic part;cytoskeletal part;c	53.994	0	30.82122463	P60660;P14649	P60660	1	1	0	1	0	0	1	1	3	2	5	0
NADH-ubiquino	**NDUFS1**	NaN	17.27957	15.25045	20.31959	NaN	NaN	15.92	20.22435	cell part;cytoplasmic part;intracellular organelle part;intracellular	53.658	0	26.77127627	P28331	P28331	0	1	1	1	0	0	1	1	3	2	5	0
Alpha-actinin-4	**ACTN4**	NaN	18.13576	14.41614	21.4893	NaN	NaN	17.02767	21.22359	adherens junction;anchoring junction;axon hillock;axon part;cell	43.071	0	28.25795311	O43707;Q9H25	O43707	0	1	1	1	0	0	1	1	3	2	5	1
Dihydropyrimidi	**DPYSL2**	NaN	19.0529	16.67135	22.76215	NaN	NaN	21.01733	20.96818	axon;cell body;cell part;cell projection;cell projection part;cytopla	42.218	0	28.46298902	Q16555	Q16555	0	1	1	1	0	0	1	1	3	2	5	0
40S ribosomal p	**RPS4X**	NaN	19.56755	19.0284	22.81059	NaN	NaN	17.25156	23.17909	cell part;cytosolic small ribosomal subunit;intracellular organelle p	36.716	0	28.12706382	P62701	P62701	0	1	1	1	0	0	1	1	3	2	5	0
60S ribosomal p	**RPL8**	NaN	20.16484	18.63403	21.16521	NaN	NaN	20.70033	21.45889	cell part;cytosolic large ribosomal subunit;intracellular organelle p	33.927	0	26.34440089	P62917	P62917	0	1	1	1	0	0	1	1	3	2	5	0
Coatomer subu	**COPA**	NaN	17.55052	14.4595	20.31163	NaN	NaN	18.89368	20.81855	cell part;COPI vesicle coat;cytoplasmic part;cytoplasmic vesicle pa	32.718	0	28.00656629	P53621	P53621	0	1	1	1	0	0	1	1	3	2	5	1
Ig kappa chain C	**IGKC**	NaN	22.33644	23.58669	23.50616	NaN	NaN	26.22505	26.90185	cell part;extracellular region;membrane;plasma membrane	28.266	0	30.12164014	P01834;P0DOX7	P01834	0	1	1	1	0	0	1	1	3	2	5	1
Aldehyde dehyd	**ALDH2**	NaN	20.35035	16.63849	22.00638	20.79844	NaN	NaN	23.25926	cell part;cytoplasmic part;intracellular organelle lumen;intracellul	28.103	0	28.58566751	P05091	P05091	0	1	1	1	1	0	0	1	3	2	5	0
Heterogeneous	**HNRNPU**	NaN	16.22955	16.98526	20.82151	NaN	NaN	18.42771	21.001	catalytic step 2 spliceosome;cell part;cell surface;CRD-mediated r	26.777	0	27.31440871	Q00839	Q00839	0	1	1	1	0	0	1	1	3	2	5	0
Catenin beta-1	**CTNNB1**	NaN	18.21618	16.06655	20.52583	NaN	NaN	16.66289	21.33783	adherens junction;anchoring junction;apical part of cell;basolater	25.262	0	27.53712216	P35222	P35222	0	1	1	1	0	0	1	1	3	2	5	0
Inter-alpha-tryp	**ITIH1**	NaN	19.51355	17.29266	20.61369	NaN	NaN	20.86861	20.01031	extracellular region	24.876	0	27.63478004	P19827	P19827	0	1	1	1	0	0	1	1	3	2	5	1
Tubulin beta-4B	**TUBB4B;TUBB4A**	NaN	17.51384	17.65291	23.13777	NaN	NaN	19.49826	22.01417	axon part;cell body;cell part;cell projection;cell projection part;cil	23.601	0	28.1212449	P68371;P0435C	P68371;P0435C	0	1	1	1	0	0	1	1	3	2	5	0
Phosphoglucom	**PGM5**	NaN	21.51562	19.88785	21.30318	NaN	18.38457	NaN	19.70952	actin filament bundle;actomyosin;adherens junction;anchoring ju	23.162	0	27.88675349	Q15124	Q15124	0	1	1	1	0	1	0	1	3	2	5	0
Serine/threonin	**PPP2R1A;PPP2R1B**	NaN	19.0164	14.4685	21.45608	NaN	NaN	18.1802	20.62925	cell part;chromosomal part;chromosome, centromeric region;cyt	23.077	0	27.35077034	P30153;P30154	P30153;P30154	0	1	1	1	0	0	1	1	3	2	5	0
Ras GTPase-acti	**IQGAP1**	NaN	17.98131	13.41667	19.9402	NaN	NaN	15.45799	19.4222	actin filament;cell leading edge;cell part;cell projection;cytoplasm	22.219	0	27.32328474	P46940	P46940	0	1	1	1	0	0	1	1	3	2	5	0
Epoxide hydrola	**EPHX1**	17.63062	19.15889	NaN	20.31849	NaN	NaN	19.81621	20.33767	cell part;cytoplasmic part;endoplasmic reticulum membrane;end	20.195	0	26.75110903	P07099	P07099	1	1	0	1	0	0	1	1	3	2	5	0
Vacuolar protei	**VPS35**	NaN	18.57673	15.49785	20.1483	NaN	NaN	18.19398	20.50959	cell part;cytoplasmic part;cytosol;endosome;intracellular membr	18.765	0	27.08598165	Q96QK1	Q96QK1	0	1	1	1	0	0	1	1	3	2	5	0
Protein kinase C	**PRKCDBP**	NaN	20.6289	21.29266	23.95589	NaN	NaN	19.72319	21.09803		17.089	0	28.07556394	Q969G5	Q969G5	0	1	1	1	0	0	1	1	3	2	5	0
Protein disulfide	**PDIA6**	16.96206	18.38734	NaN	19.26215	15.8013	NaN	NaN	20.56505	cell part;cytoplasmic membrane-bounded vesicle;cytoplasmic par	14.98	0	25.45613379	Q15084	Q15084	1	1	0	1	1	0	0	1	3	2	5	0
Dihydrolipoyllys	**DLST**	18.79341	17.79392	NaN	17.95379	NaN	NaN	15.69223	21.33249	cell part;cytoplasmic part;intracellular membrane-bounded orgar	12.635	0	26.31471987	P36957	P36957	1	1	0	1	0	0	1	1	3	2	5	0
Histidine--tRNA	**HARS;HARS2**	NaN	15.76599	14.67342	17.23491	NaN	NaN	16.41148	19.58589	cell part;cytoplasmic part;cytosol;intracellular organelle lumen;in	12.494	0	24.88976165	P12081;P4959C	P12081;P4959C	0	1	1	1	0	0	1	1	3	2	5	0
Ras-related prot	**RAP1A;RAP1B**	NaN	20.09016	19.15618	24.00333	20.36602	NaN	NaN	20.57727	cell junction;cell part;cell-cell junction;cytoplasmic part;cytosol;g	11.84	0	27.67519125	P62834;P61224	P62834;P61224	0	1	1	1	1	0	0	1	3	2	5	0
Dystrophin	**DMD**	NaN	15.53603	12.87396	18.2243	NaN	12.02115	NaN	11.99163	cell junction;cell part;cell projection;cell projection part;cell surfa	10.071	0.002	26.1245123	P11532	P11532	0	1	1	1	0	1	0	1	3	2	5	0
40S ribosomal p	**RPS27L;RPS27**	NaN	21.78177	19.53049	23.99291	NaN	19.94077	NaN	24.32279	cell part;cytoplasmic part;cytosolic small ribosomal subunit;intrac	8.0226	0.0019	27.35942612	Q71UM5;P4267	Q71UM5;P4267	0	1	1	1	0	1	0	1	3	2	5	0
Serum deprivati	**SDPR**	NaN	17.63446	18.15101	22.64106	NaN	NaN	19.01405	16.34511	caveola;cell part;cytoplasmic part;cytosol;Golgi apparatus;intrace	7.984	0.0019	27.03663897	O95810	O95810	0	1	1	1	0	0	1	1	3	2	5	0
Ras-related prot	**RAB7A**	18.2846	20.37571	19.23318	NaN	NaN	NaN	20.70599	21.6044	cell part;cytoplasmic membrane-bounded vesicle;cytoplasmic par	7.7411	0.0019	26.58591818	P51149	P51149	1	1	1	0	0	0	1	1	3	2	5	0
Ubiquitin thioes	**OTUB1**	NaN	18.43758	16.88441	21.56788	NaN	NaN	19.53191	21.32069	cell part;cytoplasm;intracellular part	7.5313	0.0018	26.63796098	Q96FW1	Q96FW1	0	1	1	1	0	0	1	1	3	2	5	0
40S ribosomal p	**RPS2**	NaN	20.23351	17.46491	21.86658	NaN	NaN	19.30405	21.25344	cell part;cytosolic small ribosomal subunit;intracellular organelle p	6.2048	0.009	27.16920876	P15880	P15880	0	1	1	1	0	0	1	1	3	2	5	0
Dihydropyrimidi	**DPYSL3**	NaN	20.16165	21.04153	24.91825	18.74685	NaN	19.87054	20.78029	cell body;cell part;cell projection;cell projection part;cytoplasmic	146.86	0	30.04648212	Q14195;Q1411	Q14195	0	1	1	1	1	0	1	1	3	3	6	1
Neutral alpha-g	**GANAB**	NaN	21.02958	17.37203	22.84986	NaN	17.78922	20.16042	23.18797	cell part;cytoplasmic membrane-bounded vesicle;cytoplasmic par	86.781	0	29.73802153	Q14697	Q14697	0	1	1	1	0	1	1	1	3	3	6	0
Complement fac	**CFH**	NaN	18.52512	18.2874	19.57108	17.59667	NaN	21.35515	20.99369	extracellular region part;extracellular space	85.651	0	28.55043122	P08603;Q0359:	P08603	0	1	1	1	1	0	1	1	3	3	6	1
Elongation factc	**EEF2**	NaN	20.09352	19.341	23.81	15.62154	NaN	19.26282	23.61009	Cajal body;catalytic step 2 spliceosome;cell part;cytoplasm;cytopl	84.677	0	30.3290293	P13639;Q1502!	P13639	0	1	1	1	1	0	1	1	3	3	6	0
Vesicle-traffickii	**SEC22B**	NaN	18.60038	16.52654	20.27901	18.62738	NaN	19.49557	21.85935	cell part;cytoplasmic membrane-bounded vesicle;cytoplasmic par	82.581	0	26.48588113	O75396	O75396	0	1	1	1	1	0	1	1	3	3	6	0
Ras suppressor	**RSU1**	NaN	16.47226	18.34043	23.58291	16.31311	NaN	17.45555	17.66595	cell part;cytoplasmic part;cytosol;intracellular part	74.834	0	27.38228496	Q15404	Q15404	0	1	1	1	1	0	1	1	3	3	6	0
Hemopexin	**HPX**	NaN	18.4186	21.08537	23.67239	18.24623	NaN	23.38811	23.321	cell part;cytoplasmic membrane-bounded vesicle lumen;cytoplas	62.151	0	29.69208894	P02790	P02790	0	1	1	1	1	0	1	1	3	3	6	1
Peptidyl-prolyl c	**PPIA**	NaN	23.38311	21.92299	25.62642	23.6424	NaN	23.14171	25.66077	cell part;cytoplasm;cytoplasmic part;cytosol;extracellular region;i	44.029	0	30.40436093	P62937;P0DN2(	P62937	0	1	1	1	1	0	1	1	3	3	6	1
Rab GDP dissoci	**GDI2;GDI1**	NaN	20.13696	17.72674	22.61547	17.65976	NaN	20.6136	22.96182	cell part;cell projection;cell surface;cytoplasmic part;cytosol;Golg	42.461	0	28.89084608	P50395;P3115C	P50395;P3115C	0	1	1	1	1	0	1	1	3	3	6	0
60S ribosomal p	**RPL18**	NaN	22.46451	20.91641	25.06682	21.22911	NaN	22.87513	24.50972	cell part;cytosolic large ribosomal subunit;intracellular organelle p	30.332	0	29.00477291	Q07020	Q07020	0	1	1	1	1	0	1	1	3	3	6	0
Alcohol dehydrc	**ADH1C**	NaN	19.26098	18.5252	20.2815	21.45141	NaN	19.83124	23.18094	cell part;cytoplasmic part;cytosol;intracellular part	27.479	0	28.14204511	P00326	P00326	0	1	1	1	1	0	1	1	3	3	6	0
4-trimethylamir	**ALDH9A1**	NaN	19.82045	19.70968	21.36432	NaN	17.74806	19.87082	23.08426	cell part;cytoplasmic part;cytosol;intracellular membrane-bounde	27.463	0	28.43884787	P49189	P49189	0	1	1	1	0	1	1	1	3	3	6	0
Tryptase delta;T	**TPSD1;TPSAB1;TPSB2**	NaN	23.48173	21.63878	24.0426	NaN	19.51655	21.99148	23.56092	extracellular region;extracellular region part;extracellular space	20.971	0	27.88442628	Q9BZJ3;Q15661	Q9BZJ3;Q15661	0	1	1	1	0	1	1	1	3	3	6	1
Tripeptidyl-pept	**TPP1**	19.97785	19.23142	NaN	22.34976	20.10827	NaN	20.1154	21.57029	cell part;cytoplasmic membrane-bounded vesicle;cytoplasmic par	20.884	0	28.14569337	O14773	O14773	1	1	0	1	1	0	1	1	3	3	6	0
40S ribosomal p	**RPS5**	NaN	20.65622	19.10774	22.44152	20.16962	NaN	20.50417	22.69011	cell part;cytosolic small ribosomal subunit;intracellular organelle p	17.478	0	27.37011094	P46782	P46782	0	1	1	1	1	0	1	1	3	3	6	0
Heterogeneous	**HNRNPA0**	19.05049	19.28695	NaN	21.72841	17.08701	NaN	20.66692	20.878	cell part;intracellular organelle part;intracellular part;macromolec	16.926	0	26.70041453	Q13151	Q13151	1	1	0	1	1	0	1	1	3	3	6	0
Integrin beta-1	**ITGB1**	17.96121	19.03628	NaN	21.63662	18.03333	NaN	18.27403	18.30412	acrosomal vesicle;adherens junction;alpha3-beta1 integrin compl	15.852	0	27.32997025	P05556	P05556	1	1	0	1	1	0	1	1	3	3	6	1
2-oxoglutarate	**OGDHL;OGDH**	NaN	17.62927	15.49361	19.38216	NaN	15.66183	18.15026	20.24458	cell part;cytoplasmic part;intracellular organelle lumen;intracellul	13.743	0	26.90724461	Q9ULD0;Q0221	Q9ULD0;Q0221	0	1	1	1	0	1	1	1	3	3	6	0
Versican core pr	**VCAN**	NaN	15.12525	15.50937	19.68876	16.94512	15.01963	16.84806	NaN	cell part;cytoplasmic part;extracellular matrix;extracellular region	13.414	0	27.23388762	P13611	P13611	0	1	1	1	1	1	1	0	3	3	6	1
ATP synthase su	**ATP5L**	18.06902	21.06375	NaN	23.34652	20.14009	NaN	21.30419	22.41483	cell part;cytoplasmic part;intracellular organelle part;intracellular	13.251	0	27.00645929	O75964	O75964	1	1	0	1	1	0	1	1	3	3	6	0
Laminin subunit	**LAMA4**	NaN	16.66108	15.56111	19.54683	15.47285	NaN	17.43518	15.25363	basal lamina;extracellular matrix part;extracellular membrane-bo	13.138	0	26.66180093	Q16363	Q16363	0	1	1	1	1	0	1	1	3	3	6	1
Chloride intrace	**CLIC1**	NaN	20.7446	16.94043	21.34484	15.24578	NaN	20.81746	22.9443	brush border;cell part;cell projection;chloride channel complex;cy	12.885	0	27.69683809	O00299	O00299	0	1	1	1	1	0	1	1	3	3	6	0
Neuroblast diffe	**AHNAK**	NaN	15.92231	15.21523	17.60711	13.17927	NaN	15.91474	15.41326	cell part;intracellular membrane-bounded organelle;intracellular	11.999	0	27.21549034	Q09666	Q09666	0	1	1	1	1	0	1	1	3	3	6	0
L-lactate dehydi	**LDHB**	NaN	20.1893	17.40374	22.66999	20.05762	NaN	20.59396	20.92129	cell part;cytoplasmic part;cytosol;intracellular membrane-bounde	11.132	0.0021	27.68605527	P07195	P07195	0	1	1	1	1	0	1	1	3	3	6	0
Biliverdin reduc	**BLVRA**	NaN	17.04228	17.50719	20.55843	NaN	14.42528	18.85583	19.24379	cell part;cytoplasmic part;cytosol;intracellular part	8.4547	0.0019	25.50821163	P53004	P53004	0	1	1	1	0	1	1	1	3	3	6	0
Olfactomedin-lil	**OLFML1**	NaN	17.26334	16.35002	18.43575	19.68859	NaN	18.8746	17.719	extracellular region	7.114	0.0017	25.48646434	Q6UWY5	Q6UWY5	0	1	1	1	1	0	1	1	3	3	6	1
Sodium/potassi	**ATP1B1**	19.23713	18.7725	NaN	19.74521	20.25994	NaN	16.92544	20.12237	apical plasma membrane;basolateral plasma membrane;caveola;c	6.789	0.0017	25.67551432	P05026	P05026	1	1	0	1	1	0	1	1	3	3	6	0
Band 4.1-like pr	**EPB41L2**	NaN	16.95572	14.61339	16.99998	18.00487	NaN	17.84328	18.53757	cell cortex part;cell junction;cell part;cytoplasmic part;cytoskelet:	6.7499	0.0016	25.92947063	O43491	O43491	0	1	1	1	1	0	1	1	3	3	6	0
60S ribosomal p	**RPL4**	15.94569	19.85965	NaN	19.14301	NaN	17.54751	19.8966	20.43817	cell part;cytosolic large ribosomal subunit;intracellular non-memb	6.2307	0.0091	25.99567538	P36578	P36578	1	1	0	1	0	1	1	1	3	3	6	0
Fibrinogen beta	**FGB**	NaN	21.66674	21.44567	24.76289	22.72594	20.02743	28.37169	26.919	blood microparticle;cell cortex;cell part;cytoplasmic membrane-b	323.31	0	33.75254526	P02675;CON__I	P02675	0	1	1	1	1	1	1	1	3	4	7	1
Tenascin	**TNC**	NaN	19.45433	18.45527	23.95358	19.72758	18.69551	17.34888	19.37373	basement membrane;extracellular matrix;extracellular matrix par	317.77	0	30.91463342	P24821	P24821	0	1	1	1	1	1	1	1	3	4	7	1
Galectin-1	**LGALS1**	NaN	24.82406	24.25443	27.14492	23.03947	22.49787	24.37385	24.74837	cell part;cell surface;cytoplasm;extracellular matrix;extracellular r	183.74	0	31.13815563	P09382	P09382	0	1	1	1	1	1	1	1	3	4	7	1
Fibrinogen gam	**FGG**	NaN	21.48247	21.74698	24.32841	23.4979	21.3208	28.13011	26.74817	blood microparticle;cell cortex;cell part;cytoplasmic membrane-b	179.33	0	33.54777278	P02679	P02679	0	1	1	1	1	1	1	1	3	4	7	1
Talin-1	**TLN1**	NaN	19.49309	20.43878	23.49253	20.28173	18.41043	18.45535	20.50795	actin cytoskeleton;adherens junction;anchoring junction;cell junc	175.63	0	31.11079346	Q9Y490;Q9Y4G	Q9Y490	0	1	1	1	1	1	1	1	3	4	7	1
Fibrinogen alph	**FGA**	NaN	19.9356	20.01998	22.25358	21.93815	20.36794	26.16984	24.81568	cell cortex;cell part;cytoplasmic membrane-bounded vesicle lume	152.64	0	32.09301542	P02671;CON__I	P02671	0	1	1	1	1	1	1	1	3	4	7	1
Glyceraldehyde	**GAPDH**	NaN	21.99324	21.07901	25.28602	21.92328	20.84782	22.52334	25.18325	cell part;cytoplasmic part;cytoskeleton;cytosol;extracellular mem	145.26	0	30.62331209	P04406;O1455(	P04406	0	1	1	1	1	1	1	1	3	4	7	1
Collagen alpha-:	**COL12A1**	NaN	18.74983	17.34004	22.0046	18.29041	16.91917	20.24876	19.56791	anchoring collagen;cell part;collagen;collagen type XII;cytoplasmi	130.78	0	30.0150479	Q99715	Q99715	0	1	1	1	1	1	1	1	3	4	7	1
Annexin A4	**ANXA4**	NaN	20.4711	20.54302	23.97386	18.25257	19.51563	21.44678	24.90582	cell part;cytoplasm;intracellular part	114.67	0	30.16746313	P09525	P09525	0	1	1	1	1	1	1	1	3	4	7	0
Profilin-1	**PFN1**	NaN	23.66807	23.33525	26.90357	23.53243	22.50678	23.94771	25.84144	cell part;cell projection;cytoplasm;cytoskeleton;intracellular mem	92.475	0	31.03131086	P07737;CON__I	P07737	0	1	1	1	1	1	1	1	3	4	7	0
Very long-chain	**ACADVL**	NaN	17.91508	16.8728	18.69703	17.20505	17.33978	18.68623	23.13951	cell part;cytoplasmic part;intracellular non-membrane-bounded c	79.482	0	28.71823027	P49748	P49748	0	1	1	1	1	1	1	1	3	4	7	0
Creatine kinase	**CKB**	NaN	23.47395	19.62507	26.53936	21.99096	19.83112	22.29174	23.13017	cell part;cytoplasmic part;cytosol;intracellular membrane-bounde	65.83	0	31.0347908	P12277;P06732	P12277	0	1	1	1	1	1	1	1	3	4	7	0
60 kDa heat shc	**HSPD1**	NaN	18.52711	15.8573	22.08803	15.7819	14.40833	19.37948	23.36973	cell part;cell surface;coated pit;coated vesicle;cytoplasmic memb	62.316	0	28.97544344	P10809	P10809	0	1	1	1	1	1	1	1	3	4	7	1
WD repeat-cont	**WDR1**	NaN	21.07503	20.82143	24.78741	20.86899	18.86568	20.88181	23.52432	cell part;cytoplasmic part;cytoskeleton;cytosol;extracellular regio	60.343	0	30.46519032	O75083	O75083	0	1	1	1	1	1	1	1	3	4	7	1
Aconitate hydra	**ACO2**	NaN	19.68175	18.00574	22.15666	18.68965	17.56376	18.38457	23.16434	cell part;cytoplasmic part;intracellular membrane-bounded orgar	53.052	0	29.19197066	Q99798	Q99798	0	1	1	1	1	1	1	1	3	4	7	0
Ig gamma-1 cha	**IGHG1**	NaN	21.45623	22.11261	21.97813	21.9346	19.65318	25.2274	25.41355	cell part;extracellular region;membrane	50.043	0	31.03996234	P0DOX5;P0185	P0DOX5;P0185	0	1	1	1	1	1	1	1	3	4	7	1
Phosphoglycera	**PGK1**	NaN	20.16803	20.24063	23.31382	18.74652	15.95283	20.97092	22.85247	cell part;cytoplasmic part;cytosol;intracellular part	48.486	0	29.20853043	P00558;P07205	P00558	0	1	1	1	1	1	1	1	3	4	7	0
Heat shock 70 k	**HSPA6;HSPA7**	NaN	20.69396	20.84889	23.5341	20.80049	17.98103	21.48005	21.77925		43.044	0	29.74634327	P17066;P48741	P17066;P48741	0	1	1	1	1	1	1	1	3	4	7	0
Fermitin family	**FERMT2**	NaN	20.85377	20.68097	23.40976	20.77121	17.2534	19.37592	20.3024	actin filament bundle;actomyosin;adherens junction;anchoring ju	42.46	0	29.36131005	Q96AC1;Q9BQL	Q96AC1	0	1	1	1	1	1	1	1	3	4	7	0
Mitochondrial c	**MTCH2**	NaN	20.24086	18.22962	21.90987	16.59398	16.19476	19.69714	21.76563	cell part;cytoplasmic part;integral to membrane;intracellular mer	35.123	0	27.0717337	Q9Y6C9	Q9Y6C9	0	1	1	1	1	1	1	1	3	4	7	0
Alpha-crystallin	**CRYAB**	NaN	19.49219	20.52459	25.49896	16.94912	16.38898	18.652	17.46985	actin filament bundle;cell part;cell surface;contractile fiber part;c	34.328	0	29.04835437	P02511	P02511	0	1	1	1	1	1	1	1	3	4	7	0
40S ribosomal p	**RPS9**	NaN	21.26207	20.08472	23.6872	20.75173	19.28575	21.2596	23.14191	cell part;cytosolic small ribosomal subunit;intracellular non-meml	33.252	0	28.35934233	P46781	P46781	0	1	1	1	1	1	1	1	3	4	7	0
40S ribosomal p	**RPS8**	19.35969	20.73975	NaN	22.44225	20.57598	19.02118	21.79396	22.68705	cell part;cytosolic small ribosomal subunit;intracellular organelle p	31.836	0	27.46653282	P62241	P62241	1	1	0	1	1	1	1	1	3	4	7	0
Ribonuclease in	**RNH1**	NaN	20.14967	17.66372	20.22329	18.76678	16.21039	19.36583	22.00601	angiogenin-PRI complex;cell part;cytoplasm;extracellular region p	31.519	0	27.63277105	P13489	P13489	0	1	1	1	1	1	1	1	3	4	7	1
Ras-related prot	**RAB6B;RAB6A;RAB39A**	19.60023	20.89149	NaN	20.18701	21.14083	20.10917	21.4039	22.46742	cell part;cytoplasmic membrane-bounded vesicle;cytoplasmic par	31.508	0	27.62756238	Q9NRW1;P2034	Q9NRW1;P2034	1	1	0	1	1	1	1	1	3	4	7	0
Four and a half	**FHL1**	NaN	20.794	19.97533	25.46669	20.48925	17.78315	19.81934	20.83492	cell part;cytoplasm;cytoplasmic part;cytosol;intracellular membra	29.393	0	29.84867208	Q13642	Q13642	0	1	1	1	1	1	1	1	3	4	7	0
Cytochrome b-c	**UQCRC1**	NaN	19.7088	18.6683	22.91136	19.24695	15.608	17.69084	23.83016	cell part;cytoplasmic part;intracellular organelle part;intracellular	29.244	0	29.15805302	P31930	P31930	0	1	1	1	1	1	1	1	3	4	7	0
Serine/threonin	**PPP1CB;PPP1CC;PPP1CA**	NaN	20.12616	17.29795	23.57045	18.17612	16.01155	19.79284	21.01971	cell division site part;cell part;cell projection;cell projection part;c	28.19	0	28.1199596	P62140;P36873	P62140;P36873	0	1	1	1	1	1	1	1	3	4	7	0
Microsomal glu	**MGST3**	21.89951	21.1364	20.5515	NaN	20.65762	23.57068	24.2754	25.0976	cell part;cytoplasmic part;endoplasmic reticulum membrane;end	27.729	0	29.02572545	O14880	O14880	1	1	1	0	1	1	1	1	3	4	7	0
Pyruvate dehyd	**PDHA1**	NaN	18.29836	16.3962	22.13097	19.44901	18.38734	20.32323	21.80278	cell part;cytoplasmic part;intracellular organelle lumen;intracellul	25.344	0	27.85442053	P08559	P08559	0	1	1	1	1	1	1	1	3	4	7	0
ATP-dependent	**PFKP**	NaN	19.48552	19.79636	22.5484	17.40116	19.18848	20.49609	22.0434	6-phosphofructokinase complex;cell part;cytoplasmic part;cytosc	24.717	0	28.77457882	Q01813	Q01813	0	1	1	1	1	1	1	1	3	4	7	0
Protein S100-A6	**S100A6**	NaN	23.6299	16.82053	27.03538	20.62854	20.0692	23.47568	25.32882	cell part;cell projection;cytoplasmic part;cytosol;envelope;extrins	22.532	0	29.94823759	P06703	P06703	0	1	1	1	1	1	1	1	3	4	7	0
40S ribosomal p	**RPS24**	21.594	23.62489	NaN	24.05457	21.33025	20.64491	23.70187	23.12967	cell part;cytosolic small ribosomal subunit;intracellular non-meml	21.329	0	28.43833234	P62847	P62847	1	1	0	1	1	1	1	1	3	4	7	0
Ig lambda-1 cha	**IGLC1;IGLL5;IGLC6**	NaN	20.76773	22.19665	23.53706	22.55946	19.90739	25.4928	25.33681	cell part;extracellular region;membrane;plasma membrane	21.006	0	29.59097585	P0DOY3;P0DOY	P0DOY3;P0DOY	0	1	1	1	1	1	1	1	3	4	7	1
14-3-3 protein s	**SFN**	NaN	21.18423	19.26531	23.31879	17.61411	17.47287	20.80664	22.974	cell part;cytoplasmic part;cytoplasmic vesicle membrane;cytoplas	19.007	0	28.5124301	P31947	P31947	0	1	1	1	1	1	1	1	3	4	7	1
Lipoma-preferre	**LPP**	NaN	20.19328	20.33582	24.9522	20.28996	17.24088	20.67564	21.59117	adherens junction;anchoring junction;cell junction;cell part;cell-s	18.927	0	29.99846501	Q93052	Q93052	0	1	1	1	1	1	1	1	3	4	7	0
Plasminogen;Pla	**PLG**	NaN	17.34577	16.3135	19.81805	19.02575	14.33525	21.2394	20.42798	cell part;cytoplasmic membrane-bounded vesicle lumen;cytoplas	18.367	0	27.81268253	P00747	P00747	0	1	1	1	1	1	1	1	3	4	7	1
Microfibrillar-as	**MFAP5**	NaN	22.00477	21.92763	23.52397	23.44998	20.05232	23.8042	23.54321	extracellular matrix part;extracellular region;extracellular region p	17.381	0	28.41566641	Q13361	Q13361	0	1	1	1	1	1	1	1	3	4	7	1
Voltage-depend	**VDAC2**	NaN	21.1054	19.94978	23.05247	21.76073	20.80262	20.99293	21.65342	cell part;cytoplasmic part;intracellular non-membrane-bounded c	16.942	0	28.43845133	P45880	P45880	0	1	1	1	1	1	1	1	3	4	7	0
Clusterin;Cluste	**CLU**	NaN	17.70063	19.75861	21.19809	17.89416	17.03853	21.34825	21.33325	cell part;chromaffin granule;cytoplasmic membrane-bounded ves	15.606	0	27.38046952	P10909	P10909	0	1	1	1	1	1	1	1	3	4	7	1
Histone H3.1;Hi	**HIST1H3A;HIST3H3;H3F3C**	21.9518	24.35515	NaN	27.22674	23.00702	23.10807	25.20131	25.76724	cell part;chromosomal part;extracellular region;intracellular mem	14.004	0	30.13968097	P68431;Q1669!	P68431;Q1669!	1	1	0	1	1	1	1	1	3	4	7	1
NADH dehydrog	**NDUFA13**	NaN	21.12994	19.35029	23.48235	19.29255	17.30777	20.01059	22.75128	cell part;cytoplasmic part;integral to membrane;intracellular orga	13.822	0	27.49243634	Q9P0J0	Q9P0J0	0	1	1	1	1	1	1	1	3	4	7	0
Heterogeneous	**HNRNPC;HNRNPCL4;HNRN**	16.24674	19.95319	NaN	21.85125	19.57874	16.62428	20.7367	21.27555	catalytic step 2 spliceosome;cell part;intracellular membrane-bou	13.623	0	27.34756379	P07910;P0DMR	P07910;P0DMR	1	1	0	1	1	1	1	1	3	4	7	0
60S ribosomal p	**RPL24**	NaN	20.63361	18.36671	23.25246	20.48089	18.97166	20.91481	21.29019	cell part;cytosolic large ribosomal subunit;intracellular organelle p	12.839	0	27.13916864	P83731	P83731	0	1	1	1	1	1	1	1	3	4	7	0
Tyrosine-protei	**PTPN11**	17.61058	17.36863	NaN	20.23234	17.47477	15.65122	17.69207	18.10426	cell part;cytoplasmic part;cytosol;intracellular membrane-bounde	12.634	0	26.39879913	Q06124	Q06124	1	1	0	1	1	1	1	1	3	4	7	0
F-actin-capping	**CAPZA2;CAPZA1**	NaN	21.3362	20.96091	22.31172	20.37645	18.81903	21.93092	22.37374	cell cortex part;cell part;cortical cytoskeleton;cytoplasmic part;cy	12.518	0	28.03464652	P47755;P52907	P47755;P52907	0	1	1	1	1	1	1	1	3	4	7	1
Serine/arginine-	**SRSF4;SRSF5;SRSF6**	22.7275	23.61773	NaN	24.71356	22.42021	21.90866	22.54626	21.24574	cell part;cytoplasm;intracellular non-membrane-bounded organe	12.031	0	29.66522796	Q08170;Q1324	Q08170;Q1324	1	1	0	1	1	1	1	1	3	4	7	0
Isoleucine--tRNA	**IARS2**	17.92972	NaN	15.85309	18.59925	19.42874	17.97124	18.86686	20.04273	cell part;cytoplasmic part;intracellular organelle lumen;intracellul	11.705	0	27.04791253	Q9NSE4	Q9NSE4	1	0	1	1	1	1	1	1	3	4	7	0
Ig gamma-3 cha	**IGHG3**	NaN	18.25746	18.9748	17.7028	19.12293	17.4132	20.97708	21.2619	cell part;extracellular region;membrane	10.155	0.002	26.68939191	P01860	P01860	0	1	1	1	1	1	1	1	3	4	7	1
Actin, alpha car	**ACTC1**	NaN	22.71655	21.35418	25.25151	22.62932	21.15919	22.99695	23.52325	actin filament;actomyosin, actin part;cell part;contractile fiber pa	9.709	0.002	30.55316261	P68032	P68032	0	1	1	1	1	1	1	1	3	4	7	1
Uncharacterize	**NCBP2-AS2**	31.12725	NaN	29.89653	30.98529	31.28664	31.35621	31.15684	30.44825		8.3965	0.0019	36.0968289	Q69YL0	Q69YL0	1	0	1	1	1	1	1	1	3	4	7	0
NADH dehydrog	**NDUFB4**	NaN	19.72983	19.5652	22.94235	20.65377	18.92271	19.22576	21.76312	cell part;cytoplasmic part;integral to membrane;intracellular orga	8.1935	0.0019	26.25567709	O95168	O95168	0	1	1	1	1	1	1	1	3	4	7	0
Cytochrome c o	**COX7A2**	NaN	21.09732	20.02432	23.01888	20.361	19.09264	21.76052	23.04263	cell part;cytoplasmic part;intracellular organelle part;intracellular	8.0114	0.0019	26.62686647	P14406	P14406	0	1	1	1	1	1	1	1	3	4	7	0
Heterogeneous	**HNRNPK**	17.46044	19.48731	NaN	21.26842	18.01683	14.85531	19.57054	20.7774	catalytic step 2 spliceosome;cell part;chromatin;chromosomal pa	7.8233	0.0019	27.11326748	P61978	P61978	1	1	0	1	1	1	1	1	3	4	7	0
NADH dehydrog	**NDUFA10**	NaN	19.01392	18.6485	21.35976	17.17904	17.20103	18.84742	20.777	cell part;cytoplasmic part;intracellular organelle lumen;intracellul	7.6612	0.0018	26.99129157	O95299	O95299	0	1	1	1	1	1	1	1	3	4	7	0
Protein NipSnap	**GBAS**	NaN	19.80774	20.05205	22.4839	20.73082	18.74057	19.81649	21.06822	cell part;cytoplasmic part;integral to membrane;integral to plasm	7.6056	0.0018	27.65082047	O75323	O75323	0	1	1	1	1	1	1	1	3	4	7	0
Complement C1	**C1QC**	NaN	17.91088	16.51798	20.23034	19.35397	16.03409	20.6435	19.99673	collagen;extracellular matrix part;extracellular region;extracellula	7.4851	0.0018	25.95158176	P02747	P02747	0	1	1	1	1	1	1	1	3	4	7	1
Actin, aortic sm	**ACTA2**	NaN	21.66757	20.74148	23.11893	17.81965	19.61294	21.44415	21.37289	actin cytoskeleton;cell part;contractile fiber;contractile fiber part	7.2445	0.0017	28.63169613	P62736	P62736	0	1	1	1	1	1	1	1	3	4	7	0
ATP-dependent	**PFKM**	NaN	17.60038	16.59577	20.24493	18.85602	17.81703	17.1138	19.05807	6-phosphofructokinase complex;apical plasma membrane;cell pai	7.0684	0.0017	26.52856333	P08237	P08237	0	1	1	1	1	1	1	1	3	4	7	0
Protein AMBP;A	**AMBP**	19.69617	19.08475	19.40526	NaN	20.58013	18.77459	19.37276	20.06039	cell part;cell surface;extracellular region;extracellular region part;	6.7544	0.0016	26.48937687	P02760	P02760	1	1	1	0	1	1	1	1	3	4	7	1
Protein 4.1;Ban	**EPB41;EPB41L1;EPB41L3**	16.6708	17.68332	NaN	16.87843	17.50293	15.87896	18.66091	18.69666	axon part;cell cortex part;cell junction;cell part;cell projection pai	6.3515	0.0079	25.9625005	P11171;Q9H4G	P11171;Q9H4G	1	1	0	1	1	1	1	1	3	4	7	0
POTE ankyrin	**POTEE;POTEF;POTEI;POTEJ**	NaN	18.50157	18.586	19.73998	19.03265	16.86858	19.28261	21.90327	cell cortex part;cytoplasmic part;intracellular membrane-bound	6.2824	0.0077	26.62456758	Q6S8J3;A5A3E0	Q6S8J3;A5A3E0	0	1	1	1	1	1	1	1	3	4	7	0
Sialic acid-bind	**SIGLEC16**	NaN	20.28105	19.78123	20.065	21.84537	20.45934	25.62464	22.07698	cell part;integral to membrane;intrinsic to membrane;plasma	6.2038	0.009	30.85281446	A6NMB1	A6NMB1	0	1	1	1	1	1	1	1	3	4	7	0
Alpha-parvin	**PARVA**	18.98084	21.77949	20.6715	23.68731	NaN	21.82427	[illegible]	NaN	actin cytoskeleton;cell junction;cell part;cytoplasmic part	12.74	0	28.37164871	Q9NVD7	Q9NVD7	1	1	1	1	0	1	[illegible]	0	4	[illegible]	[illegible]	0
Guanine nucleo	**GNAI2**	21.17597	17.91485	21.82021	21.88118	NaN	21.76539	[illegible]	NaN	cell part;centrosome;cytoplasmic part;cytoskeletal part	48.848	0	27.33389851	P04899	P04899	1	1	1	1	0	1	[illegible]	0	4	[illegible]	[illegible]	0
Sodium/potassi	**ATP1A1**	15.15798	16.49199	16.7125	22.19686	NaN	18.66515	23.65665	NaN	axon;caveola;cell part;cytoplasmic part;cytosol;integral	110.34	0	29.64708447	P05023;P13637	P05023	1	1	1	1	0	1	1	0	4	2	6	0
Poly(rC)-binding	**PCBP1**	19.69559	19.8942	21.45076	24.47079	NaN	21.20148	24.05556	NaN	cell part;cytoplasmic part;intracellular membrane-bounded	56.542	0	29.55101826	Q15365;P57721	Q15365	1	1	1	1	0	1	1	0	4	2	6	0
Myosin regulat	**MYL9**	22.31041	23.3434	18.29733	26.67101	NaN	NaN	17.83053	21.61126	actin filament bundle;actomyosin;cell part;contractile fiber part	50.662	0	30.08398018	P24844	P24844	1	1	1	1	0	0	1	1	4	2	6	0

Glycogen phosp	PYGB	14.21682	18.79671	18.90947	22.04347	NaN	NaN	18.07692	18.55817	cell part;cytoplasm;cytoplasmic part;cytosol;intracellular part;me	43.214	0	28.11961337	P11216;P11217	P11216	1	1	1	1	0	0	1	1	4	2	6	0
von Willebrand	VWA1	16.93756	19.54323	20.10776	22.34101	19.49693	NaN	18.83448	NaN	basement membrane;extracellular matrix;extracellular matrix par	24.273	0	27.48515947	Q6PCB0	Q6PCB0	1	1	1	1	1	0	1	0	4	2	6	1
Biglycan	BGN	24.04693	21.70721	17.78813	23.81607	NaN	NaN	21.78229	21.29983	cell part;cell surface;cytoplasmic membrane-bounded vesicle;cytc	20.13	0	29.40926613	P21810	P21810	1	1	1	1	0	0	1	1	4	2	6	1
Aminopeptidase	RNPEP	15.39208	17.22647	16.43464	19.75608	NaN	NaN	18.56559	21.17816	cell part;extracellular region;extracellular region part;extracellula	18.795	0	26.99399254	Q9H4A4	Q9H4A4	1	1	1	1	0	0	1	1	4	2	6	1
Ras-related prot	RAB1B;RAB1A;RAB10;RAB	16.56908	20.24226	18.32043	21.83353	NaN	NaN	20.36624	22.02114	cell part;cell projection;cilium;cytoplasm;cytoplasmic membrane-	13.106	0	27.29920173	Q9H0U4;P6282	Q9H0U4;P6282	1	1	1	1	0	0	1	1	4	2	6	0
Palladin	PALLD	17.19114	20.26419	20.53251	24.53154	NaN	16.23799	18.06975	18.99604	actin filament;adherens junction;anchoring junction;cell junction	116.73	0	30.71881818	Q8WX93;Q86T(	Q8WX93	1	1	1	1	0	1	1	1	4	3	7	0
Mas-related G-p	MRGPRF	22.80951	24.01827	22.38735	24.328	23.45199	23.78347	22.73822	NaN	cell part;integral to membrane;intrinsic to membrane;membrane	103.35	0	29.64234057	Q96AM1	Q96AM1	1	1	1	1	1	1	1	0	4	3	7	0
Galectin-4	LGALS4	22.11331	23.0486	20.82073	24.31935	NaN	19.69653	22.52578	26.76939	cell part;cytoplasmic part;cytosol;intracellular part;membrane;pla	100.54	0	31.03603628	P56470	P56470	1	1	1	1	0	1	1	1	4	3	7	0
Peroxiredoxin-6	PRDX6	19.73676	22.50845	20.10303	25.25046	NaN	16.80914	22.11509	23.89356	cell part;cytoplasmic membrane-bounded vesicle;cytoplasmic par	70.167	0	29.92860688	P30041	P30041	1	1	1	1	0	1	1	1	4	3	7	0
Septin-2	Sep-02	20.24644	21.72705	20.24296	24.292	NaN	18.50541	21.33462	21.61018	actin cytoskeleton;cell cortex part;cell division site part;cell part;c	47.542	0	29.35575586	Q15019	Q15019	1	1	1	1	0	1	1	1	4	3	7	0
14-3-3 protein z	YWHAZ	17.42086	21.23122	17.43738	24.30932	NaN	16.54641	21.65172	24.23081	cell leading edge;cell part;cytoplasmic membrane-bounded vesicl	43.669	0	29.28372237	P63104;P27348	P63104	1	1	1	1	0	1	1	1	4	3	7	0
Serpin B6	SERPINB6	17.03832	17.97567	17.79931	19.97407	NaN	16.49462	19.54215	22.9455	cell part;centrosome;cytoplasmic part;cytoskeletal part;cytosol;ir	39.492	0	27.72767309	P35237	P35237	1	1	1	1	0	1	1	1	4	3	7	0
X-ray repair cros	XRCC5	16.7337	19.75901	16.17313	21.20359	17.22938	NaN	19.75888	21.8443	cell part;chromosomal part;cytoplasm;intracellular organelle part	37.996	0	28.23109715	P13010	P13010	1	1	1	1	1	0	1	1	4	3	7	0
Succinate dehyc	SDHA	18.20003	20.14631	18.80873	20.69634	NaN	18.04116	20.45784	23.15541	cell part;cytoplasmic part;fumarate reductase complex;intracellul	36.51	0	28.76081561	P31040	P31040	1	1	1	1	0	1	1	1	4	3	7	0
Poly [ADP-ribos	PARP1	15.40906	17.45177	15.76077	19.89275	17.33769	NaN	18.51357	18.74366	cell part;envelope;intracellular non-membrane-bounded organell	27.686	0	26.76141813	P09874	P09874	1	1	1	1	1	0	1	1	4	3	7	0
Heat shock cogr	HSPA8	14.89131	17.23351	18.16575	22.51627	18.6006	NaN	19.39814	20.72326	cell part;cell surface;clathrin coated vesicle membrane;clathrin sc	27.368	0	28.19272324	P11142	P11142	1	1	1	1	1	0	1	1	4	3	7	1
ADP-ribosylatio	ARF4;ARF5;ARF1;ARF3	16.65452	19.63256	19.50147	20.83214	17.28311	NaN	20.99631	23.1735	cell part;contractile fiber part;cytoplasmic part;cytosol;Golgi appa	26.657	0	27.32053299	P18085;P84085	P18085;P84085	1	1	1	1	1	0	1	1	4	3	7	0
60S ribosomal p	RPL30	22.96462	21.96208	21.32438	23.38653	NaN	17.30001	22.2064	23.89735	cell part;cytosolic large ribosomal subunit;intracellular organelle p	20.452	0	28.05532787	P62888	P62888	1	1	1	1	0	1	1	1	4	3	7	0
Proteoglycan 3	PRG3	21.12187	21.98715	18.11411	24.2851	NaN	18.09192	19.0746	20.06605		19.162	0	27.60165825	Q9Y2Y8	Q9Y2Y8	1	1	1	1	0	1	1	1	4	3	7	0
Cytochrome c o	COX6B1	17.42407	18.00053	17.1316	24.08253	NaN	17.65053	20.70961	22.71614	cell part;cytoplasmic part;intracellular organelle part;intracellular	16.826	0	27.50218329	P14854	P14854	1	1	1	1	0	1	1	1	4	3	7	0
T-complex prote	CCT4	15.73437	18.90436	17.88614	20.5682	19.36132	NaN	19.89107	20.67306	cell part;centrosome;chaperonin-containing T-complex;cytoplasn	16.777	0	27.47676474	P50991	P50991	1	1	1	1	1	0	1	1	4	3	7	0
Sushi repeat-co	SRPX	18.72301	20.75858	17.27394	19.86457	21.35939	19.76828	19.05062	NaN	autophagic vacuole;cell part;cell surface;cytoplasmic part;endopl	14.222	0	27.5829791	P78539	P78539	1	1	1	1	1	1	1	0	4	3	7	0
60S ribosomal p	RPL5	21.76272	21.46389	16.49232	22.84186	19.1188	NaN	21.23023	21.18507	cell part;cytosolic large ribosomal subunit;intracellular membrane	13.736	0	27.67451794	P46777	P46777	1	1	1	1	1	0	1	1	4	3	7	0
60S ribosomal p	RPL28	19.14338	21.32454	19.38905	23.81597	NaN	20.45232	22.01407	22.93222	cell part;cytosolic large ribosomal subunit;intracellular organelle p	13.608	0	27.9465375	P46779	P46779	1	1	1	1	0	1	1	1	4	3	7	0
Guanine nucleo	GNB1	19.23191	20.2214	20.30552	23.27014	19.97141	NaN	20.75801	21.82283	cell body;cell part;cell projection;cell projection part;cilium part;d	7.8793	0.0019	27.93663165	P62873	P62873	1	1	1	1	1	0	1	1	4	3	7	0
General transcri	GTF3C5	21.96258	22.42029	19.98579	24.90752	20.10406	16.71102	NaN	17.3403	cell part;intracellular organelle part;intracellular part;macromolec	6.2543	0.0077	30.33234129	Q9Y5Q8	Q9Y5Q8	1	1	1	1	1	1	0	1	4	3	7	0
Collagen alpha-1	COL1A1	28.7433	28.98338	28.39051	29.09071	30.20268	29.55225	29.81314	29.4548	cell part;collagen;collagen type I;cytoplasmic part;endoplasmic re	323.31	0	38.5936945	P02452	P02452	1	1	1	1	1	1	1	1	4	4	8	1
Fibrillin-1	FBN1	23.32072	25.12786	25.21327	26.15345	26.22816	24.99585	26.28579	26.16312	basement membrane;extracellular matrix part;extracellular regio	323.31	0	35.90757323	P35555;P35556	P35555	1	1	1	1	1	1	1	1	4	4	8	1
Laminin subunit	LAMB2	23.16452	23.78067	23.19683	25.63184	23.56302	22.44463	23.26914	22.82483	extracellular matrix part;extracellular region part;laminin comple:	323.31	0	33.39035964	P55268	P55268	1	1	1	1	1	1	1	1	4	4	8	1
Collagen alpha-2	COL1A2	30.77878	30.62218	29.62994	30.8464	31.29406	30.74895	31.13919	30.55536	cell part;collagen;collagen type I;cytoplasmic part;endoplasmic re	323.31	0	39.87734958	P08123	P08123	1	1	1	1	1	1	1	1	4	4	8	1
Laminin subunit	LAMC1	23.28729	23.79976	23.35891	25.30758	23.80134	22.97381	23.81734	23.04692	extracellular matrix part;extracellular membrane-bounded organ	323.31	0	33.08858385	P11047	P11047	1	1	1	1	1	1	1	1	4	4	8	1
Collagen alpha-1	COL6A1	26.31988	27.37186	26.96058	28.28679	28.66414	27.36928	27.2203	27.69803	anchoring collagen;cell part;collagen;collagen type VI;cytoplasmic	323.31	0	36.40785595	P12109	P12109	1	1	1	1	1	1	1	1	4	4	8	1
Nidogen-1	NID1	22.69196	23.70176	23.11141	25.67939	23.76678	22.56458	23.41828	23.08249	basal lamina;cell part;cell periphery;extracellular matrix part;extr	323.31	0	32.61120261	P14543	P14543	1	1	1	1	1	1	1	1	4	4	8	1
Collagen alpha-3	COL6A3	25.8061	27.04302	26.21584	27.53252	28.0592	26.66194	26.61625	26.85591	anchoring collagen;cell part;collagen;collagen type VI;cytoplasmic	323.31	0	37.43363893	P12111	P12111	1	1	1	1	1	1	1	1	4	4	8	1
Filamin-A	FLNA	21.83395	24.15236	23.00167	26.8125	23.54946	22.40754	23.15785	23.23837	actin cytoskeleton;cell cortex;cell part;chromosomal part;cytopla	323.31	0	34.53478922	P21333	P21333	1	1	1	1	1	1	1	1	4	4	8	1
Alpha-actinin-1	ACTN1	21.0142	25.26803	24.39532	27.50317	22.89232	21.99497	23.85624	25.29435	actin filament;adherens junction;anchoring junction;cell junction	323.31	0	33.96791392	P12814;P35609	P12814	1	1	1	1	1	1	1	1	4	4	8	1
Basement mem	HSPG2	23.75338	24.584	24.76946	27.05466	24.91388	24.11545	24.55286	24.81553	basal lamina;cell part;cytoplasmic part;extracellular matrix part;e	323.31	0	35.74472345	P98160	P98160	1	1	1	1	1	1	1	1	4	4	8	1
Eosinophil pero:	EPX	22.96483	26.11912	24.69413	27.20116	24.5643	23.50567	25.58523	25.40002	cell part;cytoplasmic membrane-bounded vesicle;cytoplasmic par	323.31	0	33.87499913	P11678;P05164	P11678	1	1	1	1	1	1	1	1	4	4	8	1
Laminin subunit	LAMA5	21.23005	22.75878	22.46956	24.1495	22.77187	21.65875	22.67271	22.4438	basement membrane;extracellular matrix part;extracellular regio	323.31	0	33.25222811	O15230;Q1678	O15230	1	1	1	1	1	1	1	1	4	4	8	1
Collagen alpha-2	COL6A2	25.81665	26.75977	25.9955	27.76224	27.61456	26.35072	26.40944	26.77605	cell part;collagen;cytoplasmic part;endoplasmic reticulum lumen;	323.31	0	35.42704889	P12110	P12110	1	1	1	1	1	1	1	1	4	4	8	1
Actin, cytoplasm	ACTG1;ACTB	25.05796	27.05403	26.64705	28.97714	26.61414	25.21738	26.99442	28.59292	axon;cell cortex part;cell part;cell projection;contractile fiber;cort	323.31	0	34.79275243	P63261;P60709	P63261;P60709	1	1	1	1	1	1	1	1	4	4	8	1
Calponin-1	CNN1	24.15105	25.11506	24.89264	30.01784	23.62723	22.11012	22.50198	22.51396	actin filament bundle;actomyosin;cell body;cell junction;cell part;	323.31	0	33.97083036	P51911;Q9943	P51911	1	1	1	1	1	1	1	1	4	4	8	0
Actin, gamma-e	ACTG2	29.38294	30.2415	30.38751	33.20921	29.67325	28.43571	29.2971	29.49779	cell part;cell periphery;cytoplasmic part;cytoskeleton;cytosol;intr	323.31	0	38.21399643	P63267	P63267	1	1	1	1	1	1	1	1	4	4	8	0
Myosin-11	MYH11	27.16701	28.24799	27.54642	30.54582	27.89522	26.68083	26.96895	26.65226	A band;actin filament bundle;actomyosin;actomyosin contractile	323.31	0	38.02601744	P35749;P12883	P35749	1	1	1	1	1	1	1	1	4	4	8	0
ATP synthase su	ATP5A1	19.54538	23.3868	22.62623	25.5659	23.59923	22.41815	24.21653	26.19699	cell part;cytoplasmic part;intracellular organelle lumen;intracellul	323.31	0	32.39840978	P25705	P25705	1	1	1	1	1	1	1	1	4	4	8	0
Filamin-C	FLNC	18.31924	21.41524	21.58316	24.97001	20.59714	19.69498	20.49804	20.4864	cell part;contractile fiber part;costamere;cytoplasm;cytoplasmic p	323.31	0	32.64615754	Q14315	Q14315	1	1	1	1	1	1	1	1	4	4	8	0
EH domain-cont	EHD2	21.32932	23.11902	23.45174	25.9896	23.24962	21.87346	22.84917	22.93745	cell part;cytoplasmic membrane-bounded vesicle;cytoplasmic par	323.31	0	31.73630462	Q9NZN4;Q9H4N	Q9NZN4	1	1	1	1	1	1	1	1	4	4	8	0
Desmin	DES	23.29179	26.77618	27.70728	29.87855	26.65772	25.19584	26.4062	26.49135	adherens junction;anchoring junction;axon part;cell junction;cell	323.31	0	35.62763956	P17661;Q1635	P17661	1	1	1	1	1	1	1	1	4	4	8	0
ATP synthase su	ATP5B	21.91758	23.11858	22.70634	26.12157	23.14847	22.3353	23.91698	26.46175	cell part;cell surface;cytoplasmic part;intracellular non-membrane	323.31	0	32.54291618	P06576	P06576	1	1	1	1	1	1	1	1	4	4	8	0
Tubulin alpha-1	TUBA1A;TUBA3C;TUBA3E	25.59798	27.30791	26.63367	28.38303	27.23334	26.11309	26.99938	27.50127	cell part;cytoplasm;cytoplasmic microtubule;cytoplasmic part;cyt	323.31	0	34.5831809	Q71U36;Q1374	Q71U36;Q1374	1	1	1	1	1	1	1	1	4	4	8	0
Synemin	SYNM	17.12969	22.69717	23.43873	25.70609	21.66275	20.082	20.80302	21.7959	adherens junction;anchoring junction;cell junction;cell part;contr	312.39	0	32.68085142	O15061	O15061	1	1	1	1	1	1	1	1	4	4	8	0
Transgelin	TAGLN	24.71392	26.98663	25.57917	30.18471	25.59087	24.51069	26.48305	26.88855	cell part;cytoplasm;intracellular part	309.34	0	34.68269415	Q01995	Q01995	1	1	1	1	1	1	1	1	4	4	8	0
Histone H4	HIST1H4A	27.25386	29.36982	26.29423	31.5106	27.99653	27.28938	28.67283	28.69584	actin cytoskeleton;cell part;chromosomal part;cytoskeleton;extra	300.48	0	34.88558308	P62805	P62805	1	1	1	1	1	1	1	1	4	4	8	1
Cathepsin G	CTSG	25.66031	26.74471	25.21342	27.62854	27.72611	26.65322	27.77486	26.89006	cell part;cell surface;cytoplasmic membrane-bounded vesicle;cytc	290.02	0	33.93315269	P08311	P08311	1	1	1	1	1	1	1	1	4	4	8	1
Collagen alpha-1	COL4A1	25.0818	25.95954	25.11827	26.58721	25.92583	25.56331	25.43192	25.42758	basal lamina;cell part;collagen;collagen type IV;cytoplasmic part;e	282.11	0	35.00399431	P02462;P29400	P02462	1	1	1	1	1	1	1	1	4	4	8	1
Lumican	LUM	24.72765	24.33919	23.78905	26.65267	23.4763	22.18831	24.99761	24.17188	cell part;collagen;cytoplasmic part;extracellular matrix part;extra	276.62	0	31.82547678	P51884;CON (	P51884	1	1	1	1	1	1	1	1	4	4	8	1
Myosin-9	MYH9	19.47742	21.97011	20.37698	23.78526	20.77274	19.1493	21.92169	22.24508	actin filament bundle;actomyosin;actomyosin contractile ring;adh	265.16	0	31.63079397	P35579	P35579	1	1	1	1	1	1	1	1	4	4	8	1
Dermatopontin	DPT	28.43682	28.43928	26.95593	28.2795	29.71399	29.45695	29.33415	28.89649	extracellular matrix;extracellular region part;extracellular space;p	264.77	0	34.6965438	Q07507	Q07507	1	1	1	1	1	1	1	1	4	4	8	1
Myosin light cha	MYLK	20.05073	21.21656	20.9643	24.17957	21.87815	19.87332	20.44425	20.83159	actin filament bundle;actomyosin;cell division site part;cell part;c	245.09	0	31.48534184	Q15746	Q15746	1	1	1	1	1	1	1	1	4	4	8	0
Complement C3	C3	18.38961	21.63511	20.16766	21.58183	21.97837	19.70271	23.76891	23.35178	cell part;extracellular membrane-bounded organelle;extracellular	232.55	0	31.7756466	P01024;CON (	P01024	1	1	1	1	1	1	1	1	4	4	8	1
Vimentin	VIM	19.82129	23.73014	22.72038	26.00817	23.17925	19.96621	24.26191	24.50743	cell leading edge;cell part;cell projection;cytoplasmic part;cytoske	222.97	0	32.18624292	P08670;CON (	P08670	1	1	1	1	1	1	1	1	4	4	8	1
Tubulin beta cha	TUBB	23.951	25.62995	25.05225	28.13006	25.96746	24.6435	25.8044	26.93112	cell body;cell part;cytoplasm;cytoplasmic part;cytoskeletal part;c	221.95	0	33.65234722	P07437;A6NNZ	P07437	1	1	1	1	1	1	1	1	4	4	8	1
C4b-binding pro	C4BPA	19.25739	20.50494	20.04767	21.172	22.21943	21.6468	24.99856	24.07284	cell part;cytoplasm;extracellular region;intracellular part;membra	209.28	0	30.90576803	P04003	P04003	1	1	1	1	1	1	1	1	4	4	8	1
Collagen alpha-2	COL4A2	23.78776	24.27817	23.41532	25.354	24.46663	23.84795	23.90399	23.65239	cell part;collagen;collagen type IV;cytoplasmic part;endoplasmic r	200.45	0	33.62701438	P08572	P08572	1	1	1	1	1	1	1	1	4	4	8	1
Pyruvate kinase	PKM	20.47635	23.67971	23.15814	25.84592	23.51087	22.75754	24.18109	25.30946	cell part;cytoplasmic part;cytosol;extracellular membrane-bound	195.5	0	32.3353795	P14618;P30613	P14618	1	1	1	1	1	1	1	1	4	4	8	1
EMILIN-1	EMILIN1	18.56726	21.39205	21.05966	23.85377	19.97239	19.71482	21.38137	21.10712	collagen;extracellular matrix part;extracellular membrane-bound	193.53	0	30.3205545	Q9Y6C2	Q9Y6C2	1	1	1	1	1	1	1	1	4	4	8	1
Membrane prim	AOC3	25.60549	25.5634	24.92827	25.22383	25.83567	25.02136	25.81702	25.05681	cell part;cell surface;cytoplasm;integral to membrane;intracellula	191.63	0	33.37645404	Q16853;O7510	Q16853	1	1	1	1	1	1	1	1	4	4	8	0
Hemoglobin sub	HBB	22.43278	25.59132	22.4058	27.58871	23.45312	23.33142	27.45685	27.81262	cell part;cytoplasmic membrane-bounded vesicle lumen;cytoplasi	178.9	0	32.8537627	P68871;CON (	P68871	1	1	1	1	1	1	1	1	4	4	8	1
Unconventional	MYO1C	17.77867	21.93323	21.31102	24.2863	21.7909	19.66792	20.64033	21.62185	basal plasma membrane;brush border;cell part;cell projection;cel	176.23	0	30.93325824	O00159	O00159	1	1	1	1	1	1	1	1	4	4	8	1
Heat shock-rela	HSPA2	17.92937	21.86703	21.93934	25.51566	21.93585	19.82412	22.14199	23.60784	cell part;cell surface;chromosomal part;cytoplasmic membrane-b	175.81	0	31.35400132	P54652;P11021	P54652	1	1	1	1	1	1	1	1	4	4	8	0
Vinculin	VCL	20.1029	22.07754	21.94732	24.47883	22.03413	20.60748	21.47719	21.63856	actin cytoskeleton;adherens junction;anchoring junction;cell junc	164.21	0	31.6539492	P18206	P18206	1	1	1	1	1	1	1	1	4	4	8	1
Clathrin heavy c	CLTC	16.2035	19.932	17.95106	22.0746	19.13809	17.27649	20.54444	22.68936	cell part;clathrin coat;clathrin coat of coated pit;clathrin coat of t	161.9	0	30.30845364	Q00610;P53675	Q00610	1	1	1	1	1	1	1	1	4	4	8	1
Mimecan	OGN	25.54271	26.41724	23.96305	27.43245	26.36818	24.37312	26.39971	25.33929	cell part;cytoplasmic part;extracellular matrix;extracellular region	157.34	0	33.18721682	P20774	P20774	1	1	1	1	1	1	1	1	4	4	8	1
Integrin-linked p	ILK	20.25994	22.19764	21.81714	25.95087	21.90753	19.61333	20.98357	21.43843	adherens junction;anchoring junction;axon part;cell body;cell jun	153.33	0	30.91356389	Q13418	Q13418	1	1	1	1	1	1	1	1	4	4	8	0
Ig mu chain C re	IGHM	20.34147	22.12499	22.36402	22.96712	22.56347	20.63662	26.16254	25.9336	cell part;extracellular region;integral to membrane;intrinsic to me	153.12	0	31.89616214	P01871;P0DOX(	P01871;P0DOX(	1	1	1	1	1	1	1	1	4	4	8	1
Bone marrow pr	PRG2	23.01146	25.68755	21.66822	27.16682	24.1354	23.75766	24.41558	23.74263	cell part;cytoplasmic membrane-bounded vesicle;cytoplasmic par	151.07	0	31.8964148	P13727	P13727	1	1	1	1	1	1	1	1	4	4	8	1
Coronin-1C	CORO1C	17.44289	22.92448	22.43901	26.65704	21.77876	21.93143	22.10095	22.50538	actin cytoskeleton;cell part;cytoskeleton;intracellular non-membr	143.05	0	31.28482569	Q9ULV4	Q9ULV4	1	1	1	1	1	1	1	1	4	4	8	0
Annexin A6	ANXA6	21.54406	23.88837	22.43372	25.72333	23.63267	22.98609	23.85633	23.86816	cell part;cytoplasmic membrane-bounded vesicle;cytoplasmic par	141	0	32.39634403	P08133	P08133	1	1	1	1	1	1	1	1	4	4	8	1
Fibronectin;Ana	FN1	18.92622	21.09719	20.24841	24.25768	19.72832	19.73298	21.97806	21.25367	apical plasma membrane;basement membrane;cell part;cytoplasi	140.55	0	31.60845124	P02751	P02751	1	1	1	1	1	1	1	1	4	4	8	1
Decorin	DCN	26.84995	25.09245	23.62545	27.06415	25.97353	23.74129	26.27277	25.14829	anchoring collagen;cell part;collagen;collagen type VI;cytoplasmic	139.44	0	33.16864406	P07585	P07585	1	1	1	1	1	1	1	1	4	4	8	1
Histone H2B typ	HIST1H2BL;HIST1H2BM;HIS	25.53083	27.59605	25.81968	30.31051	26.34496	25.37073	27.64774	27.70991	cell part;chromosomal part;extrinsic to membrane;extrinsic to pla	135.07	0	33.84267963	Q99880;Q9987	Q99880;Q9987	1	1	1	1	1	1	1	1	4	4	8	0
Transforming gr	TGFB1I1	21.20634	22.21573	21.31219	25.26513	22.06332	20.25983	21.77044	20.40322	adherens junction;anchoring junction;cell junction;cell part;cell-s	133.7	0	30.50189867	O43294	O43294	1	1	1	1	1	1	1	1	4	4	8	0
Annexin A2;Puta	ANXA2;ANXA2P2	16.57456	23.60885	20.94099	25.70823	21.85209	21.03053	23.89171	25.45648	basement membrane;cell part;cytoplasmic membrane-bounded v	125.61	0	31.55590711	P07355;A6NMY	P07355;A6NMY	1	1	1	1	1	1	1	1	4	4	8	1
Heat shock prot	HSPB1	23.78526	24.71879	25.67823	29.1161	23.95456	22.70654	23.70967	23.91752	cell part;cell surface;contractile fiber part;cytoplasmic part;cytosl	121.32	0	33.25124069	P04792	P04792	1	1	1	1	1	1	1	1	4	4	8	0
L-lactate dehydr	LDHA	19.98524	23.32444	22.0476	25.35347	20.34505	21.78349	23.53683	25.25994	cell part;cytoplasm;cytoplasmic part;cytosol;intracellular membra	120.72	0	30.95995815	P00338;Q6ZMR	P00338	1	1	1	1	1	1	1	1	4	4	8	0
Peripherin	PRPH	17.80908	20.73248	18.91243	23.76648	20.98231	18.27617	19.82546	18.8031	axon;axon part;cell part;cell projection;cell projection part;C-fiber	111.42	0	29.28986812	P41219	P41219	1	1	1	1	1	1	1	1	4	4	8	0
Smoothelin	SMTN	19.69756	21.91656	22.98709	25.08797	21.77612	20.99583	20.95113	20.61342	actin cytoskeleton;cell part;cytoplasm;cytoskeleton;intracellular r	103.21	0	31.37699733	P53814;Q9NUD	P53814	1	1	1	1	1	1	1	1	4	4	8	0
Chymase	CMA1	23.83297	21.59982	21.50446	23.25537	25.26778	23.06219	23.28799	23.59446	cell part;extracellular region;intracellular	103.05	0	30.42782318	P23946	P23946	1	1	1	1	1	1	1	1	4	4	8	1
Histone H3.3	H3F3A	28.21725	29.79943	27.70101	31.84019	29.26137	28.34723	29.55386	29.87818	cell part;chromosomal part;extracellular region;intracellular orga	101.89	0	34.90974274	P84243	P84243	1	1	1	1	1	1	1	1	4	4	8	1
Collagen alpha-1	COL14A1	17.47025	21.13031	21.51567	23.24811	21.62212	17.9138	22.22808	21.78532	anchoring collagen;cell part;collagen;collagen type XIV;cytoplasm	101.6	0	31.03170524	Q05707	Q05707	1	1	1	1	1	1	1	1	4	4	8	1
Ras-related prot	RRAS	20.69396	22.84322	22.55985	25.13101	22.58383	20.88748	21.27407	20.0747	cell part;cytoplasmic part;endoplasmic reticulum;intracellular me	98.028	0	29.83878974	P10301;P6207(	P10301	1	1	1	1	1	1	1	1	4	4	8	0
Plasma membra	ATP2B4;ATP2B3;ATP2B2;AT	16.26404	19.78615	19.46858	22.51205	20.03012	18.87457	19.58437	18.8087	apical plasma membrane;cell body;cell part;cell projection;cilium;	97.194	0	29.1799943	P23634;Q1672(	P23634;Q1672(	1	1	1	1	1	1	1	1	4	4	8	0
Alpha-enolase	ENO1	21.26991	20.72025	18.53024	23.83932	21.93672	19.52187	20.70168	24.64746	cell part;contractile fiber part;cytoplasmic part;cytosol;cytosolic p	95.538	0	30.10236994	P06733;P13929	P06733	1	1	1	1	1	1	1	1	4	4	8	1
Histone H2A typ	HIST1H2AC;HIST3H2A;HIST	20.03564	24.95034	23.26327	28.72546	23.73862	22.4403	25.0121	26.82457	cell part;chromatin;chromosomal part;chromosome;condensed c	94.456	0	31.6193379	Q93077;Q7L7L(	Q93077;Q7L7L(	1	1	1	1	1	1	1	1	4	4	8	0
Tubulin alpha-1	TUBA1B	23.87202	25.31482	24.68624	25.38172	25.32031	24.12825	25.40285	26.24587	cell part;cytoplasm;cytoplasmic microtubule;cytoplasmic part;cyt	93.603	0	32.60917811	P68363;A6NHL	P68363	1	1	1	1	1	1	1	1	4	4	8	0
Tubulointerstiti	TINAGL1	22.72783	24.34834	23.42726	24.6324	23.79818	21.75735	22.52174	24.00804	cell part;cytoplasm;extracellular region part;extracellular space;ir	93.583	0	31.12730986	Q9GZM7	Q9GZM7	1	1	1	1	1	1	1	1	4	4	8	1
Asporin	ASPN	24.36232	24.49644	22.488	26.36765	25.33538	23.33361	24.79005	24.02386	extracellular matrix;extracellular region part;proteinaceous extra	92.316	0	32.06628366	Q9BXN1	Q9BXN1	1	1	1	1	1	1	1	1	4	4	8	1
Heat shock 70 k	HSPA1B;HSPA1A	19.96916	21.65189	21.80692	24.71639	21.82213	19.65882	21.30602	22.39165		89.878	0	30.52215562	P0DMV9;P0DM	P0DMV9;P0DM	1	1	1	1	1	1	1	1	4	4	8	0
Heat shock prot	HSP90AB1	19.23119	21.84007	20.46374	23.25314	21.33527	19.02424	22.01437	24.13977	apical plasma membrane;basolateral plasma membrane;brush bo	88.783	0	30.35835746	P08238;Q58FF7	P08238	1	1	1	1	1	1	1	1	4	4	8	0
Plectin	PLEC	13.29175	17.99413	17.29329	20.26534	17.719	15.51067	17.88846	19.21937	actin cytoskeleton;adherens junction;anchoring junction;cell junc	81.67	0	29.60077254	Q15149;Q9UPN	Q15149	1	1	1	1	1	1	1	1	4	4	8	0
Polymerase I an	PTRF	21.99959	23.01533	21.92314	26.37044	22.70542	21.33811	22.46054	21.67607	caveola;cell part;cytoplasmic part;cytosol;endoplasmic reticulum;	81.667	0	30.86252762	Q6NZI2	Q6NZI2	1	1	1	1	1	1	1	1	4	4	8	0
Putative elonga	EEF1A1P5;EEF1A1;EEF1A2	20.37252	23.61448	21.71217	25.51482	22.68468	21.59728	23.84336	24.92021	cell body;cell part;cytoplasm;cytoplasmic part;cytosol;eukaryotic	80.231	0	31.25811041	Q5VTE0;P68104	Q5VTE0;P68104	1	1	1	1	1	1	1	1	4	4	8	0
Isocitrate dehyc	IDH2	16.60655	21.17164	19.91475	25.13716	19.64556	19.7101	18.86327	23.33743	cell part;cytoplasmic part;intracellular organelle lumen;intracellul	79.839	0	30.1858886	P48735	P48735	1	1	1	1	1	1	1	1	4	4	8	0
Transforming gr	TGFBI	18.8472	19.16357	20.293	23.79927	21.2476	19.64511	21.25194	21.75784	cell part;extracellular matrix;extracellular membrane-bounded or	78.736	0	29.60249032	Q15582	Q15582	1	1	1	1	1	1	1	1	4	4	8	1
Histone H2A typ	HIST2H2AC;HIST2H2AA3	21.28365	22.26745	21.28201	27.26401	22.74698	20.97603	23.53694	25.90157	cell part;chromosomal part;intracellular membrane-bounded org	76.919	0	30.24943337	Q16777;Q6FI13	Q16777;Q6FI13	1	1	1	1	1	1	1	1	4	4	8	0
Nidogen-2	NID2	21.16269	20.64799	18.8562	22.64801	20.58829	18.32487	21.1997	20.15956	basement membrane;cell part;cell surface;extracellular matrix pa	71.417	0	29.93213201	Q14112	Q14112	1	1	1	1	1	1	1	1	4	4	8	1
Cytoplasmic dyr	DYNC1H1	15.46932	17.59631	16.62927	20.64359	16.6683	15.15987	17.27276	19.31869	cell part;centrosome;cytoplasmic dynein complex;cytoplasmic pa	70.135	0	29.49106038	Q14204	Q14204	1	1	1	1	1	1	1	1	4	4	8	1
PDZ and LIM do	PDLIM7	19.21421	20.55441	22.0209	25.42483	19.99507	18.84684	19.61355	20.67107	actin cytoskeleton;actin filament bundle;actomyosin;adherens jui	69.58	0	30.47923432	Q9NR12	Q9NR12	1	1	1	1	1	1	1	1	4	4	8	0
Moesin;Radixin	MSN;RDX	18.07091	22.67564	20.04327	25.03624	21.63648	20.34863	22.79557	23.21838	actin filament;apical part of cell;apical plasma membrane;basolat	67.108	0	30.97814694	P26038;P35241	P26038;P35241	1	1	1	1	1	1	1	1	4	4	8	1
Elongation facto	TUFM	17.79042	21.38874	19.97393	23.95403	17.86212	18.34932	21.30011	24.25364	cell part;cytoplasmic part;intracellular non-membrane-bounded c	59.811	0	30.27841468	P49411	P49411	1	1	1	1	1	1	1	1	4	4	8	0
Cytochrome b-c	UQCRC2	17.81866	20.87942	19.19902	22.83074	21.21916	20.62364	21.41952	23.53872	cell part;cytoplasmic part;intracellular organelle part;intracellular	58.3	0	29.05082098	P22695	P22695	1	1	1	1	1	1	1	1	4	4	8	0
Peroxiredoxin-1	PRDX1	18.78947	22.45395	22.06036	24.68992	22.49636	21.4368	23.65436	25.50924	cell part;chromatin;chromosomal part;cytoplasmic membrane-bc	57.928	0	30.58468234	Q06830;Q1316	Q06830	1	1	1	1	1	1	1	1	4	4	8	1
ADP/ATP transl	SLC25A5;SLC25A6	19.75362	22.73969	21.43609	24.84321	23.80233	22.57679	23.49167	24.93656	cell part;cell projection;cilium;cytoplasmic part;cytoskeletal part;i	57.053	0	30.90217781	P05141;P12236	P05141;P12236	1	1	1	1	1	1	1	1	4	4	8	0
Vitronectin;Vitr	VTN	21.38416	20.5733	19.33313	21.6248	18.43876	19.66924	23.53196	22.52047	alphav-beta3 integrin-vitronectin complex;cell part;extracellular r	56.895	0	29.29926724	P04004;CON (	P04004	1	1	1	1	1	1	1	1	4	4	8	1
Guanine nucleo	GNB2;GNB4	21.01998	23.54404	22.80453	24.89139	23.01794	21.94332	23.29502	24.60992	cell body;cell part;cytoplasmic part;intracellular part;macromolec	54.138	0	30.29351234	P62879;Q9HAV	P62879;Q9HAV	1	1	1	1	1	1	1	1	4	4	8	0
Guanine nucleo	GNB2L1	19.47929	21.7516	20.48935	23.16516	20.07483	19.02926	22.51759	23.68667	cell body;cell part;cell projection;cytoplasmic part;cytoskeleton;d	52.492	0	29.43481791	P63244	P63244	1	1	1	1	1	1	1	1	4	4	8	0
Neutrophil defe	DEFA3;DEFA1	24.92913	27.59406	25.21278	27.29553	26.94938	28.40775	30.32421	29.44366	azurophil granule lumen;cell part;cytoplasmic membrane-bounde	52.366	0	33.48147354	P59666;P59665	P59666;P59665	1	1	1	1	1	1	1	1	4	4	8	1
Endoplasmin	HSP90B1	18.97911	19.31325	17.44354	22.97437	19.28299	17.90754	20.22635	23.26084	cell part;cytoplasmic membrane-bounded vesicle;cytoplasmic par	50.921	0	29.69639041	P14625;Q58FF3	P14625	1	1	1	1	1	1	1	1	4	4	8	0
Tensin-1	TNS1	17.24144	18.8649	19.32056	21.49941	19.44308	17.64997	18.33324	17.64688	adherens junction;anchoring junction;cell junction;cell part;cell-s	50.731	0	28.81900245	Q9HBL0	Q9HBL0	1	1	1	1	1	1	1	1	4	4	8	0
40S ribosomal p	RPS3	20.01004	22.27324	18.88148	23.82503	20.85377	19.91311	22.22034	23.06291	cell part;cell projection membrane;cell projection part;cytosolic s	50.573	0	29.42740361	P23396	P23396	1	1	1	1	1	1	1	1	4	4	8	0
Collagen alpha-2	COL5A2	21.11883	21.65272	16.89107	22.72017	21.99697	19.9812	21.53151	20.04607	cell part;collagen;collagen type V;cytoplasmic part;endoplasmic r	50.552	0	30.57686673	P05997	P05997	1	1	1	1	1	1	1	1	4	4	8	1
Mast cell carbo:	CPA3	21.37257	20.52631	20.6988	19.93876	24.02673	21.44627	22.522	22.33658	cell part;cytoplasmic membrane-bounded vesicle;cytoplasmic par	50.014	0	29.64648375	P15088	P15088	1	1	1	1	1	1	1	1	4	4	8	1
Prohibitin-2	PHB2	19.39956	21.14855	19.56192	23.29684	21.34505	20.12288	21.41033	23.08824	cell part;cytoplasmic part;intracellular membrane-bounded orgar	49.364	0	29.27879129	Q99623	Q99623	1	1	1	1	1	1	1	1	4	4	8	0
Myeloid-associa	MYADM	22.18444	23.6006	23.38337	23.98971	23.6621	23.81196	23.33224	22.98445	cell part;integral to membrane;intrinsic to membrane;membrane	46.374	0	29.26165633	Q96S97	Q96S97	1	1	1	1	1	1	1	1	4	4	8	0
Erythrocyte ban	STOM	20.48935	21.44364	21.42322	21.67111	22.48456	21.84862	23.04013	23.18494	cell part;cytoplasm;cytoplasmic membrane-bounded vesicle;cyto	46.076	0	29.09702834	P27105	P27105	1	1	1	1	1	1	1	1	4	4	8	1
Annexin A5	ANXA5	20.29927	23.07653	20.64939	25.08736	22.49597	21.58201	23.39715	23.71114	blood microparticle;cell part;cytoplasm;endothelial microparticle	45.464	0	30.73553821	P08758	P08758	1	1	1	1	1	1	1	1	4	4	8	1
Laminin subunit	LAMB1	19.33398	19.80258	18.68924	21.31562	18.31765	16.87195	19.69231	18.96011	cell part;cytoplasmic part;extracellular matrix part;extracellular m	44.748	0	28.82177204	P07942	P07942	1	1	1	1	1	1	1	1	4	4	8	1
Leucine-rich PPI	LRPPRC	16.95742	18.64902	19.33584	18.29158	19.8291	19.35402	19.52723	20.84728	cell part;chromosome;condensed chromosome;condensed nucle:	43.932	0	28.95060324	P42704	P42704	1	1	1	1	1	1	1	1	4	4	8	0
Prohibitin	PHB	20.3208	21.66973	20.48277	23.9083	20.94063	20.30084	21.8789	23.51087	cell part;cytoplasmic part;integral to membrane;integral to plasm	43.919	0	29.45795043	P35232	P35232	1	1	1	1	1	1	1	1	4	4	8	0
Collagen alpha-1	COL3A1	22.81192	24.27448	23.62634	23.66308	25.62305	24.85172	25.41925	24.8334	cell part;collagen;collagen type III;cytoplasmic part;endoplasmic r	43.349	0	33.77931107	P02461	P02461	1	1	1	1	1	1	1	1	4	4	8	1
Eosinophil catio	RNASE3	22.41522	23.4957	22.71802	26.49707	21.73905	21.227	24.61717	24.38146	extracellular region	42.424	0	30.36264824	P12724	P12724	1	1	1	1	1	1	1	1	4	4	8	1
Guanine nucleo	GNAO1	20.96578	21.87418	20.37103	24.36906	21.7487	19.73491	21.73773	21.15122	apical plasma membrane;cell body;cell part;cell projection;cell pr	42.302	0	29.3095599	P09471;P11488	P09471	1	1	1	1	1	1	1	1	4	4	8	0
Protein-glutami	TGM2	14.57648	21.50862	20.94942	23.15054	22.39598	21.51017	22.37981	22.61865	cell part;cytoplasmic part;intracellular membrane-bounded orgar	34.878	0	30.13785037	P21980	P21980	1	1	1	1	1	1	1	1	4	4	8	0
Actin-related pr	ACTR2	25.31793	26.56328	25.028	26.63686	25.90752	24.54528	25.28175	25.04356	Arp2/3 protein complex;cell part;cell projection;cytoplasmic part	32.854	0	32.42106534	P61160	P61160	1	1	1	1	1	1	1	1	4	4	8	0
Actin-related pr	ARPC4	20.36346	23.19809	21.23731	24.854	23.01446	21.90518	23.91716	24.13281	Arp2/3 protein complex;cell part;cell projection;cytoplasmic part	32.018	0	29.59985083	P59998	P59998	1	1	1	1	1	1	1	1	4	4	8	0
Dolichyl-diphos	RPN2	15.98233	19.93632	19.84238	20.26705	20.49502	19.52183	22.35665	23.40119	autophagic vacuole membrane;cell part;cytoplasmic part;endopl	31.681	0	28.91119383	P04844	P04844	1	1	1	1	1	1	1	1	4	4	8	0
Annexin A11	ANXA11	18.54574	21.19748	19.00846	23.12907	17.17962	19.86349	20.93805	22.28173	azurophil granule;cell part;cytoplasmic membrane-bounded vesic	31.59	0	28.5509449	P50995	P50995	1	1	1	1	1	1	1	1	4	4	8	0
60S ribosomal p	RPL7	17.69914	20.24714	19.36826	22.77712	19.83553	18.25907	20.20622	21.78441	cell part;cytosolic large ribosomal subunit;intracellular organelle p	31.563	0	27.46068673	P18124	P18124	1	1	1	1	1	1	1	1	4	4	8	0
Cofilin-2	CFL2	19.57939	22.17292	21.72434	25.81007	22.4146	20.65334	22.94674	23.88958	actin cytoskeleton;cell part;cytoplasm;cytoskeleton;intracellular r	30.366	0	30.01557967	Q9Y281	Q9Y281	1	1	1	1	1	1	1	1	4	4	8	0
Tubulin beta-2B	TUBB2B	20.80365	22.34422	21.24719	25.12076	22.90861	21.43166	22.33372	22.62259	cell part;cytoplasm;cytoskeletal part;intracellular organelle part;i	29.983	0	30.35310748	Q9BVA1	Q9BVA1	1	1	1	1	1	1	1	1	4	4	8	0
Collagen alpha-1	COL5A1	16.28589	19.3069	19.79497	16.80763	21.47872	21.02553	21.15542	21.18004	basement membrane;cell part;collagen;collagen type V;cytoplasn	29.913	0	29.88407687	P20908	P20908	1	1	1	1	1	1	1	1	4	4	8	1
Eukaryotic initia	EIF4A1;EIF4A2	20.42214	21.27384	20.37878	23.52456	21.39707	19.91173	22.03423	22.34997	cell part;cytoplasmic part;cytosol;eukaryotic translation initiation	28.319	0	29.39807334	P60842;Q1424(	P60842;Q1424(	1	1	1	1	1	1	1	1	4	4	8	0
Transmembrane	TMEM43	21.79954	22.44233	20.84575	23.31465	21.88643	18.67418	22.49082	22.07532	cell part;cytoplasmic part;endoplasmic reticulum;Golgi apparatus	27.142	0	29.63606017	Q9BTV4	Q9BTV4	1	1	1	1	1	1	1	1	4	4	8	0
Annexin A7	ANXA7	19.18935	21.2314	19.29771	22.88067	20.7154	19.81941	20.58187	21.91346	cell part;cytoplasmic part;cytosol;endoplasmic reticulum membra	26.976	0	28.61617695	P20073	P20073	1	1	1	1	1	1	1	1	4	4	8	0
Collagen alpha-3	COL5A3	19.81204	20.4502	20.09159	20.71507	21.45779	21.05616	21.58793	21.22152	cell part;collagen;collagen type V;cytoplasmic part;endoplasmic r	26.813	0	30.3273169	P25940	P25940	1	1	1	1	1	1	1	1	4	4	8	1
Prolargin	PRELP	17.48676	16.54312	20.02364	22.52052	15.29656	14.57377	20.02594	20.69337	cell part;cytoplasmic part;extracellular matrix;extracellular region	25.758	0	27.86555422	P51888	P51888	1	1	1	1	1	1	1	1	4	4	8	1
Ubiquitin-60S ri	UBA52;RPS27A;UBB;UBC	21.70607	24.07586	22.26831	23.54215	22.60187	20.96198	23.47828	25.29457	cell part;cytoplasmic part;cytoplasmic vesicle membrane;cytoplas	24.574	0	29.15489458	P62987;P62979	P62987;P62979	1	1	1	1	1	1	1	1	4	4	8	0
Leiomodin-1	LMOD1	19.35113	20.98905	19.94034	23.23549	20.4026	19.51607	20.59523	19.75186	cell part;cytoplasmic part;cytoskeleton;cytosol;intracellular non-r	24.563	0	28.92756179	P29536	P29536	1	1	1	1	1	1	1	1	4	4	8	0
Splicing factor, p	SFPQ	16.39322	20.28861	17.95985	22.41895	18.01078	17.9642	21.14681	22.00696	cell part;cytoplasm;intracellular organelle part;intracellular part;r	24.131	0	28.67495562	P23246	P23246	1	1	1	1	1	1	1	1	4	4	8	0
ATP synthase su	ATP5C1	16.49345	19.35954	19.42589	22.1193	21.8438	19.88699	21.35316	22.69215	cell part;cytoplasmic part;intracellular organelle lumen;intracellul	23.913	0	27.96928024	P36542	P36542	1	1	1	1	1	1	1	1	4	4	8	0
Tubulin beta-3 c	TUBB3	19.21667	20.50514	20.05616	22.44816	21.3545	19.94407	21.06329	21.2903	axon;cell part;cell projection;cytoplasm;cytoskeletal part;intracell	23.403	0	28.37085925	Q13509	Q13509	1	1	1	1	1	1	1	1	4	4	8	0
60S ribosomal p	RPL14	20.41245	21.43675	19.15632	24.92922	21.10527	20.16349	21.94059	23.98146	cell part;cytosolic large ribosomal subunit;intracellular organelle p	22.878	0	28.44213496	P50914	P50914	1	1	1	1	1	1	1	1	4	4	8	0
ATP-dependent	DDX39A;DDX39B	16.68442	19.54374	18.13796	21.41354	19.92829	18.34291	20.3393	21.44531	cell part;cytoplasm;intracellular membrane-bounded organelle;in	22.047	0	27.42189802	O00148;Q1383	O00148;Q1383	1	1	1	1	1	1	1	1	4	4	8	0
Collagen alpha-1	COL21A1	20.72542	20.66822	20.84606	20.46732	21.34299	21.30986	20.36837	21.22034	cell part;collagen;cytoplasmic part;endoplasmic reticulum lumen;	21.936	0	29.43614924	Q96P44	Q96P44	1	1	1	1	1	1	1	1	4	4	8	1
Serpin H1	SERPINH1	15.60377	20.18556	18.17685	22.41426	19.88417	18.87132	21.32597	20.56393	cell part;cytoplasmic part;endoplasmic reticulum lumen;endoplas	20.194	0	28.12804775	P50454	P50454	1	1	1	1	1	1	1	1	4	4	8	0
T-complex prote	TCP1	15.3728	18.67989	18.02269	21.43888	18.51757	17.50673	20.32882	21.03194	cell junction;cell part;centrosome;chaperonin-containing T-comp	18.827	0	27.81066165	P17987	P17987	1	1	1	1	1	1	1	1	4	4	8	0
EGF-containing	EFEMP1	17.52083	20.4109	21.28563	22.73806	21.69698	21.13057	22.00237	21.58376	extracellular matrix;extracellular region part;extracellular space;p	18.658	0	29.05050964	Q12805	Q12805	1	1	1	1	1	1	1	1	4	4	8	1
Destrin	DSTN	21.25609	22.24702	22.65875	25.85227	22.39218	20.96205	22.20051	22.55747	actin cytoskeleton;cell cortex part;cell part;cortical actin cytoskel	18.117	0	29.93353966	P60981	P60981	1	1	1	1	1	1	1	1	4	4	8	0
Microfibrillar-as	MFAP2	24.38489	26.52929	25.91582	27.23096	27.24889	26.27764	27.12967	26.81812	extracellular matrix part;extracellular region;extracellular region p	16.654	0	31.65535748	P55001	P55001	1	1	1	1	1	1	1	1	4	4	8	1
Caveolin-1;Cave	CAV1;CAV3	22.17661	23.2468	22.44048	24.61661	22.11705	22.04657	24.07806	23.2281	acrosomal membrane;apical plasma membrane;basolateral plasm	14.263	0	29.62027347	Q03135;P56539	Q03135;P56539	1	1	1	1	1	1	1	1	4	4	8	0
Aldehyde dehyd	ALDH1B1;ALDH1A3;ALDH1	17.63474	18.57976	16.88822	23.11509	19.39795	19.13102	20.16312	20.74032	cell part;cytoplasm;cytoplasmic part;cytosol;intracellular membra	14.087	0	28.19760546	P30837;P47895	P30837;P47895	1	1	1	1	1	1	1	1	4	4	8	0
Fibulin-5	FBLN5	19.59576	20.67642	20.33068	22.58903	22.36282	20.45914	21.54302	20.94364	cell part;cytoplasm;elastic fiber;extracellular matrix;extracellular	13.696	0	28.47869446	Q9UBX5	Q9UBX5	1	1	1	1	1	1	1	1	4	4	8	1
Titin	TTN	19.73845	18.91357	18.7028	19.68087	18.61076	17.81303	18.45121	17.998	cell part;chromosome;condensed chromosome;condensed nucle:	13.478	0	32.74801228	Q8WZ42	Q8WZ42	1	1	1	1	1	1	1	1	4	4	8	1
Actin-related pr	ACTR3;ACTR3C;ACTR3B	15.60418	16.65536	18.31858	22.02952	19.15338	18.41601	19.47989	22.31396	Arp2/3 protein complex;cell junction;cell part;cell projection;cell-	13.036	0	27.8647871	P61158;Q9C0K3	P61158;Q9C0K3	1	1	1	1	1	1	1	1	4	4	8	0
Kinesin-like prot	KIF20B	25.6138	24.57346	22.52095	25.67971	24.18132	23.33402	23.90692	23.3577	cell part;centrosome;cytoplasm;cytoplasmic part;cytoskeletal par	11.434	0.0021	34.1901346	Q96Q89	Q96Q89	1	1	1	1	1	1	1	1	4	4	8	0
Antigen KI-67	MKI67	21.6808	21.52545	19.00358	22.63079	19.25509	18.58498	19.21367	18.28125	cell part;chromosomal part;chromosome;chromosome, centrome	10.658	0.002	31.35515724	P46013	P46013	1	1	1	1	1	1	1	1	4	4	8	0
Pejvakin	DFNB59	24.33919	24.73371	24.16553	24.08886	25.32769	25.46986	24.06168	25.38795	cell body;cell part;neuronal cell body	10.656	0.002	32.27230885	Q0ZLH3	Q0ZLH3	1	1	1	1	1	1	1	1	4	4	8	0
Uncharacterized	C5orf42	15.49732	20.74854	19.96719	21.97698	20.34386	18.80098	17.82526	20.35359	cell part;integral to membrane;intrinsic to membrane;membrane	10.288	0.002	30.52785152	Q9H799	Q9H799	1	1	1	1	1	1	1	1	4	4	8	0
Microfibril-asso	MFAP4	25.09857	23.66936	22.47665	24.39257	25.32361	24.99053	25.48093	24.01044	extracellular matrix part;extracellular region part;fibril;microfibril	10.098	0.002	30.49505087	P55083	P55083	1	1	1	1	1	1	1	1	4	4	8	1
60S ribosomal p	RPL22	20.74788	22.6315	19.66648	24.42579	19.81666	20.35402	22.73455	23.11658	cell part;cytosolic large ribosomal subunit;intracellular organelle p	8.6408	0.0019	27.57441452	P35268	P35268	1	1	1	1	1	1	1	1	4	4	8	0
Tenascin-X	TNXB	13.34082	16.5687	15.32453	18.69326	17.57186	16.64442	16.70239	17.12	cell part;extracellular matrix;extracellular region part;extracellula	7.6627	0.0018	27.62491613	P22105	P22105	1	1	1	1	1	1	1	1	4	4	8	1
Macrophage mi	MIF	19.40522	22.44761	21.4225	25.42733	20.94821	19.08306	23.27682	23.80637	cell part;cell surface;cytoplasm;extracellular region;extracellular r	7.6272	0.0018	28.60681996	P14174	P14174	1	1	1	1	1	1	1	1	4	4	8	1
Calcium-binding	SLC25A13;SLC25A12	15.00251	18.18238	15.12	19.5285	18.57976	17.4496	18.12994	15.86986	cell part;cytoplasmic part;integral to membrane;integral to plasm	7.5993	0.0018	26.04737174	Q9UJS0;O7574(	Q9UJS0;O7574(	1	1	1	1	1	1	1	1	4	4	8	0
SH3 and multipl	SHANK3	23.15667	23.20407	18.44589	23.28926	24.09273	22.70913	23.51388	23.80961	cell junction;cell part;cell projection membrane;cell projection pa	7.5816	0.0018	32.53910695	Q9BYB0	Q9BYB0	1	1	1	1	1	1	1	1	4	4	8	0
Mitochondrial 2	SLC25A11	19.40904	20.19556	18.14674	20.24748	19.82457	19.1941	20.18689	20.92042	cell part;cytoplasmic part;integral to membrane;integral to plasm	7.033	0.0017	27.0437474	Q02978	Q02978	1	1	1	1	1	1	1	1	4	4	8	0
60S ribosomal p	RPL13	16.93928	20.28059	18.9846	22.55749	20.27424	19.25024	20.19761	21.01045	cell part;cytosolic large ribosomal subunit;intracellular organelle p	6.7558	0.0016	26.83460684	P26373	P26373	1	1	1	1	1	1	1	1	4	4	8	0
Prostacyclin rec	PTGIR	24.66514	25.51569	22.28658	27.68892	23.14504	21.90558	21.42562	22.15013	cell part;cytoplasmic part;cytosol;integral to membrane;integral t	6.44	0.0048	31.56065193	P43119	P43119	1	1	1	1	1	1	1	1	4	4	8	0
DNA-binding pro	ID1	25.30699	25.60261	22.4468	27.74606	23.20614	21.31457	21.59755	21.45131	cell part;cytoplasm;intracellular membrane-bounded organelle;in	6.4373	0.0048	31.51770466	P41134	P41134	1	1	1	1	1	1	1	1	4	4	8	0
Iron-responsive	IREB2	18.92819	21.4916	19.10308	21.39681	21.50295	21.79233	21.40551	20.92078	cell part;cytoplasm;cytoplasmic part;cytosol;intracellular membra	6.3336	0.0079	29.5388249	P48200	P48200	1	1	1	1	1	1	1	1	4	4	8	0
Condensin-2 co	NCAPG2	25.61051	24.38364	20.61791	25.90258	23.81225	20.8946	21.2498	21.50644	cell part;intracellular membrane-bounded organelle;intracellular (	6.2264	0.0091	33.27239229	Q86XI2	Q86XI2	1	1	1	1	1	1	1	1	4	4	8	0

Appendix 6 - Protein candidates potentially specific to either SI and Colon scaffolds

11 total proteins detected in either Colon or SI ECM scaffolds

Protein names	Gene names	iBAQ Colon_A	iBAQ Colon_B	iBAQ Colon_C	iBAQ Colon_D	iBAQ SI_A	iBAQ SI_B	iBAQ SI_C	iBAQ SI_D	GOCC name	Score	Q-value	Intensity	Protein IDs	Majority protein IDs	iBAQ Colon_A	iBAQ Colon_B	iBAQ Colon_C	iBAQ Colon_D	iBAQ SI_A	iBAQ SI_B	iBAQ SI_C	iBAQ SI_D	Colon	SI	Extracellular
Carbamoyl-phc	**CPS1**	NaN	NaN	NaN	NaN	NaN	14.68677	16.08535	22.25678	cell part;cytopl	73.658	0	28.55090821	P31327	P31327	0	0	0	0	0	1	1	1	0	3	0
HLA class II hist	**HLA-DRB1**	NaN	NaN	NaN	NaN	20.03106	NaN	22.47998	19.05539	cell part;clathri	49.611	0	26.83195239	Q5Y7A7;P0191	Q5Y7A7;P0191	0	0	0	0	1	0	1	1	0	3	0
Dolichyl-diphos	**DAD1**	NaN	NaN	NaN	NaN	21.36437	NaN	19.72489	22.78654	cell part;cytopl	9.2686	0.0019724	25.68658965	P61803	P61803	0	0	0	0	1	0	1	1	0	3	0
Defensin-5;HD!	**DEFA5**	NaN	NaN	NaN	NaN	25.55221	25.4776	29.23911	29.89966	cell part;cytopl	23.646	0	33.01100335	Q01523	Q01523	0	0	0	0	1	1	1	1	0	4	1
Thrombospond	**THBS4**	NaN	17.40615	16.40085	23.54345	NaN	NaN	NaN	NaN	basement mer	48.69	0	28.89573613	P35443;CON__	P35443	0	1	1	1	0	0	0	0	3	0	1
Sorbin and SH3	**SORBS1**	NaN	15.43195	17.31371	21.94474	NaN	NaN	NaN	NaN	actin cytoskele	43.274	0	27.92382716	Q9BX66;O9487	Q9BX66	0	1	1	1	0	0	0	0	3	0	0
Calcium/calmo	**CAMK2G;CAM**	17.06792	NaN	19.02429	22.53251	NaN	NaN	NaN	NaN	axon part;calci	12.43	0	27.32757389	Q13555;Q9UQ	Q13555;Q9UQ	1	0	1	1	0	0	0	0	3	0	0
Cilia- and flage	**CFAP46**	16.97668	17.99214	NaN	20.45202	NaN	NaN	NaN	NaN		8.9569	0.0019493	27.87554848	Q8IYW2	Q8IYW2	1	1	0	1	0	0	0	0	3	0	0
Protein Niban	**FAM129A**	NaN	17.53541	16.94364	20.18628	NaN	NaN	NaN	NaN	cell part;cytopl	8.3217	0.0018975	25.81066165	Q9BZQ8	Q9BZQ8	0	1	1	1	0	0	0	0	3	0	0
KN motif and a	**KANK2**	17.53397	NaN	16.44954	19.9146	NaN	NaN	NaN	NaN	cell part;cytopl	7.8978	0.0018657	25.73308941	Q63ZY3	Q63ZY3	1	0	1	1	0	0	0	0	3	0	0
Alpha-parvin	**PARVA**	18.98084	21.77949	20.6715	23.68731	NaN	NaN	NaN	NaN	actin cytoskele	12.74	0	28.37164871	Q9NVD7	Q9NVD7	1	1	1	1	0	0	0	0	4	0	0